Modeling the kinetics of the main peak and later age of alite hydration

Thèse N° 9499

Présentée le 10 mai 2019

à la Faculté des sciences et techniques de l'ingénieur
Laboratoire des matériaux de construction
Programme doctoral en science et génie des matériaux

pour l'obtention du grade de Docteur ès Sciences

par

Alexandre Reda Constantin William Caleb OUZIA

Acceptée sur proposition du jury

Prof. W. Curtin, président du jury
Prof. K. Scrivener, directrice de thèse
Prof. G. Scherer, rapporteur
Dr E. Garboczi, rapporteur
Prof. R. Flatt, rapporteur

2019

ÉCOLE POLYTECHNIQUE
FÉDÉRALE DE LAUSANNE

Pour mes parents,

In a world in which there is so much to interest,
so much to enjoy,
and so much also to correct and improve ...

Utilitarianism
— John Stuart Mill

Acknowledgements

Je tiens tout d'abord à remercier Karen de m'avoir accordé avec confiance une grande liberté dans mes recherches, une liberté exigeante et formatrice qui m'a valu plusieurs mauvaises nuits à me torturer l'esprit mais aussi quelques bonnes idées parfois. Je souhaite également lui exprimer ma gratitude pour toutes les conférences et workshops auxquels j'ai pu participer, La Havane, Londres, Beijing, Vienne, Amsterdam, Gstaad, ... c'était un rythme effréné mais des expériences fécondes.

Je souhaite aussi remercier mes rapporteurs de thèse, Professeur George Scherer, Docteur Edward Garboczi et Professeur Robert Flatt, pour leur révisions et critiques qui m'ont permis d'approfondir ma réflexion et la qualité de la thèse. J'aimerais également remercier Paul Bowen, André Nonat, Luc Nicoleau et Patrick Juilland pour nos discussions stimulantes sur les mécanismes d'hydratation, de précipitation ... ou de dissolution.

Je ne peux pas ne pas mentionner quatre chercheurs issus du LMC sur les épaules desquels ma thèse s'est construite: Amélie Bazzoni, Mercedes Costoya, Elise Bérodier et Arnaud Muller.

Une thèse, pour toute la charge de travail qu'elle représente, ne résume pourtant pas quatre ans de vie, loin s'en faut. Pourquoi dissimuler par sens du protocole la diversité des expériences vécues en quatre ans de maturations scientifique et humaine? Me retournant sur ces années, je ne peux qu'être ému de tant d'aventures, de transformations, de hauts et de bas, d'images, de paysages. Emu par l'étendue des expériences incroyables que j'ai vécu grâce à vous tous qui m'avaient tant apporté de soutiens, de changement d'air, de discussions, de joie, ou ... de critiques ! Une thèse, c'est intense surtout au début, surtout au milieu et surtout à la fin. Sans vous cela n'aurait pas été aussi riche.

Pleins de souvenirs de mes premiers mois au LMC avec l'ancienne équipe et leur chaleureux accueil. Mention spéciale à Lionel pour être allé "faire un petit tour en courant" jusqu'à la

tour Haldimand, mi-février sous la bruine et sans entraînement aucun. Mais somme toute, “sans souffrance la douleur n’est rien” et j’ai pu grâce à tes encouragements réaliser mon premier marathon! Merci à toi pour ta bonne humeur et ton dynamisme indéracinables. Je tiens également à remercier l’équipe de techniciens, Jean, Tonio et Paul pour leur aide maintes fois requise. Arnaud, combien de kilomètres le long du lac, d’heures à refaire le monde à pas d’heure, à se challenger? et ça n’est pas fini ! Hadi, pour tout ton humour aiguisé et la gaieté que tu nous as apporté, les échos de ton rire dans le corridor me restent. Encore un immense merci pour la découverte de ton antique patrie, pardonnes nous nos infernales espièglerie avec Arnaud et Pawel. Pawel, merci pour ton sens de la rigueur, ta sympathie et gaieté de coeur. Anne-Sandra, le subtil cocktail de ton humour déjanté aux saveurs rigoristes suisse-alémaniques nous ont bien manqué depuis que tu nous as quitté. Merci à Marie-Alix pour l’organization de tous ces workshops stimulants et si bien situés.

A mes étudiants de projets de licence et master, Bruno, Pablo, Edgar et Win-Wei je me réjouis autant que je suis curieux de vous voir vous élancer dans le monde de l’entreprise ou de la recherche.

Mink et Wiola, thank you for all your kindness and for sharing the PhD adventure together.

Plein de bonnes ondes à la prochaine génération: Yosra, Franco, Anna, Mahsa et Solène ... vous allez vous régaler de la fin de thèse. Solène, au delà du plaisir toujours renouvelé de te voir éclater en fou rire au milieu des meetings les plus sérieux, je te dois la plus belle photo de ma thèse, merci! Franco, je m’impatiente que tu révolutionnes notre compréhension des aluminates ... pour coder tout cela ;).

Tous mes encouragement à l’ultime équipe: Khalil, Andrea, Sara, Qiao, Maya, Gabie, Masood. Faîtes nous rêver ! Imaginez et osez !

Clin d’oeil à mes collègues et amis chinois, Lili, Yan, Shiyu, Hui, Yu et Xuerun. Thank you for all your sympathy and exchanges about the depth of our cultural differences despite my (bad) dark humour. I admire your dedication and courage !

Amis Post-docs, Adrien, François, Fabien, Diana, William, le labo s’effondrerait-il sans vous?

Un immense merci à mes colocataires, Lucile, Anne-Frédérique et Georges, pour tous ces apéros sur le balcon de Saint-Paul, tous ces univers croisés du théâtre et de l’anthropologie, ces débats autour de la table de la cuisine mais aussi pour décaler mon regard de scientifique Béotien. Et Cyril, merci pour tout ton engagement pour la nature, la jeunesse, la société et le monde ! et ces soirées aux bougies, pétards, piano et amaretto à divaguer sous le ciel étoilé du lavaux me resteront gravées!

Jérôme et Arthur, camarades, quelle aventure rocambolesque nous avons vécu avec Origine(s) et Destin(s) ! Des hauts plateaux du Vercors aux petits théâtres lyonnais, des frayeurs du premier plateau à la salle comble … et comblée, je raconterai notre histoire à mes enfants, en hurlant d'une grosse voie fourcadienne, et je vous jure qu'ils ne me croiront quand même pas ! Jérôme, quelle histoire depuis le BS en passant par ce café dominical à Austerlitz jusqu'à la troupe au grand complet pour affronter le jury parisien. Merci de m'avoir tracté dans les passages à vide et d'y avoir toujours cru.

Xavier, merci de m'avoir fait découvrir la méditation, expérience marquante et parfois salvatrice. Merci pour tout ton engagement pour le campus, pour ce bol d'air humaniste en ce bastion scientiste. Et quelle joie d'avoir organisé ensemble les Break & Brain !

Mes amis d'école, Alisson, Idriss, Laura, Anthony & Marion, Romain, Tiphaine, Hanja et Priscille. Merci de votre bienveillance malgré mon état d'abrutissement perpétuel. De se retrouver chaque année, de retrouver l'ambiance de nos années étudiantes, de garder leur tendre mémoire et d'en créer de nouvelles.

Elise, merci pour ton soutien et tes mille et un conseils discrets mais avisés en cette dernière année éprouvante. Maude, par où commencer? Combien de kilomètres du bord du lac, au sommet du moléson en passant mille fois par la tour de Gourze et les terrasses du lavaux? Combien de paysages contemplés et partagés dans cette magnifique région? Julien … quel privilège d'avoir été ton officemate ces quatre années! La moitié de ma thèse ne s'y trouverait pas sans être passé par le crible de ton esprit! Et quelle aventure astronomique nous avons vécu ensemble!

Enfin, cette thèse, comme toute mon éducation, n'aurait été possible sans mes parents, Madjid Ouzia et Maryse Carel; sans votre amour inconditionnel, à travers des années parfois difficiles, je ne serais pas arrivé là.

Épesses, le 1er Mai 2019

tour Haldimand, mi-février sous la bruine et sans entraînement aucun. Mais somme toute, “sans souffrance la douleur n’est rien” et j’ai pu grâce à tes encouragements réaliser mon premier marathon! Merci à toi pour ta bonne humeur et ton dynamisme indéracinables. Je tiens également à remercier l’équipe de technicien, Jean, Tonio et Paul pour leur aide maintes fois requise. Arnaud, combien de kilomètres le long du lac, d’heures à refaire le monde à pas d’heure, à se challenger? et ça n’est pas fini ! Hadi, pour tout ton humour aiguisé et la gaieté que tu nous as apporté, les échos de ton rire dans le corridor me restent. Encore un immense merci pour la découverte de ton antique patrie, pardonnes nous nos infernales espièglerie avec Arnaud et Pawel. Pawel, merci pour ton sens de la rigueur, ta sympathie et gaieté de coeur. Anne-Sandra, le subtil cocktail de ton humour déjanté aux saveurs rigoristes suisse-alémaniques nous ont bien manqué depuis que tu nous as quitté. Merci à Marie-Alix pour l’organization de tous ces workshops stimulants et si bien situés.

A mes étudiants de projets de licence et master, Bruno, Pablo, Edgar et Win-Wei je me réjouis autant que je suis curieux de vous voir vous élancer dans le monde de l’entreprise ou de la recherche.

Mink et Wiola, thank you for all your kindness and for sharing the PhD adventure together.

Plein de bonnes ondes à la prochaine génération: Yosra, Franco, Anna, Mahsa et Solène ... vous allez vous régaler de la fin de thèse. Solène, au delà du plaisir toujours renouvelé de te voir éclater en fou rire au milieu des meetings les plus sérieux, je te dois la plus belle photo de ma thèse, merci! Franco, je m’impatiente que tu révolutionnes notre compréhension des aluminates ... pour coder tout cela ;).

Tous mes encouragement à l’ultime équipe: Khalil, Andrea, Sara, Qiao, Maya, Gabie, Masood. Faîtes nous rêver ! Imaginez et osez !

Clin d’oeil à mes collègues et amis chinois, Lili, Yan, Shiyu, Hui, Yu et Xuerun. Thank you for all your sympathy and exchanges about the depth of our cultural differences despite my (bad) dark humour. I admire your dedication and courage !

Amis Post-docs, Adrien, François, Fabien, Diana, William, le labo s’effondrerait-il sans vous?

Un immense merci à mes colocataires, Lucile, Anne-Frédérique et Georges, pour tous ces apéros sur le balcon de Saint-Paul, tous ces univers croisés du théâtre et de l’anthropologie, ces débats autour de la table de la cuisine mais aussi pour décaler mon regard de scientifique Béotien. Et Cyril, merci pour tout ton engagement pour la nature, la jeunesse, la société et le monde ! et ces soirées aux bougies, pétards, piano et amaretto à divaguer sous le ciel étoilé du lavaux me resteront gravées!

Jérôme et Arthur, camarades, quelle aventure rocambolesque nous avons vécu avec Origine(s) et Destin(s) ! Des hauts plateaux du Vercors aux petits théâtres lyonnais, des frayeurs du premier plateau à la salle comble … et comblée, je raconterai notre histoire à mes enfants, en hurlant d'une grosse voie fourcadienne, et je vous jure qu'ils ne me croiront quand même pas ! Jérôme, quelle histoire depuis le BS en passant par ce café dominical à Austerlitz jusqu'à la troupe au grand complet pour affronter le jury parisien. Merci de m'avoir tracté dans les passages à vide et d'y avoir toujours cru.

Xavier, merci de m'avoir fait découvrir la méditation, expérience marquante et parfois salvatrice. Merci pour tout ton engagement pour le campus, pour ce bol d'air humaniste en ce bastion scientiste. Et quelle joie d'avoir organisé ensemble les Break & Brain !

Mes amis d'école, Alisson, Idriss, Laura, Anthony & Marion, Romain, Tiphaine, Hanja et Priscille. Merci de votre bienveillance malgré mon état d'abrutissement perpétuel. De se retrouver chaque année, de retrouver l'ambiance de nos années étudiantes, de garder leur tendre mémoire et d'en créer de nouvelles.

Elise, merci pour ton soutien et tes mille et un conseils discrets mais avisés en cette dernière année éprouvante. Maude, par où commencer? Combien de kilomètres du bord du lac, au sommet du moléson en passant mille fois par la tour de Gourze et les terrasses du lavaux? Combien de paysages contemplés et partagés dans cette magnifique région? Julien … quel privilège d'avoir été ton officemate ces quatre années! La moitié de ma thèse ne s'y trouverait pas sans être passé par le crible de ton esprit! Et quelle aventure astronomique nous avons vécu ensemble!

Enfin, cette thèse, comme toute mon éducation, n'aurait été possible sans mes parents, Madjid Ouzia et Maryse Carel; sans votre amour inconditionnel, à travers d'années parfois difficiles, je ne serai pas arrivé là.

Épesses, le 1er Mai 2019

Abstract

The aim of this thesis is to understand the mechanisms underlying the main hydration peak and later ages of alite hydration; it proposes new mechanistic models for these two stages.

Alite is the main constituent of Portland Cement (PC), and is responsible for the setting and hardening of concrete during the first reaction day. Because future cements will still be based on PC, alite remains worthy of investigation.

Alite hydration can be divided into five stages according to the heat flow released during the first two days of reaction. The three last stages, the acceleration and deceleration periods (which combined are called "main hydration peak" and last one day) and the later age (one day to 28 days), are still under debate. As long as the mechanisms of alite hydration are not fully understood the path toward the optimization of cements is hindered.

The two hypotheses referred in all major textbooks for the main hydration peak, the diffusion barrier and nucleation and growth by impingement suffer from critical pitfalls examined in chapter 2.

In 2015, Bazzoni suggested a new mechanism: C-S-H needles progressively cover the alite surface while simultaneously shift from a fast to a slow growth mode. The first contribution of the thesis is the Needle model. It was built onto Bazzoni's hypothesis and proved it to be right though with some shades. The peak time coincides with the time at which most of the needles have nucleated and are in their fast growth regime. As they gradually enter the slow growth regime, the rate decreases.

The Needle model also studied for the first time an old hypothesis raised by Taylor: that the small grain dissolution may explain part of the transition from the acceleration to deceleration period. The model shows that the small grains dissolution do not affect the shape of the main

hydration peak, they do not cause the transition, though they do sharpen and shift it slightly left. This effect is only visible for particle size distribution having a large fraction of grains below 10 micrometers, or alternatively for powders that reach more than 50% of degree of hydration at 24 hours.

Regarding the later ages, a new model is built to test the space-filling hypothesis. The probability of outer C-S-H growth is found to be not linear with the available space for precipitation. The later age kinetics are shown to be not controlled by a single overwhelming mechanism but rather by the cumulative effects of several coupled mechanisms.

Keywords: alite hydration kinetics, C-S-H, modelling, main hydration peak, later age

Résumé

Le but de cette thèse est de comprendre les mécanismes du pic principal et du vieil âge de l'hydratation de l'alite. Un modèle est proposé ces deux périodes.

L'alite est le constituant principal du ciment Portland, et est responsable de la prise et du durcissement du béton pendant le premier jour. L'intérêt d'étudier l'alite réside également dans le fait que les ciments futurs resteront basés sur le ciment Portland.

La cinétique de l'hydratation de l'alite est divisé en cinq étapes selon le profil de chaleur dégagé par la réaction. Les trois dernières étapes, l'accélération et la décélération (qui ensemble constituent le pic principal et s'étendent sur une journée) et le vieil âge (entre 1 et 28 jours), restent sujets de débats. Tant que les mécanismes de l'hydratation de l'alite restent incompris l'optimisation des ciments est entravée.

Les deux hypothèses mises en avant pour expliquer le pic principal et présentées dans tous les livres de références, l'hypothèse de la barrière de diffusion et l'hypothèse de nucléation et croissance par tamponnement, souffrent de plusieurs écueils critiques examinées dans le chapitre 2.

En 2015, un nouveau mécanisme a été suggéré par Bazzoni : les aiguilles de C-S-H recouvrent progressivement la surface des grains d'alite en même temps qu'elles évoluent d'une croissance rapide vers une croissance lente. La première contribution de cette thèse et le modèle de l'aiguille. Ce modèle est construit sur l'hypothèse de Bazzoni et démontrer la justesse de ce scénario malgré quelques nuances. Le pic coincide au temps auquel la majorité des aiguilles ont nuclées et croissent rapidement. Alors qu'elles entrent progressivement dans leur mode de croissance lente, la vitesse de réaction décroît.

Le modèle de l'aiguille a également permis d'étudier pour la première fois une hypothèse soulevée par Taylor en 1986 : l'hypothèse que la dissolution des petits grains puisse expliquer en partie la transition entre l'accélération et la décélération. Le modèle démontre que la dissolution de ces petits grains de modifie pas la forme du pic, elle ne cause pas la transition, mais ce phénomène réduit la largeur et hauteur du pic tout en le translatant sur la gauche. Cet effet n'est significatif que pour les poudres suffisamment fines : celles possédant une large fraction de leur granulométrie inférieure à 10 microns, ou alternativement pour les poudres dépassant 50 % d'avancement à 24 heures.

Concernant le vieil âge, un nouveau modèle a permis de tester l'hypothèse dite du remplissement de l'espace. La probabilité de croissance du C-S-H extérieur est trouvé être non-linéaire avec l'espace disponible pour la précipitation. La thèse s'achève sur une argumentation démontrant que la cinétique du vieil âge n'est pas le fait d'un unique facteur, mais ne peut être expliquée que par le couplage de plusieurs mécanismes.

Mots-clé : hydratation de l'alite, cinétique, C-S-H, modélisation, pic principal, vieil âge.

Contents

Glossary

Cement shorthand notation

C: CaO (Calcium Oxide)	S: SiO_2 (Silicon dioxide)	A: Al_2O_3 (Aluminium oxide)	
F: Fe_2O_3 (Iron oxide)	\$: SO_3 (Sulfate)	H: H_2O (water)	c: $CaCO_3$

Abbreviation of materials and phases

OPC: ordinary Portland cement

SCM: Supplementary cementitious material(s)

C_3S: Tricalcium silicate

C_2S: Dicalcium silicate

C_3A: Tricalcium aluminate

C_4AF: Tetracalcium aluminoferrite

C\$$H_3$: Gypsum

C-S-H: Calcium silicate hydrate

CH: Calcium hydroxide (portlandite)

Abbreviations of techniques

MIP: Mercury intrusion porosimetry

SEM: Scanning electron microscopy

EDS: Energy dispersive X-Ray spectroscopy

BET: Brunauer-Emmett-Teller

XRD: X-Ray diffraction

Miscellaneous abbreviations

W/C: water to cement ratio

W/S: water to solid ratio

PSD: Particle size distribution

1 Introduction

Concrete is the world most produced material. Although that material has the least embodied energy, its massive production is responsible for 4.0 to 5.8% of the world CO_2 emission. The anthropogenic CO_2 emission produced since the second industrial revolution is partly responsible for global warming and climate change.

However, no other material can compete with cement on a global scale. The cost, widespread availability, easiness of manipulation, versatility of shape for artistic architectural purposes, CO_2 emission per mass, strength and durability makes it unique. As a result, future cement will still be based on Portland cement, the gray cement that has become a hallmark of our modern world.

Alite is the main constituent of Portland Cement (PC), and is responsible for the setting and hardening of concrete during the first reaction day. Because future cements will still be based on PC, alite remains worthy of investigation.

Alite hydration can be divided into five stages according to the heat flow released during the first two days of reaction. The three last stages – acceleration (stage 3) and deceleration (stage 4) periods which together form the main hydration peak, and the later ages (stage 5) – are still under debate. As long as the mechanisms of alite hydration are not fully understood the path toward the optimization of cements is hindered.

The aim of this thesis is to build and test new mechanistic models for the main hydration peak and later ages based on Bazzoni's microstructural observations that C-S-H nucleates and grow as needles.

Contents

1.1 Concrete: the future of construction materials

1.1.1 Concrete is the most produced material

Concrete is the most produced material (figure 1.1). Concrete is a composite made of sand, aggregates, water and of course cement, its reactive component. The cement proportion for standard concrete amounts to about 10 wt.% which explains why its annual production is one order of magnitude less than concrete, but still higher than any metal or polymer.

By definition, a cement is any substance used to bind several other materials together. In practice, it is most frequently confused with Portland Cement (PC), this particular gray cement that has become ubiquitous and a marker of our civilization. Portland cement is made by calcining limestone and clays at 1450°C for two hours which makes clinker. Gypsum is added after cooling.

Portland cement was invented and patented by Joseph Aspdin (1778-1855) in 1824 but it was not before the end of the XIXth century that it spread out and became a commonplace, mostly thanks to François Hennebique (1842-1921). Hennebique associated steel bars with concrete in the bottom part of concrete slab, i.e. where tension occurs and where concrete is weak. This improved steel reinforced concrete was set to progressively overthrow all other building materials throughout the XXth century.

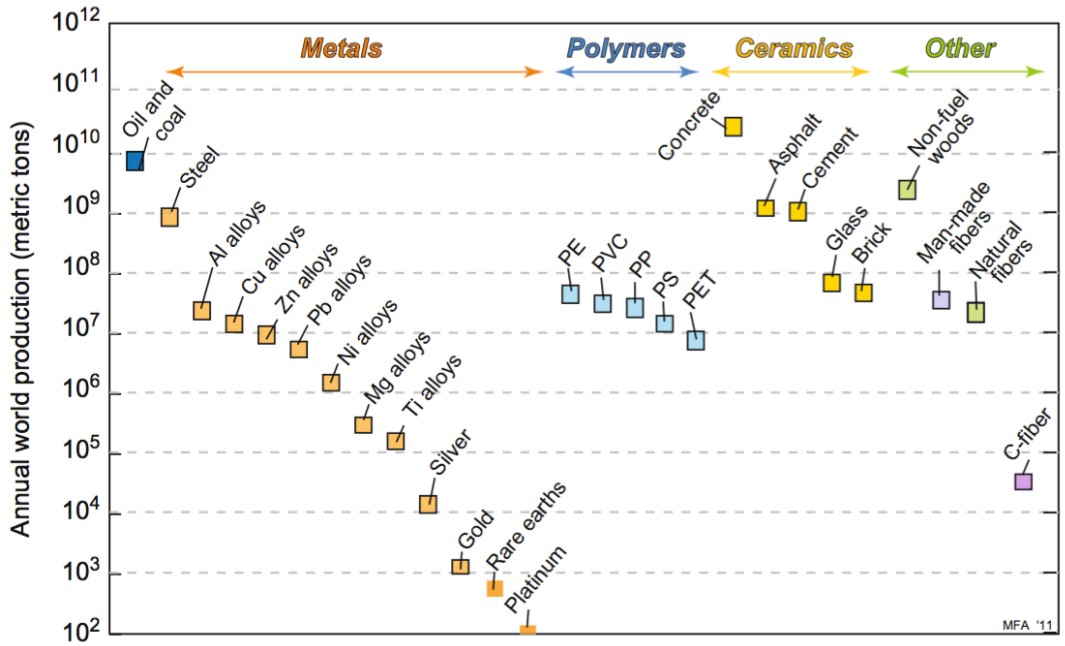

Figure 1.1 – Annual world production of materials. Concrete tops it. Cement is fourth. From [2, figure 2.3, p. 19]

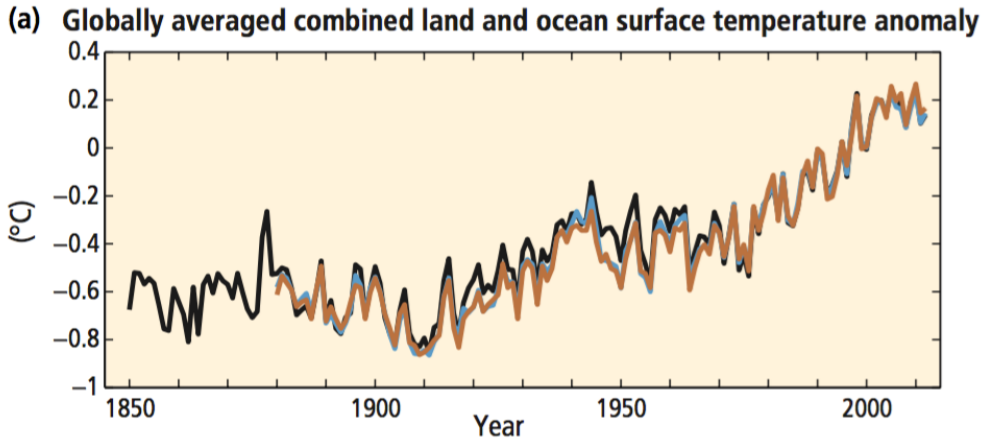

Figure 1.2 – Global temperature rise since the dawn of the second industrial revolution. From [15, Figure SPM.1 p. 3]

Much as Bronze and Iron characterize historical ages, concrete has become a marker of our age. Most of the infrastructures of our modern world are made of (Portland cement based) concrete.

1.1.2 4.0 to 5.8% of the world CO_2 emission

The formidable world economic growth since the second industrial revolution combined with the growing world population and dependence on fossil fuels have eventually led to global warming and climate change. In one century, the world average temperature has increased by about 1°C (figure 1.2). This increase of temperature is explained by the anthropogenic CO2 emissions (figure 1.3). For more details, the interested reader is referred to the synthesis report on climate change 2014 [15] issued by the International Panel on Climate Change (IPCC), a panel of one thousand scientists from 195 nations, on which the Paris agreement was signed by 174 nations and EU in 2016.

From about 1 billion people in 1800, to 1.6 billion in 1900 and up to 7.5 billion people in 2018, the world population has dramatically increased. This dramatic population growth has demanded for housing and infrastructure, which explains why concrete has become a big contributor to the world CO2 anthropogenic emission. The CO2 emission from cement production is estimated to be to range between 1.45 GT/year (GigaTons per year) [1] to 2.08 GT/year [5] which translates to 4.0% to 5.8% of the global anthropogenic emission.

1.1.3 There are no better solution to build the infrastructure the world need

Cost, widespread availability, easiness of manipulation, versatility of shape for artistic architectural purposes, CO2 emission per mass, strength and durability. No other material has a better combination of these properties.

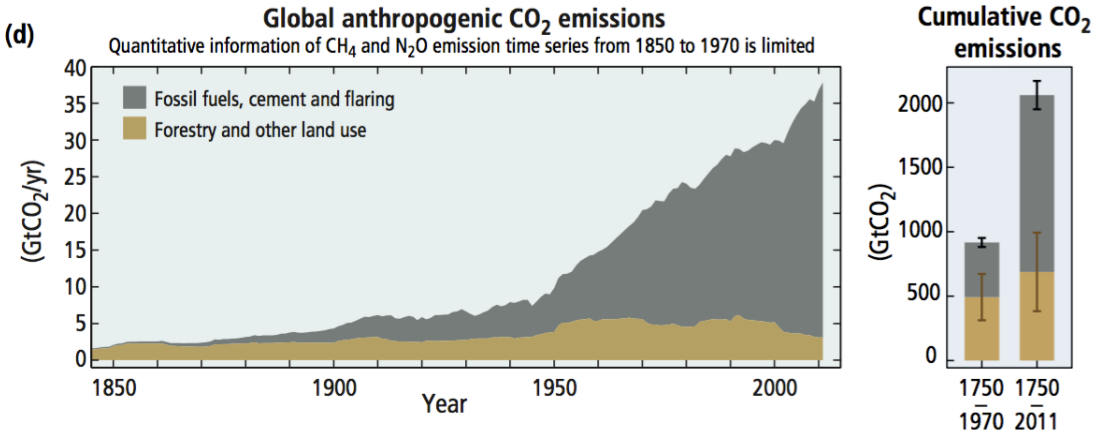

Figure 1.3 – Global anthropogenic CO2 emissions since the dawn of the second industrial revolution. From [15, Figure SPM.1 p. 3]

Wood is sometimes thought to be an ecological alternative to concrete. This is not the case in general as full life-cycle analysis have demonstrated and shown on Figure 1.4. Wood may only be a better alternative to concrete in areas close to a forest and a wood factory and for buildings lower than four stores [2, p. 283].

Crude-earth alternatives, for example adobe, require lengthy field works, specific technical skills, and achieve only moderately tall building at the expense of very thick walls. This solution however may be meaningful for poor areas that do not have access to cement plants or forests nearby and where labor time is cheap. Also, its esthetic appeal marks the culture of the place as for instance Iran Bam's citadel or Timbuktu Djinguereber mosque.

Geopolymers, or alkali-activated cements (AAC), are thought to be a promising alternative to concrete, but this does not resist a critical investigation. Geopolymers consist of slags activated with basic solutions, pH > 13. Slags are by-products of the steel industry.
Geopolymers / AAC suffer from three serious disadvantages. First, they require particular safety measures: pH 13 solutions can certainly not be manipulated without gloves or glasses; the reality of field-work, especially in developing countries, makes it unrealistic. Second, slag production amounts to only ten percent of steel production and as a consequence to about ten percent of PC production. To compete with PC, slag production would have to increase by an order of magnitude, and therefore not just rely on steel production. Third, and most importantly, the cost of geopolymers is a most serious argument against them: blended cements are always cheaper to produce than geopolymers. Blending PC with slags is always cheaper than activating slag with a base solution. Nevertheless, geopolymers may still be relevant for niche applications, such as nuclear and toxic wastes containment [10, Part III] and fireproof walls [6].

Could we imagine some new breakthrough innovation will one day overthrow "king concrete"? Probably not: The Earth's crust top 5 most abundant elements (figure 1.5) are Oxygen, Silicon, Aluminium, Iron, and Calcium... which exactly match the top five elements of PC. Together

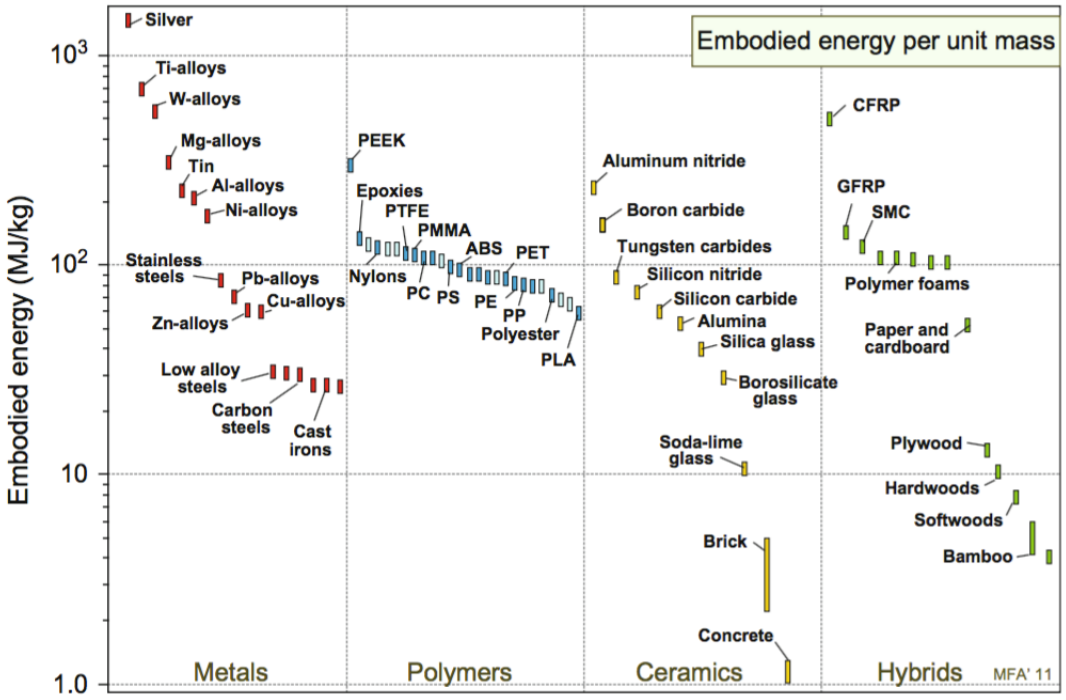

Figure 1.4 – Embodied energy per mass of common materials. Concrete has less embodied energy per mass than any other material, even woods. From [2, figure 6.11, p. 151]

they account for more than 92% of the Earth's crust elements and 95% of PC. The widespread availability of the raw minerals necessary to produce concrete therefore comes at no surprise... though it seems an extremely lucky coincidence that our planet is made of the raw minerals exactly required to produce such a versatile and useful material.

No other material can thus compete with PC-based concrete - today or in the foreseeable future – except, perhaps wood, under the specific conditions mentioned precedingly.

1.1.4 Supplementary cementitious materials: the way to mitigate CO_2 emission

To reduce concrete CO2 emissions, producers blend it with so-called Supplementary Cementitious Materials (SCM). SCMs are substances added to PC that are cheaper than PC while able to maintain or improve PC performance.

Historically, the Romans were perhaps the first to notice the strength and durability gain obtained by adding pozzolans (volcanic rocks found near the village of Pozzuoli in Italy) to cement. The pantheon dome in Rome stands to remind us of the past glory of Rome ... and of the durability of cement blended with SCMs!

Nowadays, the most common SCM is limestone: PC is almost never sold pure but always with at least 5% of limestone. Limestone is cheaper than PC, available practically in every country

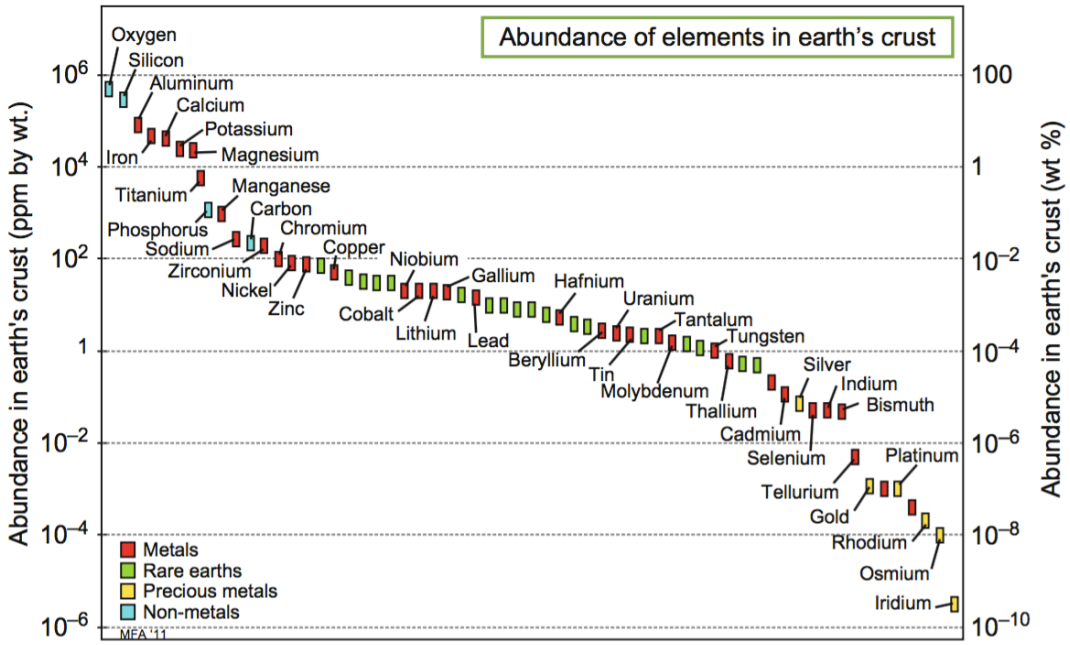

Figure 1.5 – Abundance of the elements in Earth's crust. The top five elements are precisely those required to produce Portland cement. Together, these five elements make 93% of all elements. From [2, figure 2.1, p. 17]

and is easy to grind to any desired fineness. Then comes two common by-products of the steel and coal industries respectively: slags and fly ashes.

Whatever the SCM blended with PC, they all behave as "fillers" during the first hydration day [4, p. 125]: they provide extra-surface for heterogeneous precipitation of the hydrates, but they do not chemically react with water or any other phase.
Therefore, they do not change the chemical reaction occurring during the first day: the phase assemblage by the end of the first day is close a standard PC paste.

1.1.5 Conclusion: cement based on Portland cement will be the future, alite remains relevant to investigate

PC based cements remain the future of most countries' infrastructures and housing. Because alite is the main ingredient of Portland cement, because SCM do not change the chemical reaction during the first day, and because alite is responsible for the first day strength in PC, the investigation of its hydration mechanisms remains relevant for the future. **This constitutes one motivation of the present thesis.**

1.2 Cement and alite hydration mechanisms

The development of cements throughout history has been purely empirical up to the end of the XIXc [14, p. 17]). In a century of research, the qualitative understanding of PC has started from nearly nothing to the exhaustive description of the hydration reactants and products. The composition, crystalline structure and morphologies evolutions of the hydrates and the subdivision of hydration in five stages have been deciphered by the modern characterization techniques, in particular calorimetry, electron microscopies techniques and X-Ray Diffraction (XRD).

The picture of cement pastes and concrete unraveled by these techniques is a complicated one. PC is a mix of five phases: alite (impure C3S), belite (impure C2S), tricalcium aluminate (C3A), tetracalcium aluminoferrite (C4AF) and gypsum (CaSO4). This involves at least six main chemical elements: Calcium, Oxygen, Silicon, Aluminum, Iron and Sulphur.

When mixed with water, the hydration reaction leads to setting within a few hours and hardening within a month. A variety of products whose chemical composition is whose crystallographic order range from crystalline (CH) to only a short-range order for the main reaction product: C-S-H (Calcium Silicate Hydrate). Because C-S-H is a non-stoichiometric phase, dashes are used.

The chemical reaction of alite hydration is:

$$C_3S \quad + \quad (3+x-n)HO \quad \rightarrow \quad C_x-S-H_n \quad + \quad (3-x)CH \tag{1.1}$$

Where C stands for CaO, S for SiO_2 and H for H_2O so that C_3S stands for $(CaO)_3(SiO_2)$ for example.

The calcium to silica x is typically about 1.7 +/- 0.4, and the water to silica ratio varies from 1.8 to 6 depending on what counts as water (see chapter 2 section 4.4 for more details).

In order to understand the complexity of the microstructure development, a natural path is to understand first the hydration of each reactant in order to disentangle their impact in the whole system. For that reason, alite, the main component of PC (roughly 2/3 of its mass) has been extensively studied for at least a century [12]. Yet the mechanisms of alite hydration are still in debate today [17].

The hydration of alite was first studied by Klein in 1914 [12]. He identified the hydration products as being a crystalline phase, Calcium Hydroxide, and an amorphous hydrated orthosilicate now denoted C-S-H for Calcium Silicate Hydrate. This phase is crucial as it is the main binding phase.

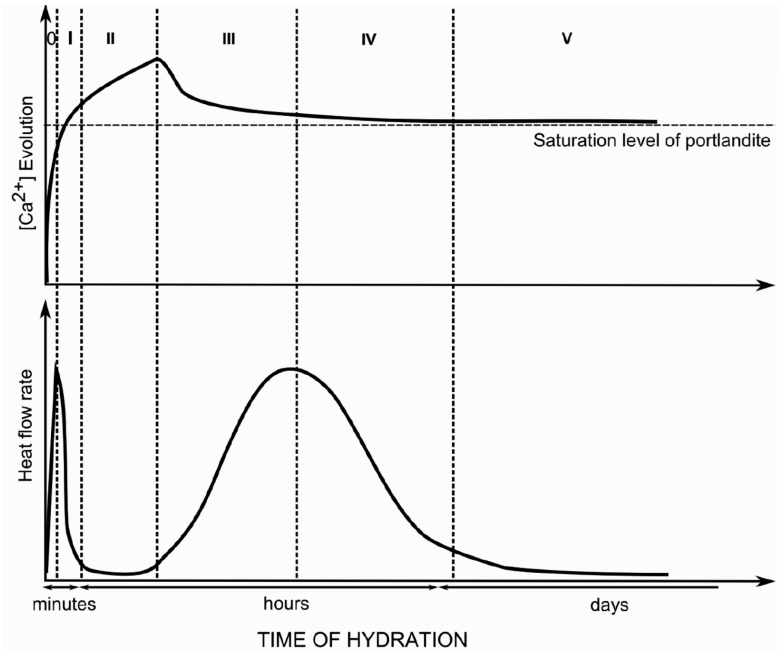

Figure 1.6 – Solution phase analysis and associated calorimetry of alite hydration (image from [9])

1.2.1 Insight on the alite hydration from calorimetry and solution phase analysis

The hydration of alite has been divided in five stages by Kondo and Ueda in 1968 [13] according to the heat flow released by the reaction. An archetypal heat flow profile is shown on figure 3.1 together with the solution phase analysis.

The recently emerging consensus regarding alite hydration concerns only the first two stages out of the five successive stages of the hydration reaction [18]. Several ideas have been proposed for the physico-chemical mechanisms involved in the remaining ones.

Stage 0. Initial fast reaction: dissolution of alite in water which leads to the release of Ca2+, OH- and H2SiO42- into solution. This dissolution is highly exothermic and only lasts a few minutes.

Stages 1 and 2: first deceleration and induction period with a transition from fast to slow dissolution rates. The transition from one rate to the other is explained by the theory of crystal dissolution as developed by geochemists and studied in detail in the thesis of Juilland [11]. At high undersaturation alite dissolution is controlled by etch pits opening while at lower undersaturation the step retreat mechanism prevails. In addition to the saturation state of the solution the crystallographic defects density is the other main rate controlling factor.

Stages 3 and 4. When calcium ions reach a peak concentration a massive precipitation of hydrates occurs. The peak is usually described as an acceleration period followed by a deceleration period. Hypotheses about this main hydration peak are detailed in the next subsection and chapter 2.

Stage 5. After 24h the reaction progresses very slowly but for months (and even years for OPC). The most common hypothesis about this stage is a combination of diffusion limited reaction, densification of the C-S-H and space-filling [18].

1.2.2 The main hydration peak debate

The debate on the main hydration peak evolves around the question: "What causes the transition from the acceleration period to the deceleration period?". The two most widespread hypotheses found in the literature are the nucleation and growth hypothesis, and the diffusion-controlled hypothesis. Both suffer from essential setbacks that are examined in chapter 2 and should be rejected. The question therefore remains open.

Bazzoni recently suggested a new hypothesis from her observation with the Scanning Electron Microscopy (SEM) of alite hydration [3]. First, she observed that C-S-H nucleates and grow as needles on the surface of alite grains during the first day. Second the peak time corresponds to the time of full surface coverage. Third, needles do stop growing even when space is still available. According to her, the combination of surface coverage and stop of the needle growth could explain the peak.

We will return to Bazzoni hypothesis in chapter 3 as it is one of the starting points of the thesis: does this hypothesis quantitatively account for the main hydration peak?

1.2.3 The later ages

After 24 hours comes the "later age", a period of very low heat flow but where strength develops from 20% at one day to 80% at 28 days of its final strength. No mechanistic, only empirical, model yet exists. Conjectures about this period suggests that space filling as well as densification of C-S-H and maybe perhaps diffusion after one month could be the leading mechanism.

One motivation of this work is to build a mechanistic model on this period to test the space filling hypothesis.

1.3 Cement and alite hydration modelling: methods and goals

1.3.1 The necessity of mathematical models

The emphasis on building mathematical models, rather than qualitative or conceptual ones, marked a shift in the scientific method introduced by Galileo in his essay "The Assayer":

> Philosophy [Nature] is written in that great book which ever lies before our eyes — I mean the universe — but we cannot understand it if we do not first learn the language and grasp the symbols, in which it is written. This book is written in the mathematical language, and the symbols are triangles, circles and other geometrical figures, without whose help it is impossible to comprehend a single word of it; without which one wanders in vain through a dark labyrinth.
>
> *The Assayer* (1623), as translated by Thomas Salusbury (1661), p. 178, as quoted in *The Metaphysical Foundations of Modern Science* (2003) by Ewin Arthur Burtt, p. 75

The complexity of most natural phenomena requires quantitative models to be built onto each hypothesis attempting to explain them. Only then can hypotheses be quantitatively tested, and a decision firmly reached on their validity or invalidity.

There certainly exist simple enough cases where qualitative arguments can be put forward and sufficient to close a discussion. For example, for the main hydration peak, the diffusion barrier hypothesis (presented in chapter 2) can be disproved by raising qualitative arguments only. By contrast, to choose among the different nuances of nucleation and growth hypotheses require quantitative arguments to be raised (presented in chapter 2).

1.3.2 The paradigm of materials science and engineering

It is commonplace to assert that the ultimate goal of materials science is to understand how the key features of microstructures arise from the elaboration process and then how these features lead to the observed resulting macroscopic properties. Likewise, the goal of materials engineering is to optimize the properties by tuning the elaboration process. This requires to be able to quantitatively predict the properties from the knowledge of the elaboration process. Schematically:

In the particular case of cement and concrete science, the key properties to optimize are the CO2 emission, the mechanical and durability properties. These macroscopic properties are influenced by the amount of each of the five phases of this cement, their Particle Size

Distributions (PSD) and specific surfaces [14]. The water to cement ratio as well as the curing conditions (temperature, relative humidity) are known to significantly impact the properties. In addition to this already long list other non-trivial factors also influence the microstructure development such as mixing speed, the possible inclusions of ions in the matrix of alite and belite or the possible defects resulting from the grinding process (see the next chapter for the detailed list).

1.3.3 Specific motivations for modelling cement hydration

The motivations to develop models can be arranged under three keywords: understanding, predicting and optimizing.

- UNDERSTANDING
  - "understanding and predicting cement hydration kinetics and microstructure" [20]
  - "understanding and predicting concrete mechanical behavior" [19]
  - "quantifying knowledge of hydration process" [8]
  - "to troubleshoot problem on the field" [7]
- PREDICTING
  - "to predict the performance of concrete" [8]
  - "long term and service life prediction" [7]
  - "predicting temperature rises" [14, p. 344]
- OPTIMIZING
  - "sustainable cement production" [16]
  - "to help design new cementitious materials" [20]
  - "reduce the number of trial and error cycle" [7]

1.3.4 Conclusion: what do we want from hydration models?

To sum up, the long-term motivation to model cement hydration is to optimize cement and concretes i.e. to lead to the strongest, most durable and least polluting cement possible.

In order to achieve that aim, models should take as input at least all the factors systematically present in any cement formulation and known to impact significantly on the properties: the amount, PSD and specific surface of each phase as well as the water to cement ratio and curing conditions. In the best case, models should be able to predict the performance of the resulting mixes. Only by comparing the predictions with experiments can the hypothesized

mechanisms of hydration be validated or refuted and thus the understanding of cement hydration be ascertained.

Because of the complexity of cement hydration, the path toward a complete cement hydration theory necessarily passes by a complete theory of alite microstructural development i.e. a theory of alite hydration.

1.4 Statement of the problem and objectives

1.4.1 The main hydration peak

The hypotheses that exist in the literature have not been able to prove their point as chapter 2 demonstrates.

Nevertheless, two new hypotheses have been raised that might possibly explain the transition: the needle hypothesis and the small grain dissolution hypothesis. These new hypotheses are considered in the needle model article (chapter 3).

1.4.2 The later ages

The second objective is to put into equations one of the conjectures about the later ages: to build a model to test the space-filling hypothesis.

1.5 Structure of the thesis

The thesis is divided in three parts: first a literature review on the hydration mechanism, then one part about the main hydration peak and a third one on the later ages mechanisms.

Each chapter opens with a one page summary of the key results. The reader may want to first read these together with the conclusion chapter to have a clear view of the key contributions of the thesis before to delve into the chapters.

1.6 References

[1] Robbie M Andrew. "Global CO2 emissions from cement production" (2018).

[2] Michael Ashby. *Materials and the environment*. Butterworth-Heinemann, 2013.

[3] Amélie Bazzoni. *Study of early hydration mechanisms of cement by means of electron microscopy*. Doctoral Dissertation Ecole Polytechnique Fédérale de Lausanne (EPFL), 2014.

[4] Elise Berodier. *Impact of the Supplementary Cementitious Materials on the kinetics and microstructural development of cement hydration*. Doctoral Dissertation Ecole Polytechnique Fédérale de Lausanne (EPFL), 2015.

[5] T. A. Boden, R. J. Andres, and G. Marland. "Global, Regional,and National Fossil-Fuel CO2 Emissions, Carbon Dioxide Information". *Analysis Center, Oak Ridge National Laboratory, U.S. Department of Energy, Oak Ridge, Tenn., USA,* ().

[6] Lorenza Carabba et al. "Alkali activated lightweight mortars for passive fire protection: A preliminary study". *Construction and Building Materials* 195 (2019), pp. 75–84.

[7] J. S. Dolado and K. Van Breugel. "Recent advances in modeling for cementitious materials". *Cement and concrete research,* 41(7) (2011).

[8] C. F. Dunant et al. "An algorithm to compute damage from load in composites". *Frontiers of Architecture and Civil Engineering in China* 5 (2011).

[9] E.M. Gartner et al. *Structure and performance of cements,Chapter 3: Hydration of Portland cement*. Vol. 14. Spon press, Bensted and Barnes, 1914.

[10] J. S. J. Van Deventer (eds.) J. L. Provis. *Geopolymers, Structures, Properties and Industrial Applications*. Woodhead Publishing, 2009.

[11] Patrick Juilland. *Early Hydration of Cementitious Systems*. Doctoral Dissertation Ecole Polytechnique Fédérale de Lausanne (EPFL), 2009.

[12] A.A Klein. "The hydration of Portland cement". *Trans. Faraday Soc.* 14 (1914).

[13] Renichi Kondo and Shunro Ueda. "Kinetics and Mechanisms of the Hydration of Cements". *Tockyo Symposium* 2 (1968).

[14] Frederick Measham Lea. *Lea's Chemistry of Cement and Concrete, Fourth edition*. Wiley & Sons, 1998.

[15] R.K. Pachauri and L.A. (eds.) Meyer. "Climate Change 2014: Synthesis Report. Contribution of Working Groups I, II and III to the Fifth Assessment Report of the Intergovernmental Panel on Climate Change". *IPCC, Geneva, Switzerland* (2014).

[16] M. Schneider et al. "Sustainable cement production—present and future". *Cement and concrete research,* 41(7) (2011).

[17] Karen L. Scrivener, Patrick Juilland, and Paulo J.M. Monteiro. "Advances in understanding hydration of Portland cement". en. *Cement and Concrete Research* 78 (Dec. 2015), pp. 38–56.

[18] Karen L. Scrivener and André Nonat. “Hydration of cementitious materials, present and future”. en. *Cement and Concrete Research* 41.7 (July 2011), pp. 651–665.

[19] H.F.W. Taylor. *Cement chemistry, Second edition*. Thomas Telford, 1997.

[20] Jeffrey J. Thomas et al. “Modeling and simulation of cement hydration kinetics and microstructure development”. en. *Cement and Concrete Research* 41.12 (Dec. 2011), pp. 1257–1278.

2 Literature review on the hydration mechanisms

Part of the information of this chapter on the past two decades of research has already been published in the article "The needle model: A new model for the main hydration peak of alite."[68].

The main hydration peak problem was first posed during the fifth international symposium in Tokyo in 1968 [54]. The 70's subsequently saw the first three main attempts to answer the challenge: the phase boundary, diffusion and nucleation and growth hypotheses were raised and were to occupy the center stage for the following three decades. From 2000 on, growing criticisms against these hypotheses lead to the emergence of the boundary nucleation and growth, the confined growth and the dissolution hypotheses.

The first mention of the later age as a problem only occurs in 1989 [36]. Before, diffusion limitation was deemed obvious and the later ages not problematic. Only two extra hypotheses have since been raised: space-filling associated with densification and the pore solution limitation.

The chapter focuses on the exposition and critical discussion of the two most widespread hypothesis about the main hydration peak debate: the diffusion hypothesis and the nucleation and growth by impingement hypothesis. These hypotheses are referenced in all major textbooks [80, pp. 150-156], [58, pp. 243 - 259], [42] [21, pp. 109-112, section 7.2.1.1] and recent reviews related to cement science and thus deserve an extensive treatment.

One of the main outputs of this chapter is the rebuttal of all six hypotheses related to the main hydration peak; this provides the motivation for the needle model presented in the next chapter.

The chapter also introduces notions about the microstructural development during the main hydration peak, later ages and the pore structure that are necessary to understand the needle model underlying assumptions.

Contents

2.1 The main hydration peak problem

2.1.1 What triggers the start of the acceleration period?

Critical supersaturation is the cause of the precipitation

The driving force for the precipitation of solid phases in aqueous solutions is well-established to be the supersaturation level [64]. Precipitation starts whenever the critical supersaturation is reached.

The critical supersaturation with respect to C-S-H occurs very rapidly: within seconds for pastes or minutes for diluted suspensions, the silicate concentration drops which indicates the precipitation of C-S-H as shown on figure 2.1. According to experimental evidence from Garrault-Gauffinet and Nonat, these first C-S-H precipitates range in the order of a few nm, which corresponds to a few dozen C-S-H molecules [32, p. 573]. Andalibi et al. call these first C-S-H precipitates primary particles or crystallites and their model suggests a range of 2 to 4 nm [2, Fig. 5 (e)].

The critical supersaturation with respect to Portlandite occurs later on. In dilute suspensions, experiments made by Damidot, Nonat and Barret [29] [27] [28] clearly shows that no precipitation of CH is necessary to observe a main hydration peak. In dilute suspensions with 22 mmol/l of lime concentration and above w/c = 15 the Portlandite critical supersaturation level is reached during or even after the main hydration peak; which results in an endothermic peak (figure 2.1b right). A drop of electrical conductivity and lime concentration accompanies Portlandite precipitation.

Is C-S-H or CH precipitating first? Two kinds of C-S-H

C-S-H surely precipitates before Portlandite, but there may be two kinds of C-S-H. The first kind, C-S-H (I), precipitates within the first seconds or minutes and has a low Ca/Si ratio: between 0.66 and 1.5 [27, p. 34] [32, p. 568] or between 0.3 and 1.5 [59, fig. 4.2 p.87]. This low Ca/Si value is likely explained the kinetic path of the reaction[1]. Dissolution is congruent up to the point where it crosses the C-S-H solubility curve. At this point, the Ca/Si ratio is low. As the calcium concentration further increases in solution up to the critical supersaturation of portlandite, so does the equilibrium Ca/Si ratio of the C-S-H [65, section 5].

The second kind, C-S-H (II)[2], coincides with the start of the acceleration period and has a higher Ca/Si ratio: between 1.5 and 2. Because there is a discontinuity in the C-S-H Ca/Si stability, these two C-S-H may have a different structure [32, fig. 2] [47], though this remains an open question.

[1] The kinetic path of a reaction is the time trajectory of the calcium and silicon concentration of the reaction. For an example of it, see the discussion of [27]

[2] Note that this C-S-H(I) and C-S-H(II) nomenclature is based on Nonat's work and does not match Taylor's nomenclature.

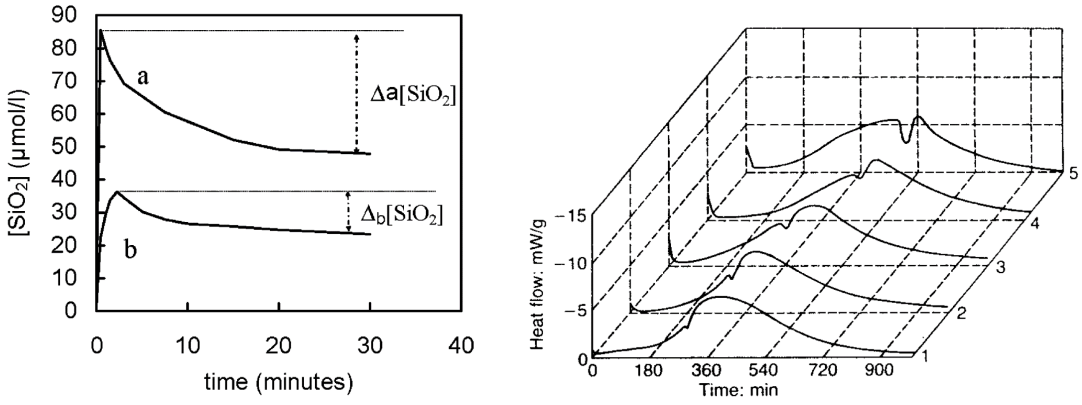

Figure 2.1 – Left: Evolution of the silicate concentration in diluted suspensions w/c = 50 of C_3S in two different lime concentrations: 11mmol/L for the top curve (a) and 22mmol/L for the lower (b) one. From [34, fig. 5]. Right: Heat flow evolution of C_3S hydrated in a 22mmol/l lime solution at w/c ratios 10, 15, 20, 35 and 50 from front to bottom. From [27, fig. 6]. The progressive shift of the endothermic peak seen corresponds to Portlandite precipitation. These two plots highlight that the silicate concentration drops within seconds or minutes whereas the calcium concentration drops later on. In other words, C-S-H precipitates first and Portlandite precipitation is not necessary for the main hydration peak to occur.

The first kind is small, it lies in the range of a few nm, and is hardly observed by SEM while the second kind is clearly observable on the surface of alite grains as presented on figure 2.2. Interestingly though, the second kind of C-S-H does not only grow, it is not just the growth of the first kind of C-S-H; it still nucleates while other nuclei are growing. Nucleation and growth of this second type is not strictly sequential, both phenomena overlap for a few hours during the acceleration period. Thermodynamically, this may seem unexpected as the critical supersaturation for nucleation is often thought to be much higher than the one for growth. Yet the observations are clear and the two phenomena do happen simultaneously for a few hours; which indicates that the driving force is still high enough to promote heterogeneous nucleation of C-S-H (II) during this time lapse. Beyond it, only growth happens.

In diluted suspensions, Portlandite precipitates after C-S-H (II) as can be inferred from figure 2.1. In pastes, the opposite seems true. Indeed, experimental observations of the surface from Bazzoni [5] and Berodier [11] indicate that heterogeneous nucleation happens within a few . Modelling approach from Andalibi et al. also suggests a similar timeframe [2, fig. 5 (f)]. But in pastes, the supersaturation relative to portlandite is certainly reached in less than an hour due to the low amount of water.

Portlandite or C-S-H (II) precedence is an open question that is not so problematic for the present thesis. What is assuredly observed in pastes is the simultaneity within an hour of: 1- Portlandite precipitation 2-C-S-H (II) precipitation, 3- a drop in the electrical conductivity and 4- a drop in calcium concentration; these four events mark the start of the acceleration period. From then on, C-S-H and Portlandite precipitate congruently modulo the possibly

varying Ca/Si ratio, electrical conductivity decreases and the calcium concentration decreases up to asymptotically to the Portlandite solubility curve.

N.B.: The controversy over the exact sequence and cause of the start of the main hydration peak is still ongoing. The interested reader can find more information in [36, section 3.2.2.3] [20] [76, section 3.3] [75, section 2.2].

2.1.2 The acceleration period: heterogeneous nucleation and growth

The cause of the acceleration period is generally recognized to be the heterogeneous nucleation and growth of C-S-H (the only dissent voice is Nicoleau [63, section 4.4] [62, p.773]. Heterogeneous nucleation and growth is caused by the critical supersaturation with respect to C-S-H (II) and Portlandite, which happens at about the same time in paste.

Once the critical supersaturation is reached, the growth rate accelerates. Gartner et al. [36] terms this “autocatalytic” growth, meaning the growth of C-S-H is proportional to the C-S-H surface area.

The amount of evidence in favor of heterogeneous nucleation and growth is huge. Electron microscopy analyses of hydrating alite or cement pastes show the nucleation and growth of C-S-H on limestone, quartz, slags, fly ashes [11], metakaolin [3]. When the surface is not alite, this extra C-S-H precipitation is named “the filler effect”. Different surfaces may have different propensities for nucleation and growth of C-S-H, for instance limestone promotes C-S-H N& G better than quartz [11, fig. 3.9 and 3.30] or even cement grains themselves (figure 2.2) and C_3S [5, p. 78].

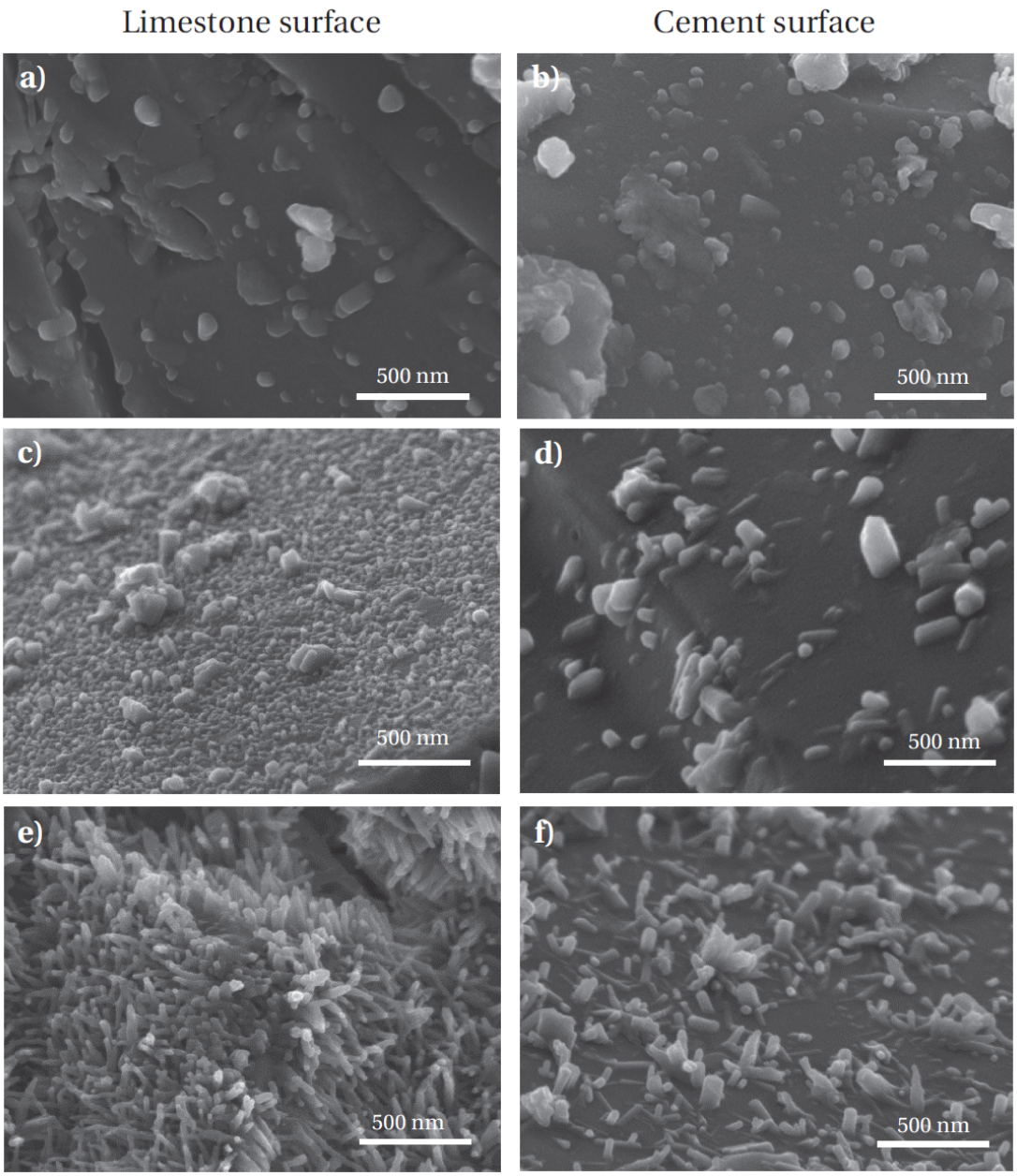

Figure 2.2 – Evolution of the surface of limestone (left) and cement (right) grains during the acceleration period (respectively: 5 min, 1 hour and five hours from top to bottom. The number and size of C-S-H needles increases over the acceleration period. Limestone provides a better surface for nucleation than cement grains. From (Berodier 2015, fig. 3.30 p. 57).

Factors that significantly influence the acceleration period

Fineness / Particle size Distribution (PSD) The particle size distribution has long been known to dramatically influence the hydration rate. As far back as the Tokyo symposium in 1968, in the discussion of the Kondo and Ueda paper where they introduce the five stages of the hydration reaction, Taplin criticized the misinterpretation of the mechanisms by models that neglect the PSD effect:

> *"Nucleation, crystal growth, dissolution and diffusion are some of the possible rate controlling processes in the hydration of cement. In trying to distinguish between them, the effect of particle size distribution can hardly be ignored. In the later stages of the reaction, this size distribution effect is generally about as great in comparison with a mono-sized powder as is a change from a linear to a parabolic reaction mechanism"*
>
> Taplin written discussion, 1968 Tokyo symposium, p. 250.

Surprisingly it took 14 years for the first model to take into account the PSD effect [53]. In his article, Knudsen builds on top of Taplin's remark by pointing that merely using the average grain size instead of the whole PSD is not correct.

In her Ph.D thesis, Costoya quantitatively studied the PSD impact on C_3S [25] and her experiments has since served as a benchmark for testing models.

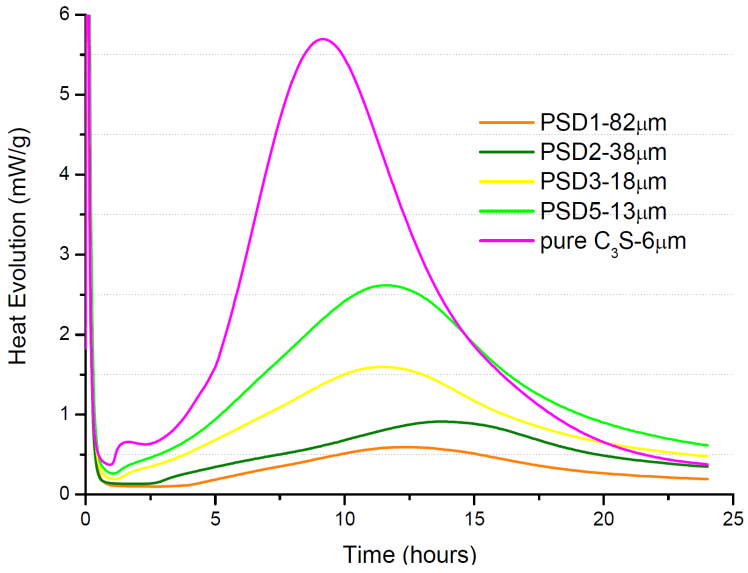

Figure 2.3 – Costoya PSD experiment on alite and C_3S. The finer the PSD the higher the reactivity. This experiment has repeatedly been used to benchmark models. From [25, p. 56]

Filler effect: amount and fineness C-S-H has been proved to precipitate on many surfaces by Bazzoni, Berodier and Avet in their Ph.D theses. Quartz, limestone, fly ashes, slags, calcined clays all provide nucleation sites, though with different propensities.

Although often thought of as "active phases", C_2S, C_3A, C_4AF also behave as fillers during the first day of hydration of PC: they have been observed to be covered by C-S-H by Scrivener in (Scrivener thesis, 1984). Because the average combined amount of these phases is about one third of PC mix design, and because they are about the same fineness as alite, PC behaves in a similar way to and alite with 50% of filler system. This *partly* explains why PC is more reactive than alite during the first day.It seems this has been left unnoticed. Another part of the explanation of why PC reacts more comes from the sulfate enhancement (see corresponding paragraph).

The higher the surface of filler added the higher the surface available for precipitation. Therefore, both the amount and the PSD of the filler play a role on the overall reactivity.

Doping ions In her thesis, Bazzoni studied the influence of magnesium and zinc on C_3S and observed a significant increase with the latter one. With zinc, she observed the peak height and the acceleration period slope to increase in the same proportion as the C-S-H needles did. Moreover, she measured by EDX the composition of the C-S-H and found that zinc was incorporated in it whereas magnesium was not [5, fig. 4.30]. This corroborates the findings of [79] who found zinc to incorporate in the interlayer of gyrolite, a crystalline counterpart of C-S-H. This suggests that zinc influences the precipitation whereas magnesium does not and reinforces the hypothesis that precipitation controls the acceleration period.

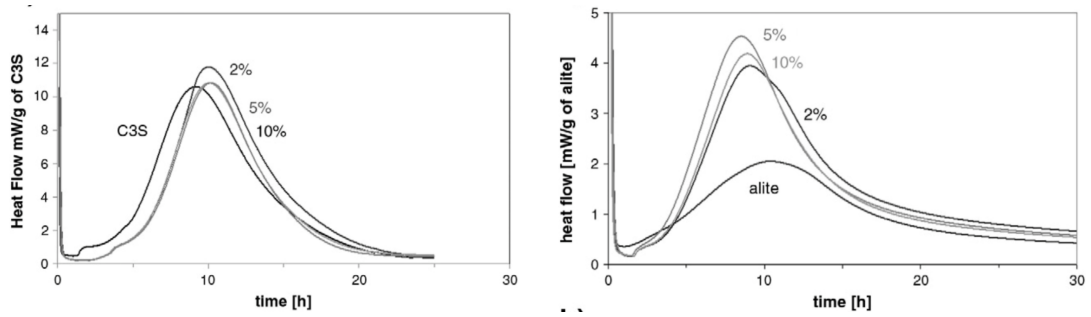

(a) *(b)*

Figure 2.4 – Influence of gypsum on C_3S (left) and alite (right) hydration. Gypsum significantly increase the peak height of alite, but not of C_3S, suggesting that the aluminium in alite plays a role. From [70, fig. 5].

Sulfate ions For research purposes, pastes are most frequently mixed with pure water so as to avoid any interference with the ions present in tap water.

Mixing alite in lime or silicate solutions influences the ionic solubility product and thus the nucleation and growth of C-S-H and Portlandite. The impact of the initial lime concentration in diluted suspensions has been extensively studied at Dijon [34].

The presence of gypsum also significantly increases the peak height on alite hydration but not on C_3S hydration as is shown on figure 2.4. Gypsum very quickly dissolves and releases sulfate in solutions. Surprisingly, the gypsum effect is not monotonic on alite, Quennoz's experiment suggests there is an optimum between 2% and 10%. To explain the difference of impact between C_3S and alite, Quennoz and Scrivener argue that alite contains aluminium which inhibits its dissolution. Whenever gypsum is present, it removes the aluminium (by Aft precipitation for instance) from the solution and restores the normal C_3S reactivity.

Alite polymorphism C_3S commonly adopts three different polymorphic forms: rhombohedral, monoclinic and triclinic [80, pp. 4-6]. According to Young and Skalny in their review on the mechanisms of PC hydration at the Paris ICCC [78, section 2.1.3], the various crystal forms of pure C_3S have comparable reactivities. Harada et al. [41] found the following order of reactivities: monoclinic < triclinic < rhombohedral. Doping ions can further stabilize preferentially one polymorph [67].

However, Stewart and Bailey found a different order of reactivities [4], including a significant difference between the triclinic and monoclinic forms: the acceleration slope and peak height varied by a factor of two.

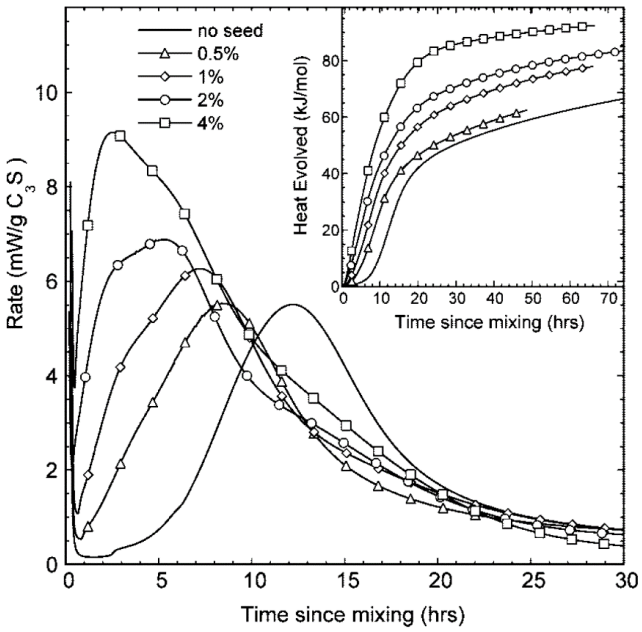

Figure 2.5 – Effect of C-S-H seeds on C_3S hydration. The seed amounts refer to the masse of solid C-S-H per mass of C_3S. Note how the peak progressively shift left as it increases. From [85, fig. 2].

Unfortunately, these authors did not check whether the PSD of their different polymorphs were identical or not so that no conclusion can be reached. What seems yet sure is that there is no significant change of intrinsic reactivity across the different polymorphs.

C-S-H seeds Seeding alite paste with C-S-H results in dramatic changes as presented on figure 2.5. Not only do the acceleration slope and peak height increase with the seed dosage, but the induction period also vanishes.

This experiment highlights the autocatalytic growth of C-S-H. Information about the supposed mechanisms can be found in [48, section 2.2].

Mixing rate In his thesis [50], Juilland studied the impact of the mixing rate from hand mixing up to 2000 rpm with a steel paddle (figure 2.6). The acceleration slope and peak height significantly increases with the rate up to about 2000 rpm.

To explain this observation, Juilland argues that higher mixing rates result in thinner boundary layers, which consequently results in higher nucleation rate of C-S-H (I). Simultaneously, high shearing rates promote the distribution of these nuclei in the capillary pore space away from the alite surface. Both effects could play a role though it remains difficult to assess them experimentally [50, pp. 74-79].

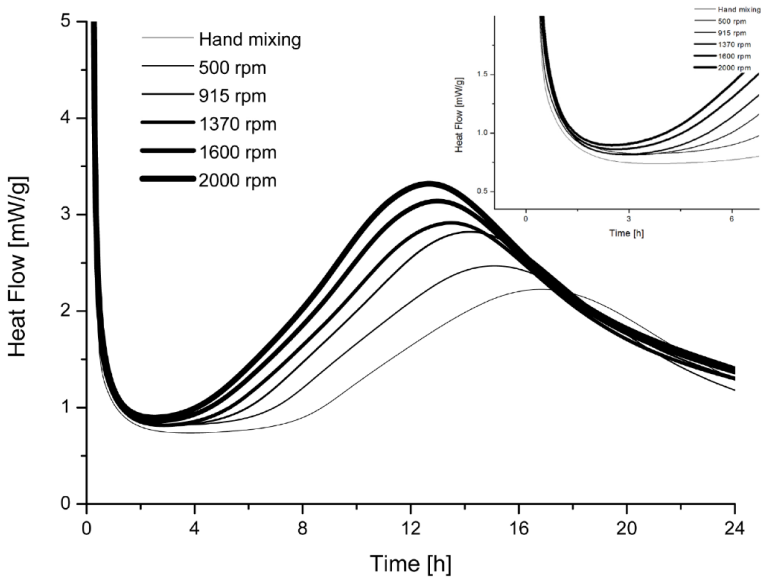

Figure 2.6 – Effect of the mixing rate on alite hydration kinetics (w/c = 0.4). From [50, fig. 4.1 p. 74]

Alkali salts In her thesis [61], Mota-Gasso investigated the effect of alkali salts on alite hydration as presented on figure 2.7. All salts increase the acceleration slope and peak height but the effect is more pronounced when alkali salts are combined with a sulfate source.

In a similar fashion to Quennoz and Scrivener, she argues that whenever sulfates are present, they remove the alkali from solutions and restore the normal C_3S reactivity.

Brown, Harner and Prosen [17] also investigated the effect of other inorganic (alkali) salts on C_3S hydration (figure 2.7 right) and did not find any strong influence, maybe because they were not combined with a sulfate source as Mota Gasso suggests.

N.B. *The difference of reactivity between PC and alite may partly come from the sulfate enhancement. Another part of the explanation comes from the filler effect of the $C2_S$, $C3A$ and C_4AF. Which effects is quantitatively more important remain an open question; the sulfate contribution might me more important because it alone is sufficient to nearly double the peak height. It seems this dual explanation of the difference between the alite and PC reactivities has been left unnoticed.*

Admixtures Some admixtures are used deliberately to influence the hydration, typically: retarders and accelerators. Other admixtures may also indirectly influence it, for instance water-reducers may influence the later age hydration.

The influence mechanisms are thought to be the complexation of calcium ions, a modification of the anhydrous phase dissolution (by adsorption for instance) and/or of the hydrates nucleation and growth (by nuclei poisoning) and/or a perturbation of the aluminate-silicate-sulfate balance.

As admixtures are out of scope of this thesis, the interested reader may refer to the reference book from Aïtcin and Flatt "Science and Technology of Concrete admixtures", in particular chapter 12.

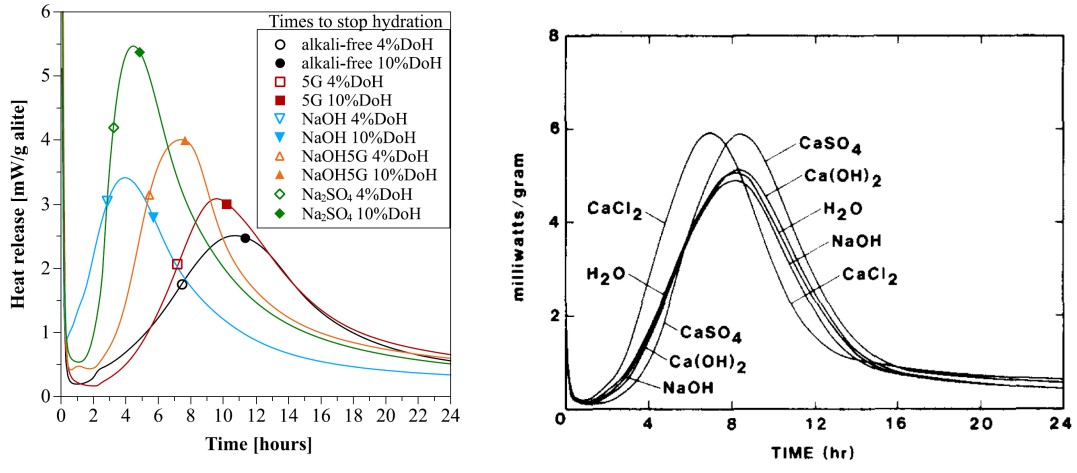

(a) *(b)*

Figure 2.7 – Impact of alkali salts on hydration. Left on alite from [61, fig.3]. Right on C_3S from [17]

Factors that barely influence the acceleration period

Thermal treatment: annealing

In her thesis [5, section 3.3.2] and in [6], Bazzoni investigated the influence of annealing on the hydration of alite. Annealing is supposed to decrease the number of crystallographic defects and thus alter the dissolution rate of alite. She varied either the annealing time at constant temperature 650∘C (figure 2.8 left), or varied the temperature at constant annealing time of one hour (figure 2.8 right).

The increase of the induction period corroborates the geochemical hypothesis that dissolution controls hydration up to the onset of acceleration. Inversely the very small influence of annealing on the acceleration period slope and peak height rather denies that dissolution controls this stage.

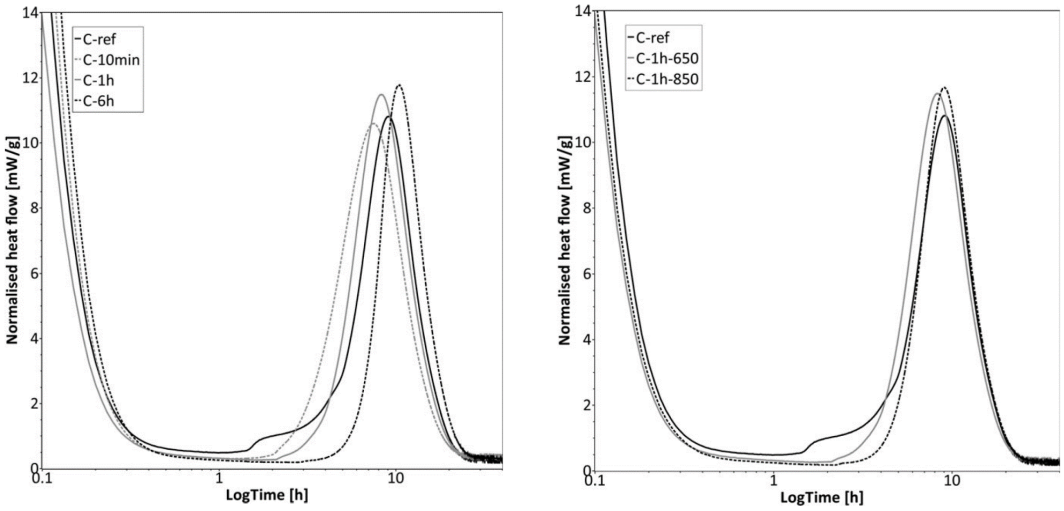

(a) *(b)*

Figure 2.8 – Influence of annealing on alite hydration. Left: annealing at 650°C with varying time. Right: annealing for one hour at 650°C or 850°C. From [6].

w/c ratio Several researchers have investigated the impact of water to cement ratio on alite hydration. Most notably Kirby and Biernacki demonstrated in [51] that the water to cement ratio had a negligible effect on C_3S, alite, and PC hydration within the range 0.4 to 0.8.

The negligible influence of the water to cement ratio on hydration in this range can be attributed to the fact that there is more than enough space for the hydrates to precipitate. At water to cement ratio below 0.2, for instance for Ultra-High Performance concrete, the acceleration slope and peak height may indeed be decreased due to a lack of space.

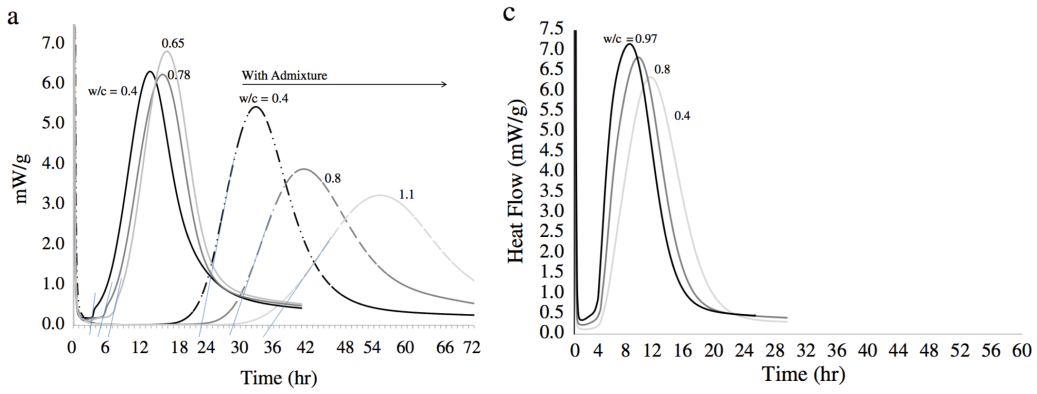

(a) *(b)*

Figure 2.9 – Influence of the w/c ratio on alite (left) and C_3S (right) hydration. The admixture used in this study was the commercial organic admixture polyheed N. From [51, fig. 5]

2.1.3 Exposition of the main hydration peak problem: why is there a transition to a deceleration period?

Origin of the main hydration peak problem

Although isothermal calorimetry has become today mainstream in the investigation of cement hydration, it was not even mentioned in the section "Methods of investigation of the chemical reactions occurring during the hydration of Portland Cement" of the review paper of Copeland, Kantro and Verbeck at the Washington symposium in 1960 [24, pp. 431-433]. From the record of articles involving isothermal calorimetry as a tool to study the hydration kinetics at the Tokyo symposium in 1968 and then at the ICCC Paris in 1980, we can deduce it became common during the 60's and mainstream only in the 70's.

Though Kondo et Ueda were not the first to use isothermal calorimetry on cement, they were the first to separate hydration in five stages (figure 2.10 as is commonly known today. Thereby emerged the question of the transition between each stage of the reaction and in particular from the acceleration to the deceleration period.

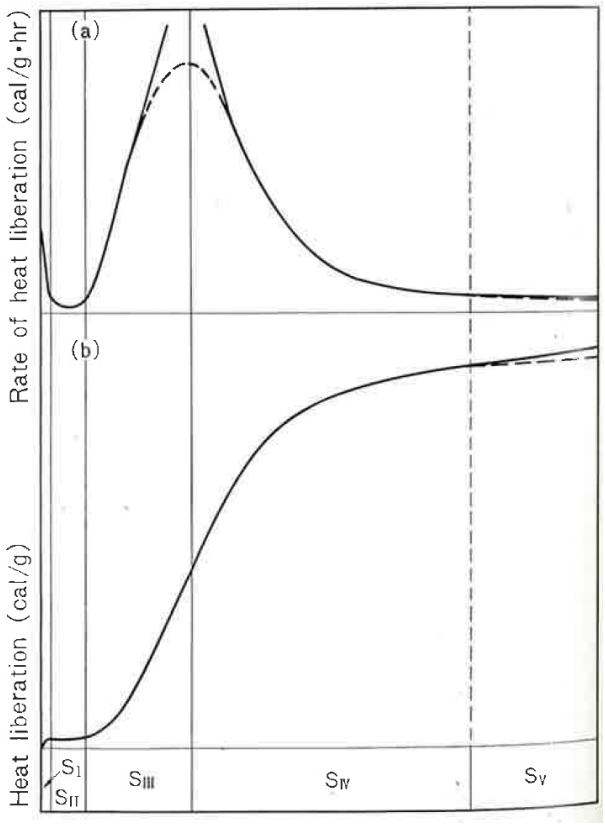

Figure 2.10 – First time the calorimetry curve was divided in five stages. This division is not anodyne: it opened five decades of debates on the questions of the transitions from one stage to the next. Should the focus have been on the heat instead of the heat flow, the question of the transition from acceleration to deceleration period would perhaps have not occurred. From [54, p. 232].

2.1.4 The diffusion barrier hypothesis (1968 - 2011)

Exposition of the hypothesis

The diffusion barrier hypothesis states that as C-S-H precipitates on the surface of cement grains, it forms a thickening layer that ultimately becomes thick enough to act as a diffusion barrier. As cited by Pommersheim and Clifton [23], the first to raise the hypothesis in the context of cement hydration were De Jong, Stein and Stevels in [49] based on microscopic observations of a hydrated grains. They illustrated the theory through figure 2.11 reproduced from [23].

Historical development of the hypothesis

The diffusion layer theory subdivides in different shades depending on how many sublayers the hydrate layer is supposed to have: some considered three sublayers as shown on figure 2.11: outer and inner C-S-H plus an intermediate middle layer [23]; other went for only one aggregated layer and thus diffusion coefficient [12].

Other variations include different geometries: the Ginstling-Brouhnstein equation [37] took into account the 3D geometry of the reaction by contrast with the Jander equation which is a 1D simplification [44] [45]. Both equations however comes from the field of solid-gas reaction at high temperature (several hundreads of °C). The 3D platform HYMOSTRUC is also based on this theory.

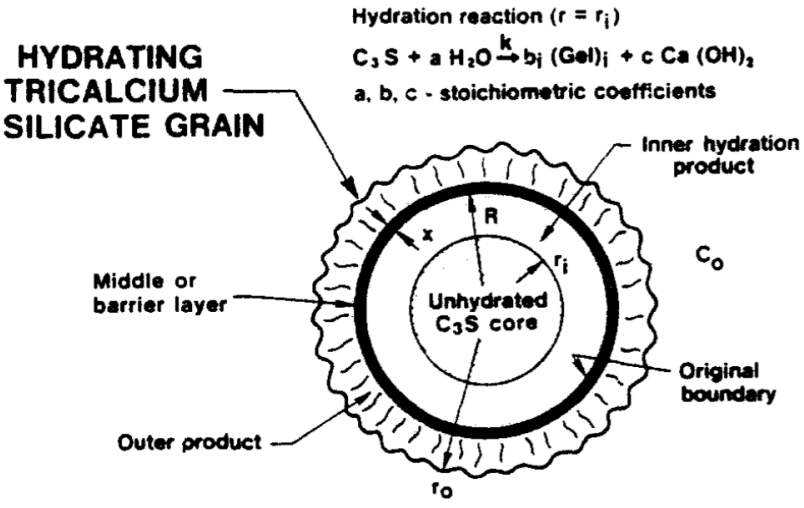

Figure 2.11 – Schematic representation of a hydrating C_3S grain according to [23]. Three different kinds of C-S-H were invoked so as to better fit the calorimetry curve. In short, this states that as C-S-H precipitates on the surface of cement grains, it forms a thickening layer that ultimately becomes thick enough to act as a diffusion barrier.

Evidence against the diffusion barrier hypothesis

1 - There is no uniform or dense layer forming around alite grains; C-S-H nucleates as needles or foils leaving the anhydrous grain in direct contact with the pore solution.

TEM or SEM observations in secondary electron mode of hydrating alite and cement pastes clearly reveal that C-S-H does certainly not precipitate as uniform layers but as fibrils/needles or foils [77] [39] [38] [58, p. 256] [80, p. 124-125] [5]. As a consequence, cement grains are in direct contact with the pore solution, during the acceleration period at least[3]. Figure 2.12 shows a representative alite grain one hour before the peak. Even after the peak, when not all but most of the surface is covered by needles [68, section 3.1] this contact weakens the assumption that the C-S-H behaves like a continuous layer because transport phenomena always take the shortest path.

To draw an analogy with the thermal insulation of building, the power required to heat a single-room house covered by a 10 centimeters of insulation layer but without any windows or doors is clearly different than the power consumption of a single-room house with 20 centimeters of insulation on half of its walls and the other half plainly open windows/doors. Both have an average 10cm of insulation but surely it would be quite exaggerated to affirm that the second house can be modelled as the first one with an apparent wall/layer thickness of 10cm and apparent diffusion coefficient equal to the first one.

Perhaps the confusion comes from observations in the later ages, when the inner C-S-H has eventually precipitated. The inner C-S-H does ultimately form a uniform layer around the grain and is ultimately in direct contact with it, but the inner C-S-H only starts to precipitate in cement pastes at about 18 hours, that is in the middle of the deceleration period and thus *after* the peak. In this sense, figure 2.11 may be misleading as it does not tell the chronology of events; some readers might intuitively but wrongly conclude that the different layers of C-S-H grow on top of each other.

2 - The presence of a gap between the receding anhydrous grain and the outer C-S-H scaffold. The inner C-S-H precipitates in the gap left by the receding grain. This gap separates the anhydrous grain from the detached outer C-S-H scaffold as shown on figure **??**. The inner C-S-H does not precipitate on the surface of the anhydrous grain but from the outer C-S-H scaffold toward the anhydrous core as shown on figure 2.14. As a consequence, as long as the inner C-S-H has not yet reached the anhydrous core, both the grain and the thickening inner C-S-H layer are still in direct contact with the pore solution and face each other.

As the contact between the inner C-S-H layers and the anhydrous cores are achieved only beyond three days, the diffusion layer theory can only be soundly raised then.

[3] Some may argue that the SEM does not allow to resolve needles that would longitudinally grow along the surface and isolate the grain from the pore solution. But looking at figure 2.12, this does not seem to be the case; even if it was, the thickness of the layer would then be of the order of the diameter of the needles, less than 50nm, which is more than one order of magnitude lower than the value assumed in diffusion based model

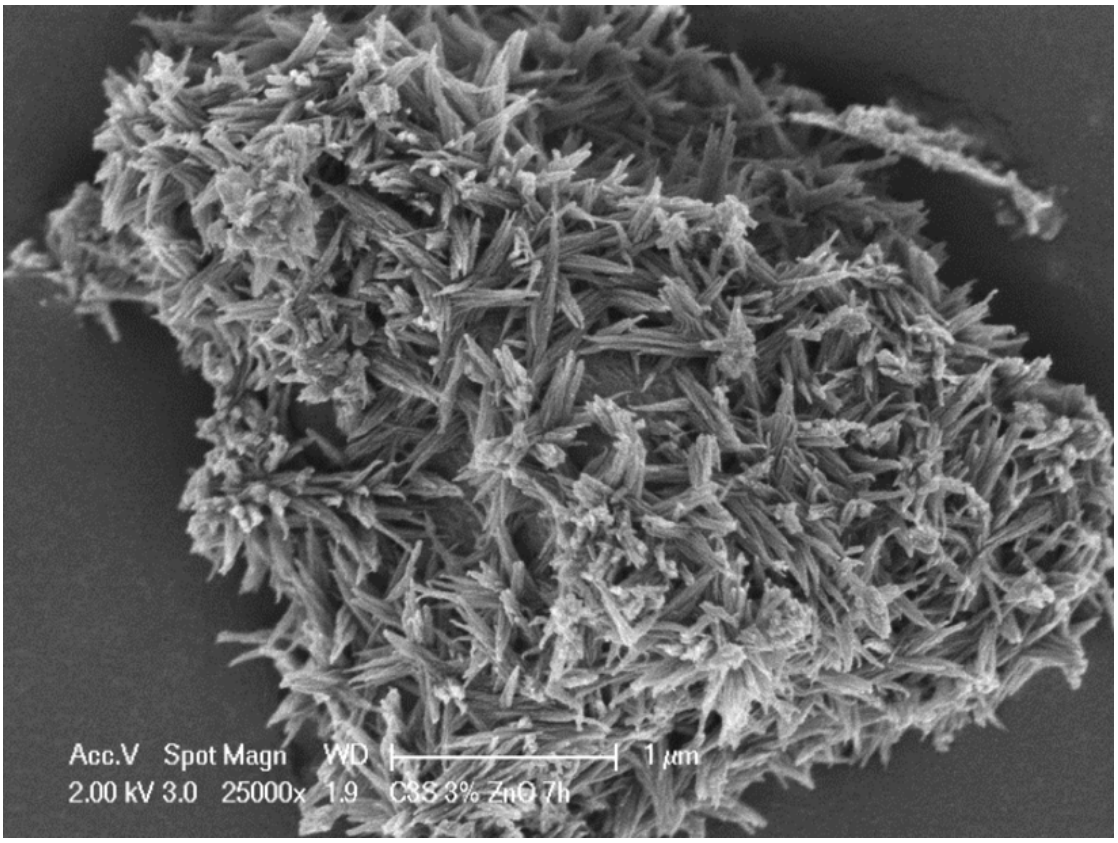

Figure 2.12 – SE-SEM image of a hydration C_3S grain one hour before the peak (this C_3S was doped with 3% ZnO). Note that C-S-H does not form a continuous layer around the grain, its surface is actually still in contact with the pore solution. This weakens the diffusion barrier hypothesis. Courtesy of Dr. Xuerun Li.

But the presence of a gap between the receding anhydrous grain and the outer C-S-H underlies yet another argument against the diffusion layer theory that has already been raised in a previous review [76]. If the outer C-S-H shell acted as a diffusion barrier, then the concentration of species within the gap would be higher, and thus the supersaturation higher as well, so that precipitation should rather happen inside it than outside the shell at the tip of the needles. Yet precipitation does carry on at the tip of the needles, not in the gap, up to the end of the first day up, that is well after the peak[4].

[4] Some may argue that the inner C-S-H starts precipitating in the middle of the deceleration period and may from this point on act as a diffusion barrier; but careful SEM observation reveals that the needles still grow for the first 28 days at least, i.e. even in the presence of a growing layer of inner C-S-H (see the outer C-S-H input parameter section of chapter 4 for more details).

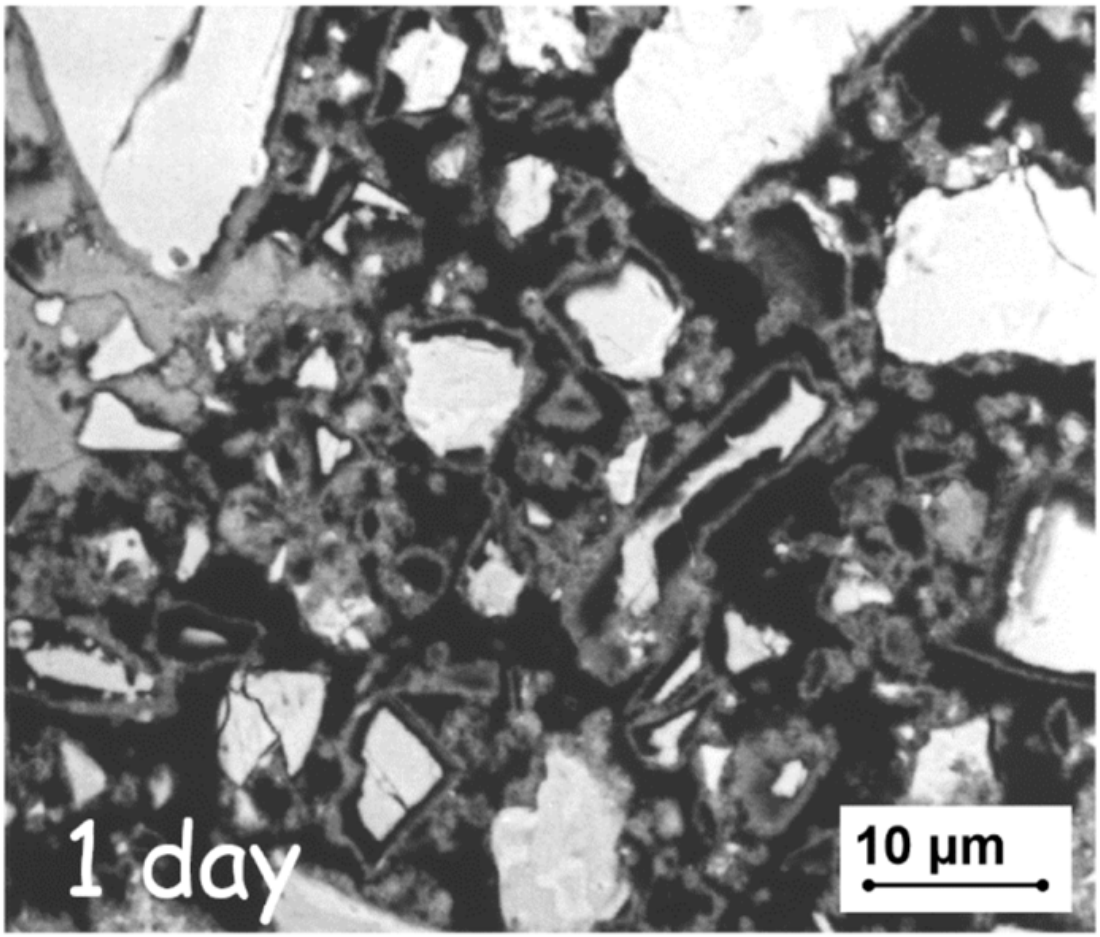

Figure 2.13 – A typical PC paste at one day. Outer C-S-H in dark grey are seen around white anhydrous grains. A Portlandite cluster in intermediate grey level is seen on the top left. Some anhydrous grains are polyphase as in the bottom of the image (different shades of whites are seen). Some small outer C-S-H shells have lost their anhydrous core: these are called "Hadley grains" after the researcher who noticed them first. The black background is the pore network, filled by a mixture of water and air (due to chemical shrinkage). From [77].

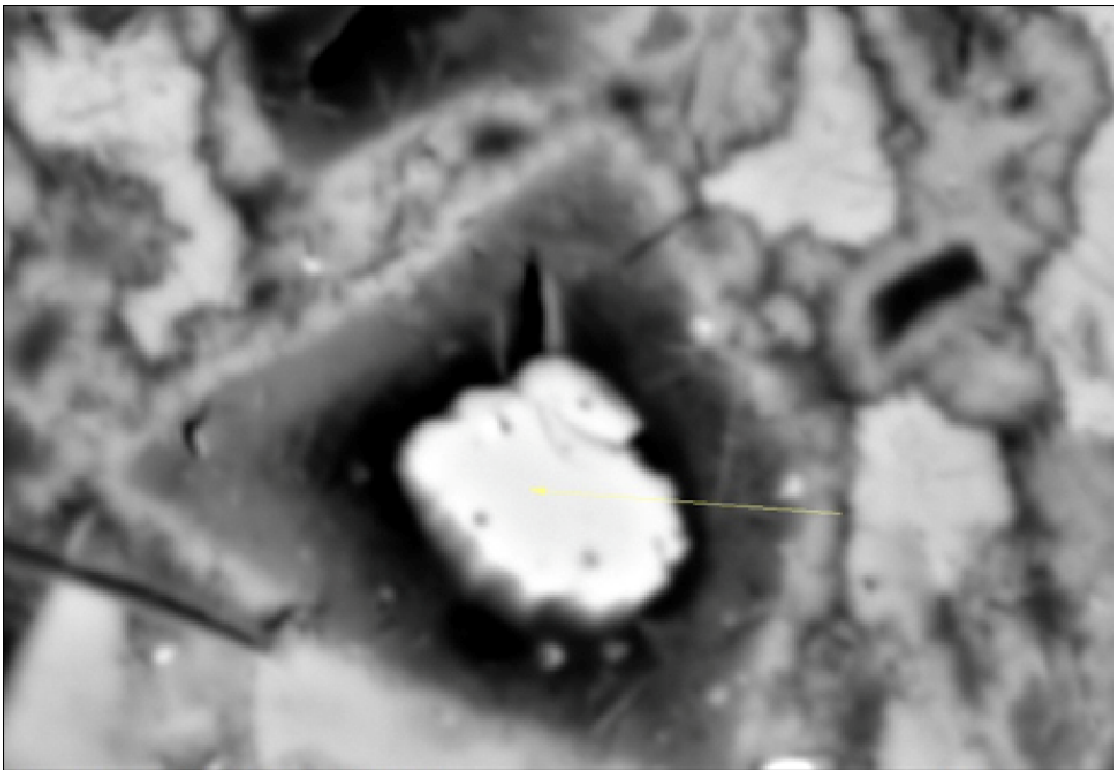

Figure 2.14 – Inner C-S-H filling up the gap left by the receding anhydrous grain. The inner C-S-H nucleates on the outer C-S-H shell and grows inward.

3 - The activation energy is constant throughout the whole peak.

If there was a transition of mechanism at the peak time, then the activation energy of the first mechanism, during the acceleration, and the second mechanism, during the deceleration, would likely be different. However, the activation energy has been measured to be constant not only throughout the whole peak but up to a few days [84], thus suggesting no change of mechanism during the first few days.

4 - The variation of the C-S-H diffusion coefficient vary by an order of magnitude with the PSD: it does not make sense.

Ten years ago, Bishnoi modeled the diffusion hypothesis through his then newly developed platform μic (pronounced "mike") and showed that the C-S-H diffusion coefficient had to be varied over one order of magnitude to fit C_3S powders having different fineness [15]. Such a variation appears ad hoc and required only to save the hypothesis and not grounded in reality: no variation of any C-S-H properties has ever been measured to depend on the alite fineness.

5 - The ability to fit a bell shape curve with four freely varying parameters or more is not convincing.

The only argument so far in favor of the diffusion layer theory is the fact that models based on it are able to fit the calorimetry curve. Yet these models always rely on four fitting parameters or more: typically, two for the mechanism assumed to control the acceleration period, and two for the deceleration period. Four being the sufficient number of parameters to satisfactorily fit any asymmetric bell shape curve, the fitting ability of these models comes as no surprise.

Moreover, the Jander and Ginstling-Brounstein equations (or variation of these) come from another field, namely solid-state reactions between two crystals at high temperature. Obviously, the applicability of these equations on 1- a dissolution-precipitation reaction between 2- a crystal and non-crystalline porous material (C-S-H) 3- at low temperature is questionable. To apply these equations to cement hydration would require a dedicated argumentation which is never found in the literature. Even if these equations are shown to be able to fit the calorimetry curve, they interpret it in terms of a physical situation completely different to the real case. In other words, a dedicated diffusion equation should have been derived from the low temperature reaction of a crystal – non-crystalline and porous material case.

6 - No publications in favor of it in one decade have answered any of the former arguments

Most of the former points against the diffusion layer theory have already been raised in previous publications over this last decade and no attempt at all was made to rebut them.

Conclusion on the diffusion barrier hypothesis

Even if all textbooks refer to this hypothesis as plausible [80, pp. 124-125] [58, pp. 243-248], [42][5], [21], the evidence built over the last decade against it is overwhelming. This undermines models like HYMOSTRUC based on the diffusion barrier hypothesis.

[5] At the time of writing this thesis, the fifth edition of Lea's *Chemistry of Cement and Concrete* was just released in March 2019 and unfortunately still refer to the diffusion barrier as the right mechanism explaining the transition.

2.1.5 Nucleation and growth with impingement (1968-2011)

Exposition of the hypothesis

This theory states that the progressive impingement of C-S-H hydrates of neighboring grains lead to the transition from acceleration to deceleration. Alternatively, as hydrates impinge against each other the surface in contact with water decreases; because the reaction is assumed proportional to the surface of contact with water this leads to a decreasing rate. Figure 2.15 illustrates this theory.

Historical development of the hypothesis

This idea originated first in the context of metal melts and was modelled by Avrami (Avrami, 1929). Upon cooling, some metal melts nucleate homogeneously and the nuclei grow proportionally to their contact surface with the liquid. As they progressively impinge against one another, the total surface of contact with the melt decreases and so does the reaction rate.

The analogy between nucleation and growth in metal melts and the hydration reaction was first proposed by Tenoutasse and DeDonder [82].

As the nucleation and growth of C-S-H was then pointed out to be heterogeneous, so-called Boundary Nucleation and Growth (BNG) models were developed where precipitation occurs on the surface of cement grains. Models again were built from an analogy with the field of metallurgy [83] though of metal recrystallisation instead of metal solidification this time [22]. In his recrystallisation model, Cahn assumes nucleation to take place at the grain boundaries, which is analogous to heterogeneous nucleation.

BNG models were further refined to consider a C-S-H densification mechanism [15] or anisotropic growth [74].

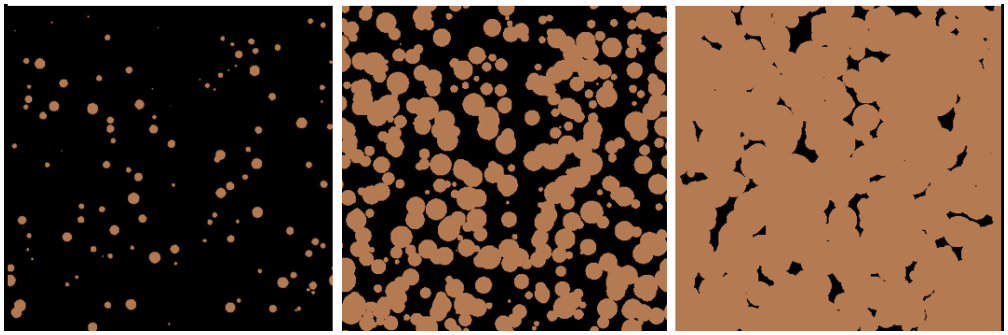

Figure 2.15 – Avramian homogeneous nucleation and growth in a metal melts. When the metal start solidifying a few nuclei randomly appears (left). The growth is assumed proportional to the contact surface with the liquid. Progressively the nuclei impinge (central picture) up to the point where most of the growth is blocked by impingement (right picture). Schematically the central picture is suggested to be the analog to the main hydration peak. From this point impingement gets stronger and stronger and lead to the deceleration period. From [15]. This analogy with metal solidification however does not hold as is explained in the text: impingement is not *the mechanism explaining the transition.*

Evidence against the N& G with impingement:

1 - Impingement is barely visible under the SEM

Observations of 0.5 water-to-cement ratio pastes at one day - that is significantly after the peak - do not show much impingement: figure 2.13 does not look like the third image of the triptych figure 2.15. The amount of porosity on figure 1-14 is also much larger than on the third image of the triptych 2.15; and so are as well the contact surfaces between the alite grains and water, or between the C-S-H shells and water.

2 - The value of the nucleation and growth rates lie beyond experimental incertitude intervals

The perpendicular growth rates G of BNG models such as [15, table 7] [74, table 3] tested on Costoya PSD experiment [25] are found to be respectively in the range [0.032 - 1.10] $\mu m/h$ and [.04 - 0.10] μm/h and monotonically *increasing* with the average particle size. This translates to C-S-H thicknesses of respectively [320 - 11000] nm and [400 - 1000] nm at the time of the peak. But Costoya measured the thickness to lie within [100 - 400] nm [25, p. 88] and monotonically *decreasing* with the average particle size: the average thickness measured for the coarsest powder is 100nm $\pm 100nm$ whereas the fitted ones are 11 000 nm and 1000nm.

Furthermore, because of such high growth rates, and because of the ellipsoid shapes of the nuclei, these models correspondingly underestimate the nucleation rates in order to fit the calorimetry curve. Therefore, the microstructural story underpinning these models is one where *few dozens of big ellipsoids* nucleates per micron square. By contrast, the story observed by SEM is the opposite: *hundreds of small needles*[6] nucleate per micron square.

3 - The main hydration peak still occurs at w/c = 50 where there is clearly no perpendicular impingement

Even more convincing is the evidence that the main hydration peak barely evolves from water to cement ratio 0.4 to 0.8 as pointed out by Kirby and Biernacki in [51] and reproduced on figure 2.9. If impingement was to explain the transition from acceleration to deceleration then surely the interparticle distance, which is directly linked to the water-to-cement ratio, should influence it; yet this not the case. More dramatic is Garrault, Behr and Nonat experiment in dilute suspension [33], with water-to-cement ratio of 50, where the interparticle distance is then in the order of tens of microns, well beyond any C-S-H thickness measured at any time, and where a main hydration peak is still observed at the same time and same height.

4 - The ability to fit a bell shape curve with four freely varying parameters or more is not convincing

[6] To avoid confusion, bunches of needles are sometimes observed radiating from the *exact same point*, they look like sea anemone. But that is only one of the many arrangements needles take: figures 2.2 and 2.12 illustrate the variety of needles aggregations states.

The same argument used against the diffusion layer theory applies to the N&G with perpendicular impingement models: they were only shown to be able to fit calorimetry curves with different set of input parameters each time.

Conclusion on perpendicular N& G

This theory is referenced in all the old [80, pp. 124-125] [58, pp. 243-248] [21], as the only alternative to the diffusion layer theory. Yet, as for the diffusion layer theory, the evidence raised in the last decade against it is overwhelming.

The case of parallel impingement: impingement from nuclei growing on the same grain

If perpendicular impingement is not the right mechanism, then could parallel impingement be it[7]? Very likely not for parallel impingement would result in a transition to a lower heat flow, but not to a decrease toward zero. Indeed, once nuclei have grown and all impinge laterally on each other, their only growth direction is outward; then the C-S-H growth would be linear in case of needles or foils, or quadratic in case of layers so that it would result in a transition to a plateau or lesser, but still positive, slope after the acceleration period; not in a drop about as steep as the acceleration period. This argument was numerically demonstrated in [15].

Mixture between diffusion barrier and N& G: The Parrott-Killoh approach of connecting in sequence the rate limiting mechanism

The diffusion layer theory has actually most frequently been used in conjunction with nucleation and growth since at least Bezjak and Jelenic [13] and Parrott and Killoh [69]. The slowest mechanism is assumed to control the overall reaction rate. As nucleation and growth always starts as the slowest reaction, it always precedes the diffusion control. Bezjak and Jelenic were the first to introduce the idea on alite, but Parrott and Killoh extended to all four phases of PC clinker, each phase receiving a set of five (!) fitting parameters [69, table 1].

This approach faces the same issues as the previous explanation and only save the phenomena in even a more ad hoc manner: whenever nucleation and growth are not anymore able to fit the calorimetry curve another mechanism is invoked.

[7] By parallel impingement is meant the impingement from needles belonging to the same grain.

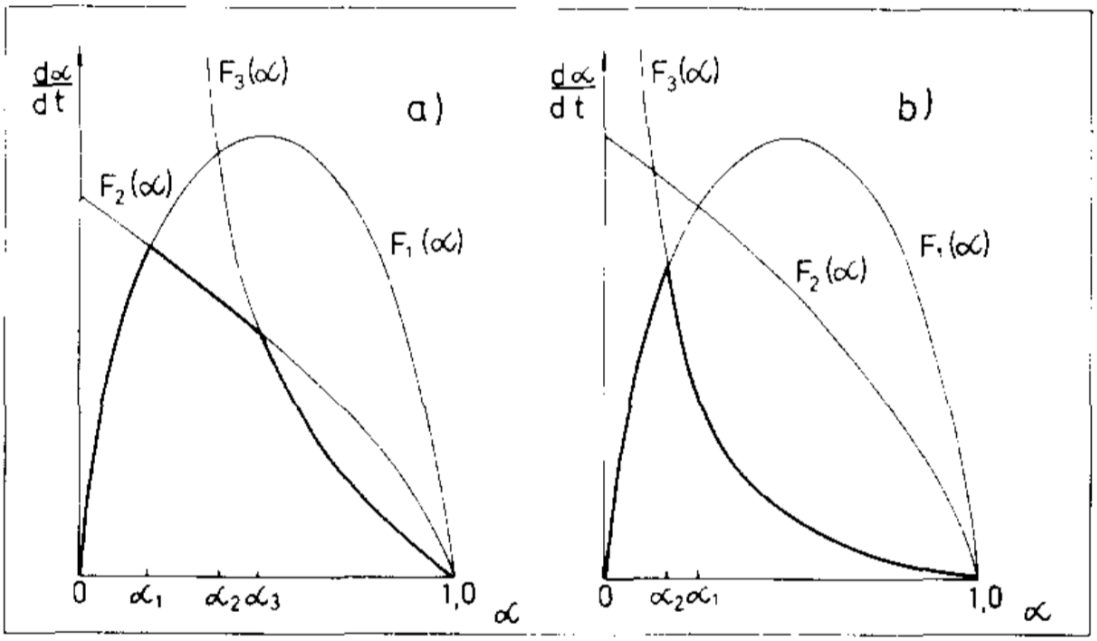

Figure 2.16 – Illustration of the "sequential" hypothesis [13, fig. 1]: Nucleation and growth (F1) is the first mechanism up to the point where either phase boundary (F2) or diffusion (F3) growth takes on. Bezjak and Jelenic were the first to introduce it; but this as extended to PC by Parrott and Killoh [69].

2.1.6 Confined growth (2011 - Present)

Following the criticisms addressed to the nucleation and growth models by Kirby and Biernacki, the confined growth hypothesis forces the nucleation and growth to happen no more than one micron from the grain surface in closer agreement with SEM observations.

In 2011, Biernacki and Xie developed a single particle model exploring this hypothesis [14]. By definition this model does not consider the particle size distribution and can therefore not be tested against experiments. Yet this model predicts 2 μm particles to release more heat at 24 h than any bigger particle ([14, fig. 11]. This is in contradiction with SEM microstructural observations: at 24 h particles below 5 μm have completely been consumed [52], and 2 μm particles vanish even before 10 h [77].

In 2013, Masoero et al. built another model based on the confined growth hypothesis [60]. By contrast with the previous model, this one allows for the particle size distribution and enable the comparison with experimental data. They showed the model is able to fit Costoya's PSD experiment [25, p.57] while keeping the exact same set of parameters, except for the thickness of the confined growth zone which fluctuates around an average of 1 μm. This value is questionable: it is beyond the thickness uncertainty interval measured by Costoya by more than a factor of two [25, p.88]. Bazzoni [5, fig. 4.35]and Garrault, Behr and Nonat [33, fig. 7] also found the average thickness at one day to lie in the range 200–500 nm. Moreover, the starting time of hydration is assumed to be negative (equal to minus 3 h) which is unphysical.

In 2016, Honorio et al. published yet another confined growth model, this time assuming an increasing C-S-H density and a diffusion control mechanism after the peak [43]. As explained in the preceding subsection, diffusion is certainly not the underlying mechanism behind the transition. Also, the model neglects the small grains consumption so that the 2 μm grains release more heat at 24 h than any bigger size thus being the biggest contributor to the heat release beyond one day. As already mentioned, this is in contradiction with SEM observations.

2.1.7 Small grain dissolution / surface reduction (1986 - Present)

That the consumption of the small grains could possibly explain part of the transition from acceleration to deceleration has been raised by Taylor in 1986 though he did not expect it to be the sole mechanism [81, sections 5.3.1, 5.4.1 and 10 pp. 92-94;103] [80, p. 155]. Grains below 3 µm have been observed to be completely reacted by 10 h and grains below 7 µm by 24 h by Scrivener [77]. Kjellsen and Justnes reached similar conclusions with most of the grains below roughly 5 µm having disappeared by 24 h [52, p. 905]. Though some models like µic [16], CEMHYD3D [7], HydratiCA [19] and HYMOSTRUC [86] implicitly take into account the dissolution of the small grains, the significance of the impact of the consumption of the small grains on the transition has not been studied in details and thus remains an open question.

In [9] and [8] Bergold, Goetz-Neunhoeffer and Neubauer argue that the dissolution of the small grains explains the transition to the deceleration period. But the PSD of their powder is much finer than usual: the BET specific surface they have ranges from 0.6 to 35.2 m2/g; which translates to a range of about 20 μm down to a few microns only. Following the observations of Kjellsen and Justnes reproduced on figure 2.17, such small grains do indeed vanish before the peak time. Even if the small grains dissolution play a role, they nevertheless are insufficient to explain the transition for coarser powders, such as the three coarsest powders on figure 2.3.

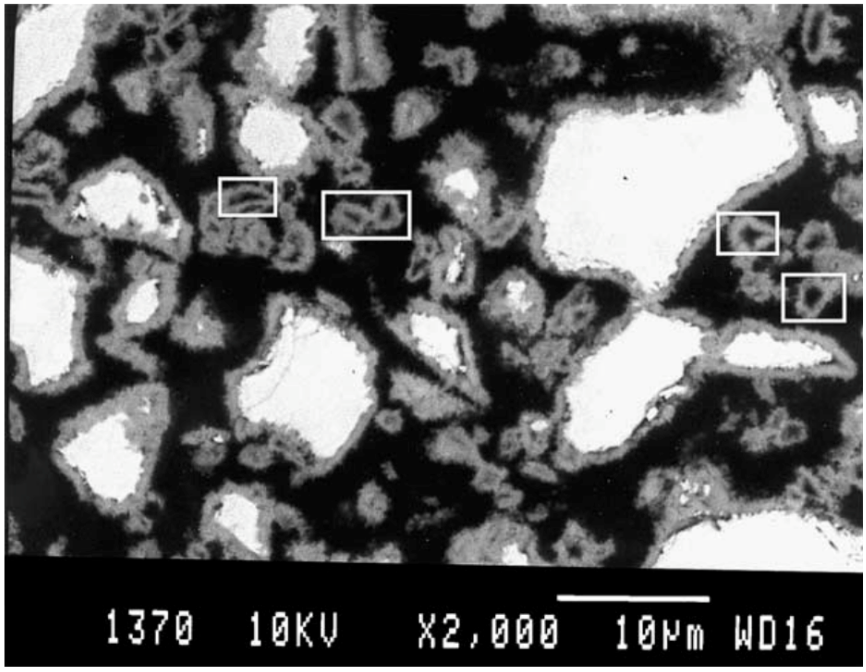

Figure 2.17 – C_3S paste at 24 h. Hadley grains are highlighted by white boxes. Their maximum size is about 5 µm: grains below this threshold have vanished. From [52, fig. 4].

2.1.8 Bazzoni's Needles N & G (2014 - Present)

In her thesis, Bazzoni characterized the microstructure of C-S-H during alite hydration by electron microscopy. She showed that C-S-H nucleates and grows mainly as needles on the surface of alite grains during the main hydration peak. She suggested that the transition from the acceleration to the deceleration happens when the surface is completely covered with needles while at the same time the needles finish their growth. She also proposed that a transition in the growth mode of the C-S-H occurs at the time of the peak: when needles finish their growth the inner C-S-H start forming. Finally, she studied the influence of magnesium and zinc as doping ions and found the latter to significantly increase the heat flow and degree of hydration while at the same time the C-S-H needle length increased significantly.

The present thesis is an attempt to build a model based on Bazzoni's observations, and quantitatively test the underlying hypothesis. This is dealt with in the next chapter and proved to be quantitatively correct except for the inner C-S-H contribution which is negligible at this stage.

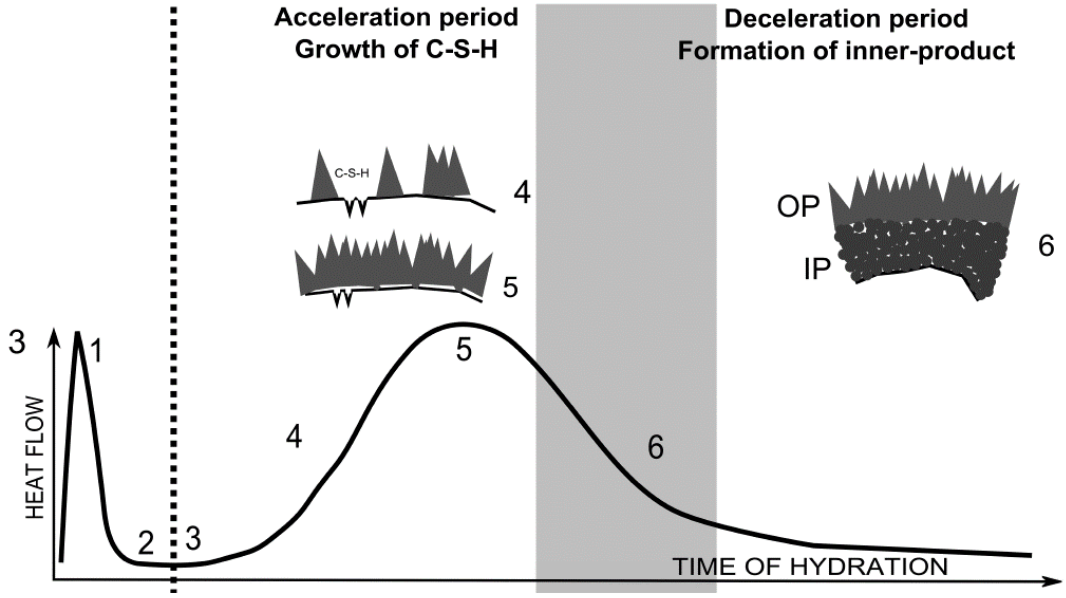

Figure 2.18 – Bazzoni's scenario for the main hydration peak. Needles gradually cover the surface during the acceleration period and progressively enter the slow growth regime. At the peak time, the surface is completely covered and the inner C-S-H start precipitating. One of the contribution of the present thesis is to demonstrate this hypothesis is quantitatively correct although the inner C-S-H contribution is negligible during the main hydration peak. . From [5].

2.2 The later age

By contrast with the main hydration peak, no model has yet been specifically built to investigate the later age and thus the later ages mechanisms are only discussed qualitatively.

2.2.1 The later age mechanisms

From the division in five stages of the reaction from Kondo and Ueda, the later ages start at the end of the deceleration period, which is about one day in alite at 20°C, and sometimes close to two days in some PC.

As mentioned earlier, the later age was first discussed specifically only in 1989 in [35]:

> *"Considering our very limited understanding of stage 4 [the deceleration period], stage 5 [the later age] is even more mysterious, which is unfortunate because it is the most important stage with respect to strength building and porosity reduction"*

Before the mechanism was deemed obvious and assumed to be diffusion (as can be found in all textbooks and review papers of international symposia before 1989). All models that attempted to model the later ages switch to a diffusion limitation at the latest by the end of the deceleration period. Twenty years later, in 2011, Scrivener and Nonat emphasized the fact that barely anything had been achieved yet on this period, except sheer diffusion model fitting. They highlight the need to build a model that considers the PSD and product overlap (impingement). The needle model as presented in chapter 5 exactly meets this requirement.

Based on activation energy arguments, Thomas criticized the hypothesis that diffusion was rate-limiting even up to 70% Degree of Hydration (DoH) which roughly corresponds to the first three days [84].

2.2.2 One key factor influencing the later ages: the w/c

All the factors listed in the previous section that either significantly influenced or not the main hydration peak apply to the later ages except for one big exception: the water to cement ratio now has a significant influence. Experiments from Berodier have demonstrated that if the cement pastes from w/c 0.4 to 0.6 had the same rate during the first day, they dramatically differ afterwards; this is presented on figure 2.19.

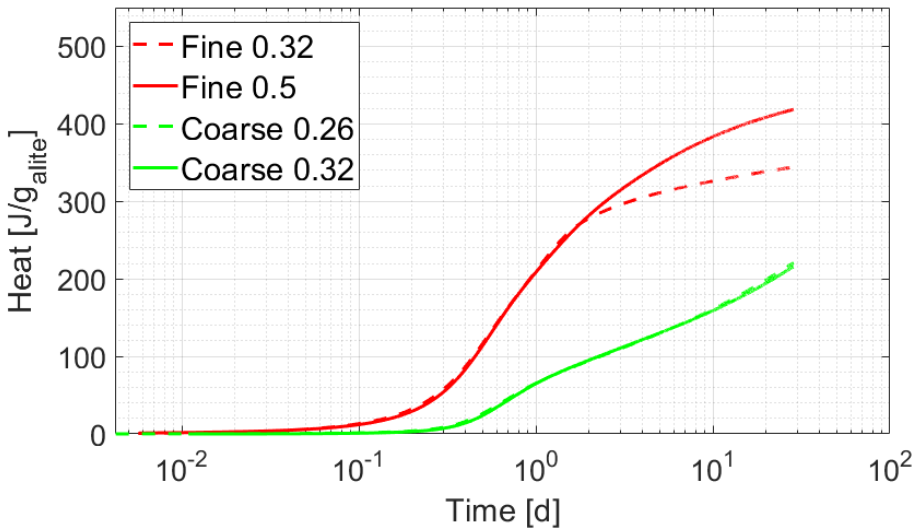

Figure 2.19 – Influence of the w/c on the hydration kinetics of alite pastes in the later age. The red curves are the fine powders whereas the green ones are coarse powders; dashed line are the low w/c ratios and continuous the high w/c ratios. The influence of the w/c ratio is very significant for the fine powder: there is a split between the low and high w/c ratios curves. This plot is a subset of the dataset to benchmark hydration models presented in chapter 4 on the later age.

2.3 The microstructural development

2.3.1 Main hydration peak

C-S-H: mostly outer C-S-H, inner C-S-H starts precipitation during the deceleration period

During the acceleration period, C-S-H nucleates and grows as "outer C-S-H" and adopts a morphology ranging from needles to foils (more discussion on this point in the next section). The term "outer" highlights the fact that C-S-H heterogeneously precipitates on the surface, grows outward and forms a shell that eventually detaches from the dissolving and thus shrinking anhydrous core.

Between the shell and the receding anhydrous core a gap opens up. This gap is more marked in PC than in alite: at 24 h it is about 1 μm in PC [77, p. 147] and less than 0.5 μm in alite [52]. These gaps are clearly seen on figure 2.13.

Correspondingly, the outer C-S-H shell in PC is about 0.5 μm to 1 μm at 12h and 1 to 2 μm at 24 h [77, p. 180] whereas it is closer to 0.5 μm in alite [52] and actually probably even smaller [25, p. 88] [5, pp. 73, 95] at 24h.

Authors differ on the time at which inner C-S-H starts precipitating. The inner C-S-H is that phase that precipitates in the gap left by the shrinking anhydrous core. It nucleates from the outer C-S-H shell and grows inward. In PC, it starts at about 18h, that is in the middle of the deceleration period. In alite pastes, Bazzoni suggests the inner starts as early as the peak time [5, p. 74]. But considering that gaps opening are difficult to observe in alite pastes this might be underestimated. What is safe to state is that the inner C-S-H start precipitating somewhere during the deceleration period.

Small grains and Hadley grains

In PC pastes, grains below 3 μm vanish by the peak time, and 7 μm by the end of the first day. In alite pastes, Kjellsen and Justnes found 5 μm as observed on figure 2.17. This means that the gap opening depends on the grain size: bigger grains tend to develop smaller gaps. A 5 μm grain has by definition vanished when the gap reached 2.5 μm. This influence of the gap size on the grain size can also be seen on figures 2.13.

2.3.2 Later ages (1 day - 1 month)

At the later ages the hydrates further fill the space: there is much less pore space (in black). The gap between the anhydrous core and the outer shell increases up to about 4 days where they reach a thickness of 3 μm. Then the inner C-S-H growth eventually fills the gap by 28 days. Striking features of this age are the thick inner C-S-H layer, which reach a few microns in

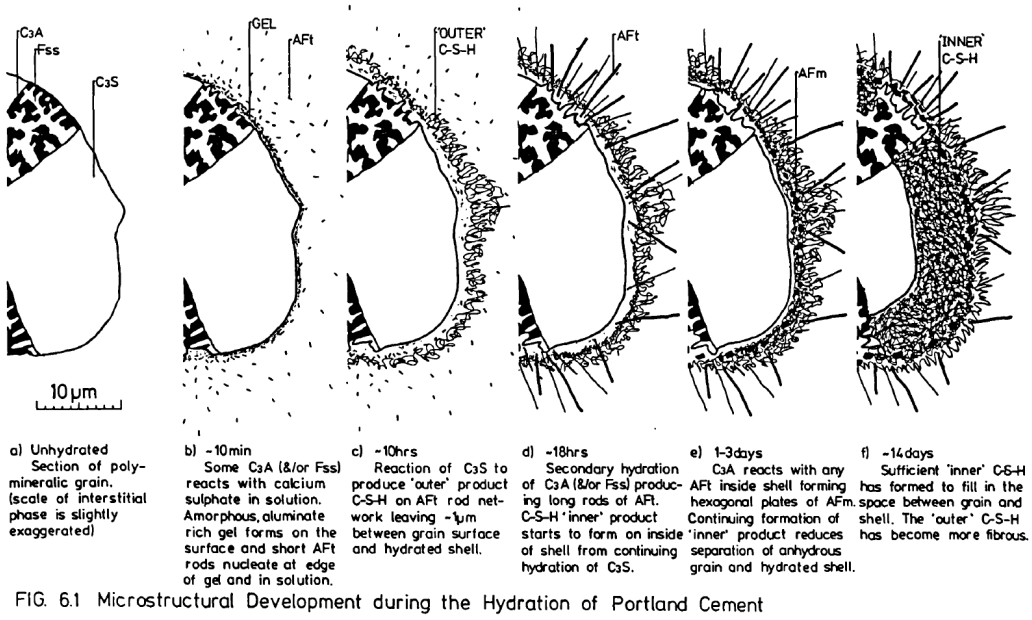

Figure 2.20 – Microstructural development during the hydration of Portland cement. From [77, p. 176]. In alite paste, the structure is simpler: there is no C_3A nor ferrite phase and thus no Aft or Afm but only outer and inner C-S-H. The time frame remains similar.

alite pastes, and up to 10μm in PC pastes by 28 days. Grains smaller than 10 to 12 μm in alite pastes vanish, 15-20 μm in PC pastes.

Portlandite clusters

In alite pastes, Portlandite forms clusters whose size depends on the PSD of the alite powder [25, p. 148]. They range from 45 μm in diameter to 220 μm for alite powders whose d_v50 ranges from 6 μm to 82 μm respectively. As a consequence, Portlandite clusters are always much bigger than alite grains and they engulf them (as seen on figure 2.21).

In PC pastes, the Portlandite is much more finely dispersed and nearly no engulfment is ever observed (figure 2.22).

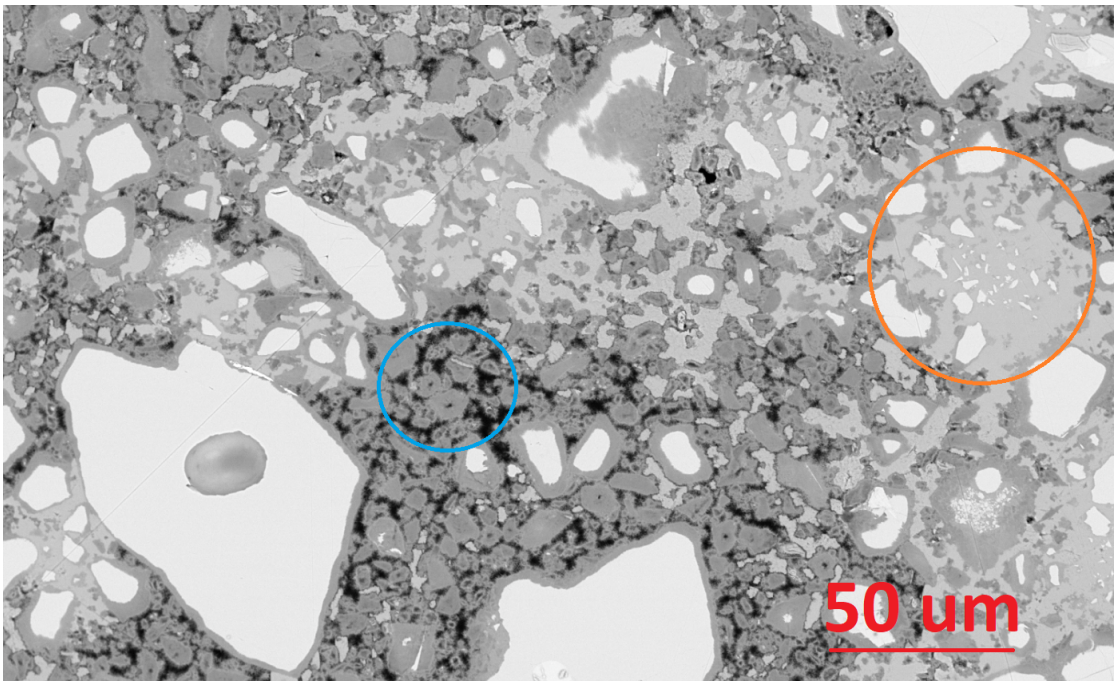

Figure 2.21 – SEM picture of a 28 days alite paste at w/c = 0.7 and 20°C. Big Portlandite clusters (by contrast with the PC paste in the next picture) and numerous Hadley grains are seen (within the blue circle in the center of the figure for example). All grains below 10 µm have vanished except those engulfed by Portlandite clusters (within the orange circle on the right of the picture). Picture taken at 10 kV and working distance of 8 mm.

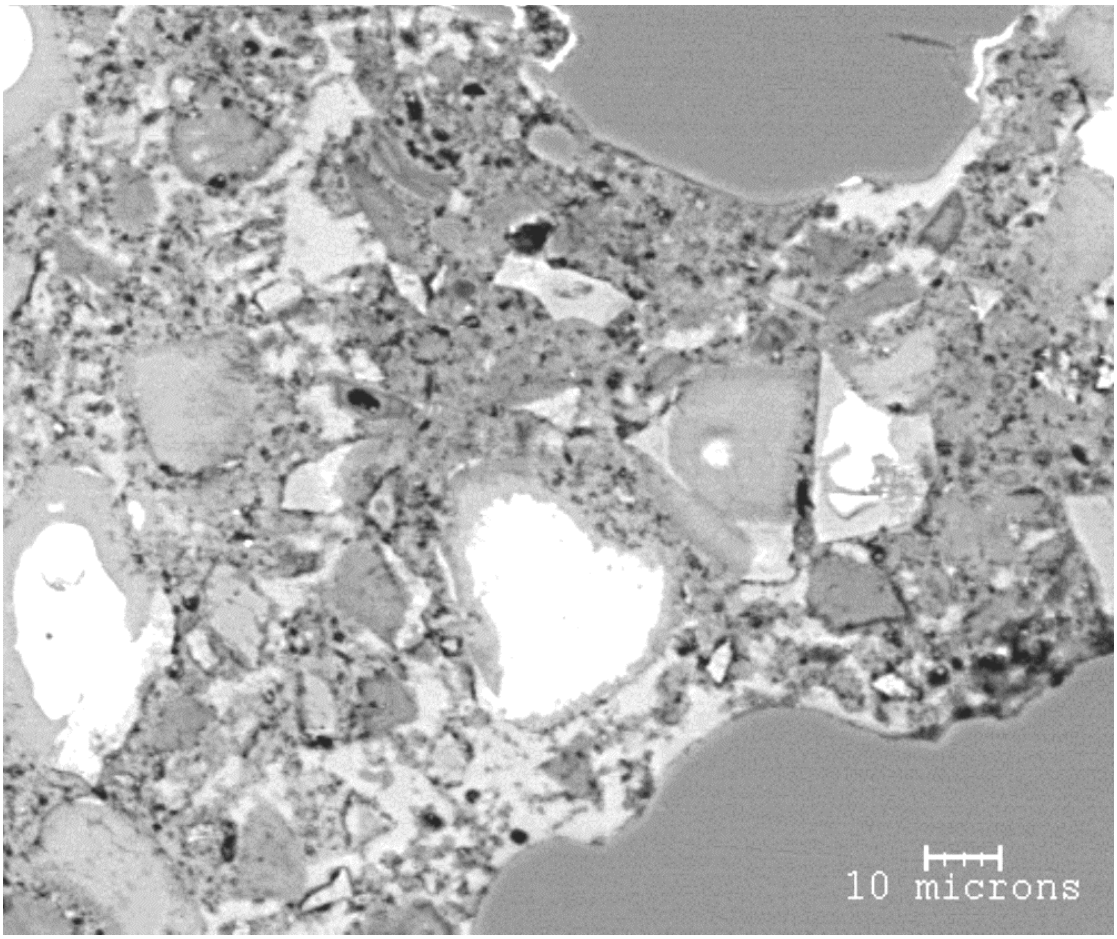

Figure 2.22 – PC paste hydrated at 28 days. Most of the space is filled compared with 24 h. All grains below 15 µm have dissolved. Grains below 5 µm leave Hadley grains. Portlandite is finely dispersed by contrast with the previous figure and does not engulf the grains.

2.3.3 Very late ages (beyond 1 month)

Beyond one month the hydrates continue filling the spaces though at a lower rate. As it is in contact with the anhydrous core, the inner C-S-H then possibly reacts by a topochemical reaction. At least in the case of PC with silica fumed, a distinction between the early inner product and the later inner product must be made in order to avoid confusion (figure 2.23). Whether this very late age product also appear in alite pastes remains an open question to this date. One may suppose that the reaction between alite and inner C-S-H carries on as long the inner C-S-H still contains water-filled gel pores.

Hadley grains 5 μm in diameter are still observed on polished surfaces up to 23 years old [81, section 5.4.1].

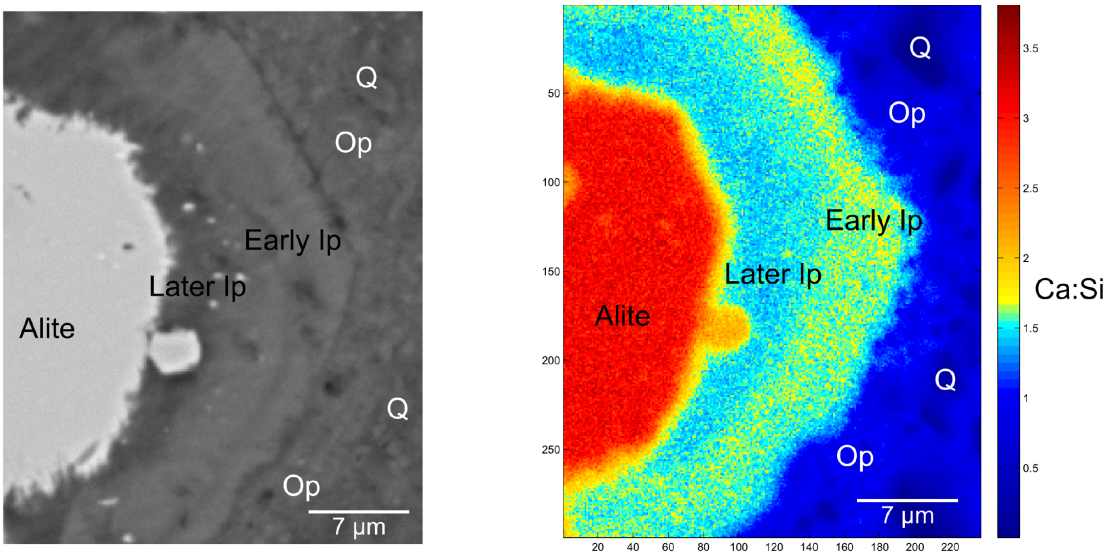

Figure 2.23 – SEM and corresponding EdX picture of a hydrating alite grain in a PC pastes blended with 25 % of Silica fume at 90 days. Two types of inner C-S-H are observed. Whether the distinction between these two inner C-S-H holds in alite pastes remains an open question. From [72, p. 106].

.

2.4 Structure, morphology and stoichiometry of the C-S-H

2.4.1 Structure of the C-S-H at the nanometer scale: sheets

As far back as 1952, the C-S-H structure was already established to be similar to tobermorite [10, p. 235]:

> *"The main conclusion from the X-ray and physical chemical study of cement hydration compounds is that there is only one or possibly two very similar crystalline forms, C-S-H(I) and C-S-H(II), [. . .] closely related to the mineral tobermorite. Even at the present stage of the research it is possible to show that the structure of this hydrate is that of a layer lattice with a variable thickness indicating the presence of interstitial sheets of water molecules."*

There have been considerable controversies over the past seven decades over the exact nature of C-S-H, whether there was different closely related phase such as jennite, jaffeite, metajennite or other similar minerals [71]. All these structures are sheet like minerals.

Yet, recent research rather suggests that C-S-H always conforms to a defective tobermorite structure. Modelling effort from Kunhi et al [56] suggest "a defective, nanocrystalline tobermorite structure with missing bridging silicate tetrahedra, leading to a decreased silicate chain length, and deprotonated silanol groups, the charge of which is compensated by additional calcium ions in the water-interlayer and with additional Ca-OH groups".

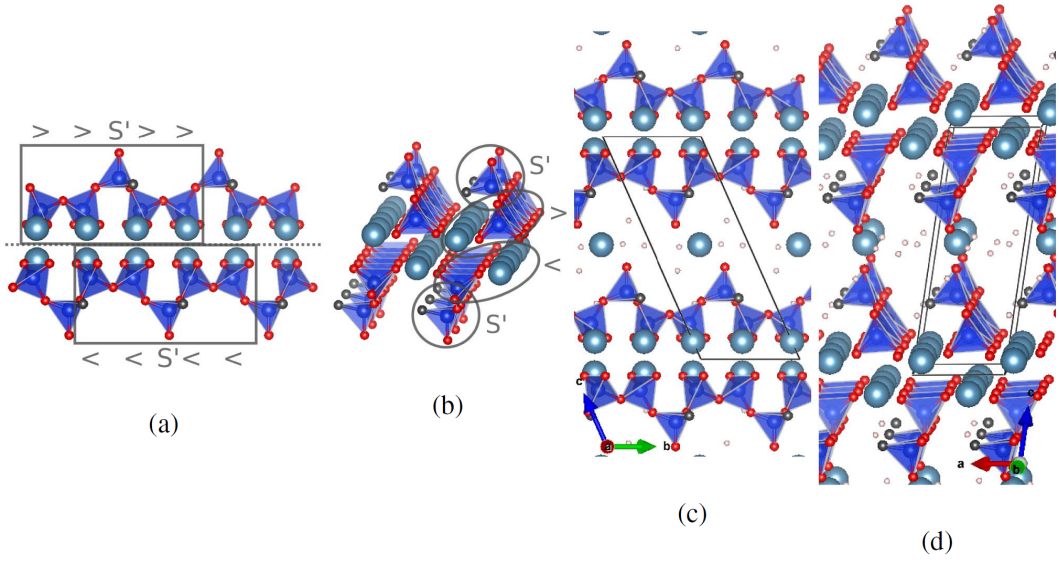

Figure 2.24 – Ca-Si layer of 14 Angstroms tobermorite with characteristic linear dreierketten structure of silicate chains ((a) and (b)) as well as their stacking in 14 Angstrom tobermorite ((c) and (d)). Si: blue, Ca: turquoise, O: red, OH: black. From [56].

Experimental works on homogenous C-S-H nucleation from Krautwurst et al. [55] aligns with these findings and propose a two-step nucleation process of C-S-H. The first step would produce amorphous crystallites of the order of the nm, while the second step would lead to a defective tobermorite structure.

As the nanostructure of C-S-H is not necessary to understand the content of this thesis, the interested reader is referred to the numerous works of Hal Taylor and Ian Richardson in addition to the already mentioned articles.

2.4.2 Morphology of the outer C-S-H at the micrometer scale: foils, reticulate network and needles

The first investigation of the outer C-S-H produced by C_3S hydration by SEM was done by Grudemo as early as 1952 [10, pp. 247 253] who describe it as "bundles of fibrous particles, often with broom-shaped structures at the ends". A few years later, at the Washington symposium held in 1960, Brunauer and Greenberg [18, p. 145] summarizes Grudemo's findings:

> *"The first extensive electron optical studies of tobermorites prepared at room temperature have been published by Grudemo. The low-lime tobermorites consist predominantly of very thin crinkled foils; some of which are so thin that Grudemo estimated them to be of unit cell thickness. Some of these foils or sheets appear to roll, partial or completely, into tubes or fibers. Kaloused and Prevus obtained similar electron microsgraphs and came to similar conclusions. Gaze and Robertson obtained tobermorite foils from hydrated Portland cement, and they estimated that these foils were of the order of two molecules in thickness.*
>
> *At lime saturation, the micrographs show predominantly tubes or fibers. Grudemo states, "In saturated and supersaturated lime solutions, a fibrous or needle-like growth of the crystals seems to be promoted, probably caused by a degeneration of the sheets into lath-like structures, and by twisting and rolling of the crystal sheets."*

Here, the influence of the concentration of the solution is thought to have an influence on the morphology of the C-S-H. But it seems that Grudemo's findings of a fibrous C-S-H troubled him because C-S-H was already known to be a defective tobermorite, how could sheets fold into a needle?

> *"It is a question open to discussion if the distortion and rolling of the crystal sheets of this and other specimens of C-S-H are caused by lattice strains set up in the lattice as a consequence of misfit layers, or if it is a secondary effect caused by dehydration processes in the vacuum within the microscope tube."*
>
> (Grudemo, 1952) [10, p. 248]

Three decades later, Bayley and Stewart rather suggested that the substrate could influence the morphology of the C-S-H:

> *With a monoclinic modification the foils that had grown previously lifted and peeled, giving crumpled sheets, but with triclinic or rhombohedral preparations, needle like outgrowths were formed. All three specimens eventually gave similar structures, in which needle like outgrowths were bridged by crumpled foils. [Studies using a cryo stage indicated that the outgrowths were not an artifact of drying].*
>
> (Bayley and Stewart, 1984) [4].

At Rio's symposium, Taylor suggested there was rather a continuum of morphologies, and proposed several other causes to explain the observed range:

> *These and other morphological varieties of C-S-H gel are, almost certainly, not distinct categories, but points in a continuum of forms all derived from sheets which tend to roll, crumple or shred in a preferred direction. The way in which they do this, and the extent, appear to depend largely on the amount of space available, perhaps together with such other factors as the mechanism or rate of formation, presence of admixtures, and can be further modified by drying, fracture, or other processes after formation."*
>
> (Taylor, 1986) [81, section 5.4.1]

In the following two decades, it has repeatedly been described as "acicular" which etymology means "needle-like" in [57], fibril-like [30] or directly as needles [77] [30] [26] [46].

In their review paper of 2002 [36], in table 3.3, Gartner et al. indicate that the middle products, the one observed during the main hydration peak by SEM and TEM, are "needles radiating from grains (acicular)"; suggesting the morphology of the C-S-H depends on the stage of the reaction.

Observations of synthetic C-S-H made at Laboratory of Powder Technology (LTP) at the EPFL rather exhibits foil like morphologies. Could it be explained by Grudemo's remark that foil tend to form at lower lime concentration (which is the case in synthetic C-S-H in order to avoid Portlandite precipitation) and fibrils at higher ones?

Observations made at the LMC from Costoya [25], Bazzoni [5], Rossen [72], Berodier [11], Mota Gasso [61] and Xuerun Li invariably favor the needle/fibril morphology (for example figure 2.12). A picture I took is shown on figure 2.25, needles are radiating and sections of them are seen in the bottom right.

Other authors such as Kjellsen and Justnes [52], or Sakkali and Trettin rather use the term fibrils [73]. This latter term is also recurrent in Richardson's TEM studies.

Jennings advocated outer C-S-H to be 5 nm globules and argued that sample preparation, especially the high-vacuum required for TEM and SEM, would damage the globules and create artefacts [31]. The observation that led to the globule hypothesis stems from neutron scattering experiment [1] a technique which per se does not give any geometric representation. It is not clear how the high-vacuum of the SEM and TEM chambers would transform 5 nm globules into hundreds of nanometres long fibrils or needles; nor why they would behave so on some C-S-H but not on synthetic C-S-H that has been observed, in the ultra-high vaccum of the TEM, as foils. Moreover, fractured sections made by Bazzoni to measure the needle length with time show a well-defined trend, not a random distribution, they grow longer with time. Also, observations in Environmental-SEM by [73] show fractured and polished sections to be indistinguishable to high-vacuum SEM: on Figs. 3 and 4 of this paper fibrils/needles are clearly observed. Finally, the question of drying creating needles seems to be excluded by the recent report of needles in supercritically dried C-S-H [88].

2.4.3 Conclusions on the outer C-S-H morphology

What seems certain is the sheet/layer/foil morphology adopted by C-S-H at the nanometer scale. Regarding the micron scale, after 70 years of observation, the question is still open: there is a range of observed morphologies from foils to fibrils / needles. Researchers have raised a number of possible causes:

- The lime concentration at which the C-S-H forms. Low lime concentration would favor foils, high ones needles
- The substrate on which they grow: monoclinic would favor the foils, triclinic and rhombohedral the needles
- The stages of hydration: the nucleation and growth path could start with an amorphous C-S-H and then turn it into fibrils/needles
- The rate of formation
- The presence of admixtures

What is however clear is that outer C-S-H neither forms a uniform layer, as most diffusion-based models assume, nor spheroids as most nucleation and growth models assume. Given that the shape of the C-S-H has an impact on the equations and values taken by the parameters of the model, such as the n-exponent in the Avrami model, and given that foils can be considered as aggregates of needles, to model C-S-H as fibrils/needles is the closest approximation of the outer C-S-H geometry.

Figure 2.25 – SEM polished section of a w/c = 0.7 alite paste at 28 days. Sections of needles are observed (points) in many different areas, in particular in the bottom right. Etch pits are still plainly visible on the anhydrous core. The central grain largest diameter is 12 µm, the vertical length of the image is 20 µm. Image taken at 5 kV, working distance 6 mm. See the online version to get a better view of the needles sections.

2.5 Historical appendix

2.5.1 Phase boundary limitation

This hypothesis only appears in few papers before year 2000 and has since disappeared from the literature. It is part of the sequential approach of Bezjak and Jelenic, and Parrot and Killoh.

Phase boundary dissolution of the anhydrous

As cited in Van Breugel [86], Werner [87] was perhaps the first to suggest the reaction rate to be proportional to the surface of contact of the anhydrous with the liquid:

$$\frac{d\alpha}{dt} = k\frac{S(t)}{S_0} \tag{2.1}$$

Where α is the degree of hydration, S the surface of the reactant at time t, S_0 at time 0 and k a proportionality constant. In the case of a spherical grain this becomes:

$$\frac{d\alpha}{dt} = k\frac{4\pi r(t)^2}{4\pi r_0^2} = k\frac{r(t)^2}{r_0^2} \tag{2.2}$$

Because $\alpha = \frac{V(t)}{V_0}$, the ratio of the actual volume at time t over the initial volume, and $V(t) = 4/3\pi r^3$, r_0 is the initial radius of the grain and the equation becomes:

$$\frac{d\frac{4/3\pi r^3}{4/3\pi r_0^3}}{dt} = \frac{1}{r_0^3}\frac{dr}{dt} = k\frac{r(t)^2}{r_0^2} \tag{2.3}$$

So that:

$$\frac{dr}{dt} = kr_0 \tag{2.4}$$

Which means a constant rate of thickness dissolution: $r = r_0(1-kt)$ The volume and reaction rates can now be written as a function of time:

$$V(t) = k\frac{4}{3}r_0^3(1-kt)^3 \tag{2.5}$$

$$\frac{d\alpha}{dt} = -k4\pi r_0^2(1-kt) \tag{2.6}$$

Although the idea of a solid-liquid reaction proportional to the surface of contact may intuitively seem appealing, in the case of isotropic dissolution this equation means a decreasing rate only [8], and thus cannot explain the acceleration period. Regarding the deceleration period

[8] At any time the amount of surface is lower than at the previous time step so that the heat flow can only decrease. This is implicitly shown on figure 2.16 where the F2 curves are shown to always be decreasing with DoH.

this equation cannot either account for it as it predicts a parabolic decreasing rate which is concave instead of being convex as the deceleration slope is.

Historically, the abandonment of this hypothesis was however not grounded on these two arguments but rather on the observation that the PSD turned out to be a most important parameter, as observed by [66], [89] and [40] (as mentioned in [86, pp. 106-107]). This illustrates the fact that often in the history of Science, a hypothesis is put aside not because of arguments against it, but because more trendy questions and new fields of investigation direct the attention of researchers away of it.

Phase boundary growth of the hydrates / autocatalytic reaction

The idea of a reaction proportional to the surface nevertheless likely paved the way to the phase boundary growth of hydrates layer in symmetry to the boundary dissolution of the anhydrous. This is also called the autocatalytic reaction of C-S-H. Assuming again spherical particles, the same derivation holds but now concerns the hydrate layer instead of the anhydrous. The hydrate layer thickness then linearly increases with time, the volume therefore increases with the cube of time and the rate of reaction is parabolic.

The qualitative shape of the acceleration period can thus be reproduced but not the quantitative one as the acceleration periods usually does not exactly follow a parabolic increase with time. Furthermore, a monotonic growth obviously does only account for the acceleration, not the deceleration. Therefore, it has to be coupled in sequence with another mechanism such as diffusion to account for the whole peak. Even then the transition is discontinuous and questions the validity of the model and hypothesis.

2.6 References

[1] Andrew J. Allen, Jeffrey J. Thomas, and Hamlin M. Jennings. "Composition and density of nanoscale calcium-silicate-hydrate in cement". *Nature materials* 6 (2007), pp. 311–316.

[2] M. Reza Andalibi et al. "On the mesoscale mechanism of synthetic calcium–silicate–hydrate precipitation: a population balance modeling approach". *Journal of Materials Chemistry A* 6 (2018), pp. 363–373.

[3] François Avet. *Investigation of the grade of calcined clays used as clinker substitute in Limestone Calcined Clay Cement (LC3)*. Doctoral Dissertation Ecole Polytechnique Fédérale de Lausanne (EPFL), 2017.

[4] J.E. Bailey and H.R Stewart. "C3S hydration products viewed using a cryo stage in SEM". *Journal of Materials Science Letters* 3 (1984), pp. 411–414.

[5] Amélie Bazzoni. *Study of early hydration mechanisms of cement by means of electron microscopy*. Doctoral Dissertation Ecole Polytechnique Fédérale de Lausanne (EPFL), 2014.

[6] Amélie Bazzoni, Marco Cantoni, and Karen Scrivener. "Impact of Annealing on the Early Hydration of Tricalcium Silicate". *J. Am. Ceram. Soc.* 97 (2014), pp. 584–91.

[7] Dale P. Bentz. "CEMHYD3D: A Three-Dimensional Cement Hydration and Microstructure Development Modelling Package". *NIST Internal Report* https://ciks.cbt.nist.gov/bentz/cemhyd3dv20/useg (last visited on 24 April 2019) (2000).

[8] S.T. Bergold, F. Goetz-Neunhoeffer, and J Neubauer. "Influence of the reactivity of the amorphous part of mechanically activated alite on its hydration kinetics". *Cement and Concrete Research* 88 (2016), pp. 73–81.

[9] S.T. Bergold, F. Goetz-Neunhoeffer, and J Neubauer. "Mechanically activated alite: New insights into alite hydration". *Cement and Concrete Research* 76 (2015), pp. 202–211.

[10] J.D. Bernal. "The structures of cement hydration compounds". *Proceedings of the third international symposium on the chemistry of cement, London 1952* (1952).

[11] Elise Berodier. *Impact of the Supplementary Cementitious Materials on the kinetics and microstructural development of cement hydration*. Doctoral Dissertation Ecole Polytechnique Fédérale de Lausanne (EPFL), 2015.

[12] A. Bezjak. "Nuclei growth model in kinetic analysis of cement hydration". *Cement and Concrete Research* 16 (1986), pp. 605–609.

[13] A. Bezjak and I. Jelenic. "On the determination of rate constants for hydration processes in cement pastes". *Cement and Concrete Research* 10 (1980), pp. 553–563.

[14] Joseph J. Biernacki and Tiantian Xie. "An Advanced Single Particle Model for C3S and Alite Hydration". *J. Am. Ceram* 94 (2011), pp. 2037–2047.

[15] Shashank Bishnoi and Karen Scrivener. "Studying nucleation and growth kinetics of alite hydration using μic". *Cement and Concrete Research* 39 (2009), pp. 849–860.

[16] Shashank Bishnoi and Karen Scrivener. “μic: A new platform for modelling the hydration of cements”. *Cement and Concrete Research* 39 (2009), pp. 266–274.

[17] Paul Wencil Brown, Caroline L. Harner, and Edward J Prosen. “The effect of inorganic salts on tricalcium silicate hydration”. *Cement and Concrete Research* 16 (1985), pp. 17–22.

[18] Stephen Brunauer and S.A. Greenberg. “The Hydration of Tricalcium Silciate and beta-Dicalcium Silicate at Room Temperature”. *Proceedings of the fourth international symposium on the chemistry of cement, Wahsington* 1 (1960), pp. 135–166.

[19] Jeffery W. Bullard et al. “A parallel reaction-transport model applied to cement hydration and microstructure development”. *Modelling and simulation in materials science and engineering* 18 (2010).

[20] Jeffrey W. Bullard et al. “Mechanisms of cement hydration”. *Cement and Concrete Research* 41 (2011), pp. 1208–1223.

[21] Gerry C. Bye. *Portland cement: Composition, production and properties, Second edition.* Thomas Telford, 1999.

[22] J.W. Cahn. “The kinetics of grain boundary nucleated reactions”. *Acta Metallurgica* 4 (1956), pp. 449–459.

[23] James R. Clifton and James M. Pommersheim. “Mathematical modeling of tricalcium silicate hydration”. *Cement and Concrete Research* 9 (1979), pp. 765–770.

[24] L.E. Copeland, D.L. Kantro, and George Verbeck. “Chemistry of Hydration of Portland Cement”. *Chemistry of Cement, Fourth International Symposium, Washington* 1 (1960), Paper IV-3 pp. 429-468.

[25] Mercedes Costoya. *Effect of Particle Size on the Hydration Kinetics and Microstructural Development of Tricalcium Silicate.* Doctoral Dissertation Ecole Polytechnique Fédérale de Lausanne (EPFL), 2008.

[26] M Daimon, S Ueda, and R Kondo. “Morphological study of hydration of tricalcium silicate”. *Journal of materials science* 1 (1971), pp. 391–401.

[27] Denis Damidot and André Nonat. “C3S hydration in diluted and stirred suspensions: (I) study of the two kinetic steps”. *Advances in Cement Research* 6 (1994), pp. 27–35.

[28] Denis Damidot and André Nonat. “C3S hydration in diluted and stirred suspensions: (II) properties of C-S-H precipitated during the two kinetic steps”. *Advances in Cement Research* 6 (1994), pp. 83–91.

[29] Denis Damidot, André Nonat, and Pierre Barret. “Kinetics of Tricalcium Silicate Hydration in Diluted Suspensions by Microcalorimetric Measurements”. *J. Am. Ceram. Soc.* 73 (1990), pp. 3319–22.

[30] D.D. Double, A. Hellawell, and S.J. Perry. “The hydration of Portland cement”. *Proceedings of the Royal Society, London* 3 (1978), pp. 435–451.

[31] P.C. Fonseca and H.M. Jennings. “The effect of drying on early age morphology of C-S-H as observed in environmental SEM”. *Cement and Concrete Research* 40 (2010), pp. 1673–1680.

[32] S. Garrault-Gauffinet et al. “Experimental investigation of calcium silicate hydrate (C-S-H) nucleation”. *Journal of Crystal Growth* 200 (1999), pp. 565–574.

[33] Sandrine Garrault-Gauffinet, Tanja Behr, and André Nonat. “Formation of the C-S-H Layer during Early Hydration of Tricalcium Silicate Grains with Different Sizes”. *J. Phys. Chem. B* 110 (2005), pp. 270–275.

[34] Sandrine Garrault-Gauffinet and André Nonat. “Study of C-S-H growth on C3S surface during its early hydration”. *Langmuir* 38 (2001), pp. 435–442.

[35] E.M. Gartner and J.M. Gaidis. “Hydration Mechanisms, I”. *Materials science of concrete, edited by Jan Skalny* 1 (2011).

[36] E.M. Gartner et al. *Structure and performance of cements,Chapter 3: Hydration of Portland cement*. Vol. 14. Spon press, Bensted and Barnes, 1914.

[37] A.M. Ginstling and B.I. Brounhstein. “On diffusion kinetics in chemical reactions taking place in spherical powder grains (in Russian)”. *Zhur. Priklad. Khim.* 23 (1950).

[38] A. Grudemo. “An electronographic study of the morphology and crystallization properties of calium silicate hydrates”. *Swedish Cement and Concrete Research Inst. Proc. No 26* 23 (1955).

[39] A. Grudemo. “Discussion of "The structures of cement hydration compounds"”. *Proceedings of the third international symposium on the chemistry of cement, London 1952* 23 (1952), pp. 247–253.

[40] P.E. Halstead and C.D. Lawrence. “Kinetics of Reaction in the System CaO-SiO2-H2O”. *Fourth International Symposium on the Chemistry of Cement, Washington* (1960).

[41] T. Harada, M Ohta, and S Takagi. “Mechanisms of Portland Cement hydration”. *J. Ceram. Soc. Jpn* 86 (1979).

[42] Peter. C. Hewlett. *Lea’s Chemistry of Cement and Concrete, Fifth edition*. Butterworth-Heinemann, Elsevier, 2019.

[43] Tulio Honorio et al. “Modeling hydration kinetics based on boundary nucleation and space-filling growth in a fixed confined zone”. *Cement and Concrete Research* 83 (2016), pp. 31–44.

[44] Wilhelm. Jander. “Reacktionen im festen Zustande by höheren Temperaturen. Reaktiongeschwindigkeiten endotherm verlaufender Umsetzungen”. *Zeitschrift für Anorganische und Allgemeine Chemie* (1927), pp. 1–30.

[45] Wilhelm. Jander. “Reacktionen im festen Zustande by höheren Temperaturen. Reaktiongeschwindigkeiten exotherm verlaufender Umsetzungen”. *Zeitschrift für Anorganische und Allgemeine Chemie* (1927), pp. 31–52.

[46] H.M. Jennings, B.J. Dalgleish, and P.L. Pratt. "Morphological Development of Hydrating Tricalcium Silicate as Examined by Electron Microscopy Techniques". *Journal of materials science* 64 (1981), pp. 567–572.

[47] Hamlin Jennings. "Aqueous Solubility Relationships for lhvo Types of Calcium Silicate Hydrate". *J. Am. Ceram. Soc* 69 (1986), pp. 614–18.

[48] Elizabeth John, Thomas Matschei, and Dietmar Stephan. "Nucleation seeding with calcium silicate hydrate – A review". *Cement and Concrete Research* 113 (2018), pp. 74–85.

[49] J. G. M. de Jong, H. N. Stein, and J. M. Stevels. "Hydration of tricalcium silicate". *Journal of applied chemistry* 17 (1967), pp. 246–250.

[50] Patrick Juilland. *Early Hydration of Cementitious Systems*. Doctoral Dissertation Ecole Polytechnique Fédérale de Lausanne (EPFL), 2009.

[51] David M. Kirby and Joseph J. Biernacki. "The effect of water-to-cement ratio on the hydration kinetics of tricalcium silicate cements: Testing the two-step hydration hypothesis". *Cement and Concrete Research* 42 (2012), pp. 1147–1156.

[52] Knut O. Kjellsen and Harald Justnes. "Revisiting the microstructure of hydrated tricalcium silicate – a comparison to Portland cement". *Cement and Concrete Research* 26 (2004), pp. 947–956.

[53] Torben Knudsen. "Modelling hydration of Portland cement, The effect of Particle Size Distribution". *Proceedings of the engineering foundation conference, Hennicker, New Hampshire. Publication Department, Engineering Foundation, New York* (1982), pp. 125–149.

[54] Renichi Kondo and Shunro Ueda. "Kinetics and Mechanisms of the Hydration of Cements". *Tockyo Symposium* 2 (1968).

[55] Nina Krautwurst et al. "Two-Step Nucleation Process of Calcium Silicate Hydrate, the Nanobrick of Cement". *Chemistry of materials* 107 (2018), pp. 2895–2904.

[56] Aslam Mohamed Kunhi et al. "An atomistic building block description of C-S-H - Towards a realistic C-S-H model". *Cement and Concrete Research* 107 (2018), pp. 221–235.

[57] F.V. Lawrence and J.F. Young. "Studies on the hydration of tricalcium silicate pastes. I scanning electron microscopic examination of microstructural features". *Cement and Concrete Research* 3 (1973), pp. 149–161.

[58] Frederick Measham Lea. *Lea's Chemistry of Cement and Concrete, Fourth edition*. Wiley & Sons, 1998.

[59] Delphine Marchon. *Controlling cement hydration through the molecular structure of comb copolymer superplasticizers*. Doctoral Dissertation Eidgenössische Technische Hochschule Zürich (ETH Zurich), 2016.

[60] Enrico Masoero, Jeffrey J. Thomas, and Hamlin M. Jennings. "A Reaction Zone Hypothesis for the Effects of Particle Size and Water-to-Cement Ratio on the Early Hydration Kinetics of C3S". *J. Am. Ceram. Soc.* 97 (2013), pp. 967–975.

[61] Berta Mota-Gasso. *Impact of alkali salts on the kinetics and microstructural development of cementitious systems*. Doctoral Dissertation Ecole Polytechnique Fédérale de Lausanne (EPFL), 2015.

[62] Luc Nicoleau and Maria Alice Bertolim. "Analytical Model for the Alite (C3S) Dissolution Topography". *J. Am. Ceram. Soc* 99 (2016), pp. 1–11.

[63] Luc Nicoleau and André Nonat. "A new view on the kinetics of tricalcium silicate hydration". *Cement and Concrete Research* 86 (2016), pp. 1–11.

[64] Arne. C. Nielsen. *Kinetics of Precipitation*. Pergamon, Oxford, 1964.

[65] André Nonat. "The structure and stoichiometry of C-S-H". *Cement and Concrete Research* 34 (2004), pp. 1521–28.

[66] T.L. O'Conner and et al. *J. Phys. Chem.* 62 (1958), pp. 1195–1198.

[67] Ivan Odler and Samir Abdul-Maula. "Polymorphism and Hydration of Tricalcium Silicate Doped With ZnO". *J. Am. Ceram. Soc.* 66 (1983).

[68] Alexandre Ouzia and Karen L. Scrivener. "The needle model: A new model for the main hydration peak of alite". *Cement and Concrete Research* 115 (2019), pp. 339–360.

[69] L.J. Parrot and D.C. Killoh. "Prediction of Cement Hydration". *British Ceramic Proceedings, The chemistry and chemically-related properties of cement, edited by F.P. Glasser* (1984), pp. 41–53.

[70] Alexandra Quennoz and Karen Scrivener. "Interactions between alite and C3A-gypsum hydrations in model cements". *Cement and Concrete Research* 44 (2013), pp. 46–54.

[71] I. G. Richardson. "The calcium silicate hydrates". *Cement and Concrete Research* 38 (2016), pp. 137–158.

[72] John. E. Rossen. *Composition and morphology of C-A-S-H in pastes of alite and cement blended with supplementary cementitious materials*. Doctoral Dissertation Ecole Polytechnique Fédérale de Lausanne (EPFL), 2014.

[73] Y Sakalli and R Trettin. "Investigation of C3S hydration by environmental scanning electron microscope". *Cement and Concrete Research* 259 (2015), pp. 53–58.

[74] George W. Scherer, Jie Zhang, and Jeffrey. J Thomas. "Nucleation and growth models for hydration of cement". *Cement and Concrete Research* 42 (2012), pp. 982–993.

[75] Karen L. Scrivener, Patrick Juilland, and Paulo J.M. Monteiro. "Advances in understanding hydration of Portland cement". en. *Cement and Concrete Research* 78 (Dec. 2015), pp. 38–56.

[76] Karen L. Scrivener and André Nonat. "Hydration of cementitious materials, present and future". en. *Cement and Concrete Research* 41.7 (July 2011), pp. 651–665.

[77] Karen Louise Scrivener. *The development of microstructure during the hydration of Portland cement*. Doctoral Dissertation Imperial College, University of London, 1984.

[78] J. Skalny and J.F. Young. "Mechanisms of Portland Cement hydration". *7th International Congress on the Chemistry of Cement* 1; Principal reports. Sub-Theme II-1 - 1/3 to 1/11 (1980).

[79] Andreas Stumm et al. "Incorporation of zinc into calcium silicate hydrates, Part I: formation of C-S-H(I) with C/S=2/3 and its isochemical counterpart gyrolite". *Cement and Concrete Research* 35 (2005), pp. 1665–1675.

[80] H.F.W. Taylor. *Cement chemistry, Second edition*. Thomas Telford, 1997.

[81] H.F.W. Taylor. "Chemistry of Cement Hydration". *8th International Congress on the Chemistry of Cement, Rio de Janeiro* (1986).

[82] N Tenoutasse and A. De Donder. "The kinetics and Mechanism of Hydration of Tricalcium Silicate". *Silicates Industrielles* 12:7 (1970).

[83] J.J. Thomas. "A New Approach to Modeling the Nucleation and Growth Kinetics of Tricalcium Silicate Hydration". *J. Am. Ceram. Soc.* 90 (2007), pp. 3283–3288.

[84] J.J. Thomas. "The Instantaneous Apparent Activation Energy of Cement Hydration Measured Using a Novel Calorimetry-Based Method". *J. Am. Ceram. Soc.* 95 (2012), pp. 3291–3296.

[85] J.J. Thomas, H.M. Jennings, and Jeffrey J. Chen. "Influence of Nucleation Seeding on the Hydration Mechanisms of Tricalcium Silicate and Cement". *J. Phys. Chem.* 113 (2009), pp. 4327–4334.

[86] Klaas Van Breugel. *Simulation of hydration and formation of structure in hardening cement-based materials, Hymostruc*. Doctoral Dissertation Delft University of Technology, 1991.

[87] D. Werner and et al. *Zement* (1928), 1002-1005 and 1071-1076.

[88] Zhidong Zhang, George W. Scherer, and Alexandre Bauer. "Morphology of cementitious material during early hydration". *Cement and Concrete Research* 107 (2018), pp. 85–100.

[89] H Zur Strassen. "Zur Frage der nicht-selectiven Hydratation der Zementminerale" (1959).

3 The main hydration peak

Note: This chapter was published in Cement and Concrete research in January 2019 "The needle model: A new model for the main hydration peak of alite.".

Before the article, this chapter starts with a summary of the key findings of the article and answers to frequently raised questions and criticisms.

Contents

Summary of the article

The conclusions brought forward in this summary draw on the test of the model on 14 experiments, which is a wider set of experiments than any other alite hydration model yet published. All the model parameters were constrained within experimental confidence intervals, in particular the nucleation and growth rates are quantitatively true to SEM observations. Across the 14 experiments, the average error on the heat flow and DoH were respectively of $16.2 \pm 9.1\%$ and $10.1 \pm 9.9\%$.

The main hydration peak should be seen as a single event, the separation into acceleration and deceleration period is arbitrary and a heritage of Kondo and Ueda in 1968 who were the first to qualitatively describe the calorimetry curve of alite hydration. There is no qualitative change of mechanisms, only a quantitative and progressive one. Their division of the peak into two stages biased the debate for the following five decades.

A quantitative deepening of Bazzoni's thesis

The qualitative microstructural story proposed by Bazzoni in her thesis has been quantitatively demonstrated, though with some shades.

- The transition from the acceleration to the deceleration period coincides with the covering of the alite grain surface in combination with the progressive slowdown of the needles growth. Neither the full coverage of the surface nor the progressive slowdown of the needles is alone sufficient to account for the transition.
- The contribution of the inner C-S-H to the output heat flow is quantitatively negligible up to the end of the deceleration period. Even if the inner C-S-H starts to form as early as at the peak time as Bazzoni observed, the computation of the heat released demonstrate it is quantitatively negligible: at least 80% of the heat released during the deceleration is accounted by the outer C-S-H only.
- To model C-S-H as needles enabled to show that the increase of needle size due to the Zinc doping quantitatively explains the heat flow increase
- 90% of the needles nucleate within a window of 4 hours +/- 1hour.

An answer to Taylor's question about the role of small grain dissolution

That the consumption of the small grains could possibly explain part of the transition from acceleration to deceleration has been raised by Taylor though he did not expect it to be the sole mechanism [27, p. 155].

The impact of the small grain dissolution on the hydration has been quantified for the first time.

- Grains below $4 \pm 1 \mu m$ completely dissolve within 24 hours for w/c between 0.32 and 0.5.
- The heat flow release of PSDs that incorporate a large fraction of small grains are sharpened and shifted left, but the overall shape remains the same. The dissolution of the small grain is not per se the mechanism causing the transition except perhaps for PSDs entirely below 1um
- As a rule of thumb, for common log-normal PSDs encountered for alite and cement powders, the impact of the small grains dissolution on the heat flow is negligible below 50% DoH; in practice this corresponds to powders with d_v50 coarser than $10 \mu m$.

Two bilinear equations with needles length and powder specific surface

The heat and heat flow for needle length and specific surface were derived:

$$DoH = \frac{\eta_1}{\eta_3} * S_{spe} * M_{alite} * l_{24h} * f(k_n, s_0, t_c, t)$$

$$HF(t) = \Delta_r \frac{\eta_1}{\eta_3} * S_{spe} * M_{alite} * l_{24h} * \frac{df(k_n, s_0, t_c, t)}{dt}$$

The DoH and heat flow are thus *proportional*, not simply monotonously increasing, to the 24 hour needle length and specific surface of the powder. These equations hold for the first day as long as the DoH is lower than 50% or for powders with d_v50 coarser than $10 \mu m$.

The slope of the acceleration period when plotted per unit surface is a characteristic function of the surface chemical reactivity

Within the range [1 100]μm where the model has been tested, the slope of the acceleration period when plotted per unit of surface is independent of the PSD. In this sense, it allows for the comparison of the reactivity of different alites.

In particular, the fact the model could fit 14 experiments with very similar parameters entails that the surface reactivity of grains is independent of their size within the range [1 100] μm: $1 \mu m$ grains react in exactly the same manner as $100 \mu m$. The difference in specific surface is sufficient to account for the increased reactivity of smaller grains, there is a priori no need to invoke a higher density of defects for all experiments quoted or made in this thesis.

Whenever it comes to comparing the chemical reactivity of alites, the representation per unit surface is thus more relevant than the widespread representation per unit of mass.

Answers to frequently raised questions and criticisms

1 - The fact that the model has been tested on a large number of experiments is not sufficient to state that the model is definitely validated. For example, a large set of identical experiments would not prove that a fitted model is valid.

The model has indeed only been validated on the available data in the literature, and the stringency of its test is limited by this data. Still, the variation of the peak height vary by a factor of 30: the peak height of Costoya 82 μm shown in orange on figure 15 is about 0.5 mW/g whereas Bazzoni's zinc doping experiments on a fine powder on figure 13 right exhibits a 15 mW/g height. The model is able to capture this wide amplitude. This does not prevent the model to be refuted in the future.

2 - The setting time is fixed each time based on the measured heat flow. In the event that this parameter has an impact on all that follows, then the argument that the large fitted data set is sufficient would not hold.

This parameter has only a translational effect. This is based on the assumption that the main hydration peak is relatively independent from the preceding induction period; this justifies the separation into two stages of the hydration kinetics. For instance annealing experiments made by Bazzoni, Cantoni & Scrivener on C_3S (reproduced on figure 8 of chapter 2) did not show strong quantitative influence of the initial density of defects on the main peak. Yet, this is indeed only an approximation: strictly speaking the topography of the alite surface might be altered during the induction period and influence the main hydration peak.

3 - The statement that the reactivity of small grains is identical to those of bigger grains may only be valid for the main hydration peak, not for the induction period.

Indeed the article only show under the subsection 4.2 on the impact of the dissolution of the small grains that the surface reactivites of small and big grains are exactly identical, but this is actually only shown to apply to the main hydration peak.

4 - Are the roughness factor Rou and form factor F computed separately or is their ratio computed directly?

The ratio $\frac{Rou}{F}$ is indeed computed directly as it is not possible to separate both without an image analysis by SEM. This ratio represents the "grain intrinsic specific surface" and its value is assumed to be equal to 6 for all experiments in the paper (except for Xuerun Li where it could be measured). This means that for any grain of size r, its surface is 6 times larger than a spherical smooth grain with the same volume. This corresponds to a slightly rough rugby ball.

This ratio can be directly computed with a formula derived in the appendix "Derivation of the Rou/F ratio from the PSD and BET specific surface".

5 - The function for nucleation and growth rates have no physical basis. These functions are said to have no free parameters, which is not true (rather, the parameters were arbitrarily chosen to match certain observations, and those values were found to provide good fits to a variety of data). The composition of the pore liquid, which provides the driving force for nucleation and growth, is not considered

The function for nucleation and growth rates are justified by the fact that:

- they have been *measured* (see for instance the figures 31 and 33 of chapter 4 where the fitting function overlaps the measurements). Measured incertitude intervals for the input parameters are given in the table at then of chapter 3.
- the bell shape nucleation profile is justified not only by the observations but also by theoretical considerations exemplified in the paper from Andalabi et al. ("On the mesoscale mechanism of synthetic calcium–silicate–hydrate precipitation: a population balance modeling approach", Journal of Materials Chemistry A, 2018) where it is shown that the nucleation rate profile in the case of synthetic C-S-H precipitation does have a bell shape (fig. 5 a) of this article).

As a consequence, by contrast with all other existing models at the time of writing this thesis, the number of needles per unit surface and their sizes with time *precisely* fall within the measured incertitude intervals. However, the reason why the the nucleation rate is bell shaped and why the needle initially grow fast and then slowly is not known though discussed in section 4.3 and 4.4 of this chapter. The discussion explains that these could be explained by the combination of the pore solution concentrations evolution as well as defects accumulation in the needles.

6 - The model is said to have no fitting parameters but there is a long table of fitted values at the end of the article.

By contrast with all other models, the needle model has no *free* fitting parameters but only *constrained* parameters (section 6.2 of this chapter). In other words, there *is* a fitting process, but the values are *not just* selected to provide good fits, they match the measurements. This is stated twice: once in the introduction to the section 3 "Comparison of the model with experiments and discussion" and repeated in the conclusions.

7 - The model is only phenomenological, it merely describes the peak, but does not explain it. To achieve that, the pore solution concentration evolution with time should be considered.

There is no agreement on the definition of a phenomenological model versus a mechanistic model[1]. If we consider the definition of a phenomenological model given by Wikipedia, a phenomenological model is a model not derived from first principles. But the first principles of quantum mechanics are not the ultimate principles as they do not consider general relativity. Even if they were, to explain the main hydration peak by injecting Schrödinger equations into a computer that could handle it would only reproduce what nature does, it would not provide a satisfying explanation for the human mind.

Behind this criticism perhaps lies the argument that a mechanistic model should explain the nucleation and growth rate in terms of pore solution concentrations. Though I agree that this is one of the next step to reach (as is detailed in subsections 4.3 and 4.4 of this chapter, and repeated in the conclusions of this thesis), whether this constitutes a mechanistic model remains subjective: the function describing the dependence of the nucleation and growth rate with the pore solution could still be qualified as "empirical" or "phenomenological". This function would then be possibly explained in terms of atomistic events (atoms detachment, attachment, diffusing on the surface, etc.)

What the model unequivocally defends is the scenario that the combination of needles covering the surface while gradually entering a slow growth regime. This scenario is fecund as it pushes the investigation forward by asking new questions such as why is there a transition from a fast to a slow growth regime of the C-S-H needles.

[1] Whether Science aims at *explaining* or *describing* the world is a classic debate in philosophy of Science. The debate opposes "realists" who believes that Science uncovers the true nature of the phenomena against the pragmatists, instrumentalists and conventionalists who believes that Science only aims at predicting or describing the phenomena. Conventionalists, like Quine and Duhem for instance, defend that the ultimate aim of Science is to describe the world in the most economic manner (with as low a number of concepts, principles and equations as possible), to provide a structured classification of the phenomena. According to this view, scientific theories are not even approximations of a elusive essence of the phenomena.

The needle model: a new model for the main hydration peak of alite

Authors: Alexandre Ouzia and Karen Scrivener EPFL STI IMX LMC, MXG 230, Station 12, CH-1015, Lausanne, Switzerland

Corresponding author: alexandre.ouzia@epfl.ch

Abstract

This article presents a new model for the main hydration peaks of tricalcium silicate and alite on the assumption that C-S-H nucleates and grows as needles. The model relies only on directly observable quantities and reproduces the transition from the acceleration to deceleration periods without assuming a diffusion barrier or impingement. Simulations of the model based on measured characteristics of the grains and needles are compared with experimental data and satisfactory agreement is found across a wide range of experiments. Because the model disentangles the impact of each input parameter, it sheds new light on some aspects of alite hydration. In particular the model provides a quantification of the impact of the consumption of the small grains and shows that it should not be neglected as soon as several tens of percent of the hydration reaction is reached. Finally, the article provides a critical examination of other models.

Key words: *alite, C3S, hydration, modelling, C-S-H needles/fibrils.*

3.1 Introduction

Portland cement is the most produced material in the world. It contains four major phases: alite, belite, calcium aluminate, calcium aluminoferrite, which along with calcium sulphate added during grinding, release six main chemical elements: calcium, oxygen, silicon, aluminium, iron and sulfur, into solution, where they react and form new solid hydrate phases. To understand the complexity of its microstructural development during hydration, a common strategy has been to study the hydration of each reactant separately.

For that reason, alite, an impure form of tricalcium silicate (C_3S) and the main phase of PC, which amounts to roughly 2/3 of its mass, has been the focus of many studies for at least a century [1] [2] [3]. The hydration of alite has been divided into six stages according to its calorimetry curve [3] [4] (figure 1). This curve presents two peaks: the first one corresponds to the initial dissolution of alite in water and the second one to the massive precipitation of hydrates, namely Portlandite and Calcium Silicate Hydrate (respectively CH and C-S-H in cement chemistry notation) which results in the setting and hardening.

This paper focuses on the mechanisms operating during the second peak, i.e. the main hydration peak corresponding to the third and fourth stages, also called acceleration and deceleration periods. For the first periods, the interested reader might refer to [5] or to two recently published reviews [6] [7] or to an older and more exhaustive one summing up the literature before the year 2000 [3].

3.1.1 The main hydration peak debate

Although there is a general agreement that nucleation and growth is the underlying mechanism behind the acceleration period, there is as yet no consensus on the mechanism causing the transition to the deceleration period. Though many models have been developed ([8] is a recent review) two core hypotheses emerge on which models have been built.

The nucleation and growth hypothesis and related models This hypothesis states that the transition from acceleration to deceleration period can be explained by the progressive impingement of the hydrates. A variety of models have been built on this hypothesis, each of them introducing different nuances in the pattern of nucleation and growth.

The first cluster of nucleation and growth models stems from the Avrami model, originally derived in the context of the solidification of metals [9] [10] [11] and imported into the field by Tenoutasse and DeDonder [12]. In these models the growth is assumed proportional to the amount of surface of the hydrate. Because observations show that the C-S-H nucleation is heterogeneous rather than homogeneous, a subsequent refinement of the Avrami model led to the subclass of the boundary nucleation and growth (BNG) models where nucleation is assumed to take place on the surface of alite grains [13] [14]; following the Cahn model

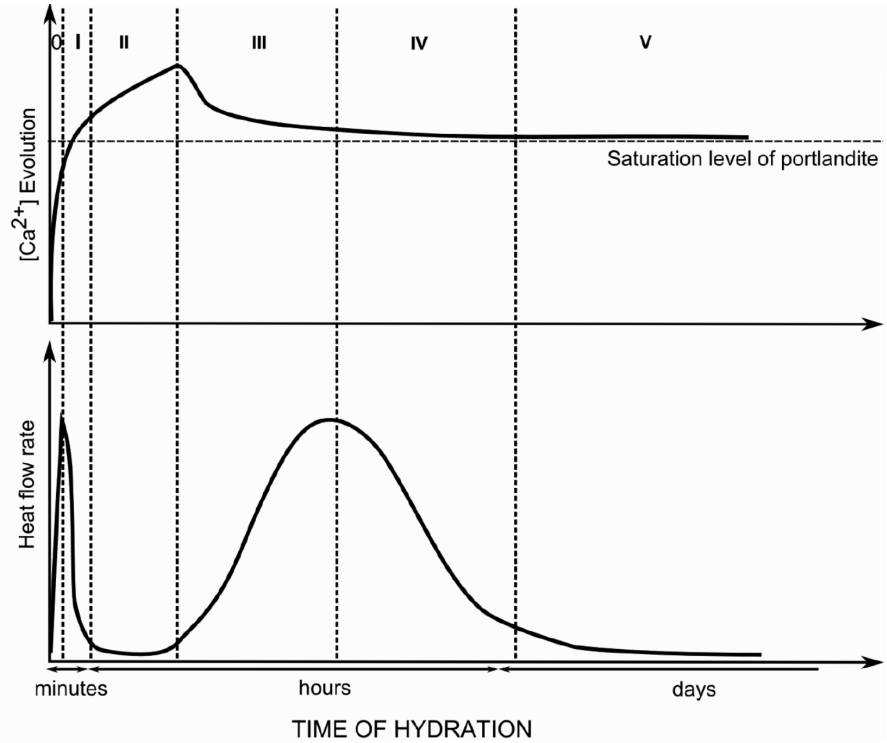

Figure 3.1 – Typical pore solution analysis and calorimetry curve of PC and its interpretation in five stages; from [3].

for metal recrystallization from grain boundaries [15]. Further refinements include a varying C-S-H density [16][17][18] or an anisotropic growth of the C-S-H [14]. The varying density hypothesis was raised as all constant C-S-H density simulations were shown to lead to almost no impingement and therefore no transition at the peak. The anisotropic growth was raised as outer-C-S-H hydrates are never observed by SEM (Scanning Electron Microscopy) to be uniform layers but rather foils or needles.

The second cluster of nucleation and growth models are the recently developed confined growth models [19] [20] [21] that explicitly limit the space where the products can precipitate to account for the impingement. When the hydrates reach the borders of the spherical box around the particle, the reaction stops at this place.

The third cluster are the simulation platforms that model the hydration of a whole powder and thus explicitly calculate the impingement of the hydrates: the former Jennings and Johnson model [22], subsequently developed by Navi and Pignat [23] [24] and finally the recently developed μic (pronounced “Mike”) platform [16] [17][18]. This last platform allows a range of mechanisms to be simulated, including varying C-S-H density and the diffusion barrier hypothesis.

The diffusion barrier hypothesis and related models This hypothesis supposes that the transition from acceleration to deceleration period can be explained by the progressive thickening of the C-S-H layer around the alite grain. When the C-S-H layer becomes thick enough, it acts as a diffusion barrier and the reaction switches from the nucleation and growth mode to the diffusion mode. By contrast with the previous hypothesis, this one suggests a transition from one controlling mechanism to another one thus legitimating the description of the main hydration peak into two periods.

A variety of models have been built on this hypothesis, dating back to the first analytical model by Kondo [25] in 1968 to the simulation platform HYMOSTRUC [26] that can take into account a realistic PSD. The interested reader may refer to [3] or [7] to get more information on these models.

Additional consideration: the consumption of the small grains The hypothesis that the consumption of the small grains could possibly explain part of the transition from acceleration to deceleration period has been raised by several researchers though they do not expect it to be the sole mechanism [27] [28] [29]. Grains below 3 μm have been observed to be completely reacted by 10 hours and grains below 7 μm by 24 hours by Scrivener [29]. Kjellsen and Justnes reached similar conclusions with most of the grains below roughly 5 μm having disappeared by 24 hours [29]. Though some models like μic, CEMHYD3D [30], HydratiCA [31] and HYMOSTRUC [26] implicitly take into account the dissolution of the small grains, the significance of the impact of the consumption of the small grains on the transition has not been studied in detail and thus remains an open question.

3.1.2 Shortcomings of previous hydration models and their underlying hypothesis

Shortcomings of nucleation and growth models assuming perpendicular impingement

The water to cement experiments of Bazzoni (reproduced in figure 8) [32] and the numerous experiments of Kirby and Biernacki [33] and Nonat made at high water to cement ratio challenge the view that perpendicular impingement (impingement between hydrates belonging to different grains) could be the mechanism leading to the transition. In their paper [33] Kirby and Biernacki showed that doubling the w/c ratio should also double the heat released if impingement was the mechanism (to double the w/c ratio is to double the volume between the grains so that the volume of hydrates and thus peak height and width should be doubled). However, it is not what they observed experimentally: the heat released by C_3S, alite or OPC barely changed.

Perhaps most convincing are direct SEM observations of polished sections of alite and C3S pastes at the end of the first day, that is long after the peak. The majority outer C-S-H shells are plainly not seen to impinge even at w/c = 0.4 as shown in chapter 3 of [32] or on figure 4 of [28]

reproduced here on figure 2 right. Recent observations by electron microscopy techniques made by Bazzoni [32][34] reinforces this point. By making precise observations of the C-S-H needles she noticed that needles stop growing in the range 200nm to 500nm, even if there is still space available. She suggested that the transition from acceleration to deceleration is caused by the cumulative effect of the needles covering alites and the end of the needle growth. We will return to this hypothesis.

As a conclusion, all models assuming perpendicular impingement to play a major role are in contradiction with experimental evidences from calorimetry and microstructural observations. All the nucleation and growth models developed before year 2000 are concerned by this conclusion and also the recently Boundary Nucleation and Growth (BNG) models assuming perpendicular impingement [13][14][18].

Shortcomings of diffusion-based models

Several arguments challenge the assumption that the C-S-H acts as a barrier. First the activation energy does not change with temperature. Then simulations made by Bishnoi on μic [18] showed that the diffusion coefficient needed to be varied by an order of magnitude from one alite PSD to another one to fit the calorimetry curve, a variation too wide to be realistic considering the C-S-H is the same. Third the presence of a gap between the anhydrous grain and the C-S-H scaffold as shown on figure 2 questions this explanation: if the C-S-H shell acts as a diffusion barrier then the supersaturation of the water enclosed in this gap would be higher than at the outward extremity of the shell (i.e. at the needles tip); yet the growth does not take place within this gap before the end of the first day.

Shortcomings of confined growth models

Following the Kirby and Biernacki paper, a set of new models has come out that assume the C-S-H to nucleate and grow only within a zone of approximately one micron around the alite grain.

In 2011, Biernacki and Xie developed a single particle model exploring this hypothesis [20]. By definition this model does not take into account the particle size distribution and can therefore not be tested against experiments. Yet this model predicts 2 μm particles to release more heat at 24 hours than any bigger particle (figure 11 of [20]). This is in contradiction with SEM microstructural observations: at 24 hours particles below 5um have completely been consumed [28], and 2 μm particles vanish even before 10 hours [29].

In 2013, Masoero et al. built another model based on the confined growth hypothesis [19]. By contrast with the previous model, this one allows for the particle size distribution thus enabling the comparison with experimental data. They showed the model is able to fit Costoya's PSD experiment [35] while keeping the exact same set of parameters, except for the thickness of

the confined growth zone which fluctuates around an average of 1um. This value is, however, questionable: it is beyond the thickness uncertainty interval measured by Costoya by more than factor of two (p88 of [35]); Bazzoni (fig 4.35 of [32]) and Gauffinet [36] also found the average thickness at one day to lie in the range 200-500 nm. Moreover, the starting time of hydration is assumed to be negative (equal to minus three hours) which is unphysical.

In 2016, Honorio et al. published yet another confined growth model, this time assuming an increasing C-S-H density and a diffusion control mechanism after the peak [21]. As explained in the preceding subsection, diffusion is certainly not the underlying mechanism behind the transition. Also, the model neglects the small grains consumption so that the 2 µm grains release more heat at 24 hours than any bigger size thus being the biggest contributor to the heat release beyond one day. As already mentioned, this is in contradiction with SEM observations.

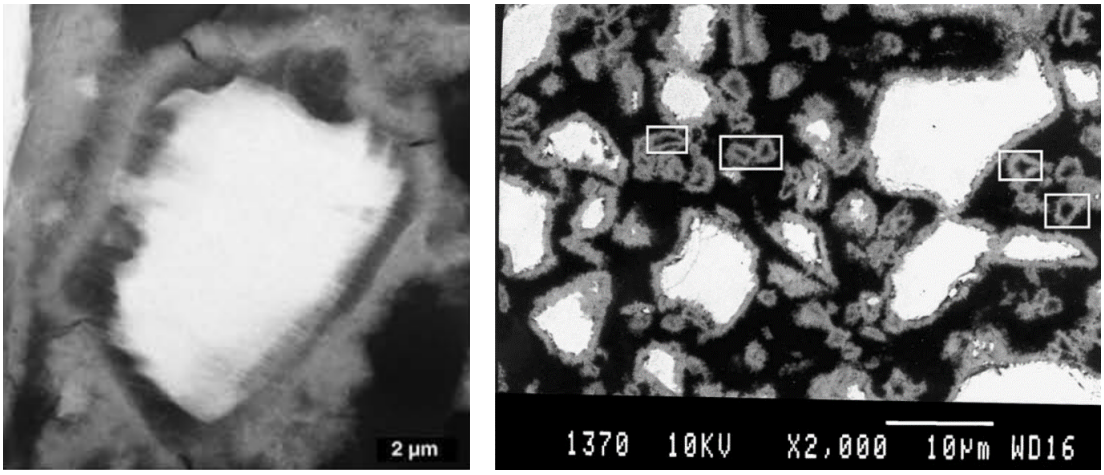

(a) *(b)*

Figure 3.2 – BSE-SEM images of alite grains at one hydration day. A gap is observed between the grain and the product layer. Note the complete consumption of grains below 3 µm leaving the so-called hollow grains behind them. Left: image taken from [37]. Right: image taken from [28].

Two other issues shared by most models: an opaque testing and fitting process

All hydration models developed so far rely on at least four fitting parameters which is the required number of parameters to fit asymmetric bell peaks [38] such as the typical calorimetry curve profile; mathematically this means the fit is underconstrained so that different combinations of parameters could fit the curve. Moreover, except for Honorio [21], Masoero[19] and Termkajornkit models [39], models are most frequently shown to be able to fit about the same number of calorimetry curves as fitting parameters which does not seem to be a stringent enough test.

Although it may be argued that the fitting parameters from hydration models have a physical meaning (growth rate, diffusion coefficient, nucleation rate, etc.) in most cases the values

obtained for these parameters are neither taken from nor compared with experiments and are left free to vary over large intervals. In the absence of any experimental constraints it is hard to objectively criticize these fitted values and their variability; or in other words: it is difficult to know if these are realistic or not and thus hard to draw firm conclusions with confidence. Another issue stems from input parameters that are not directly measurable at all, like the diffusion coefficient of ions through layers of product, or unphysical, like negative starting times for examples. For the values of those input parameters that cumulate these deficits it becomes impractical to decide whether they have any basis in reality.

In addition, the absence of a common experimental benchmark set further complicates the comparison and tests of hydration models. Though Costoya's PSD experiments has frequently been used for that purpose, it only deals with four curves.

Finally, the fitting process is never explicit[2] . When no error definition is clearly stated, one might assume that curves are fitted by visual trial and error instead of standard optimisation techniques such as the gradient method for instance [40]. In that case, fits are likely subjective and more critically the question of the uniqueness of the solution is not raised: the possibility for a given model to fit the exact same curve with different combinations of values for its input parameters is not explored. By contrast with other scientific fields using statistical models, these tools have not yet been imported in cement hydration modelling and hinder impartial model comparison.

Conclusions on the shortcomings of previous models

As a first conclusion, all hydration models based either on perpendicular impingement or diffusion during the first day fall short of experimental observations. Confined growth models developed so far also fail to be convincing for more specific reasons detailed previously. Yet they are closer to reality by assuming that C-S-H only grows within a confined zone around the grains.

Even if these models were compatible with experimental observations most of them would still suffer from an opaque testing and fitting process thus weakening their pretention to back up their underlying hypothesis. These statements do not mean these models cannot be used as interpolation or extrapolation tools, as such they retain their relevance; but in our opinion these models do not yet provide a firm defence of their underlying hypothesis regarding the main hydration peak.

3.1.3 Can outer C-S-H be modelled as needles?

The investigations about the C-S-H structures in the decade following World War II already established the existence of a fibril like C-S-H polymorph based on X-ray and electron diffraction evidence (by Taylor and Grudemo as cited by Bernal in [41]). The development of the

[2] At least in all the hydration models quoted in this article.

scanning electron microscope enabled further progress and perhaps the first outer C-S-H SEM observation revealing its topography was made by Grudemo in 1960 [42]: "Apart from larger unhydrated particles, the material seems to consist of about equal amounts of finely textured irregular masses, of rather long branched needles, and of thin plates, presumably CH crystals". In the following two decades, it has repeatedly been described as "acicular" which etymology means "needle-like" in [42][43], fibril-like [44] or directly as needles[45][47][48][29]. In reference books such as Taylor "Cement Chemistry" [27] or Leas "Cement and Concrete chemistry" [49], the same characteristic picture is shown and represented again on figure 3.

Recent SEM observations from Costoya [35], Bazzoni [32][34], Berodier [50][51], Mota-Gasso [52][53] also consistently describe outer C-S-H explicitly as needles. Other authors such as Kjellsen and Justnes [28], or Sakkali and Trettin rather use the term fibrils [58]. This latter term is also recurrent in TEM studies from Richardson [54] and Rossen [55]. Careful SEM observations show that C-S-H precipitates are tapered foils, or fibrils, we use the term "needle" here to cover all these morphologies and believe the differences arising from the exact morphology are of second order.

Jennings advocated outer C-S-H to be 5nm globules and argued that sample preparation, especially the high-vacuum required for TEM and SEM, would damage the globules and create artefacts [56]. The observation that led to the globule hypothesis stems from neutron scattering experiment [57] a technique which per se does not give any geometric representation. It is not clear how the high-vacuum of the SEM and TEM chambers would transform 5 nm globules into hundreds of nanometres long fibrils or needles. Moreover, fractured sections made by Bazzoni to measure the needle length with time show a well-defined trend, not a random distribution, they grow longer with time. Also, observations in Environmental-SEM by [58] show fractured and polished sections to be indistinguishable to high-vacuum SEM: on figure 3 and 4 fibrils/needles are clearly observed. Finally, the question of drying creating needles seems to be excluded by the recent report of needles in supercritically dried C-S-H [59].

It is also clear that outer C-S-H neither forms a uniform layer, as most diffusion-based models assume, nor spheroids as most nucleation and growth models assume. Given that the shape of the C-S-H has an impact on the equations and values taken by the parameters of the model, such as the n-exponent in the Avrami model, to model C-S-H as fibrils/needles is the closest approximation of the outer C-S-H geometry.

3.1.4 Motivation and novelties of the article

The goal of the needle model is to explore and sharpen key questions regarding the main hydration peak, first and foremost whether or not nucleation and growth of needles can account for the whole peak. In other words, the goal of this model is not to predict the calorimetry curve based on PSD, BET and SEM microstructural measurements. The questions it aims to answer and the shortcomings it avoids are detailed in the next paragraphs.

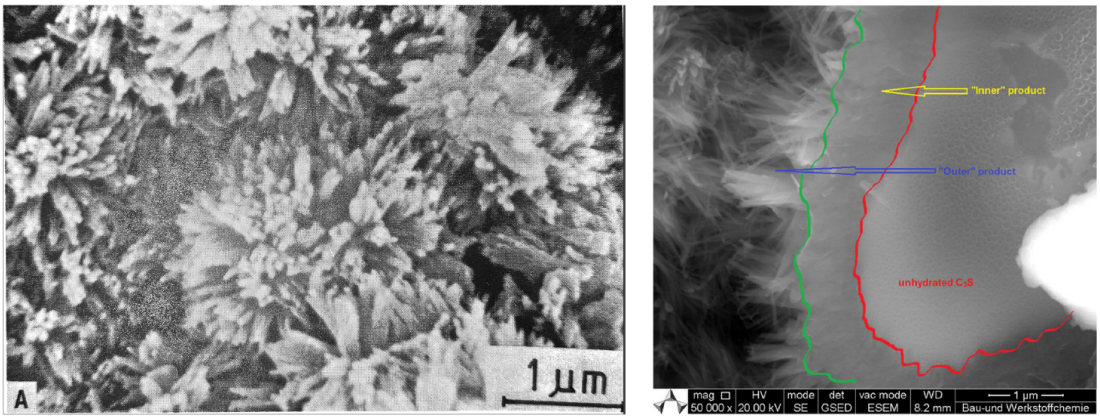

(a) *(b)*

Figure 3.3 – Pictures of outer C-S-H "needles" on alite grains. Left: surface of an alite grain during the acceleration period observed by SE-SEM taken by Scrivener[29] and as cited in Taylor textbook [27]. Right: ESEM observation of the alite surface at 4 days [58] both the outer (blue arrow that indicates the needles) and the inner (yellow arrow that indicates a smooth layer without clear structural features) C-S-H are shown. Note that the inner only start to form by the end of the first day when the reaction occurs at 20°C, before there is a gap opening between the outer C-S-H and the anhydrous core.

Initial motivation: Bazzoni's work and the main hydration peak

In her thesis [32], Bazzoni characterized the microstructure of C-S-H during alite hydration by electron microscopy. She showed that C-S-H nucleates and grows mainly as needles on the surface of alite grains during the main hydration peak. She suggested that the transition from the acceleration to the deceleration happens when the surface is completely covered with needles while at the same time the needles finish their growth. She also proposed that a transition in the growth mode of the C-S-H occurs at the time of the peak: when needles finish their growth the inner C-S-H start forming. Finally, she studied the influence of Magnesium and Zinc [34] as doping ions and found the latter to significantly increase the heat flow and degree of hydration while at the same time the C-S-H needle length increased significantly.

The first motivation of the present model is thus to quantify these qualitative statements and check:

- whether the nucleation and growth of needles is sufficient to account for the transition and the measured heat flow released; or if something else had been left unnoticed by Bazzoni
- Whether an increase in the needle length (due to zinc doping) is sufficient to account for the increased heat flow or whether something else is missed
- What could be the contribution of the formations of inner C-S-H to the measured heat released.

Second motivation: to avoid the shortcomings of the previous model and be consistent with SEM microstructural observations

Existing models have not yet been able to definitively tip the balance in favour of one hypothesis or another with regards to the transition from acceleration to deceleration. This absence of consensus may partly come from the list of shortcomings detailed in the previous section.

As a consequence, the present model *only uses physical and measurable input parameters that are constrained within experimental confidence intervals; it is consistent with SEM microstructural observations; it is tested on twice its number of parameters; errors are calculated and the fitting process is the gradient descent method.*

Third motivation: to quantitatively understand the impact of the small grains on the heat release

The third motivation is to quantitatively understand the impact of the small grain consumption. To be more specific: how much it lowers or shifts the peak? What are the contribution of different populations in a PSD? and more importantly for future models: can the consumption of small grains be neglected?

3.1.5 A model without explicit representation

Another advantage of the model is that it is an algorithm without 2D or 3D representation. This avoids the computational costs due to the representation of grains in numerical platforms". Digitisation as in CEMHYD3D or HydratiCA only allows a limited size difference between the largest and smallest grains, while vector representation as in μic or HYMOSTRUC necessitates simple geometrical shape such as spheres- this has two major consequences: first it neglects specific surface effect of the powder and second it underestimates the consumption of small grains. The drawback is that there is no explicit representation of the microstructure and the impingement of products is not considered.

3.2 Construction of the model

3.2.1 General idea

The chemical reaction between C_3S and water is:

$$Ca_3SiO_5 + xH_2O \rightarrow (CaO)_\alpha(SiO_2)(H_2O)_(x-3+\alpha) + (3-\alpha)Ca(OH)_2 \tag{3.1}$$

which in cement chemistry notations is rewritten:

$$C_3S + xH \rightarrow C_\alpha - S - H_(x-3+\alpha) + (3-\alpha)CH \tag{3.2}$$

Assuming x equal to 5.3, a density of $3.15g/cm^3$ for C_3S, a C-S-H density of $2.0g/g/cm^3$, a CH density of $2.2g/cm^3$ and a calcium to silicon ratio of 1.7 this equation can be converted in volume [18]:

$$\eta_1 V_{alite}^{consumed} + \eta_2 V_H^{consumed} \rightarrow \eta_3 V_{C-S-H}^{produced} + \eta_4 V_{CH}^{produced} \tag{3.3}$$

the η_i are respectively equal to 1.0, 1.32, 1.57 and 0.59; H is water and CH is Portlandite.

The central quantity of the model is the volume of C-S-H at any time: $V_{C-S-H}^{produced}$. Once this quantity is determined, the volume of alite consumed can be readily computed from equation (3).

From these quantities, the Degree of Hydration, DoH, and heat flow per gram of alite, H(t), can be calculated according to:

$$DoH(t) = \frac{m_{alite}^{consumed}(t)}{m_{alite}^{initial}} = \frac{V_{alite}^{consumed}(t)}{V_{alite}^{initial}} = \frac{\frac{\eta_1}{\eta_3} V_{C-S-H}^{produced}(t)}{V_{alite}^{initial}} \tag{3.4}$$

$$H(t) = \frac{d}{dt}\frac{\Delta_r H m_{alite}^{consumed}(t)}{m_{alite}^{initial}} = \frac{V_{alite}^{consumed}(t)}{V_{alite}^{initial}} = \Delta_r H \frac{d}{dt}\frac{\frac{\eta_1}{\eta_3} V_{C-S-H}^{produced}(t)}{V_{alite}^{initial}} \tag{3.5}$$

To calculate the volume of C-S-H, the volume of C-S-H produced by each grain size population is calculated and is then summed up according to the PSD:

$$V_{C-S-H}^{produced}(t) = \int_0^\infty p(R).V_{C-S-H}^{produced}(t,R)dR \tag{3.6}$$

where p(R) is the particle size density distribution in number and $V_{C-S-H}^{produced}(t)$ is the volume of C-S-H produced by one grain of radius R at time t. We assume interactions between each grain size population to be negligible, or to put it another way that the hydration kinetics of alite is a linear addition of individual isolated particles. This was studied and corroborated by Costoya on pages 80 to 82 of her thesis [35].

All the input parameters of the model are presented in table 1 and defined in the next sections.

3.2.2 Geometrical description of the needles

C-S-H "needles" are shown on figure 3 and 4. They are modelled as cylinders with radius r(t) and length l(t). They possess a characteristic nucleation rate $k_n(t)$ whose unit is a number per unit time per unit of available area. The order of magnitude of $k_n(t)$ is about $40/(\mu m^2)/h$ and the uncertainty interval wide: $[20\ 200]/(\mu m^2)/h$ as estimated from [32][50].

Bazzoni also observed the length of the needles with time (figure 4.11 of her thesis). The physical or chemical origin of this profile is uncertain: probably the needles grow faster when the supersaturation is higher, as it is the case at the onset of the main hydration peak (see figure 1), and then decreases with it, the supersaturation decreasing slowly thereafter (idem). The following function has been used to fit the experimental data:

$$l(t,t_c) = l_{max}(1-\exp((-t)/t_c)) \tag{3.7}$$

where l_{max} is the final length of a needle and t_c the characteristic growth time. This characteristic time expresses that needles have finished 95% of their growth after three times this quantity which is $t_c = 5h \pm 2h$. This profile reflects the fact that needles tend to initially have a quick growth followed by as slower growth as they asymptotically approach their final length. All needles are assumed to reach the same final length. Needles are assumed to grow laterally and keep a constant aspect ratio lying in the range [20%30%] following Bazzoni's observations (p99 of [32]): $r(t,t_c) = C.l(t,t_c)$ with $C \in$ [10% 15%] where r is the radius to that the thickness is twice larger.

The model neglects lateral and perpendicular impingement between the needles. The perpendicular impingement is neglected according to the remarks made in section 1.2. Regarding the lateral impingement, at the moment a needle nucleates, a "parking slot" corresponding to its final size is allocated to it so that other needles cannot grow on this area. On this assigned parking slot the needles can grow parallel. As a consequence, any lateral impingement is neglected.

3.2.3 The nucleation rate profile

The nucleation rate is determined by the supersaturation level and the surface energies of alite grains. The nucleation starts at the peak supersaturation level (third vertical dashed line of figure 1) which corresponds roughly with the minimum of the induction period; this time is assumed to be the starting time of the simulations in this work. Nucleation lasts a few hours according to the observations of Bazzoni [32] and Berodier [50]. The function chosen for the nucleation rate should mimic these observations as for instance the following one:

$$k_n(t) = K_n\Big(1-\exp\big(-\frac{t-t_{start}}{t_n}\big)^2\Big)Heaviside(t-t_{start})\frac{1}{1+\exp\big(\frac{t-t_{start}}{t_n}\big)^4} \tag{3.8}$$

Table 3.1 – List of all the input parameters of the Needle model.

Parameters	Quantity	Symbol	Measurement method	Typical interval	unit
Grain Parameters	Radii	R	Laser diffraction or SEM or tomography[3]	[1 100]	μm
	Form Factor	F	Cf appendix (SEM or PSD+BET)	[1/15 1]	No unit
	Roughness Factor	Rou	Cf appendix (PSD + BET)	[1 4]	No unit
Needles Parameters	Final length	l_{max}	HR-SEM or STEM	[200 500]	μm
	Final radius	r_{max}	HR-SEM or STEM	[20 50]	μm
	Characteristic growth time	t_c	HR-SEM or STEM	[20 200]	Hours
	Characteristic nucleation rate	K_n	SEM	1	$/\mu m^2/hour$
	Characteristic nucleation transition time	t_n	HR-SEM		Hours
	Nucleation starting time	t_{start}	HR-SEM	[0 5]	Hours
	Nucleation stopping time	t_{stop}	HR-SEM	[2 7]	Hours
Thermodynamic parameters	Heat of reaction	$\Delta_r H$	Calorimetry [26]	524	J/g
	C_3S density	M_{C_3S}	Archimedes method	3.1	
	Stoichiometric coefficients	η_1	[46]	1.00	
		η_2	[46]	1.32	
		η_3	[46]	1.57	
		η_4	[46]	0.59	

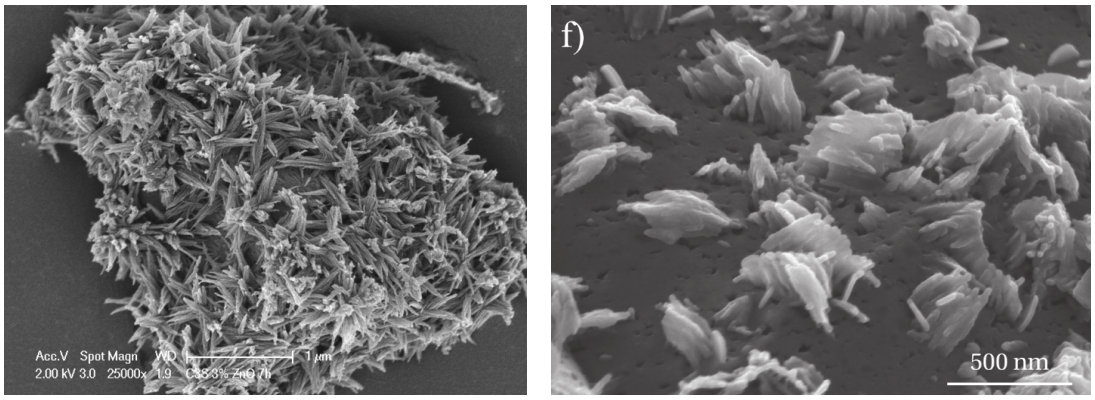

(a) *(b)*

Figure 3.4 – SEM pictures of C-S-H "needles" on alite grains during the acceleration period. Left: Xuerun Li's zinc doping experiment [61]; bunches of half a micron long needles are seen. Right: alite surface in a quartz-alite system, etch pits are visible as black dots on the surface; image taken from [50] p39. These images show the range of morphologies commonly encountered from foils to fibrils, for the purposes of the model these are all represented as cylinders (foils being cluster of them).

which simply means that the nucleation rate increases from zero to K_n within a time t_n (in order to avoid a discontinuity) and stays at this value until t_{stop} where it drops to zero within a time t_n again. This function is merely empirical and has no quantitative, only qualitative, basis in nucleation theory. Its profile is sketched on figure 7.

3.2.4 Geometrical description of the grains

Images of alite grains are shown in figure 5. The first and most obvious quantity that describes a grain is its size, or radius R. The radius of a grain A is meant here as half its diameter where by diameter is meant the equivalent diameter as obtained by laser diffraction measurement. Such a definition is a matter of choice and other possible definitions of a grain radius are discussed in [62].

However, this single quantity fails to capture the difference between a spherical smooth grain and a highly distorted and rough grain. Though both grains may have the same radii, their specific surface might well be completely different, and the specific surface of a powder is well known to have a significant effect on the degree of hydration [47] [63]. To account for that effect two additional parameters are added in the model (see figure 6).

First, a real grain may be closer to an ellipsoid than a sphere. Thus, a form factor is added to account for that difference. This factor, denoted by F, is defined as the ratio of the volume of the real grain over the volume of the equivalent grain. By "equivalent grain" is meant a

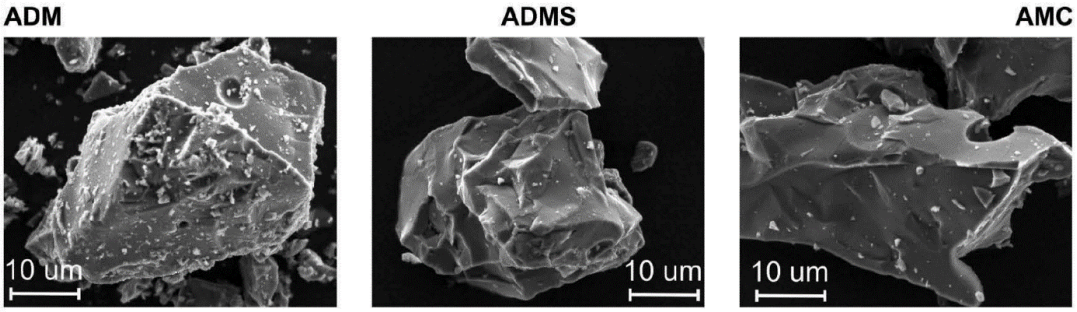

Figure 3.5 – SE-SEM images of alite grains depending on the grinding method used. ADM stands for disc mill, ADMS for disc mill followed by sedimentation and AMC for Mc-crone micronizer grinding. Note that these grains are not exactly representative of all the grain inasmuch as they are bigger than the d_v90 (90th percentile in volume) of the powder; being bigger they are more likely to be polycrystalline and thus more deformed than smaller ones. Image from [32] p 38.

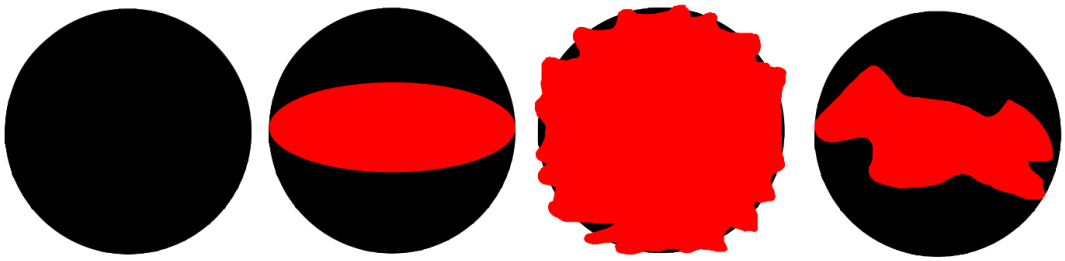

Figure 3.6 – Different possible models for alite grains. The simplest one would be to assume rains to be perfectly spherical and smooth. However realistic grains may not be perfectly spherical (second figure) or may be spherical but rough (third figure) or neither spherical nor smooth (fourth figure). In this last representation a grain is defined by a triplet (R, F, Rou) where R is its radius, F its form factor and Rou its roughness factor. These two last parameters are directly linked to the specific surface of the powder.

perfectly smooth spherical grain whose radius is the same as the grain we deal with.

$$F = \frac{V_g rain}{\frac{4}{3}\pi R^3} \tag{3.9}$$

From figure 5, F might be estimated to be about 1/15 for highly deformed grains to 1/2 for lightly deformed ones. To give an order of magnitude of F: a rugby ball has a form factor of 1/4, the 46th CRC Handbook of Physics and Chemistry 1/5 and an elongated bottle of white wine 1/15.

Secondly, even an ellipsoid shape may be unsatisfactory since two grains may have the same shape but different specific surface as it is exemplified on figure 6. To take that effect into account another parameter called "roughness" and denoted by Rou is introduced. It is defined

as the ratio of its surface over the surface of the equivalent grain:

$$Rou = \frac{S_{grain}(R)}{4\pi R^2} \tag{3.10}$$

The ratio Rou/F and the specific surface of a powder

As seen later the quantity Rou/F occurs in all the key equations of the model. This ratio is equal to one for a perfectly smooth sphere and superior to 1 otherwise. It can be interpreted as the specific surface of a grain and as such is related to the specific surface of the whole powder. One assumption of the model is that though the grains of the powder may not have the same roughness or deformation they have the same ratio Rou/F. It can be determined if the BET specific surface area and particle size distribution are known as explained in the appendix.

The difference between the nucleation surface and the grain surface

Although the first generations of C-S-H needles clearly nucleates on the surface of alite grains, observations made by SEM by [28] on alite and cement or by Gallucci [37] on cement (see figure 2, or by [50] p119 on slag and fly ashes systems during early hydration suggest that later generations of needles do not track the receding grain surface. This suggests that the needles nucleate and grow on a scaffold left by the initial grain surface. This assumption is consistently used in the needle model.

3.2.5 The single grain model

This model calculates the volume of C-S-H needles produced by one single grain: $V_{C-S-H}^{produced}(R,t)$. From now on the symbol $V_{C-S-H}^{produced}(R,t)$ will be shortened to V(R,t) to lighten the writing.

The single grain algorithm

The algorithm is schematically[4] represented in figure 7. At the top of this figure are represented the different stages of the reaction. C-S-H needles are represented as cylinders. Each colour corresponds to one generation of needles. When the cylinder is represented hollow the needle growth speed is fast. When they are represented filled they have reached at least 80% of their final length and grow more slowly.

At time of mixing and until precipitation starts (first dotted line) the grain surface is free from any C-S-H. As a consequence, the nucleation rate, volume of C-S-H and heat flow are zero. This

[4] For matter of illustration, the number of needles and number of generations of needles have been reduced to the minimum to remain understandable. Also, the time frame is approximate. In reality, the process is of course continuous. Also note the representation of needles hollow or filled is *only for the sake of illustration:* needles are of course always filled with C-S-H at any time.

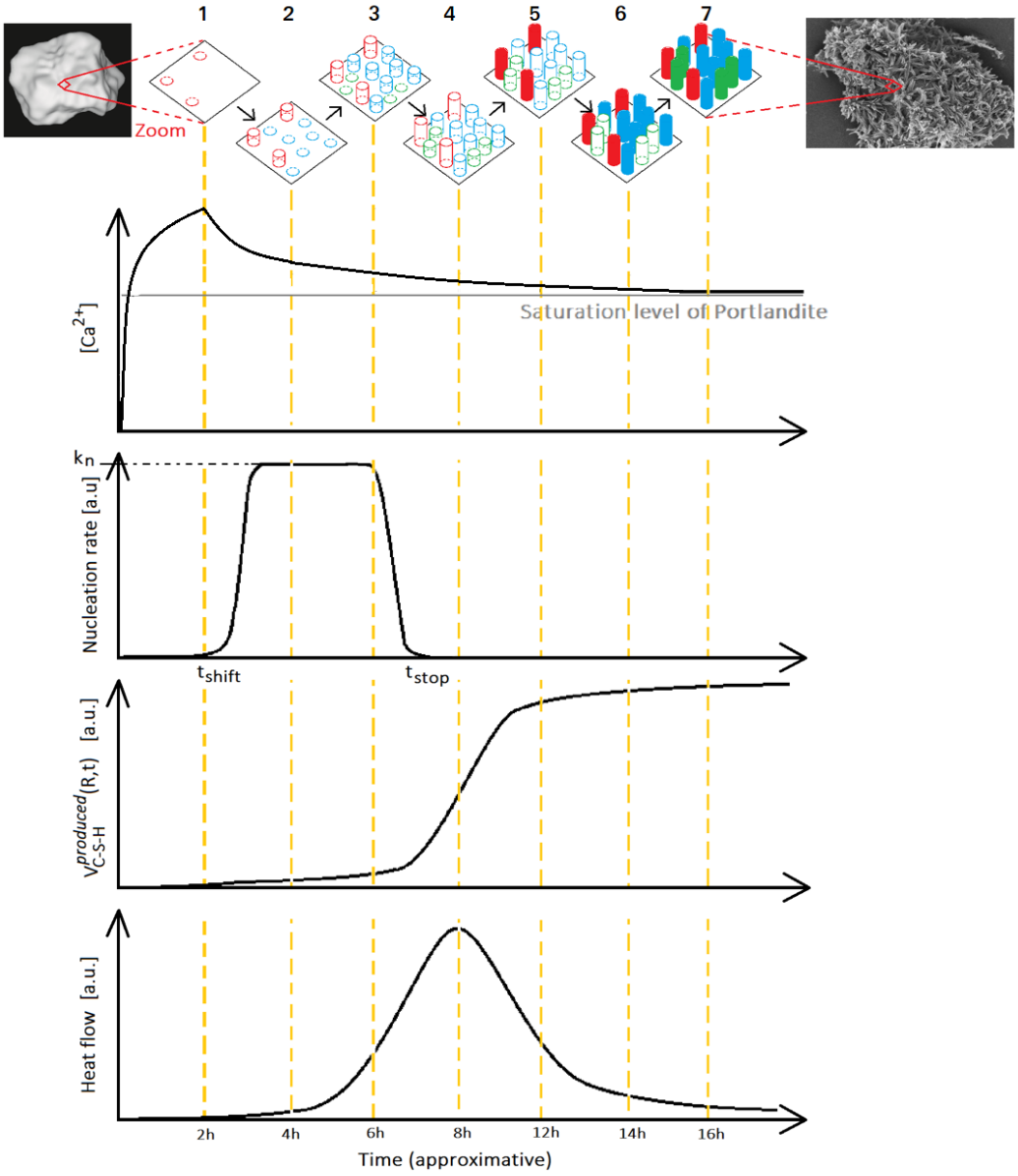

Figure 3.7 – Schematic representation of the algorithm together with the pore solution analysis, nucleation rate profile, volume of C-S-H and calorimetry curve. When needles are represented *hollow they are in their fast growth period whereas when* represented *filled they have reached their slow growth period. The peak in the heat flow corresponds to the time where most generations have nucleated and are still in their fast growth period. Then each generation gradually enters the slow growth leading to less heat released. Note that for the sake of simplicity only three generations and seven steps (numbers in the top) have been represented though the actual process is of course continuous. In the algorithm, the time step is 5 minutes: every 5 minutes a new generation is allowed to nucleate so that a few hundreds of generations are involved in total. Note the dashed lines and stages of this figure do not correspond with those of figure 1. Top left image taken from [60], top right from [61].*

part of the reaction corresponds to the dissolution and induction periods and is not modelled. To avoid overloading the illustration figure 7, the algorithm is described for 3 generations of needles only and seven steps (numbers on the top of figure 7), but in the actual simulations new generations are generated every 5 minutes according to the nucleation rate function.

- **STEP 1:** The single grain model starts at t_{start} when the first nuclei (in red) appear on the surface. Since the nucleation rate is still low, only a few nuclei appear.
- **STEP 2:** The first generation of needles (in red) has grown while another one (in blue) has nucleated. This second generation is more numerous than the first one though the free surface has decreased since the nucleation rate overcompensates it.
- **STEP 3:** The first and second generations are growing while a third one (in green) has nucleated. This last generation is a bit less numerous than the previous because the free surface has decreased while the nucleation rate has kept constant since the previous step.
- **STEP 4:** All generations are now growing fast. As a consequence, the C-S-H volume increases very quickly at this point. Therefore, the heat peak occurs exactly at this time.
- **STEP 5:** The first generation (in red) has now reached 80% of its final length and is now growing at a slower pace. The C-S-H volume still increases significantly thanks to the following two generations which are still in the fast growth period.
- **STEP 6:** The second generation (in blue) joins the first one in the slow speed growth.
- **STEP 7:** All generations have now reached 80% of their final length at least so that they all grow slowly resulting in an overall slow C-S-H volume increase and thus a low heat release.

The key equations of the single grain model

The full derivation of the model based on the algorithm is presented in appendix. We here summarise the main findings.

The key quantity V(R,t) is shown to be equal to the Volterra equation:

$$V(R,t) = \int_0^t k_n(\tau)\big(S_0(R) - S(R,\tau)\big).v(t,\tau)d\tau \tag{3.11}$$

where k_n is the nucleation rate per unit of free area and time, $S_0(R)$ the initial surface of the grain, $S(R,\tau)$ the surface of the grain occupied by the needles at time τ and $v(t,\tau)$ the volume of a needle at time t which has nucleated at time τ.

This equation possesses an analytical reformulation where the variables are found separable:

$$V(R,t) = S_0(R) l_{max} f(t) = [4\pi R^2 Roul_{max}] f(k_n, s_0, t_c, t) \tag{3.12}$$

where l_{max} is the final needle length, t_c is the characteristic growth time of the needles, s_0 the area of their basis and f is an increasing sigmoidal function[5] of time which is equal to 0 at time 0 and is always inferior to 1. The term in brackets represents the maximum reachable volume of the needles around the grain and the f function represents the fraction of that volume filled at time t. Whether the grain gets completely consumed during the reaction or not, this volume may or may not be reached. Alternatively, whether the grain gets completely consumed during the reaction, f may or may not reach 1.

Now that V(R,t) is known, the degree of reaction and heat flow can be expressed according to the $f(k_n, s_0, t_c, t)$ function:

$$DoH = \frac{\eta_1}{\eta_3} * \frac{1}{R}\frac{3Rou}{F} * l_{24h} * f(k_n, s_0, t_c, t) \tag{3.13}$$

$$HF(t) = \Delta_r \frac{\eta_1}{\eta_3} * \frac{1}{R}\frac{3Rou}{F} * l_{24h} * \frac{df(k_n, s_0, t_c, t)}{dt} \tag{3.14}$$

For reasons proved in appendix B, $1/R * 3Rou/F = S_{spe} M_{alite}$ where S_{spe} is the specific surface and M_{alite} is the volumetric mass of alite so that these equations can be rewritten to:

$$\boxed{DoH = \frac{\eta_1}{\eta_3} * S_{spe} * M_{alite} * l_{24h} * f(k_n, s_0, t_c, t)} \tag{3.15}$$

$$\boxed{HF(t) = \Delta_r H \frac{\eta_1}{\eta_3} * S_{spe} * M_{alite} * l_{24h} * \frac{df(k_n, s_0, t_c, t)}{dt}} \tag{3.16}$$

Note that these equations hold not only for single grains but also for powders as long as the consumption of the small grains in negligible. They show that the DoH and heat flow rate during the first day are *proportional* to the specific surface (as experimentally demonstrated by Bazzoni (figure 4.19 c) of [32]) and the needles length as could be expected.

Evolution of the grain radius with time

Since the alite grain provides the reactant for the hydration to occur, the hydration reaction abruptly stops if the grains get totally consumed.

[5] f is not any sigmoidal function, it is specifically the function generated by the algorithm described here above.

To model the grain consumption, we assume that grains shrink concentrically as is suggested by figure 3. Therefore, the evolution of the grain radius with time is searched, and especially the time at which the radius reaches zero if it does.

On the one hand the volume of alite consumed is naturally linked to the alite grain radius: $V_{alite}^{consumed} = 4/3\pi(R_0^3 - R(t)^3).F$. On the other hand, the volume of alite consumed is linked to the volume of C-S-H produced by the reaction equation 3: $\frac{V_{alite}^{consumed}(R,t)}{\eta_1} = \frac{V(R,t)}{\eta_3}$. This leads to:

$$R(t) = \sqrt[3]{R_0^3 - \frac{\frac{\eta_1}{\eta_3}V(R,t)}{4/3\pi F}} \tag{3.17}$$

and by inserting equation 12 into V(R,t) it can be rewritten:

$$R(t) = \sqrt[3]{R_0^3 - \frac{\eta_1}{\eta_3}\frac{3Rou}{F}R_0^2 l_{max}.f(t)} \tag{3.18}$$

Depending on the initial size R_0 of the grain, it may either be slightly or totally consumed at time t. The critical radius $r_{critical}(t)$ below which all grains have been consumed and above which grains have so far survived is:

$$R_{critical}(t) = \frac{\eta_1}{\eta_3}\frac{3Rou}{F}R_0^2 l_{max}.f(t) \tag{3.19}$$

Since f converges to 1 at infinite time, the critical grain radius separating those grains that will eventually be consumed to those which will survive is:

$$R_{critical}(t=\infty) = \frac{\eta_1}{\eta_3}\frac{3Rou}{F}l_{max} \tag{3.20}$$

To sum up, the needles will carry on nucleating and growing as long as the initial size R_0 of their associated grain is higher than the critical radius $r_{critical}(t)$, or to put it another way, as long as $H(R - R_{critical}(t)) = 1$ where H is the Heaviside step function. Therefore, the only modification that should be added for the models presented above to take into account the grain consumption is to change the f(t) in each equation for $f(t).H(R - R_{critical}(t))$.

The single grain model: simulations and discussion

The simulated calorimetry curves for two grains of respectively 2 μm and 6 μm (6 μm is roughly the d_v50 of the PSD of the C_3S used by Bazzoni) are shown on figure 9 left. The experimental curve for the whole powder is shown for comparison in figure 8.

The first striking thing is that the correct magnitude is obtained for the position and height of the peak for the black curve. Secondly the complete dissolution of the 2 μm grains (red dashed curve on the left plot and blue curve on the right one) occurs at about 8h after precipitation

begins, in agreement with SEM observations [29]. A grain three times bigger does not dissolve during the first day (black curve) and its heat flow is three times smaller because its specific surface is also three times smaller. In any case, a transition from acceleration to deceleration period is observed.

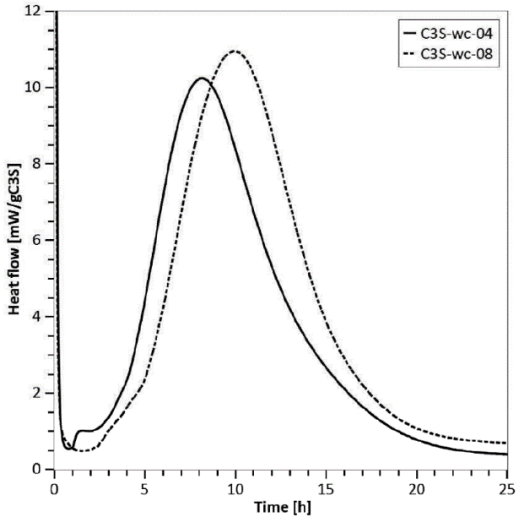

Figure 3.8 – Calorimetry curve of Bazzoni's C3S experiment with water to cement ratio of 0.4 and 0.8 (figure 4.10 of her thesis [32]).

3.2.6 The PSD model

The PSD models are obtained through a straightforward summation of the volume produced by each grain size population of size r weighted by the particle size density of this population p(r):

$$V_{C-S-H}^{produced}(t) = \int_0^{\infty} p(r).V_{C-S-H}^{produced}(t,r)dr \tag{3.21}$$

The parameters to run the PSD model are the same as the single grain model except for the PSD of the powder which is now required and the starting time of the precipitation. This straightforward summation implicitly means that each grain is assumed in isolation. The dissolution of the grain only gives hydrates to its associated scaffold. This assumption will be discussed in subsection 4.2 on the dissolution of the small grains.

3.2.7 Sensitivity study

Because some input parameters always appear together in the equations of the derivation of the model, there are only 7 genuine parameters: the PSD, $Rou/F.l_{max}$, t_{stop}, $k_n s_0$, t_c, t_n and t_{start} (arranged by order of impact on the heat release).

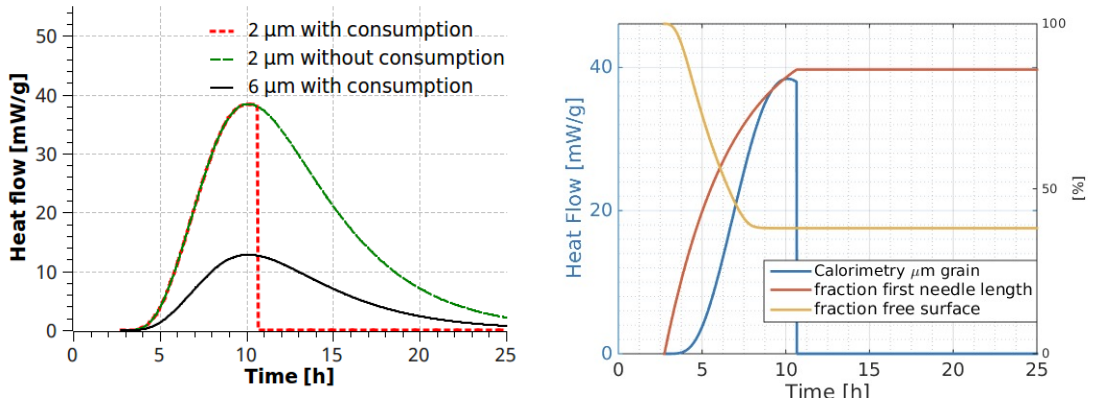

(a) *(b)*

Figure 3.9 – Left: calorimetry curve predicted by the single grain model for a 6 µm grain (which also is the d_v50 of Bazzoni's C_3S) and a 2 µm grain; input values are shown on line 1 of table 2. A 2 µm grain dissolve at about 11 hours. Right: in addition to the heat flow are shown the fraction of surface left free at any time (yellow) and the relative size (in % of the final length) of the first generation of needles (in red).

The PSD has a tremendous effect and we will be studied along Costoya PSD experiment in the next section. The DoH and heat release are nearly proportional to $Rou/F.l_{max}$ as the equations 13 and 14 indicate. The proportionality is lost whenever the consumption of small grains is no longer negligible as will be shown in subsection 4.2. The other three intermediate parameters t_{stop}, $k_n s_0$ and t_c are studied on figure 10 on Bazzoni's 0.8 water to cement ratio. The last two parameters t_n and t_{start} have only a trivial translation effect.

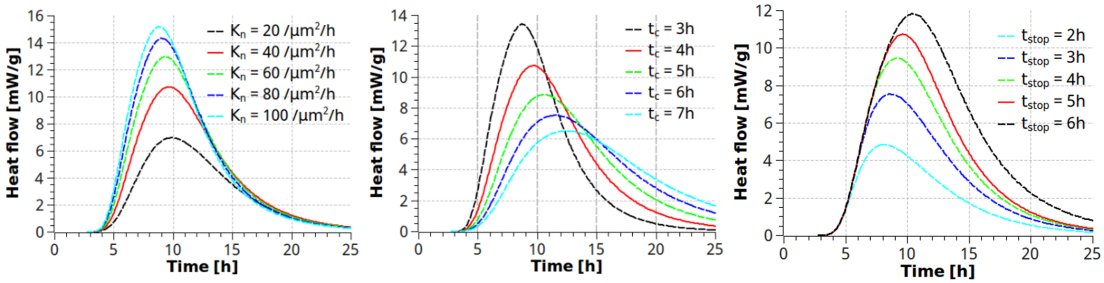

Figure 3.10 – Sensitivity study on the peak nucleation rate (left), characteristic growth rate (middle) and nucleation stopping time (right). The continuous red line of each plot is the reference Bazzoni 0.8 w/c experiment. To increase the peak nucleation rate maintain the peak position but increases both the height and area below the curve, to increase the characteristic growth rate increases the peak height but not its area, to increase the nucleation window slightly shift the peak right and increases both the height and area.

3.3 Comparison of the model with experiments and discussion

The needle model has been tested on 14 experiments. All the values taken by the input parameters of the model for the different experiments are presented in table 2 in the appendix 10.3. These values are constrained to vary only within the uncertainty intervals mentioned in the table.

Within these intervals the values chosen are obtained by the gradient descent method [40] starting from the centre of each experimental uncertainty interval. The values chosen are those giving the lowest error (see the appendix for its definition).

In table 2, out of the seven parameters of the models only 5 are shown since the other two are fixed:

- the starting time t_{start} is systematically set as the time of the minimum heat released during the induction period
- The Rou/F ratio is systematically set to 6 except for the Li's doping ions experiment where the PSD and BET having been measured the ratio could be retrieved (see related section) and found to be close to 6. 6 corresponds to a "rough rugby ball".

3.3.1 Bazzoni's water to cement experiment on C_3S

Bazzoni's experiments on C_3S for the 0.4 and 0.8 water to cement ratio are shown in figure 8. The simulations are plotted in blue on figure 11 and the experiments data are plotted in red.

For both experiments the order of magnitude of the size and time of the peak are correct and a transition from acceleration to deceleration is present in both cases. The available free surface at the time of the peak is about 40% which is not so far from being a complete coverage[6] and the first generation of needles has reached about three quarters of its final length at that time (see figure 9 right).

The difference between the experimental and simulated curves may come from approximations such as roughness and deformation constant with grain size or the profile of the nucleation rate could account for the slight deviation.

3.3.2 Bazzoni's doping experiment

In her thesis and in [34] Bazzoni studied the impact of doping ions on alite hydration. In particular, she observed that doping alite with about 1% of zinc led to a significant increase in

[6] The maximal circle density in a hexagonal packing arrangement is 91% (free surface = 9%) while in the square packing it is 78% (free surface = 22%) so that a random packing as can be expected in the present case should be below these two values (and thus the free surface above 22%). Note that in 2D there is no thermodynamically stable random packing of circular disks.

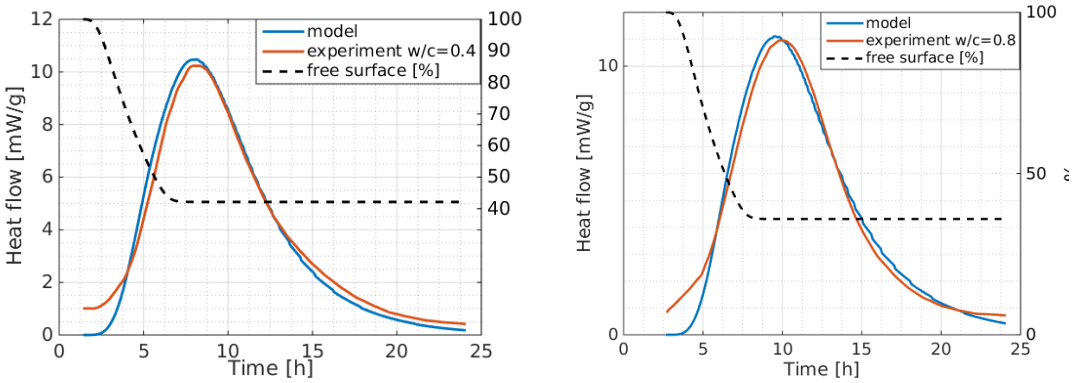

(a) *(b)*

Figure 3.11 – Comparison of the model simulations (in blue) to the calorimetry curves (in red) of Bazzoni w/c experiment. On the left, the water to cement ratio is 0.4, on the right it is 0.8.

the heat released. The zinc was well incorporated within the crystalline alite structure. The calorimetry curves for her two alites respectively sieved between 25 to 36 µm and ground 10 minutes in a Mc-Crone micronizer are reproduced on figure 12.

She also measured the maximum needle length to be about 400 nm when zinc was added compared with 270 nm without. As a consequence, she suggested that the heat increase was caused by the needles length increase. This observation is in complete agreement with equations 10 and 12 where the heat released is proportional to l_{max}: as expected the ratio of the zinc curves over non-doped ones are of the order of 400/270.

The results are shown in figure 13 where the continuous lines are the experimental data and the dashed lines the simulations. As can be seen from table 2, apart from the needle length increase, the other parameters only slightly change.

3.3.3 Xuerun Li's doping experiment

Xuerun Li replicated the impact of zinc on alite and cement [61]. We here only use his results on alite on figure 14.

Xuerun Li did three experiments: one alite without zinc, one with 1% of zinc doping and a last one with 3% of zinc doping. Moreover he also measured the PSD and BET specific surface which enables the calculation of the Rou/F ratio: he respectively measured $1.58 m^2/g$, $1.43 m^2/g$ and $2.21 m^2/g$ for no zinc, 1% zinc and 3% zinc which respectively correspond to 6.1, 6.3 and 11.5.

It is striking to note how good are the fits given the final needles lengths l_{max} and radii r_{max}, nucleation rate k_n and characteristic growth time t_c are found *exactly* identical than for Bazzoni doping experiments as shown in table 2. Only t_{stop} slightly changes. So, the model

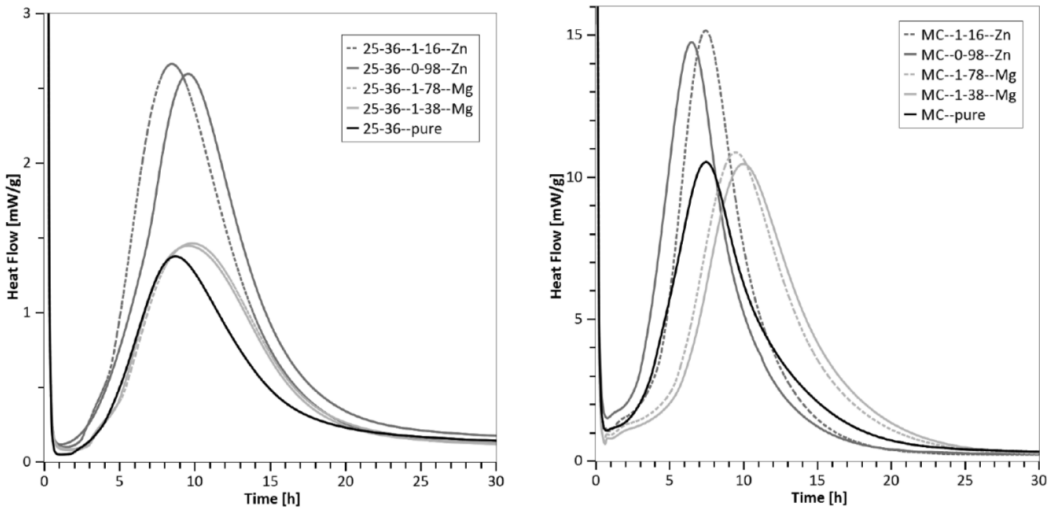

Figure 3.12 – Calorimetry curves of alite doped with magnesium and zinc respectively at 1.16% and 0.98% for Zinc and 1.78% and 1.38% for Magnesium. Left: alite sieved between 25 µm and 36 µm; right: alite ground for 10 min in the Mc-Crone micronizer. Pictures taken from [34].

spontaneously suggests that the C-S-H characteristic parameters and therefore the surface reactivities are very similar for both Bazzoni and Li's doping experiment, as could be expected. This supports the soundness of the model.

3.3.4 Costoya's PSD experiment

In her thesis [32] Costoya studied the effect of PSD on the hydration kinetics of alite hydration and showed it to have a dramatic impact. Since then her experiments have been consistently used as a benchmark for alite hydration models [14] [16] [19] [21].

This new model was tested on the set of data presented on page 56 of her thesis. Two tests are proposed: one in which all the input parameters are kept identical except the PSD, and the other one in which they are optimized to get the best fit while remaining within the experimental uncertainty intervals. The first test aims at testing whether or not the model can roughly get the trend with changing only the PSD while the other one focus on the sheer ability of the model to fit the data.

The results are shown in figure 15. On the left in dashed lines are the model simulations when all the values are kept constant and on the right when they are optimized.

On the left plot, it is striking the fits capture the changes with PSD given that the input parameters are taken from the observations of Bazzoni on a different batch of alite.

On the right, all the model simulations are all close to their experimental counterparts. Although left free to vary within their respective intervals, the input parameters remain close to

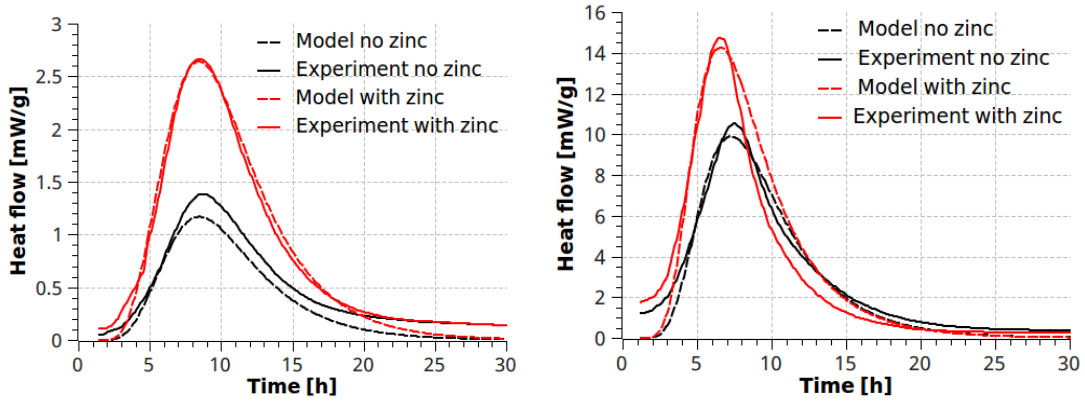

(a) *(b)*

Figure 3.13 – Comparison of the model simulations to the calorimetry curves of pure (black curves) and 1.16 zinc-doped (red curves) alites from Bazzoni. The continuous lines are the experimental curves, the dashed lines the model. The Left plot correspond to her alite ground down to a dv50 of 28µm whereas the right one has a dv50 of 2µm

the previous experiments except perhaps for the characteristic growth time that fluctuates within a range of one hour.

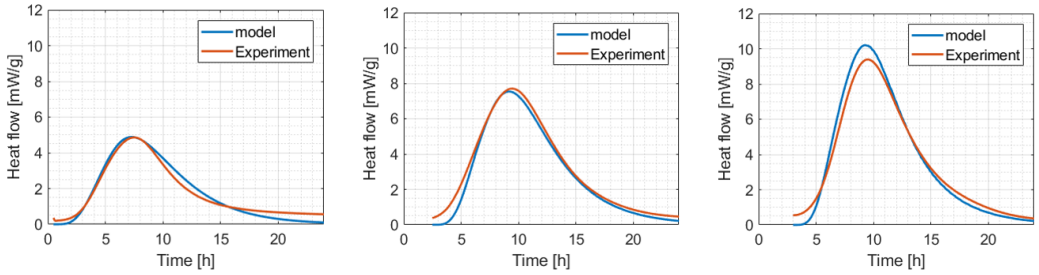

Figure 3.14 – Xuerun Li's doping experiments. On the left no zinc was added in the raw materials before synthesis, in the middle 1% in mass and on the right 3%. The needle size for the 1% and 3% experiments are identical but the grains were rougher for the 3%; this suggests zinc does not only change the needle length but also the alite growth.

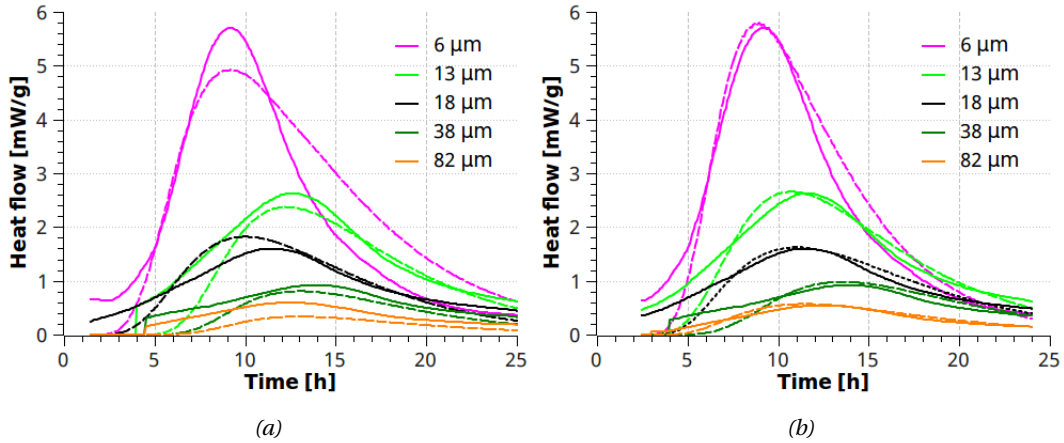

Figure 3.15 – Comparison of the model simulations to the calorimetry curves of Costoya PSD experiments (p56 of her thesis [35]). The continuous lines are the experimental curves, the dashed lines the model ones. On the left, exactly the same set of input parameters has been used (except the PSD of course), while on the right the fit was improved by letting the variables free to change (still within the experimental uncertainty intervals though).

3.3.5 Conclusion on the comparison simulations / experiments. The mechanism behind the transition from the acceleration to the deceleration

A model tested on a wide set of experiments

The model has been tested on 14 calorimetry curves, which is twice its number of input parameters, and its input parameters are shown to vary reasonably within their experimental interval (as shown in table 2). All the simulations exhibit a transition, and a transition in satisfactory agreement with the experiments. To be quantitative: an average error of 16.2% and 10.1% respectively have been found for the calorimetry and degree of hydration with standard deviation of 9.1% and 9.9% respectively (errors computed over the entire curves as detailed in the appendix). These values are similar to those found in [21].

The mechanism behind the transition: the nucleation and growth rate of needles

Given that the model has been tested on a wider set of experiments than any other model in the field, and given it has no **free** fitting parameters, but only parameters **constrained** by experiments, we believe it provides substantial support to the hypothesis that the whole hydration peak can be rationalized in terms of nucleation and growth even if this does not entail any perpendicular impingement or diffusion barrier. The heat peak in the calorimetry curve is interpreted as the time where most of the needles have nucleated (and thus most of the surface is filled) and are in their fast growth period. Beyond this point needles gradually enter their slow growth period and asymptotically reach their final length leading to a decrease in the heat flow.

3.4 Insights on alite hydration from the needle model

Because the model quantifies the impact of all the input parameters listed in table 1, it enables the disentanglement of the impact of each of them independently of the others.

For the sake of brevity, the aim of this section is not to study the evolution of the calorimetry curve when each parameter changes in a given range, but to answer specific questions related to these parameters and that shed a new light on the mechanisms of alite hydration.

3.4.1 Contribution of each population of the PSD to the total heat released

The PSD used by Bazzoni is presented on figure 16 left and clearly shows two populations. These two populations were fitted with log-normal distributions (dotted lines). The right plot of this figure shows the contribution of the finer population of the PSD is close to negligible. This might be unexpected since common sense is that the finer the powder the higher the reactivity. Nevertheless, this is not so unexpected in as much as the abscissa of the PSD is logarithmic so that the volume of the powder contained in the coarser part is at least one order of magnitude bigger than in the finer part. This very large difference of volume outbalances the difference in specific surface between the finer and coarser part.

Thus, in this case it is seen that the left population is clearly not the population that contributes the most to the overall surface area and thus reactivity of the powder.

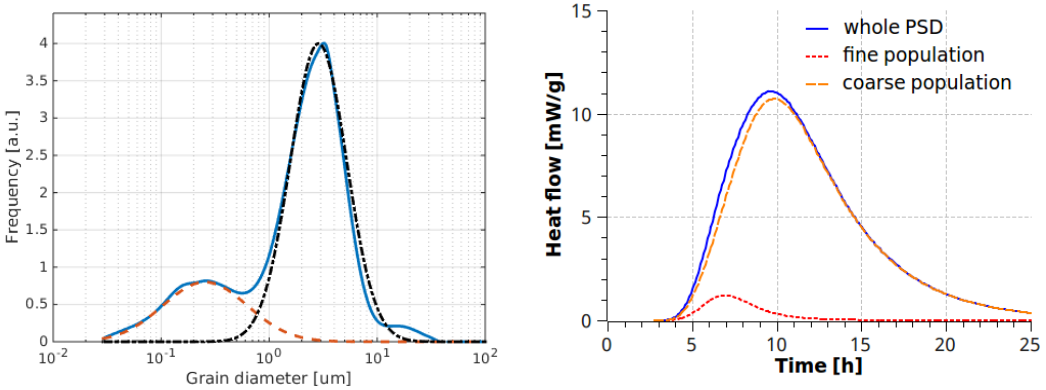

(a) *(b)*

Figure 3.16 – Left: deconvolution of the two populations of Bazzoni C_3S PSD (in volume) and their corresponding contribution to the total heat flow on the right. The vertical bar on the left plot marks the limit between those grains that survive the first hydration day, and those that do not.

3.4.2 Impact of the dissolution of the small grains

The impact of the dissolution of the small grains was raised by Taylor at least three decades back [27]. Although he speculated they would impact the hydration kinetics he did not try to

quantify this effect. The impact of the dissolution of the small grains was studied for Bazzoni's water to cement experiment and an artificial set of PSDs.

Bazzoni's w/c experiment

In figure 17 left, the blue curve is the model simulation for the water to cement ratio 0.8 when dissolution is enabled and the red curve when it is disabled (thus allowing nucleation and growth to continue on each scaffold though the grain is actually dissolved). At any given time, the maximum size of grains consumed is shown on the black dotted line. The right-hand figure shows the evolution of the grain diameter with time for different initial grain sizes. The model predicts that all grains below 5µm in diameter vanish at the end of one day, a value close to those already reported [28][29]. As a significant part of the grains of C_3S are smaller than 5 µm (see figure 16 left) it is not surprising that the difference between the blue and red curves is quite big.

Note that by contrast with other models, different thicknesses are removed from different grain sizes: as shown on the figure 17 right, an 8 µm grain loses about 2.2 um in diameter by 25 hours whereas a 5 µm loses … 5 µm by that time. The fact that less thickness is removed from bigger grains than smaller ones is consistent with SEM observations as seen from figure 2 for instance. These SEM observations support the assumption that each grain behaves mostly in isolation and the straightforward summation used to pass from the single grain model to the PSD model (see subsection 4.2.3 for more details).

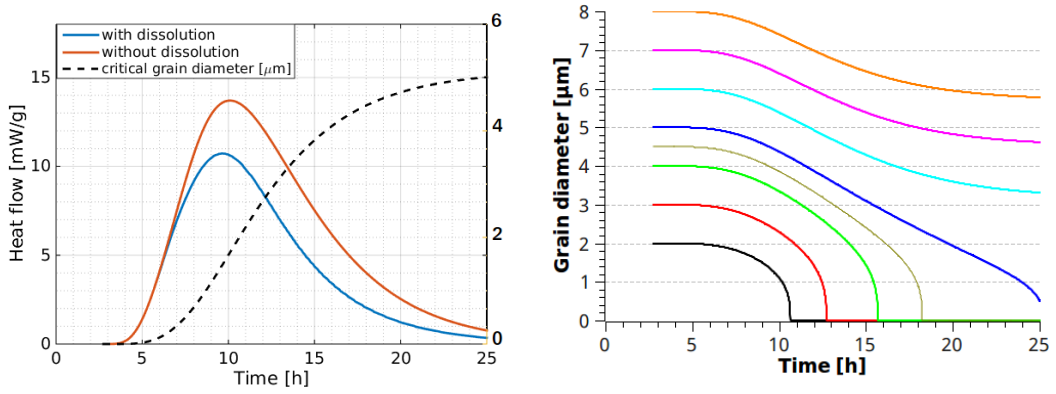

(a) *(b)*

Figure 3.17 – Impact of the dissolution of the small grains for the 0.8 w/c experiment. In red is plotted the calorimetry curve if the consumption is neglected. The dotted line represents the critical grain radius. On the right are shown the evolution of different grain radii with time; those grains that are roughly smaller than 5 µm will not survive the first day of hydration.

Artificial set of PSDs

In figure 18 is plotted a set of PSDs with their associated calorimetry curves in figure 19 left (the other input parameters are kept similar to those for Bazzoni's water to cement experiment). The central PSD chosen (in blue) corresponds to the main PSD peak of figure 16 whose mode is at 5.7 μm.

When the calorimetry curves are renormalized per unit of initial surface area (on the right plot of figure 19) the plots shed another light on the phenomenon: all the PSDs coarser than 11.5 μm in diameter align on the same curve while the finer ones are smaller and shifted because the small grains consumption becomes significant. Even more striking is the alignment of all curves, whether from fine or gross powders, during the acceleration period. To put it another way **when the curves are renormalized per surface area, the acceleration period slope is a fundamental characteristic of the chemical reactivity of the powder surface**.

This representation is compelling because it shows in a simple way that systems that could have appeared different on the usual representation (in [mW/g]) are actually behaving chemically in the exact same manner. Also, the impact of the dissolution of the small grains is easier to grasp.

It is also striking to observe the resemblance of these simulations with experiments done by Scrivener in 1984 and replotted on figure 20. In a similar way to Costoya, she measured the influence of the PSD on the calorimetry curve but also normalized them by specific surface. They exhibit the very same trend as the artificial set presented on figure 19. Note the alignment of the acceleration periods entails that the reactivities of small and big grains surfaces are identical; *there is no need to invoke here a higher density of defects to explain the higher reactivity of small grains*, Scrivener 1984 experiment suggests their higher specific surface is a sufficient cause.

To conclude, no matter whether grain consumption is negligible or not, the surface reactivity of different alites can be easily compared by comparing the slope of their acceleration periods **when renormalized per surface area**[7]. It seems this practical method has not been widely used so far though highly pertinent in addition to the usual normalization per gram of cement to understand the reaction.

Justification of the assumption of isolated grain reaction and its consequence

The straightforward summation done when passing from the single grain model to the PSD model entails that grains are assumed to react in isolation. Once a grain has completely reacted, nucleation and growth on its associated scaffold stops. As a consequence, the total active surface for nucleation and growth decreases with time.

[7] To be relevant the specific surface area method used should not make any kind of spherical approximation: Laser PSD specific surface or Blaine fineness are thus a priori inappropriate (by contrast with the BET specific surface for example).

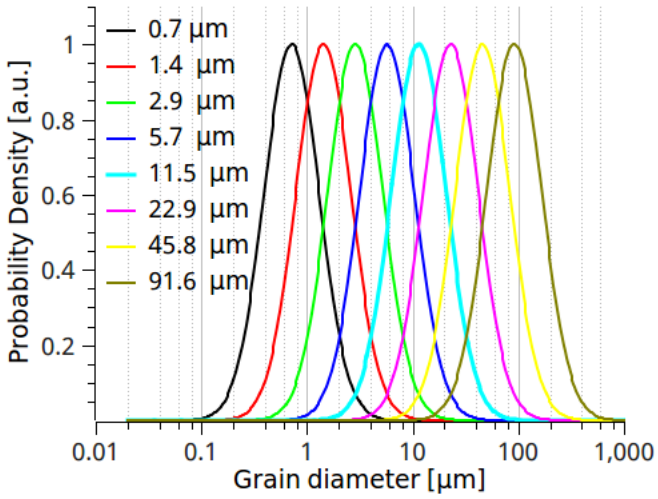

Figure 3.18 – Set of PSDs simulated in order to better grasp the impact of PSD of the calorimetry curves (see next figure). The blue curve corresponds to the second population of Bazzoni's C_3S which is the leading one.

This may at first sight seem rather unlikely because it may be thought that all grains supply equally to the pore solution supersaturation and thus to the precipitation, so that whenever a grain would vanish, its associated scaffold would still be supplied by neighbouring grains: nucleation and growth would carry on. The total active surface for nucleation and growth would then stay perfectly constant with time and equal to the initial specific surface; this total surface would remain active as long as there are some big enough grains left to feed all the scaffolds, be they empty or not. As a consequence, the heat flow rate per unit of initial specific surface would be exactly identical for any powder as long as there are some big enough grains left.

Yet, this is in contradiction with Scrivener 1984 experiment as presented on figure 20 right. From 10 to 15 hours the F4 and F5 curves are not nil; therefore there must be some big enough anhydrous cores remaining. Nevertheless, the heat released per unit of initial surface is significantly lower for both of these fine powders than for the F1 and F3 gross powders. The simplest explanation perhaps is a decrease of the active surface for nucleation and growth, and this decrease would come from the loss of the activity of those scaffolds whose anhydrous cores have completely reacted.

Surely the reality is not black or white and scaffolds do not abruptly stop contributing to the total active surface when their anhydrous core has vanished, but the Scrivener 1984 experiment entails that they contribute significantly less to the total active surface once their core have vanished. This provides some ground for the assumption that grains react in isolation to each other and to the straightforward summation.

Several consequences follow from this observation. First, if empty scaffolds contribute less to the total active surface for nucleation and growth, then their local supersaturation must

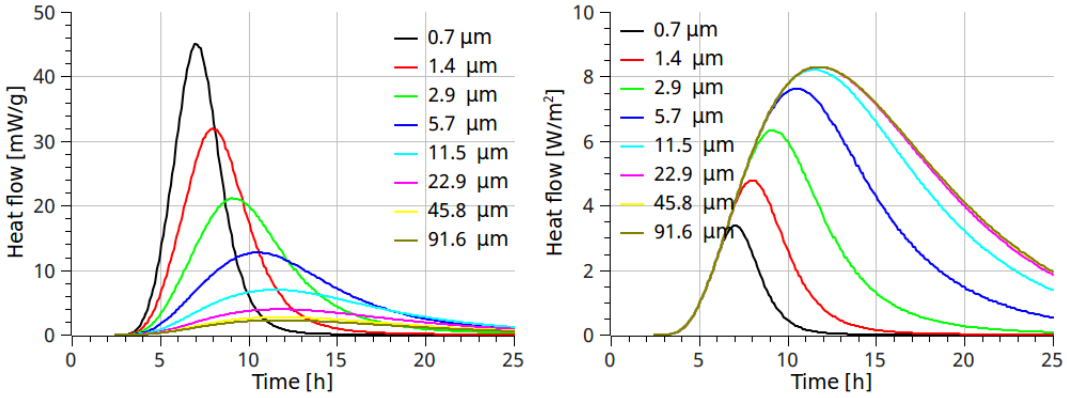

(a) *(b)*

Figure 3.19 – Calorimetry curves corresponding to the PSD plotted in the previous figure. On the right, the calorimetry curve has been normalized by surface area. The right plot show that the impact of the small grains consumption can be dramatic for PSD below 11.5 µm: if grain consumption was neglected all the curves would align. Note the resemblance with the next plot. The alignment of all curves during the acceleration period indicates their surfaces react fundamentally in the same manner independently of the PSD. This would have been left unnoticed with the usual representation (left figure).

be lower than on scaffolds still possessing their anhydrous core; or at least sufficiently lower for the scaffold to contribute much less. The explanation could be that these scaffolds are farther away from an ion source, an anhydrous core, and because ions leaving an anhydrous core first feed their associated scaffold before diffusing further away to feed the neighbours, their local supersaturation could be lower. This would imply that diffusion of species on the average distance between two shrinking anhydrous cores, i.e. around a few microns, in ordinary cementitious powders, plays a role[8].

A second consequence has already been mentioned in subsection 4.2.1 and shown on figure 17 right: different thicknesses are removed from different grain sizes: the smaller the grain the bigger the thickness removed; in agreement with SEM observations.

3.4.3 When does the inner C-S-H start forming? Why do needles stop growing? The transition occuring at the end of the first day

When does the inner C-S-H start forming?

For all the simulations presented here a transition from acceleration to deceleration systematically happens though the inner C-S-H is never invoked. Despite all the assumptions concerning the geometries of the needles and grains and finally despite lacking some precise measurements that would be needed to clearly corroborate or refute the model it seems the

[8]This should not be confused with the diffusion limitation as considered in the context of diffusion-based models dealt with in the introduction.

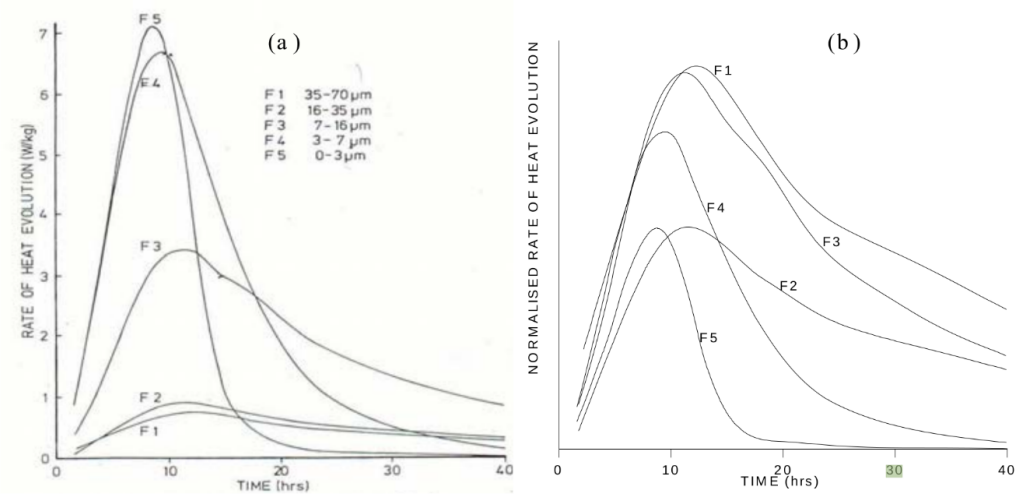

Figure 3.20 – Calorimetry curves for different cement PSD. On the right, the curves are renormalized by specific surface instead of grams. Image taken from [29]. Note the resemblance with the previous plot.

model indicates that the formation of inner product does not contribute a significant amount to the heat released during the initial part of the deceleration.

However, after roughly 20 hours all the simulations cross the experimental curves and rapidly decrease to zero. This could mean that even if the inner C-S-H starts forming before 20 hours as suggested by Bazzoni its contribution to the total heat only becomes significant at about that time. As a consequence, the model indicates that an actual transition in mechanism does not occur at the time of the peak but rather at about 20 hours.

This corresponds well with SEM observations that show the first appearance of inner-C-S-H at about that time [28][29]. To understand this transition is crucial in order to better understand the microstructural development of alite and cement pastes beyond one day.

Why do needles stop growing? Why does the inner C-S-H start to form

Why is there then a transition from one phase, the outer C-S-H needles, to another one, the inner C-S-H? Thermodynamically, the local nucleation and growth of a phase are determined by the local temperature, pressure and chemical potentials fields. Given that the temperature and pressure fields remain uniform and constant in an isothermal calorimetry experiment, the composition of the pore solution and the interfacial energies of the anhydrous grains and the hydrates are the only possible causes for this transition.

Three causes may explain the transition:

- a change in the calcium to silicon ratio that would favour the inner over the outer C-S-H. This seems unlikely as Bazzoni did not measure any significant difference between the

end of the first day, when there are mostly outer C-S-H needles, and one month, when there is a mixture of outer and inner C-S-H (figure 5.8 of [32]).

- A change of supersaturation is almost certain: it is well known it decreases and then plateaus with time, but is it more than that? The pore solution concentrations are likely not uniform - the outer and inner C-S-H growth overlaps: some inner C-S-H start to form even before all outer C-S-H finish growing - perhaps there is a gradient from each anhydrous grain surface to the outward extremity of its outer C-S-H shell that combined with a global decrease of the supersaturation would account for the transition? perhaps the local concentrations of species between the inner gap solution and the outer shell solution slightly changes?

- Perhaps needles incorporate defects during their growth, thus modifying their interfacial energies, to the point where their structure is too defective to carry on growing? This is difficult to experimentally assess, and C-S-H is known to have an intrinsic defective structure.

Perhaps the reality is a combination of these different options. Thus, again, the question remains open, and the possibility to test each of the causes separately seems remote given characterization methods existing today.

Requirements for mechanistic models dealing with the later ages

Whatever be the mechanism behind this transition it seems that new concepts and parameters are required to model the hydration kinetics beyond the main hydration peak, where the formation of inner-C-S-H becomes dominant. Some models already try to predict the hydration beyond one day but again rely on one single set of parameters for both outer and inner-C-S-H. Moreover, they often use a diffusion law which is very unlikely to be the mechanism because the inner-C-S-H forms from the outer-C-S-H shell and propagates **toward** the remaining anhydrous grain; ions only need to cross the water gap between the anhydrous grain and the inner C-S-H, they do not need to cross the outer plus inner C-S-H layers as the growth does not carry on at the outward extremity of the hydrate shell but on its inside face. This period lasts several days beyond which diffusion might eventually be the leading mechanism.

3.4.4 What factors influence the nucleation and growth rate of the needles?

If the transition corresponds to the time when most of the surface is filled and most of the needles are in their fast growth mode, what then control the nucleation and growth rates profile? Why is there a burst of nucleation within only very few hours? Why do needles exhibit a transition from a fast growth mode to a slow growth mode? The mechanisms behind them remain unspecified despite their importance in causing the transition; the model takes

the nucleation and growth rates as input parameters from Bazzoni measurements and says nothing regarding their causes.

As stated before, the local nucleation and growth of a phase are thermodynamically determined by the local temperature, pressure and chemical potentials fields. Given that the temperature and pressure fields remain uniform and constant in an isothermal calorimetry experiment, only the composition of the pore solution and the interfacial energies are possible causes to explain these rates.

The initial nucleation rate burst As in any nucleation and growth phenomenon, nucleation always precedes growth and requires an equal or higher supersaturation to occur: once stable nuclei are formed it costs equal or less energy to grow than to nucleate elsewhere. For nucleation to occur a high enough supersaturation is required, beyond which nucleation starts massively and thus drops the supersaturation down to a point where growth become favourable over nucleation.

The growth rate profile: from fast to slow growth Because the average supersaturation is known to quickly decrease and then plateaus with time, it could provide at first sight an explanation for the nucleation and growth rate profiles. Certainly, the needles nucleate and grow quickly to a certain length when the pore solution is highly supersaturated with respect to calcium hydroxide (as shown on figure 7). As most of the grain surface is covered and the supersaturation slowly reaches a plateau the nucleation rate drops to zero while the needles enter the slow growth mode.

But then, what determines the supersaturation field at any given time? Most generally it is determined by the whole preceding history of the interaction between alite dissolution, speciation and diffusion through the solution and precipitation, and the initial conditions (here the supersaturation field at the onset of precipitation). This interaction is mathematically expressed by a set of coupled partial differential equations (PDE): one expressing the local needle growth rate as a function of the local supersaturation, one set for the speciation, one expressing the tranport of the species through solution from the alite surface to the needle tip from which the supersaturation field can be computed, and one expressing the dissolution rate as a function of the local supersaturation and alite specific surface and energy.

A priori none of these phenomena is limiting [65] – it is hard to see how dissolution or precipitation could be decoupled from their dependence on their respective local supersaturation field - so that each of them is itself determined by the whole preceding history of their interaction. To commit an abuse of language, we could say that supersaturation, diffusion, dissolution and precipitation are the “four faces of the same pyramid”: if dissolution abruptly stopped the ions in solution would quickly be depleted by the precipitation and the whole reaction would stop, conversely if precipitation stopped the undersaturation of the solution would quickly decrease and the pore solution would quickly be saturated and dissolution would stop.

3.5 Comparison and discussion with other models

3.5.1 Can the dissolution of the small grains be neglected?

The dissolution of the small grains has been assumed negligible in several analytical hydration models. In the case of the simplest nucleation and growth model, the Avrami model, the question of grain consumption was not raised by Avrami because it made no sense in the case of the solidification of metals. However, when the model was imported in the field by Tenoutasse and DeDonder [12] the question was not raised either and as such neglected in the calculations. An improved nucleation and growth model (from Cahn [15]) for polycrystalline metals was imported into the field by Thomas [13]. In a similar fashion, the question of grains consumption made no sense in the context of the recrystallization of a polycrystalline metal and is thus neglected in this model (and its refinement [14]) though in a subtler way. Indeed, in the case of a nucleation and growth event at a grain boundary the growth is not prevented by the disappearance of the initial boundary though in the case of alite (and cement) the hydrate growth can be prevented if the grain on which it grows gets completely consumed. The phase-boundary and diffusion limited analytical models also systematically neglect the dissolution of the small grains. The interested reader may refer to section 3.2.2.4 and 3.2.3.1 of [3] for a review of the equations involved in these models and observe that none of them involve a Heaviside step function dropping the reaction rate to zero once the grain is totally consumed.

One novelty brought by this model is the emphasis put upon the role of the critical diameter. When an important part of the PSD is below this critical diameter the impact of the dissolution of the small grains is very significant. The simulations shown in figures 17 left and 19 right illustrate how big the difference can be when dissolution is neglected.

A consideration of the critical radius is therefore necessary to establish the range of validity for these models. Models that neglect the dissolution do not suffer much from this approximation as long as most of the PSD lies significantly above the critical radius. As a rule of thumb, the simulations shown in figure 19 and the experiments of figure 20 show that alite powders whose d_v50 (50th percentile in volume) is larger than 10 µm will not really be affected by the consumption of small grains during the first hydration day. However, if the d_v50 is smaller than 10 µm these models that are still able to fit the curve will (mis)interpret it in terms of their own parameters: they may for instance see a variation of the nucleation rate or growth rate for two different PSD when there really is only grain consumption.

Beyond one day the small grains may nevertheless be an issue for all models because the critical radius is intrinsically linked with the degree of hydration: by definition 100% of hydration means that all the grains have been consumed. Therefore, an alternative rule of thumb is that powders, whether alite or cement, that reach more than 50% of DoH will be affected by the consumption of the small grains. Because the degree of hydration of Portland cement at

one month is about 80%, any mechanistic model aiming at predicting the hydration over that period or longer must therefore necessarily take into account the consumption of the grains.

Finally, the value of the critical radius depends on the roughness and sphericity of the grains as equation 20 explicitly shows. Therefore, even for those models that take into account the dissolution, assuming the grains to be smooth and spherical may quite substantially underestimate the dissolution of the small grains.

3.5.2 On the assumption of sphericity and smoothness of the grains

Although the assumption of sphericity and smoothness of the grains has been made in several analytical as well as numerical models of alite hydration for the sake of simplicity in the derivation of the equations and fast computations it has not yet been quantified: is neglecting the roughness and form factor a small or gross approximation?

The analytical models concerned are in particular: the diffusion controlled models originally based on the Jander equation [65] or its variations (Kondo [25], Pommersheim and Clifton [66] [67], Ginstling and Brounshtein [68], Brown [69]) or models using the slowest mechanism out of nucleation and growth, boundary controlled and diffusion controlled (Bezjak and Jelenic approach [70] [71], Parrott and Killoh [72]). More recent models such as the Biernacki and Xie model [20] and Masoero and Co-workers [19] explicitly assume the particles to be spherical and smooth. Finally, the nucleation and growth models are all affected except for the Cahn-Thomas model [13] and its evolution [14].

The numerical models concerned are: the Johnson-Jennings model [22], the HYMOSTRUC model [26], the Navi-Pignat model [23] [24] and the μic model [16] [9].

The evolution of the calorimetry curve for three different values of the ratio Rou/F is plotted on figure 21. In blue is replotted the result of the 0.8 water to cement ratio model simulation, in red and black the curves if the grains were assumed to be respectively smooth rugby balls or spheres. In dotted lines are plotted the corresponding evolution of the critical radius. As can be seen the assumption of sphericity and smoothness does not shift the time of the peak significantly but produces a notable underestimation of the height of the heat released (the factor is roughly the value of Rou/F) and also of the degree of hydration.

The difference between the curves goes beyond a dilatation coefficient: the red curve is not simply the black curve times 6. Indeed because of the strong impact of the dissolution of the small grains, due to the relatively high proportion of these grains for the PSD used here, the right arm of the calorimetry curve evolves from strongly asymmetric to the left arm when the grains are assumed spherical and smooth to nearly symmetric when the grains are assumed rather aspherical and rough.

[9] Nevertheless, CEMHYD3D and VCCTL do consider non-spherical and rough grains

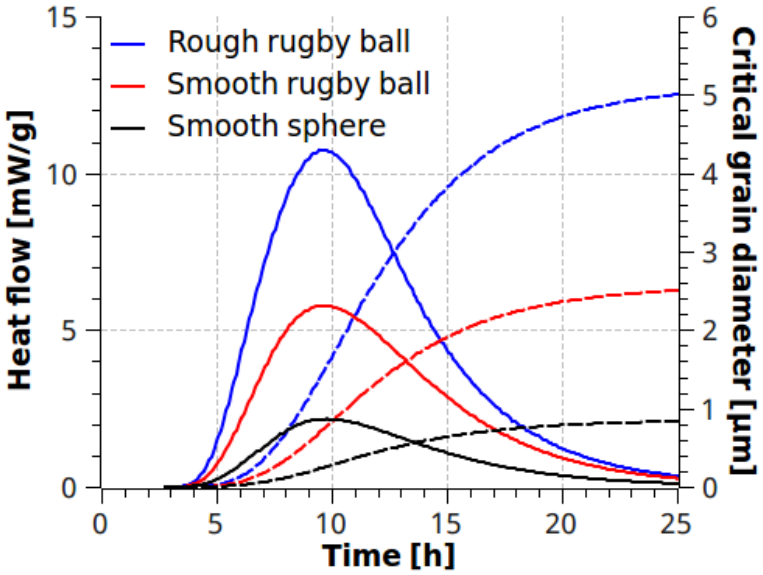

Figure 3.21 – Evolution of the heat flow and the critical radius with time for different value of the Rou/F ratio: 6 for the blue curve (a rough rugby ball), 3 for the red (a smooth rugby ball) and 1 (perfectly spherical and smooth grains).

3.5.3 On the indeterminacy of the interpretation of the calorimetry curves - The need for new criteria and a proper benchmark to assess the models

It is remarkable that among the 5 models that attempted to fit Costoya's calorimetry curves [14] [16] [19] [21] and the needle model) all of them succeeded though they defend quite different mechanisms as the cause of the transition from acceleration to deceleration. Even when they defend the nucleation and growth hypothesis their interpretations are significantly different: the model of Scherer [14] backfitted parameters on Costoya's data indicates a decrease of nuclei density while an increase in perpendicular growth rate with increasing PSD size, the Bishnoi variable C-S-H density µic model indicates that the growth rate fluctuates over a one order of magnitude - a large interval without clear trend, and finally the needle model that these parameters remain constant.

There is therefore a need to adopt stricter criteria to test models in order to really be able to get firm conclusions that will definitely tip the balance in favour of one of the position regarding the transition. Crucially models should remain falsifiable: they should take the risk to be experimentally refuted [73] [74]. Ideally, models should propose experiments that would represent a stringent test to them [74]. One way exploited with the needle model is to use input parameters that can be retrieved experimentally; constrain them within narrow enough experimental incertitude intervals and prove there is a single minimum of the error within this region.

Another way exploited by Honorio and Co-workers [21] is to make true predictions: no input parameter is backfitted from the calorimetry curve (they rely only on the PSD for their alite

model and additionally on the mass fraction for their cement model). This requirement is rather stringent and reflected by the relatively high error they obtain (24% for the Costoya calorimetry curves and about the same for their associated cement hydration model).

Models which use 4 or more unconstrained parameters, which are not directly observable or measurable (like the diffusion coefficient of C-S-H) or vague (like the fractional n-exponent of the Avrami model) can be easily fit the experimental curves often with several different combinations of parameters and so give little diagnostic information on underlying mechanisms.

This indicates that models that are able to fit any kind of calorimetric curve should be looked at suspiciously. On the one hand, because they can fit any curve they cannot state whether or not they missed some new phenomena so that they cannot bring new positive knowledge. On the other hand, since the falseness of their underlying hypothesis cannot be demonstrated either, they cannot bring new “negative” knowledge (since proving that a hypothesis is wrong is an advancement of knowledge). What is more critical is that because they cannot identify a new phenomenon (either because it is neglected or simply unknown yet), if there ever is one new phenomenon happening, they will still fit the curve and thus interpret the data in term of their own parameters; this leads to meaningless backfitted values and so is any trend that might appear. The interpretative usefulness of such models is then questionable.

To sum up, the Avrami model is the perfect example: it has 4 fitting parameters, 2 of which are neither directly observable nor measurable in the context of a cement paste (the n-exponent and the pre-exponential coefficient) and one is in addition vague and non-physical (the interpretation of fractional values of the n-exponent), it can fairly well fit any calorimetry curve though it does not take into account one of the most impacting factor: the PSD. Yet "coherent" trends in the backfitted values can be found: the n-exponent increases with decreasing powder size [77].

Finally, on the observation that five different hydration models based on different hypothesis fit all the calorimetry curves of Costoya’s PSD experiment, the article indicates the need to set up a proper benchmark for hydration models and new criteria to assess the quality, relevance and fertility of hydration models.

3.6 Conclusions

A new model for alite hydration during the first day based on the thesis of Bazzoni has been built. It is a nucleation and growth model based on the assumption that C-S-H nucleates and grows as needles or clusters of needles during the first day.

3.6.1 Answers to the initial motivations

Answers to Bazzoni's question

The point to point answer to her qualitative statements offered by the model are:

- The nucleation and growth of the needles is indeed sufficient to account for a transition, there is no need to invoke any other phenomenon. The model systematically predicts the correct order of magnitude of the calorimetry curve. To quantitatively grasp the transition the dissolution of the small grains needs to be taken into account. Yet its predictions are still slightly beyond the calorimetry experimental incertitude intervals leaving room free for discussion about whether some simplifying assumptions are too gross or whether some important factor has been missed.
- An increase in the needle length is indeed sufficient to explain the increase in the heat flow and degree of hydration in the proportion measured
- The contribution of the inner C-S-H is negligible during the first part of the deceleration period at least. However, from 20 hours on it should be responsible for part of the heat released.

A mechanistic model that avoid shortcomings of previous ones

The model has been tested on 14 experiments which is a wider set of experiments than any other set used to test other alite hydration models in the field. All its seven input parameters can be measured and are constrained by experimental confidence intervals, in particular they are true to SEM microstructural observations. As a consequence, the model satisfies Popper's criterion of being falsifiable.

The fits are made according to the standard gradient method and found to be satisfactory: the slight deviations from experiment can reasonably be accounted by the simplifications made for the grain and needles geometries for instance. The variability of the parameters found across all 14 experiments is small as exhibited in table 2, in agreement with the intuition that any alite surface reacts in a similar way.

The impact of the consumption of the small grains

The model has highlighted the role played by the small grains during the first hydration day whenever the d_v50 is smaller than 10 µm or whenever the DoH is higher than 50%. Beyond

one day models however need to account for the grains consumption because the DoH at one month amount to typically 50% for alite paste and 80% for cement pastes. Moreover, as shown in section 5.2, grains shape and roughness need to be realistic not to underestimate the grain consumption and misinterpret the heat curve in terms of other parameters.

3.6.2 Mechanisms causing the transition of the main hydration peak

Given that the model has been tested on a wider set of experiments than any other model in the field, and given it has no **free** fitting parameters, but only parameters **constrained** by experiments, we believe it provides substantial support to the hypothesis that part of the hydration peak can be explained in terms of nucleation and growth of needles.

Nevertheless, by contrast with most other nucleation and growth models, the cause of the transition is not impingement. The heat peak in the calorimetry curve is interpreted as the time where most of the needles have nucleated (and thus most of the surface is filled) and are in their fast growth period. Beyond this point needles gradually enter their slow growth period and asymptotically reach their final length leading to a decrease in the heat flow. The dissolution of the small grains further sharpens and slightly shifts the peak left but is not per se the mechanism causing the transition.

3.7 Acknowledgements

The authors thank Paul Bowen, Hadi Kazemi-Kamyab, Arnaud Muller and Julien Ston for many useful discussions and also Amélie Bazzoni and Xuerun Li for many useful inputs.

3.8 References

1. Klein, A. A. (1914). The Hydration of Portland Cement.Transactions of the Faraday Society, 14, 14-22.

2. Klein, A. A. (1919). The constitution and hydration of Portland cement.Transactions of the Faraday Society, 14, 14-22.

3. Gartner, E. M., Young, J. F., Damidot, D. A., & Jawed, I. (2002). Hydration of Portland cement. Structure and performance of cements, 13, 978-0.

4. R. Kondo and S. Choi, 5th Int. Symp. Chem. Cement, SP-98, Tokyo (1968)

5. Scrivener, K. L., Juilland, P., & Monteiro, P. J. (2015). Advances in understanding hydration of Portland cement. Cement and Concrete Research, 78, 38-56.

6. Scrivener, K. L., & Nonat, A. (2011). Hydration of cementitious materials, present and future. Cement and concrete research, 41(7), 651-665.

7. Thomas, J. J., Biernacki, J. J., Bullard, J. W., Bishnoi, S., Dolado, J. S., Scherer, G. W., & Luttge, A. (2011). Modeling and simulation of cement hydration kinetics and microstructure development. Cement and Concrete Research, 41(12), 1257-1278.

8. Dolado, J. S., & Van Breugel, K. (2011). Recent advances in modeling for cementitious materials. Cement and concrete research, 41(7), 711-726.

9. Avrami, M. (1939). Kinetics of phase change. I General theory. The Journal of Chemical Physics, 7(12), 1103-1112.

10. Avrami, M. (1940). Kinetics of phase change. II transformation-time relations for random distribution of nuclei. The Journal of Chemical Physics, 8(2), 212-224.

11. Avrami, M. (1941). Granulation, phase change, and microstructure kinetics of phase change. III. The Journal of chemical physics, 9(2), 177-184.30

12. Tenoutasse, N., & De Donder, A. (1970). The kinetics and mechanism of hydration of tricalcium silicate. Silicates Ind, 35, 301-307.

13. Thomas, J. J. (2007). A new approach to modeling the nucleation and growth kinetics of tricalcium silicate hydration. Journal of the American Ceramic Society, 90(10), 3282-3288.

14. Scherer, G. W., Zhang, J., & Thomas, J. J. (2012). Nucleation and growth models for hydration of cement. Cement and Concrete Research, 42(7), 982-993.

15. Cahn, J. W. (1956). The kinetics of grain boundary nucleated reactions. Acta Metallurgica, 4(5), 449-459.

16. Bishnoi, S., & Scrivener, K. L. (2009). μic: A new platform for modelling the hydration of cements. Cement and Concrete Research, 39(4), 266-274.

17. Bishnoi, S. (2008). Vector modelling of hydrating cement microstructure and kinetics.

18. Bishnoi, S., & Scrivener, K. L. (2009). Studying nucleation and growth kinetics of alite hydration using μic. Cement and Concrete Research, 39(10), 849-860.6

19. Masoero, E., Thomas, J. J., & Jennings, H. M. (2014). A Reaction Zone Hypothesis for the Effects of Particle Size and Water-to-Cement Ratio on the Early Hydration Kinetics of C3S. Journal of the American Ceramic Society, 97(3), 967-975.

20. Biernacki, J. J., & Xie, T. (2011). An advanced single particle model for C3S and alite hydration. Journal of the American Ceramic Society, 94(7), 2037-2047

21. Honorio, T., Bary, B., Benboudjema, F., & Poyet, S. (2016). Modeling hydration kinetics based on boundary nucleation and space-filling growth in a fixed confined zone. Cement and Concrete Research, 83, 31-44.

22. Jennings, H. M., & Johnson, S. K. (1986). Simulation of microstructure development during the hydration of a cement compound. Journal of the American Ceramic Society, 69(11), 790-795.

23. Navi, P., & Pignat, C. (1996). Simulation of cement hydration and the connectivity of the capillary pore space. Advanced Cement Based Materials,4(2), 58-67.

24. Navi, P., & Pignat, C. (1996). Simulation of effects of small inert grains on cement hydration and its contact surfaces. In The Modelling of Microstructure and its Potential for Studying Transport Properties and Durability (pp. 227-240). Springer Netherlands.

25. Kondo, R., & Daimon, M. (1969). Early hydration of tricalcium silicate: a solid reaction with induction and acceleration periods. Journal of the American Ceramic Society, 52(9), 503-508.

26. Van Breugel, K. (1970). Numerical simulation of hydration and microstructural development of cement-based composites. WIT Transactions on Engineering Sciences, 4.

27. Taylor, H. F. (1997). Cement chemistry. Thomas Telford.

28. Kjellsen, K. O., & Justnes, H. (2004). Revisiting the microstructure of hydrated tricalcium silicate—a comparison to Portland cement. Cement and Concrete Composites, 26(8), 947-956.

29. Scrivener, K. L. (1984). The development of microstructure during the hydration of Portland cement (Doctoral dissertation, Imperial College London (University of London)).

30. BENTZ, Dale P. CEMHYD3D: A three-dimensional cement hydration and microstructure development modelling package. Version 2.0. National Institute of Standards and Technology Interagency Report, 2000, vol. 7232.

31. BULLARD, Jeffrey W., ENJOLRAS, Edith, GEORGE, William L., et al. A parallel reaction-transport model applied to cement hydration and microstructure development. Modelling and Simulation in Materials Science and Engineering, 2010, vol. 18, no 2, p. 025007.

32. Bazzoni, A. (2014). Study of early hydration mechanisms of cement by means of electron microscopy (Doctoral dissertation, École Polytechnique Fédérale de Lausanne).

33. Kirby, D. M., & Biernacki, J. J. (2012). The effect of water-to-cement ratio on the hydration kinetics of tricalcium silicate cements: Testing the two-step hydration hypothesis. Cement and Concrete Research, 42(8), 1147-1156.

34. Bazzoni, A., Ma, S., Wang, Q., Shen, X., Cantoni, M., & Scrivener, K. L. (2014). The effect of magnesium and zinc ions on the hydration kinetics of C3S. Journal of the American Ceramic Society, 97(11), 3684-3693.

35. Costoya Fernández, M. M. (2008). Effect of particle size on the hydration kinetics and microstructural development of tricalcium silicate. (Doctoral dissertation, École Polytechnique Fédérale de Lausanne).

36. Gauffinet

37. Gallucci, E., Mathur, P., & Scrivener, K. (2010). Microstructural development of early age hydration shells around cement grains. Cement and Concrete Research, 40(1), 4-13.

38. Bukin A. D. Fitting function for asymmetric peaks (2007). arXiv preprint arXiv:0711.4449

39. Termkhajornkit, Pipat et Barbarulo, Rémi. Modeling the coupled effects of temperature and fineness of Portland cement on the hydration kinetics in cement paste. Cement and concrete research, 2012, vol. 42, no 3, p. 526-538.

40. Snyman, J. (2005). Practical mathematical optimization: an introduction to basic optimization theory and classical and new gradient-based algorithms (Vol. 97). Springer Science & Business Media.

41. Bernal, J. D. (1952). 3rd Symposium Chemistry of Cement.

42. Grudemo, A (1960). Chemistry of cement. In Proceedings of the 4th International Symposium, Washington (Vol 244)

43. Lawrence Jr, F. V., & Young, J. F. (1973). Studies on the hydration of tricalcium silicate pastes I. Scanning electron microscopic examination of microstructural features. Cement and Concrete Research, 3(2), 149-161.

44. Double, D. D., Hellawell, A., & Perry, S. J. (1978, March). The hydration of Portland cement. In Proc. R. Soc. Lond. A (Vol. 359, No. 1699, pp. 435-451). The Royal Society.

45. Walsh, D., Otooni, M. A., Taylor, M. E., & Marcinkowski, M. J. (1974). Study of Portland cement fracture surfaces by scanning electron microscopy techniques. Journal of Materials Science, 9(3), 423-429.

46. Daimon, M., Ueda, S., & Kondo, R. (1971). Morphological study on hydration of tricalcium silicate. Cement and Concrete Research, 1(4), 391-401.

47. Diamond, S. (1972). Identification of hydrated cement constituents using a scanning electron microscope energy dispersive X-ray spectrometer combination. Cement and Concrete Research, 2(5), 617-632.

48. Pratt, P. L., & Jennings, H. M. (1981). The microchemistry and microstructure of Portland cement. Annual Review of Materials Science, 11(1), 123-149.

49. Lea F.M.; The Chemistry of Cement and Concrete. Edward Arnold (Publishers) Ltd, London (1983)

50. Berodier, E. M. J. (2015). Impact of the Supplementary Cementitious Materials on the kinetics and microstructural development of cement hydration (Doctoral dissertation, École Polytechnique Fédérale de Lausanne).

51. Bérodier, E. et Scrivener, K. Understanding the Filler Effect on the Nucleation and Growth of C-S-H. Journal of the American Ceramic Society, 2014, vol. 97, no 12, p. 3764-3773.

52. MOTA GASSÓ, Berta. Impact of alkali salts on the kinetics and microstructural development of cementitious systems. 2015.

53. Mota, B., Matschei, T., et Scrivener, K. The influence of sodium salts and gypsum on alite hydration. Cement and Concrete Research, 2015, vol. 75, p. 53-65.

54. Richardson, I. G. (2000). The nature of the hydration products in hardened cement pastes. Cement and Concrete Composites, 22(2), 97-113.

55. Rossen, John Espen. Composition and morphology of CASH in pastes of alite and cement blended with supplementary cementitious materials. 2014.

56. Fonseca, P. C. et Jennings, Hamlin M. The effect of drying on early-age morphology of C–S–H as observed in environmental SEM. Cement and Concrete research, 2010, vol. 40, no 12, p. 1673-1680.

57. Allen, Andrew J., Thomas, Jeffrey J., et JENNINGS, Hamlin M. Composition and density of nanoscale calcium–silicate–hydrate in cement. Nature materials, 2007, vol. 6, no 4, p. 311-316.

58. Sakalli, Y. et Trettin, R. Investigation of C3S hydration by environmental scanning electron microscope. Journal of microscopy, 2015, vol. 259, no 1, p. 53-58.

59. Zhang, Z., Scherer, G. W., & Bauer, A. (2018). Morphology of cementitious material during early hydration. Cement and Concrete Research, 107, 85-100.

60. Garboczi, E. J., & Bullard, J. W. (2017). 3D analytical mathematical models of random star-shape particles via a combination of X-ray computed microtomography and spherical harmonic analysis. Advanced Powder Technology, 28(2), 325-339.

61. Xuerun Li private communication

62. Kelly, R. N., DiSante, K. J., Stranzl, E., Kazanjian, J. A., Bowen, P., Matsuyama, T., & Gabas, N. (2006). Graphical comparison of image analysis and laser diffraction particle size analysis data obtained from the measurements of nonspherical particle systems. AAPS PharmSciTech, 7(3), E93-E106.

63. Bye. G. C. (2011). Portland cement.

64. Bullard, J. W., Scherer, G. W., & Thomas, J. J. (2015). Time dependent driving forces and the kinetics of tricalcium silicate hydration. Cement and Concrete Research, 74, 26-34.

65. Jander, W. (1927). Reaktionen im festen Zustande bei höheren Temperaturen. Reaktionsgeschwindigkeiten endotherm verlaufender Umsetzungen. Zeitschrift für anorganische und allgemeine Chemie, 163(1), 1-30.

66. Pommersheim, J. M., & Clifton, J. R. (1979). Mathematical modeling of tricalcium silicate hydration. Cement and Concrete Research, 9(6), 765-770.

67. Pommersheim, J. M., & Clifton, J. R. (1982). Mathematical modeling of tricalcium silicate hydration. II. Hydration sub-models and the effect of model parameters. Cement and Concrete Research, 12(6), 765-772.

68. Ginstling, A. M., & Brounshtein, B. I. (1950). Concerning the diffusion kinetics of reactions in spherical particles. J. Appl. Chem. USSR, 23(12), 1327.

69. Brown, P. W., Pommersheim, J., & Frohnsdorff, G. (1985). A kinetic model for the hydration of tricalcium silicate. Cement and Concrete Research, 15(1), 35-41.

70. Bezjak, A. (1986). Nuclei growth model in kinetic analysis of cement hydration. Cement and Concrete Research, 16(4), 605-609.

71. Bezjak, A., & Jelenić, I. (1980). On the determination of rat constants for hydration processes in cement pastes. Cement and Concrete Research, 10(4), 553-563.

72. Parrot, L. J., & Killoh, D. C. (1984). Prediction of cement hydration. In Proc. Br. Ceram. Soc. (No. 35, p. 41).

73. Popper, K. R. (1959). The logic of scientific discovery. Hutchinson & Co Publishers

74. Popper, K. R., & Hudson, G. E. (1963). Conjectures and refutations. Routledge and Kegan Paul Publishers

75. MATLAB and Statistics Toolbox Release 2016b, The MathWorks, Inc., Natick, Massachusetts, United States

76. GNU Octave: a high-level interactive language for numerical computations

77. Scherer, G. W. (2012). Models of confined growth. Cement and Concrete Research, 42(9), 1252-1260.

3.9 Appendices

3.9.1 Full derivation of the single grain model

Derivation of the algorithm

Let

- $V_{C-S-H}^{produced}(R,t) = V(R,t)$ be the total volume of C-S-H contained in the needles that have nucleated and grown during [0,t[on one grain of radius R
- S_0 be the initial surface of the grain
- N(t) be the number of needles that have nucleated during [0,t[
- S(t) be the surface occupied by the needles at time t
- $v(t,\tau)$ the volume at time t of one needle that has nucleated at time τ
- $s(t,\tau)$ the surface at time t of the base one needle that has nucleated at time τ
- s_f the final surface occupied by a needle
- $S_p(t)$ be the surface occupied by the needles parking slots at time t (see subsection 9.1.2)

Let the time be discretized by steps of length Δt. A look at figure 7 will help follow the derivation, colours have been chosen to match this figure and help understand the sequence. At time $t = 0\Delta t$, nothing lies on the grain surface:

- $N(0\Delta t = 0$
- $S(0\Delta t) = 0$
- $S_p(0\Delta t) = 0$
- $V(0\Delta t) = 0$

At time $t = 1\Delta t$, a first generation of needles nucleates on the surface:

- $N(1\Delta t = k_n(1\Delta t)\Delta t(S_0 - S_p(0\Delta t))$
- $S(1\Delta t) = N(1\Delta t)s(1\Delta t, 1\Delta t)$
- $S_p(1\Delta t) = N(1\Delta t)s_f$
- $V(1\Delta t) = N(1\Delta t)v(1Dt, 1\Delta t)$

At time $t = 2\Delta t$,the first generation of needles grows while a second one nucleates:

- $N(2\Delta t = N(1\Delta t) + k_n(2\Delta t)\Delta t(S_0 - S_p(1\Delta t))$
- $S(2\Delta t) = N(1\Delta t)s(2\Delta t, 1\Delta t) + (N(2\Delta t) - N(1\Delta t))s(2\Delta t, 2\Delta t)$
- $S_p(2\Delta t) = N(1\Delta t)s_f + (N(2\Delta t) - N(1\Delta t))s_f$
- $V(2\Delta t) = N(1\Delta t)v(2Dt, 1\Delta t) + (N(2\Delta t) - N(1\Delta t))v(2\Delta t, 2\Delta t)$

At time $t = 3\Delta t$, the first and second generations of needles grows while a third one nucleates:

- $N(3\Delta t = N(2\Delta t) + k_n(3\Delta t)\Delta t(S_0 - S_p(2\Delta t))$
- $S(3\Delta t) = N(1\Delta t)s(3\Delta t, 1\Delta t) + (N(2\Delta t) - N(1\Delta t))s(3\Delta t, 2\Delta t) + (N(3\Delta t) - N(2\Delta t))s(3\Delta t, 3\Delta t)$
- $S_p(3\Delta t) = N(1\Delta t)s_f + (N(2\Delta t) - N(1\Delta t))s_f + (N(3\Delta t) - N(2\Delta t))s_f$
- $V(3\Delta t) = N(1\Delta t)v(2Dt, 1\Delta t) + (N(2\Delta t) - N(1\Delta t))v(2\Delta t, 2\Delta t) + (N(3\Delta t) - N(2\Delta t))v(3\Delta t, 3\Delta t)$

At time $t = k\Delta t$,k generations of needles have nucleated and grown:

- $N(k\Delta t = \sum_{i=1}^{k} k_n(i\Delta t)\Delta t.\Big(S_0 - S_p\big((i-1)\Delta t\big)\Big)$
- $S(k\Delta t) = \sum_{i=1}^{k} \Big(N(i\Delta t) - N\big((i-1)\Delta t\big)\Big).s(k\Delta t, i\Delta t)$
- $S_p(k\Delta t) = \sum_{i=1}^{k} \Big(N(i\Delta t) - N\big((i-1)\Delta t\big)\Big)s_f$
- $V(k\Delta t) = \sum_{i=1}^{k} \Big(N(i\Delta t) - N\big((i-1)\Delta t\big)\Big).v(k\Delta t, i\Delta t)$

S and V can be rewritten:

- $S(k\Delta t) = \sum_{i=1}^{k} \frac{N(i\Delta t) - N\big((i-1)\Delta t\big)}{\Delta t}.s(k\Delta t, i\Delta t)\Delta t$
- $S_p(k\Delta t) = \sum_{i=1}^{k} \frac{N(i\Delta t) - N\big((i-1)\Delta t}{\Delta t}s_f\Delta t$
- $V(k\Delta t) = \sum_{i=1}^{k} \frac{N(i\Delta t) - N\big((i-1)\Delta t\big)}{\Delta t}.v(k\Delta t, i\Delta t)\Delta t$

By letting Δt converges to 0 as fast as k converges to infinity (so that $k\Delta t$ remains constant) we get:

- $N(k\Delta t = \int_0^t k_n(\tau)\Big(S_0 - S_p(\tau)\Big)d\tau$

- $S(k\Delta t) = \int_0^t \frac{dN}{d\tau}(\tau).s(t,\tau)d\tau$
- $S_p(k\Delta t) = \int_0^t \frac{dN}{d\tau}(\tau).s_f d\tau$
- $V(k\Delta t) = \int_0^t \frac{dN}{d\tau}(\tau).v(t,\tau)d\tau$

3.9.2 Derivation of the Rou/F ratio from the PSD and BET specific surface

see the published version in Cement and Concrete research

3.9.3 Limitations of the needle model

see the published version in Cement and Concrete research

3.9.4 Errors calculation and fitting process

see the published version in Cement and Concrete research

3.9.5 Matlab code and associated files to rune the Bazzoni w/c = 0.8 simulation

see the published version in Cement and Concrete research

Experiment	l_{max}	r_{max}	t_c	K_n	t_{stop}	E_{Calo}	E_{DoH}
	[nm]	[nm]	[h]	[/µm²/h]	[h]	[%]	[%]
Single grain model simulation							
w/c Bazzoni experiment							
Confidence interval 0.4	[275 340]	[28 51]	[3 7]	[20 200]			
w/c = 0.4	340	41	3.5	40	5	7	2
Confidence intervals 0.8	[345 450]	[28 51]	[3 7]	[20 200]			
w/c = 0.8	370	44	4.0	40	5	7	1
Average Error						***7***	***1.5***
Bazzoni's doping experiment							
Confidence interval pure	[220 290]	[20 50]					
Pure	290	29	3.5	40	5	21	18
Pure McCrone	290	29	3.5	40	4	15	5
Confidence interval Zinc	[370 430]	[30 50]					
Zinc	400	35	3.5	40	5	11	4
Zinc McCrone	400	35	3.5	40	3	21	10
Average Error						***17***	***9***
Li's doping experiment							
No Zinc	290	29	3.5	40	5	15	3
1% Zinc	400	35	3.5	40	5	12	10
3% Zinc	400	35	3.5	40	5	9	6
Average Error						***12***	***6***
Costoya PSD experiment							
6 µm	290	35	5.5	40	4	27	9
13 µm	Id	Id	Id	Id	Id	14	15
18 µm	Id	Id	Id	Id	Id	16	8
38 µm	Id	Id	Id	Id	Id	22	21
82 µm	Id	Id	Id	Id	Id	48	46
Average Error						***25***	***20***
6 µm optimized	270	27	4	60	4	11	6
13 µm optimized	300	30	5.5	60	4	13	10
18 µm optimized	300	36	6	50	3	10	4
38 µm optimized	300	35	6	40	5	17	8
82 µm optimized	370	44	5.5	60	3	11	5
Average Error						***12***	***7***
Total average						***16.2***	***10.1***
Standard deviation						***9.1***	***9.9***

4 The Later Ages

Cement typically hydrates up to 50% within one day but only reaches about 85% of hydration at 28 days. Why does cement hydrate more within one day than in the following 27? Why does it never reach 100% ?

Space filling, diffusion limitations, dissolution limitations and changes in the pore solution saturation are the hypotheses raised in the literature. So far, they have not been expressed mathematically and therefore escape a rigorous quantitative assessment.

The goal of this chapter is to test the first hypothesis: is space-filling sufficient to quantitatively account for the later ages slow down? The model presented here is an upgrade of the main hydration peak one published [13] and presented in the previous chapter.

In order to build the later age model, the chapter opens with the introduction of new concepts, some of them are trivial, some other like the Distance Map Distributions (DMD) are new and deserve a special treatment. Then, the role of the gap opening phenomenon is highlighted, a rule of thumb that estimates the characteristic DoH (Degree Of Hydration) at which the kinetics slows down due to the space filling is derived.

Following this qualitative overview of the space filling mechanisms, the model is derived. In short, it computes the volume of C-S-H, derives the whole phase assemblage from the stoichiometric equation and distributes the phases in space with DMDs. A test on a dedicated benchmark follows.

The model is shown to capture the PSD and w/c ratio influence at 1 and 28 days though with strong deviation for two out of six curves. The chapter closes with the answer to the initial question: space-filling is a leading mechanism in the later ages but entails sub-mechanisms. Furthermore, other mechanisms also play a role. In short, the later age kinetics is not controlled by a single mechanism but by the cumulative effect of several non-linear and coupled mechanisms. To quantitatively account for the later age kinetics all these effects and their coupling must be considered.

Contents

4.1 New concepts to describe the microstructure evolution

The derivation of the later age model requires the introduction of new concepts. Some of these new concepts, shell detachment or inner/outer space, are just useful vocabulary and hide no mysteries. Other ones, like the Distance Maps Distributions (DMD) are new to the field and deserve a special attention. These concepts allow for a more precise description of the microstructural phenomena, in particular space-filling.

This section also aims to progressively build a qualitative mental representation of the later age mechanisms. This paves the way for the derivation of the model.

4.1.1 Shell, scaffold and cell

OUTER SHELL means the outer C-S-H plus the water and air possibly contained between and inside the needles. INNER SHELL means the inner C-S-H plus the water and air possibly contained within it. Together they form the SHELL.

SCAFFOLD means the surface on which the needles grow. Initially this corresponds to the grain surface, but the shell eventually detaches from the receding anhydrous grain so that the scaffold corresponds to the last surface where the alite grain and shell were in contact. Note that the scaffold has no volume - by contrast with a shell - because it is a surface.

CELL means the combination of an anhydrous core, its shell, the water area closest to its outer C-S-H shell than any other shell, the water inside the gap left between the anhydrous core and the inner shell (or the scaffold if the inner C-S-H has not yet precipitated).

These terms are illustrated on figure 4.1.

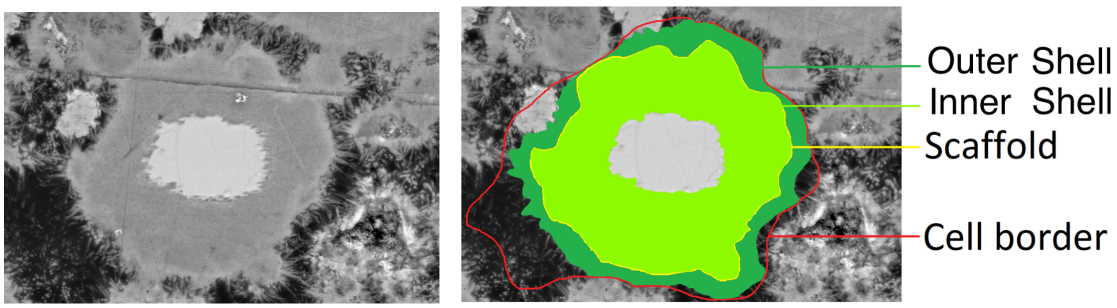

Figure 4.1 – Illustration of a shell, scaffold and cell border on a SEM polished section. Only the cell border is represented: the cell contains everything within its border. SEM picture of an alite paste at 28 days, w/c = 0.7. Image taken at 7 kV, WD = 5.5 mm, the width of the image is 20 µm.

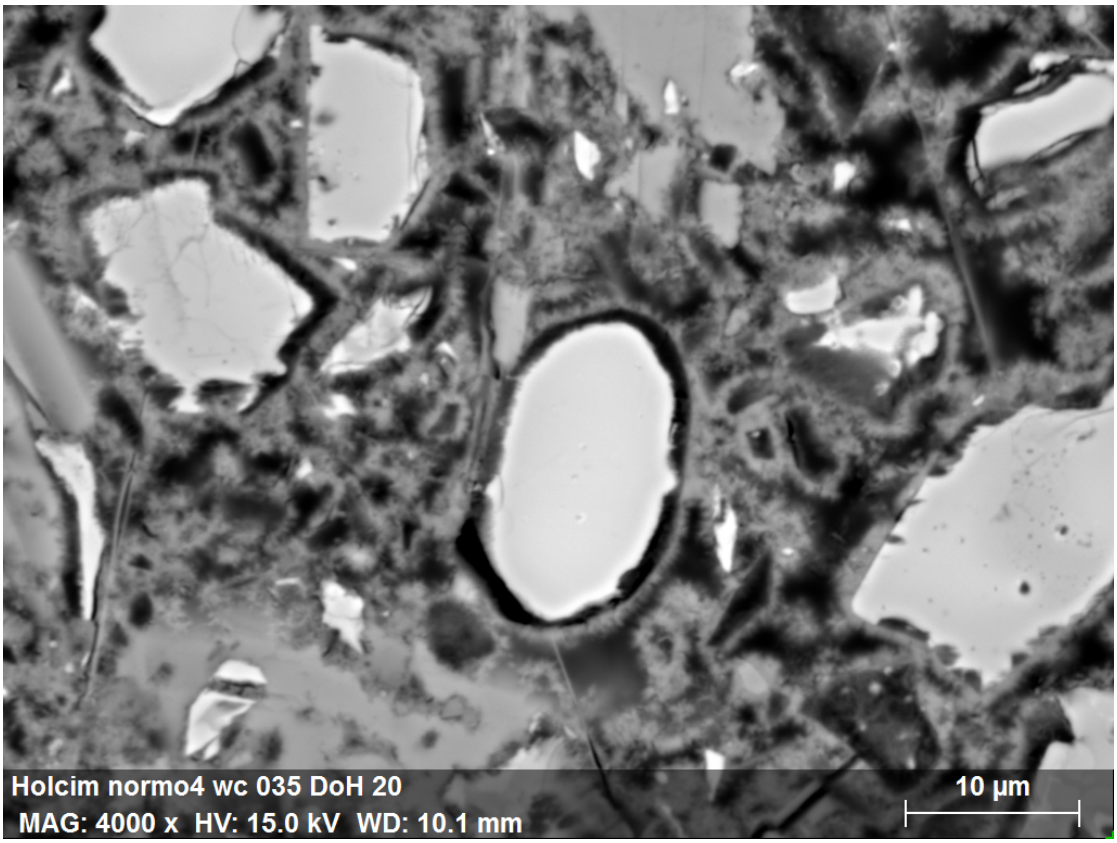

Figure 4.2 – A w/c = 0.35 PC paste at 18h and DoH = 30 %. The gap is about 1 µm +/- 1 µm. Notice the scaffold detachment and gap opening. Grains below 3 µm have vanished leaving empty shells.

4.1.2 Shell detachment and the gap opening

A striking feature of pastes at one day is the gap that opens between the shell and the receding anhydrous grains (figure 4.2). This gap means the shell detached earlier in time. As the needles nucleate and grow on the surface, they eventually form a rigid shell. The whole assemblage of needles then behaves as a single rigid object and detaches from the anhydrous core (figure 4.3).

Before the shell is completed, the needles carry on nucleating on a receding scaffold. As is demonstrated in subsection 4.5.2, the shell is completed on average at about 20% local gel-to-space ratio (see figure 4.35) after the scaffold has receded by about 100 nm. This marks the start of the gap opening and corresponds roughly to the final setting time.

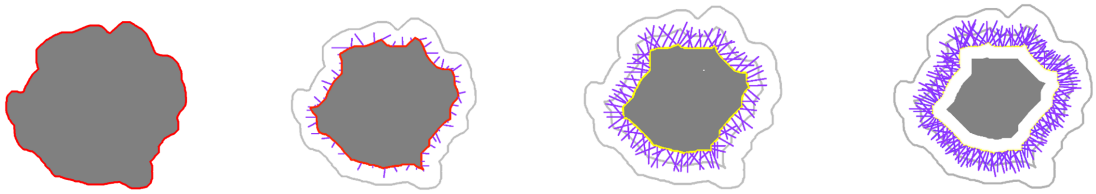

Figure 4.3 – Illustration of the scaffold receding as hydration progresses. First picture: initial grain with the scaffold in red, at this time it matches the initial grain surface. Second picture: as hydration proceeds some needles have nucleated and grown, the grain has slightly dissolved and the scaffold has tracked the receding grain surface. Third image: as hydration further carries on, already existing needles have grown longer and new ones have nucleated; the scaffold has furthered receded but the truss is now complete, the shell is rigid, so that it will not shrink anymore. Fourth figure: still more and longer needles on the scaffold as hydration goes on; the scaffold has stayed at the previous position but the gap has opened. Note that the scale of the receding is here exaggerated by one order of magnitude for the sake of illustration – otherwise the receding would be imperceptible: it is about 100 nm as computed by the model on the experiments used to test it in section 4.5.

Shell detachment and final setting time

The setting time is by definition the time at which the paste loses plasticity[1]. For this to happen the skeleton of hydrates must 1- percolate and 2- behave as a rigid whole. As hydration proceeds, the number and thickness of the percolation paths increase: the skeleton branches out and thickens. When a sufficient number of percolation paths are completed, the paste is stiff enough to bear the capillary pressure exerted by opening air voids (before it, the skeleton is not stiff enough and the overall paste volume decreases: it shrinks). The skeleton is eventually made by the assemblage of all the grains shells.

The skeleton thus becomes stiff enough above a minimum gel to space ratio and when most shells are sufficiently rigid. When both events have occurred, the paste is no longer plastic: this corresponds roughly to the final setting time. In practice, for common alite fineness and w/c, this happens at about the peak time.

The gap opening happens earlier and is larger for smaller grains

The smaller the grain the earlier and the higher the gap opening. The gap is thicker for small grains because of a specific surface area effect; that was already demonstrated in the main hydration peak model on figure 17 of [13] and replotted here on figure 4.4. This is consistent with SEM observations that show more prominent gaps for smaller grains than bigger ones. Because small grains shrink faster than big ones, their surface decreases faster than big ones so that their concentration of needles per unit of surface is higher: their shell is completed

[1] There is no sharp setting time but rather a range. The agglomeration of grains due to the sedimentation plays a role that is not modelled in the present thesis. This does not change the fact that air voids only nucleate when the paste is stiff enough, which translates to a gel-space ratio threshold as explained in the paragraph.

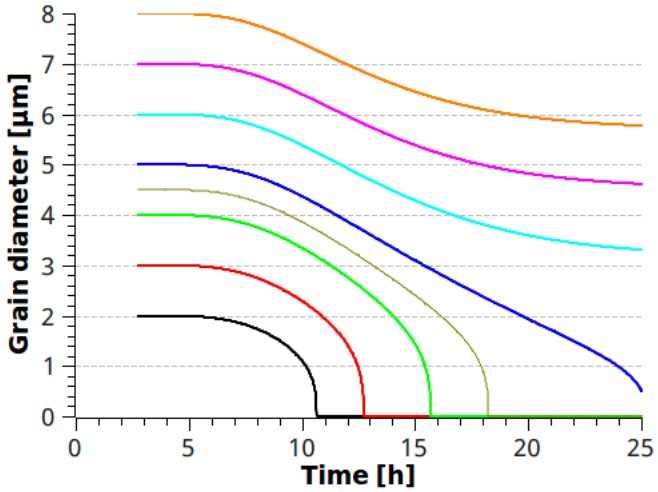

Figure 4.4 – Evolution of grain diameters from the needle model on Bazzoni's w/c=0.8 alite experiment. The gap opening is more prominent on small grains because they shrink quicker. At 16h, 4 µm grains have vanished: their gap is 2 µm thick, whereas 8 µm grains have lost about 1.8 µm in diameter at 24h, which makes a 0.9 µm thick gap. From [13].

earlier.

4.1.3 Inner / Outer space

INNER SPACE means the space between the scaffold and the receding anhydrous core (black area on figure 4.5). It may or not contain inner C-S-H, (inner) Portlandite, (inner) capillary water and air.

OUTER SPACE means the complementary set: it contains the outer C-S-H shell, (outer) Portlandite, (outer) capillary water and air (red area on figure 4.5). The scaffolds mark the frontier between the two domains.

4.1.4 Empty shells, living/dead shells

As hydration goes on, small grains eventually dissolve (figures 4.4 and 4.5). By 24h, 5 μm grains have dissolved in alite pastes, and about 7 μm in PC pastes. An EMPTY SHELL is a shell whose anhydrous core has completely dissolved . If a scaffold is close to a source of ions, i.e. if it still has its anhydrous core or if a neighboring cell still possess it AND if there is enough capillary water for ions transport to occur between them, then this is a LIVING SHELL; otherwise it is a DEAD SHELL.

N.B.: To avoid confusions, an empty shell is necessarily a Hadley grains but the opposite is untrue: a Hadley grains may hide a core below the 2D polished section that is not observed by SEM. A Hadley grain is a grain whose anhydrous core is not observed on 2D SEM sections, but

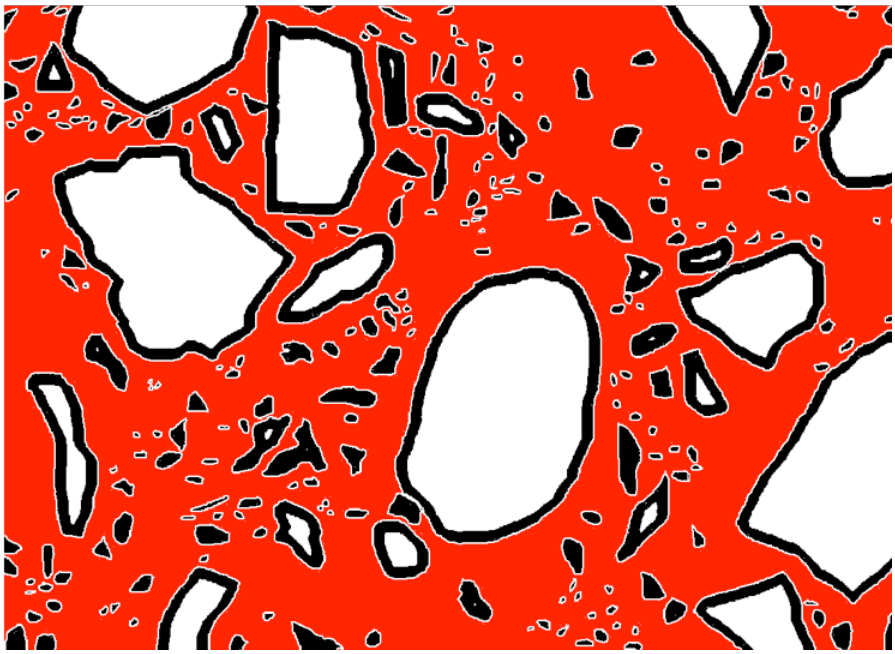

*Figure 4.5 – Illustration of the division of space in **outer space (red)** and **inner space (black)**. In white are represented the scaffolds and anhydrous grains within (if any left). N.B. the anhydrous core have been obtained by numerically eroding the scaffold: in reality grains do not systematicaly shrink concentrically: see figure 4.2.*

this does not tell whether or not the core is beneath the surface. As a consequence, Hadley grains are directly observable on polished sections and can be quantified whereas empty shells are not.

4.1.5 Cells influence domains, the living/dead subdomains

If we now take the point of view of the living grain that supplies the ions, then all the empty shells that are closer to this cell than to any other define the CELL INFLUENCE DOMAIN. At time t = 0, all cells are living and their influence domain only contains one shell: their own. As hydration proceeds, grains progressively dissolve and the surviving cells have wider and wider influence domains, in the order of ten to twenty microns bigger than their anhydrous core at 80% DoH for common w/c. This is illustrated on figures 4.6 and 4.7.

Within this domain, the supply cell will feed in priority the closest empty scaffolds. Depending of the capillary water left and volume fraction of C-S-H, the cell may only be able to feed the empty shells closer than a characteristic extinction distance. This distance separates the LIVING SUBDOMAIN, all empty shells that are close enough to the source, from the DEAD SUBDOMAIN, all empty shells that are too far from the source. The probability of growth of the needles on an empty cell will therefore vary with its distance from the source cell and the

space filling.

4.1.6 Five water reservoirs and the emptying hierarchy

As hydration proceeds, the water is emptied from the coarsest water pore to the smallest ones. This emptying process justifies the water division in five reservoirs.

The WATER BETWEEN THE NEEDLES is as expected the water adsorbed between the needles. Its characteristic pore size lies within the range of 10 to 100 nm.

The EXTERNAL CAPILLARY WATER is the capillary water in the outer space minus the water between the needles. Its characteristic pore size starts at 100 nm and has no upper bound.

The INTERNAL CAPILLARY WATER is the capillary water in the gap (if any). Its characteristic pore size lies between zero and a few microns.

The OUTER C-S-H WATER is the water locked within the C-S-H needles. Its characteristic pore size varies from 1 to 10 nm.

The INNER C-S-H WATER is the water possibly contained within the inner C-S-H. Its characteristic pore size varies from 1 to 10 nm. At the time of writing this manuscript, it remains an open question whether the inner C-S-H contains water porosities.

Because they have the coarsest pores, the first reservoirs to empty are the external and internal capillary ones. The balance between the two is addressed below in the section dealing with the Distance Maps Distribution (DMDs) (there it is shown that the water is actually emptied first in the external capillaries for most practical cases). Whenever these two reservoirs are exhausted, the model assumes then the depletion of the water between the needles, followed by the outer C-S-H water and eventually the inner C-S-H water are depleted.

The same nomenclature applies to the air pores.

N.B.: This categorization of water in five reservoirs resembles the one from Muller but is not exactly identical: what Muller calls “capillary water” corresponds here to the sum of external plus internal capillary water together with the water between the needles. Muller suggest “interhydrates” corresponds to the water between the needles (Muller’s Ph.D thesis, p. 88). What Muller calls “gel pores” corresponds here to the outer (and possibly inner C-S-H) water.

4.1.7 The phases are NOT randomly distributed in space

Looking at an SEM section for the first time may be confusing, hydrates seem spread all over the place, but their distribution is actually absolutely not random.

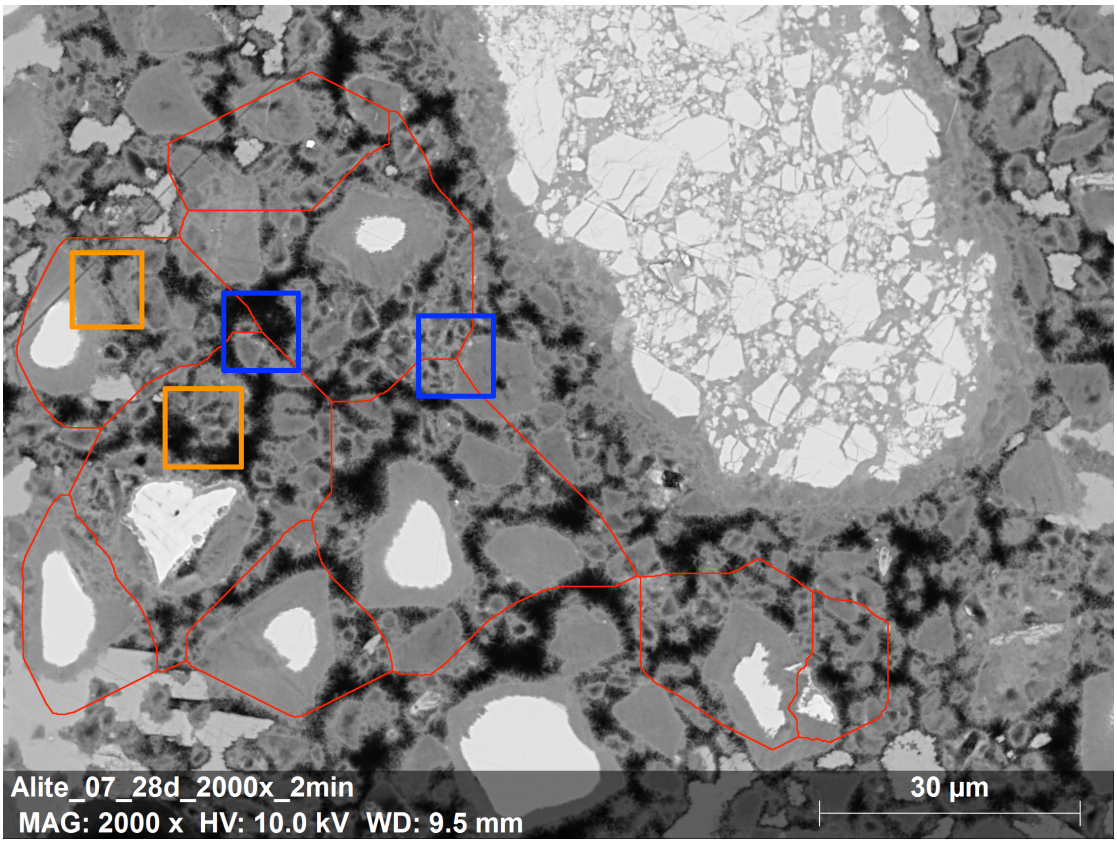

Figure 4.6 – Alite paste at 28 days and w/c = 0.7. In red are represented a few cell influence domains. The blue squares spot intersections of three domains: zones where shells are particularly far from any core and are thus more likely to be dead shells. On the opposite, the orange squares spot shells that are closer to anhydrous cores and are thus more likely to be living shells. The distinction between living and dead shells cannot however be simply made by visual inspection, not only because of the sectioning effect, but also because the transport of ions depends on the amount of water left in the external capillaries, which is not visible or deducible from an SEM section. Many Hadley grains are seen throughout the pastes: all grains smaller than 10 µm have completely dissolved. Because of the sectioning effect, some these shells hide an anhydrous core below the surface (in that case these are living shells), other do not (in that case they may or not be living shells depending how close they are to a neighbouring anhydrous core).

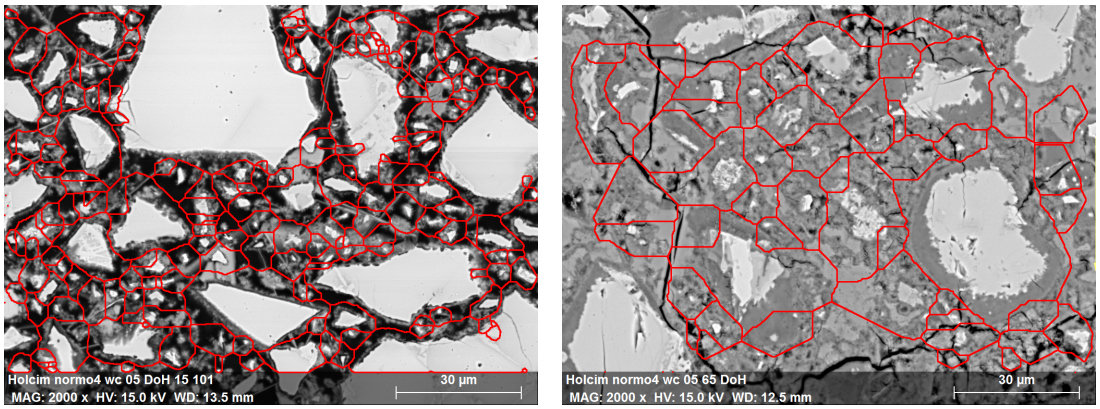

(a) a *(b) b*

Figure 4.7 – Normo 4 PC paste at 12 hours/DoH = 25% (left) and 14 days/DoH = 75% (right) for a w/c = 0.5. In red are represented the cell influence domain. As the DoH increases, the influence domains grow because of the small grains consumption (the density of grains smaller than 10 µm is much higher on the left than on the right). The size of the influence domains also increase with the w/c (compare the right figure with figure 4.6 dealing with an alite paste at w/c = 0.7). By contrast with the alite paste of the previous figure, the right figure here has a much lower external capillary fraction. Even if the cell domains are smaller here than on the alite paste, the shells that are at the intersection of three red lines, i.e. shells that are far from any anhydrous core, may likely be dead shells because the ions cannot easily travel through the pore network. Note that some of the grains are actually ferrites, this figure only aims at qualitatively illustrating the notion of influence domain.

First, the C-S-H, be it the outer or inner C-S-H, always nucleates heterogeneously on the scaffolds. On the contrary, the air voids always nucleate in the largest capillary pores, that is as far as possible from any shell. Portlandite preferentially forms in the outer space (it is barely seen mixed with the inner C-S-H). In alite pastes, Portlandite forms big clusters, whereas in PC pastes it is finely distributed.

This hydrate distribution allows for an analytical way of representing space-filling: through Distance Map Distributions introduced in section 1.9.

4.1.8 What does space mean? How to quantify space filling? Space / Water available for precipitation / Impingement: three faces of the same phenomenon

To say that space filling limits the reaction rate amounts to saying that the water filled spaces available for precipitation are depleted.*The water available for precipitation is any water pore where the crystallization pressure is insignificant*; that is any pore larger than about 10nm in the context of cement pastes[2] . Following the classification in five water reservoirs, this corresponds to the external and internal capillary water as well as the water between

[2] In (Scherer, 1998, p. 1355) we read: "For the crystal to advance arbitrarily deeply into the body, the driving force must be sufficient for the crystal to pass through the breakthrough radius. This is the radius of the largest opening leading into a percolating network of larger pores; it is the characteristic pore size that controls the permeability and it corresponds roughly to the inflection point in a mercury-intrusion or nitrogen- desorption curve". The

the needles. This other formulation of space filling, capillary water plus water between the needles, means that space filling plays a role whenever there is not such water left. From Muller experiments [11, fig. 4.22 c)], we guess this phenomenon is in practice significant for w/c about 0.5 or lower.

These considerations suggest a first formula to quantify space-filling: the ratio of external (/internal) capillary water over the outer (/inner) space:

$$f^{v}_{ext_{space}} = \frac{V_{H_{cap_{ext}}}}{V_{outer-space}} \tag{4.1}$$

And in a similar way:

$$f^{v}_{int_{space}} = \frac{V_{H_{cap_{int}}}}{V_{inner-space}} \tag{4.2}$$

Yet another way to say that space filling limits the reaction rate is to say that impingement significantly limits the hydrates growth. To quantify the space filling in term of impingement raise the need to quantify the probability of impingement of the phases.

The impingement of the hydrates can be estimated through probability considerations. Under the assumption of random distribution of the hydrates, the probability of impingement is the ratio of the volume of hydrate over the total volume; this reasoning intervenes in the derivation of the Avrami model. But as explained earlier, the hydrates are not randomly distributed in space, so that the probability of impingement needs more work and is presented in section 3.7.

4.1.9 Where do air voids open up? capillary water distribution between the internal and external reservoirs, pore size and Distance Map Distributions (DMD)

Although it may seem obvious that C-S-H shells impinge against one another or other solid phases like Portlandite, it may seem less obvious that they impinge against air voids. By contrast with some minerals that can still grow in air, C-S-H does not grow in that condition as Therefore, the evolution of the air voids, their distribution between the outer and inner space, are required to compute the probability of C-S-H impingement and capture the later ages kinetics.

One particularly germane tool is the Distance Map Distribution (DMD) of the pore structure. Not only does it enable the computation of the distribution between the internal and external

critical pore entry radius in a PC paste hydrated at w/c = 0.4 is about 20 nm at three days, and 8 nm from 14 days on as seen on (Berodier's thesis, 2015, fig. 5.15).

air and water reservoirs, but it provides the distribution of the whole phase assemblage in space: it replaces the qualitative term space-filling by a quantitative description of it.

Furthermore, because external DMDs are shown to have a Gaussian shape, they can be readily predicted without any simulation but purely from knowledge of the w/c ratio, the specific surface of the powder and the average interparticle distance. As a consequence, the computation cost is dramatically reduced compared to explicit microstructural simulations: only a simple analytical equation need to be solved to get the DMD.

Air voids preferentially open in the biggest pores ... but what is a pore size?

Thermodynamically, air voids should preferentially open in the biggest pores so as to minimize their interface curvature. Unfortunately, the pore network is a connected set: there is no unique way to divide it into pores and to define the contour or size of a pore, where they start or end. Pore sizes are commonly defined according to an experimental technique, like MIP or NMR. Each technique proposes a different interpretation of pore size that depends on its underlying physical principles: MIP rather computes a pore throat distribution than a pore size distribution, NMR interprets a *characteristic signal decay distance* which corresponds to a surface to volume ratio according to the theory.

What definition of a pore size would then fit the physical air void opening principle? Let us make a thought experiment on figure 4.5 where should the voids first open? Intuitively in the "biggest pores": on the top border of the image in the middle (slightly right) or perhaps on the left border also in the middle where there are two wide areas free of any grains. These two pores are shown in purple on figure 4.8. Once the air voids have grown in these pores, they eventually touch neighbouring grains (yellow spots). At this point, growing further would require the surface curvature to suddenly bend strongly to pass through the necks. This seems less favorable than further nucleating in other places where the curvature is lower: in the green areas[3].

If we now try to formulate the intuitions to set up a definition of pore size true to the surface curvature minimization, we may propose: "air pores preferentially open in the widest available zones, that is in zones whose points are as far as possible from any shell". If we could compute the distance of each pixel to the closest shell, we could guess where the air voids should open. That exactly is what Distance Maps (DM) do. On the figure 4.8 right is presented the distance map associated to the left image: the brightest areas correspond to the purple and green zones of the left image.

[3] Note that this approach is conservative: real mixes spontaneously incorporate air bubbles because of the mixing. Air would a priori rather propagate from these already existing bubbles than opening new ones [8], at least initially. This does not harm one of the main conclusion of this thesis, but rather reinforce it: that the air rather fill the external space than the internal one and therefore exacerbate the external space filling.

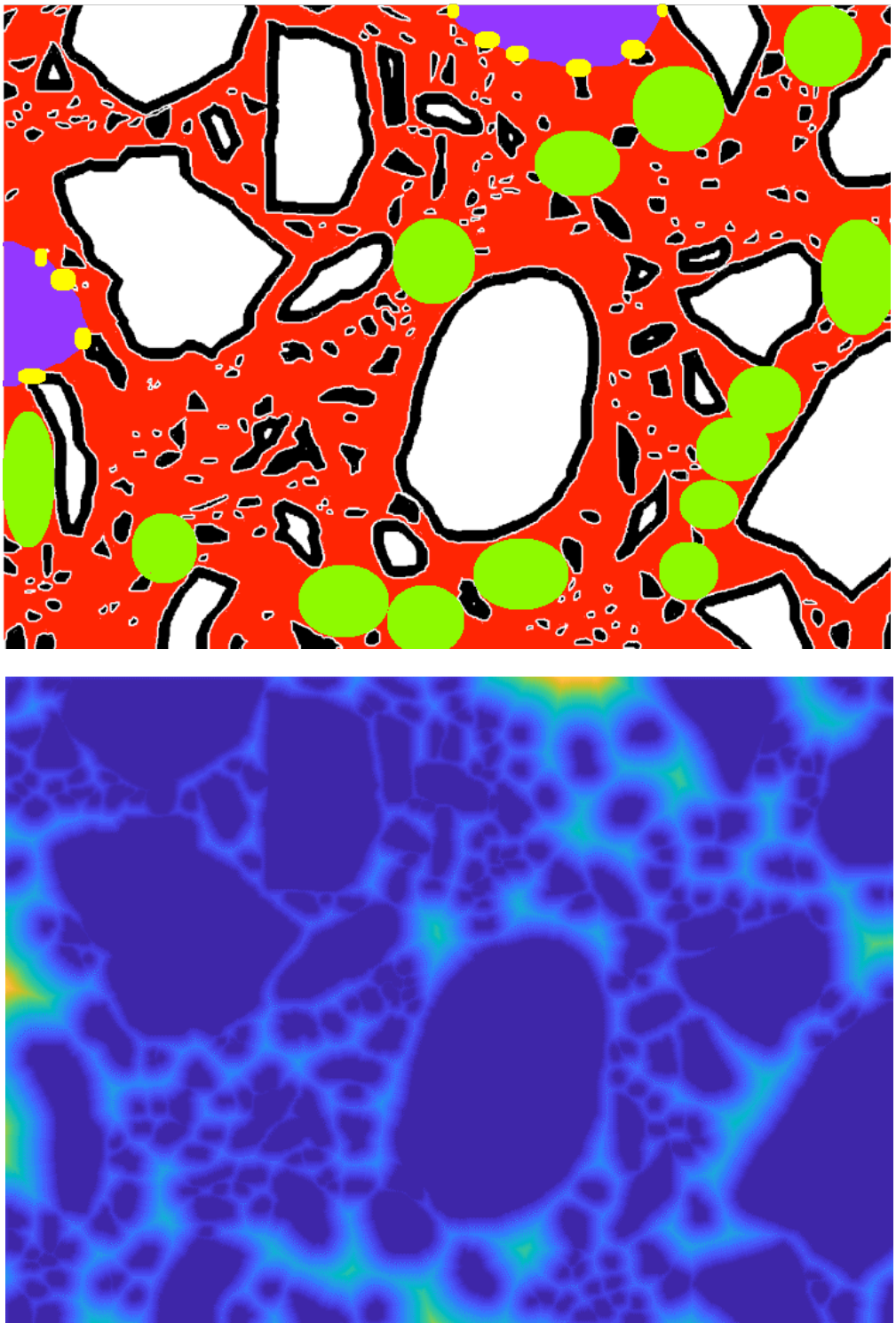

Figure 4.8 – Left: Illustration of where the air voids intuitively open (purple and green areas). The two biggest pores are in purple on the top and left side. Right: associated distance map: The brightest area matches the purple and green areas of the left image, which suggests the distance map is a relevant tool to determine where the air bubble open. These pictures are only there for illustration, the rigorous way to determine the biggest pores rely on 3D microstructures, not 2D sections.

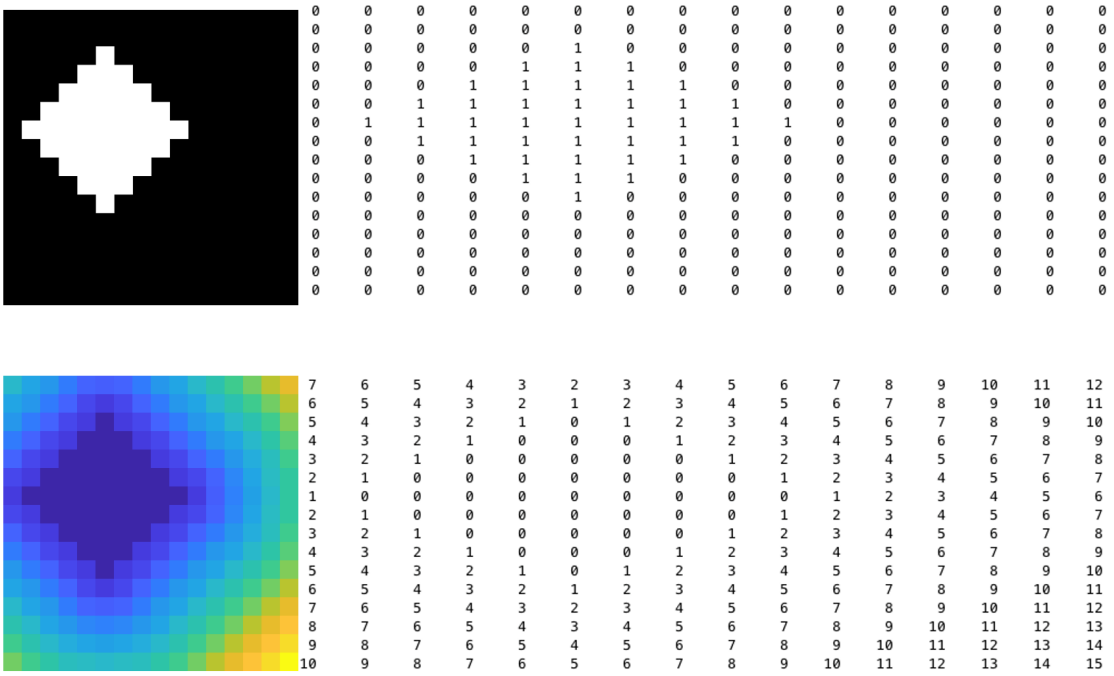

Figure 4.9 – Illustration of a simple binary image (top left) together with its associated matrix (top right); 1 code white pixels and 0 code black pixels. The DM associated to this image is shown below together with its associated matrix. On this DM matrix, the 1 are the closest pixels to the surface, their sum represents the perimeter of the particle. By analogy, in 3D, the sum of the 1 corresponds to the surface of a particle, or of a powder if there are several particles.

Distance Maps: definition and examples

Let us consider the 2D image presented on figure 4.9. This image hides a matrix of zeros (black pixels) and ones (white pixels). The distance map associated to this image computes for each pixel its shortest distance to a white pixel. Notice that the number of 1 on the DM matrix is the perimeter of the particle; by analogy, in 3D, they would represent its area.

Let us now consider a 2D section output of the µic model and compute its DM (figure 4.10). On the DM the brightest yellow pixels are those that are the farthest from a scaffold, they are the biggest pores and thus where the first air voids open.

Distance Maps Distributions and the distribution of the phases in space

External DMDs Let us now consider the distributions of ones, twos, threes, etc. of the DM matrix of 3D microstructures simulated with µic. Figure 4.11 shows 2D section of µic output with varying w/c and figure 4.13 displays the associated DMD per unit of volume (left) or per unit of mass of alite. On figure 4.13, the four relevant pieces of data to look at are: i) the maximum pore size, ii) the area below each curve, iii) the value of the distribution at 0 and iv) the distance of the peak.

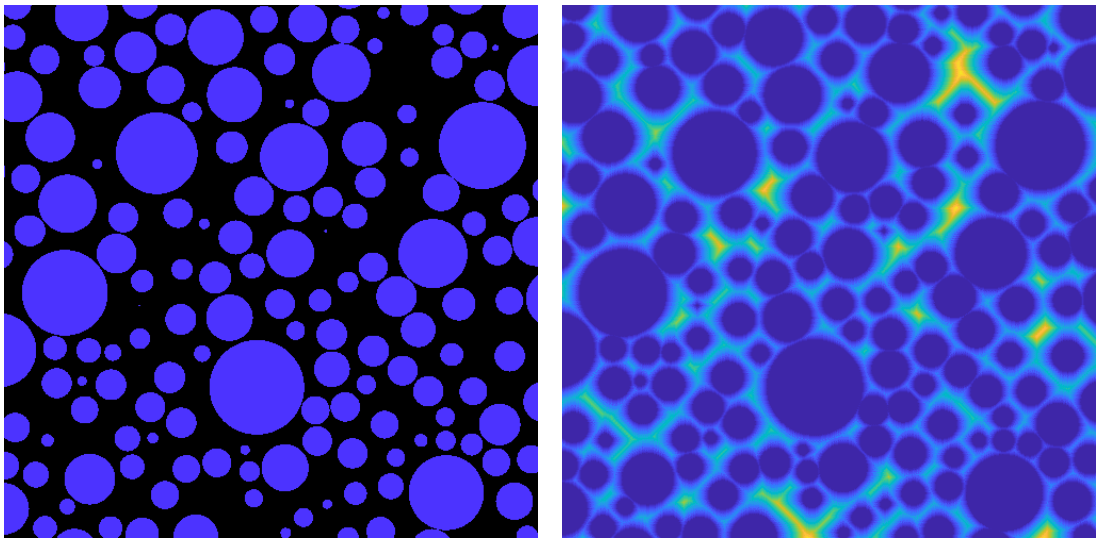

(a) *(b)*

Figure 4.10 – 2D section of a µic simulation (left) together with its associated distance map (right). The bright yellow areas on the right image are the pixels that are the farthest from a scaffold (compare with the left image), they are the biggest pores and where the air bubble will preferentially nucleate and grow. In reality, the DM should be processed on 3D structure, not on a 2D section; this figure only serves as illustration.

- The maximum pore radius is about 3.5 μm for the w/c = 1 paste whereas it is only of about 1 μm for the w/c = 0.2 paste. A 3.5 μm pore size means a 7 μm spherical ball can fit somewhere in the microstructure. These values may seem low when compared with their corresponding sections on figure 4.11, especially the w/c = 1 whose section shows large black areas. Nevertheless, considering figure 4.12 where the grains hidden behind the surface are displayed, this value seems more correct.

- The area below each curve represents the space volume, initially the volume of water that is represented in black on figure 1-11. On the DMD per unit of paste (left), the area under each curve is proportional to the corresponding black area fractions of figure 4.11.

- The value of the DMD at 0 is by definition the density of pixels lying on the surface of the grains, they represent a measure of the surface of the powder. Because there are more grains per unit volume in a low w/c paste, the amount of surface per unit of paste volume is higher than at high w/c. Replotting the DMD per unit of gram of alite yields the right image where all curves merge at a distance equal to zero; there they are equal to the specific surface of the powder: here about 0.45 m^2/g_{alite}. This value may seem low for such a fine powder, usually 5 μm powders rather ranges within 1 to 2 m^2/g_{alite}, but this is a consequence of the spherical shape of the grains in µic simulations.

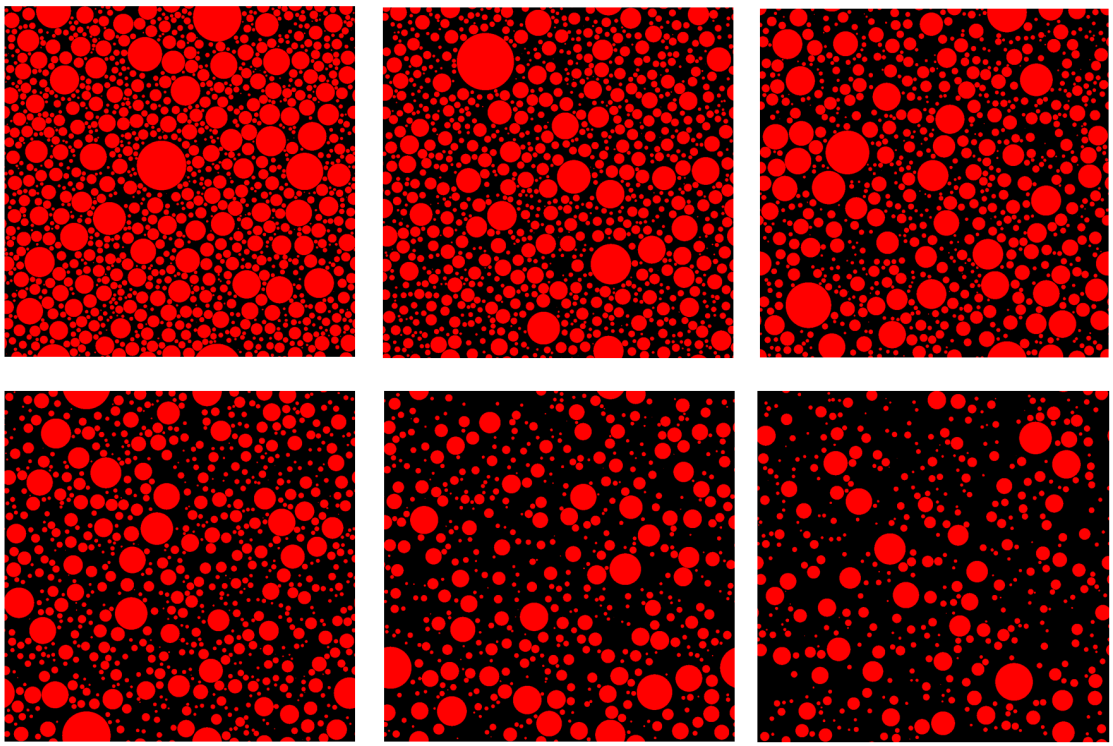

Figure 4.11 – 2D sections of µic simulations of a powder with varying w/c: from left to right and top to bottom: 0.2, 0.3, 0.4, 0.5, 0.8 and 1. The width of each image is 100 µm, the pixel size 0.1 µm. The PSD has $d_{v_{10}} = 2\mu m$, $d_{v_{50}} = 5\mu m$ and $d_{v_{90}} = 10\mu m$. Note that in reality sedimentation and agglomeration occur and matters [16] [19] which makes these µic simulations and their corresponding DMD approximate.

- For sufficiently high w/c, the DMDs increase from zero up to a peak value before decreasing. The distance of the peak value gives an estimate of the average interparticle distance.

Furthermore, figure 4.13 show that the DMDs profiles are bell shaped, to be specific they look Gaussian. Because a Gaussian is completely defined by its area, its value at 0 and its height, this opens the door to the prediction of the DMD without any simulation[4]. Indeed, the area is the initial amount of water which is known from the w/c ratio, the value at zero is the specific surface which can be measured by BET, and the height can be estimated from a regression on the curves of this figure[5]. This observation and its limitations are discussed in section 4.

Internal DMDs The DMD are not only relevant to describe the external space but also the internal space once the gaps have opened. An example of an internal DMD is shown on figure 4.14. The internal space initially increases but generally decreases once the inner C-S-H precipitates.

[4] Strictly speaking, DMD are truncated Gaussian, but this does not hinder their computation from the knowledge of these truncated Gaussian three information

[5] For w/c < 0.3 the peak height is assume to occur at zero.

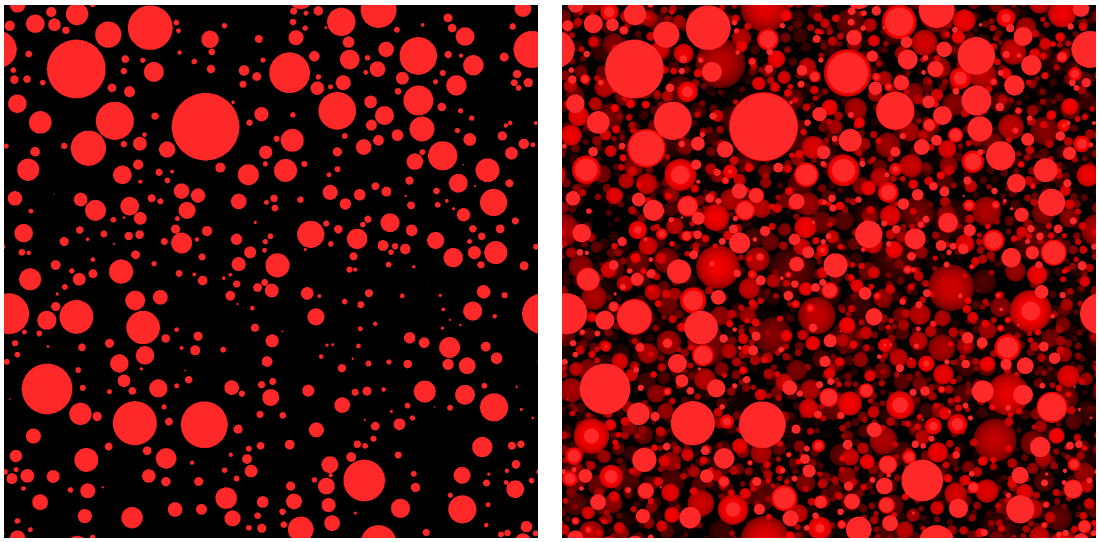

(a) *(b)*

Figure 4.12 – 2D section of the same µic simulation with w/c = 1; width of the image: 100 µm; the PSD has $d_{v_{10}} = 2\mu m$, $d_{v_{50}} = 5\mu m$ and $d_{v_{90}} = 10\mu m$. On the right the background is displayed so as to represent how misleading can the maximum pore size be from 2D sections compared with full 3D microstructures. The maximum pore diameter computed from the DMD of figure 4.12 is 7 µm for w/c =1. While this may seem that a 7 µm micron disk can easily fit in the largest pores on that image, it seems less so on the right image.

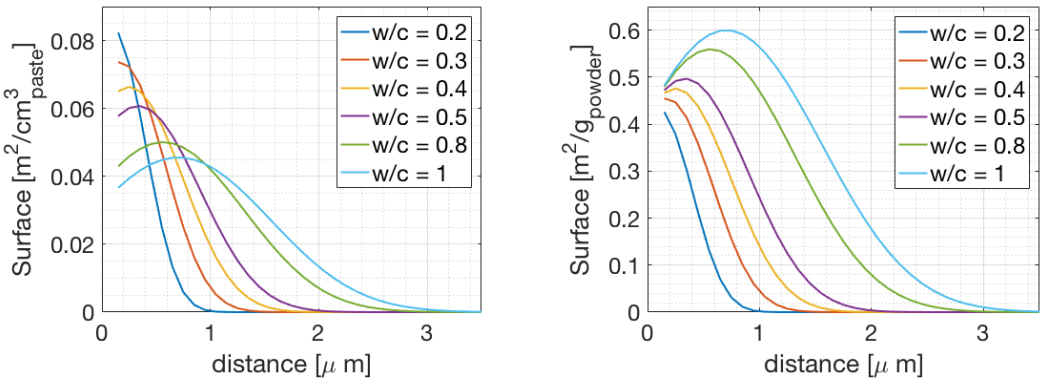

(a) *(b)*

Figure 4.13 – External DMDs of the µic simulations shown on figure 4.11. Left: DMD per unit of paste volume; right: DMD per unit of gram of powder. The four numbers to notice are: the maximum pore size (where the curve collapses to zero), the area below the curves which equals the volume of water (on the right figure it exactly is the w/c value: for instance the area below the purple curve is exactly 0.5 cm^3), the value at zero which is the surface of the powder and the position of the peak maxima which provides an estimate of the interparticle distance. N.B.: these DMD were computed from 3D simulations, not from the 2D sections.

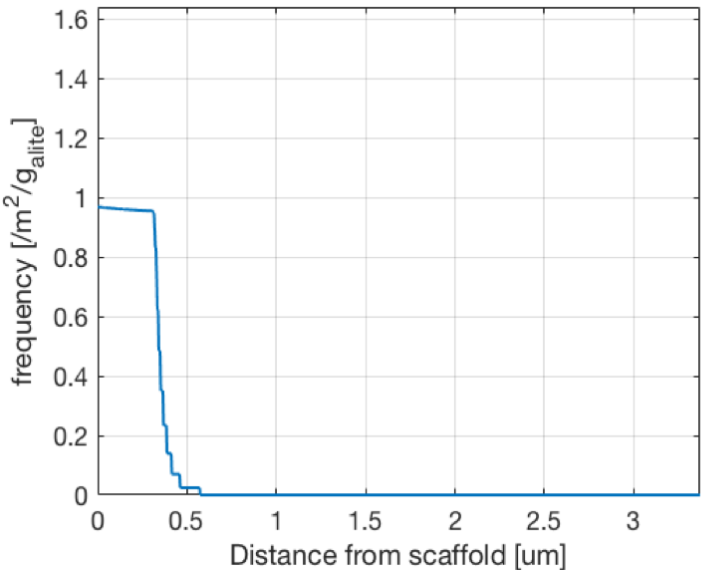

Figure 4.14 – Example of an internal DMD at 24h. By contrast with external DMD which looks Gaussian, the frequency is very stable up to 0.3 μm beyond which it suddenly drops.

On figure 4.14, most of the inner water is within 0.3 μm from the center of the gap (a 0.3 μm grain *in radius* could fit within the gap). The stair like slope that is at a higher distance comes from the small grains that dissolve faster and thus open earlier and create larger gaps.

Example of how DMDs capture the space filling of an alite paste at 24h

On figure 4.15 are plotted a set of internal and external DMDs of an alite paste at 28 days whose DoH is 79%. Because the outer C-S-H grows on the scaffold it remains close to zero distance and therefore fills the DMD from the left. On the opposite, air voids open as far as possible from the scaffold and fill the DMD from the right. Portlandite has no preference and precipitates at any distance with equal probability. Water fills whatever is left.

Air voids open first in the biggest external pores, here they are about 0.8 μm. As hydration progresses, the gap enlarges and air might get in if the inner pores become larger than the external ones. In this example, it is the case: the maximum internal pore size at this time is bigger than in the external space. On this picture the biggest air pores, about 2.5 μm, are found inside because 5 μm, or slightly bigger, grains vanish early in the reaction leaving no anhydrous grains to grow inner C-S-H. Air pores could then develop within them.

Furthermore, the volume of water within the gaps is about the volume of water in the outer space: the blue areas left and rights are close to equal. The air inside is lower than outside.

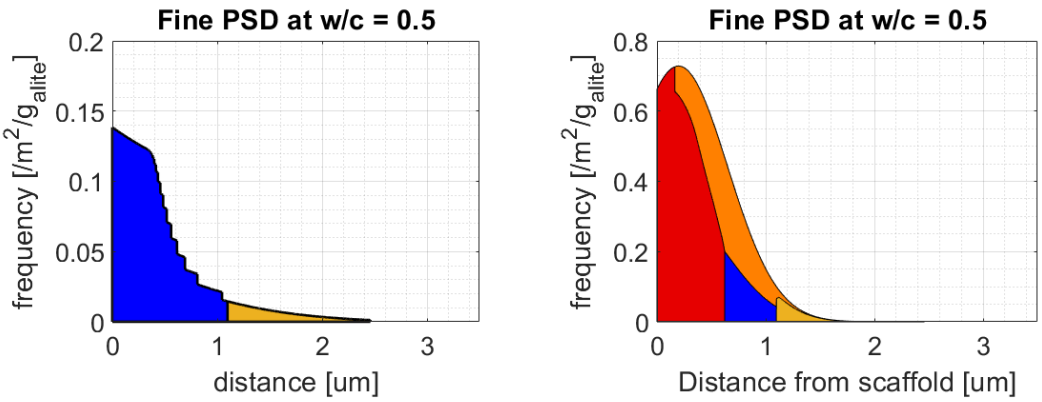

(a) *(b)*

Figure 4.15 – Simulation of the internal (left) and external (right) DMDs of an alite paste hydrated for 24h with w/c = 0.5. Blue is the capillary water, red the outer C-S-H plus water contained between and inside the needles, orange the Portlandite, and yellow the air.

4.1.10 Portlandite phagocytose

One of the main differences between alite and cement pastes is the occurrence of big Portlandite clusters in C_3S and alite pastes (as shown on figures 4.16 and 4.17). These clusters engulf alite grains which are then shut out of the hydration. In the case of cement pastes, the phenomenon is much less significant and can be neglected.

The progressive growth of the cluster is indirectly seen on figure 4.17 grains lying at the center of the clusters had no time to develop a C-S-H shell whereas those on its edge exhibit a shell only on the side facing the capillary. Note that the fraction of alite grains out of the reaction can be significant, 6% ±2% at 24h on figure 4.16; this limits the ultimate DoH to 94% ±2%.

A distinction should be made between the volume of Portlandite used for engulfing grains, the CLUSTER CORE (in red on figure 4.17) and the volume of portlandite used only for impingement: the CLUSTER TRANSITION ZONE (within the yellow border but out of the red area on figure 4.17). This distinction is required in order to correctly compute the probability for a grain to be engulfed versus the probability to impinge. This is discussed in more details in subsection 4.3.6.

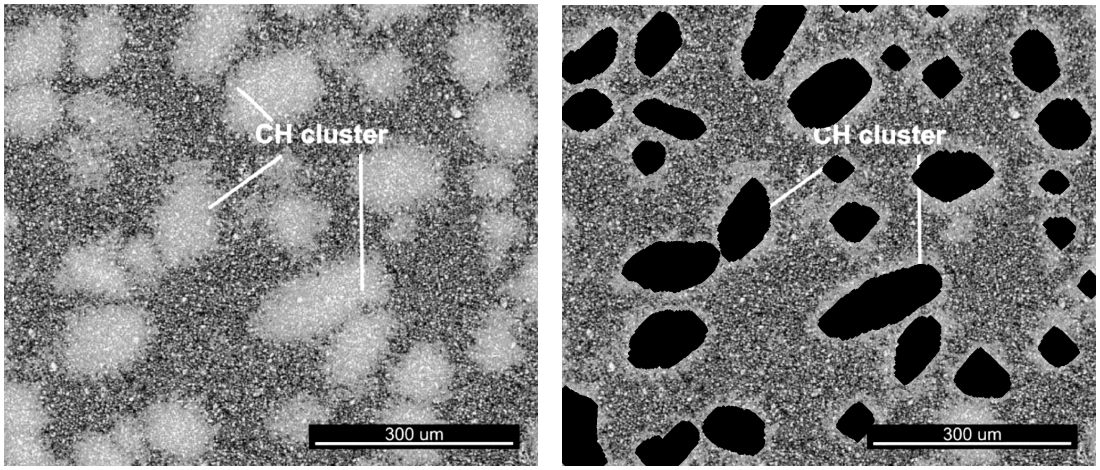

(a) *(b)*

Figure 4.16 – Portlandite clusters in a w/c = 0.4 C_3S paste hydrated for 24 hours. From segmentation, the fraction of lost grains inside these Portlandite clusters is 6% ±2%*: the ultimate DoH cannot go higher than* 94% ±2%*. The relative error of* ±2% *comes from the difficulty of clearly defining the clusters boundaries, the value of* 6% *was computed from the right image where the CH cluster boundaries seem well inside where they should be for instance. From [2, fig. 5.5 a, p. 115].*

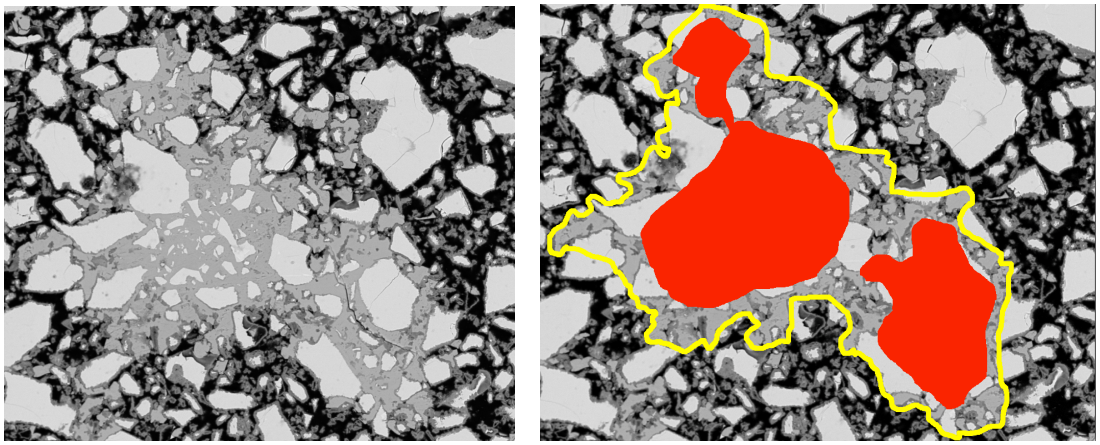

(a) *(b)*

Figure 4.17 – SEM picture of a w/c = 0.4 alite paste hydrated at 20°C for 3 days, 10kV, WD= 12.2mm, width of the image: 200 µm. One Portlandite cluster is observed. Grains that were engulfed early had no time to hydrate, they have no C-S-H shell, while those on the border of the shell, in the transition region (within the yellow border but out of the red areas), do have a shell because they just got caught; some grains show an intermediate case with only the side facing the capillary being hydrated.

4.2 The quantitative importance of the gap opening phenomenon

The quantitative importance of the gap opening phenomenon has not yet received the full attention it deserves. This section highlights that the gap opening sucks the external capillary water in the gap: it removes some available space for precipitation. As a consequence, this exacerbates the impingement in the outer space. This section demonstrates that the amount sucked in is in fact considerable for typical alite and cement PSD: it dramatically exacerbates the outer space filling.

For the sake of pedagogy, the section first considers the case of one single spherical 10 μm grain, then carries on with monodisperse spherical powders and ends with the general polydisperse case. A rule of thumb is proposed that enables a quick quantitative estimation of the critical DoH beyond which space filling decrease the hydration rate.

N.B. This section depends on one big assumption which is demonstrated in the paragraph on the importance of the gap opening phenomenon in subsection 4.5.3: the capillary water always flows from the outer space to the inner space for typical alite and cement PSD.

4.2.1 Illustration of the gap opening phenomenon on a 10 μm grain

Let us consider one single 10 μm grain at w/c = 0.32. This w/c has specifically been chosen because it implies the initial volumes of alite and water are equal. An equatorial section is represented on figure 4.18. When a 1 μm gap opens, the grain loses $(4/3\pi(5^3-4^3))/(4/3\pi 5^3)\mu m^3$ which equals 49% of its initial volume. This means the volume of the white gap on the second image of figure 4.18 is about the volume of the now 8 μm core. Because the initial volume of water and alite are equals, it also means that half of the outer water has flowed in and thus entirely fills the gap (third image). But the water consumption should in addition be considered: if the DoH is about 50%, then the amount of water consumed is about two thirds of the initial amount.

As a consequence, not only is the capillary outer space completely dry but part of the inner space is also not filled with water (the only water left is the between or within the C-S-H needles and inner C-S-H).

This example demonstrates that by 50% of DoH for a 10 μm monodisperse alite powder hydrated at w/c= 0.32, the outer space filling is complete: hydrates must then grow inside. This by the way implies that the inner C-S-H nucleation depends on the space filling: whenever the external capillary water is exhausted, there is no other choice than growing inside. Finally, all the outer black areas seen on SEM sections at this point or later on is then only air, not water.

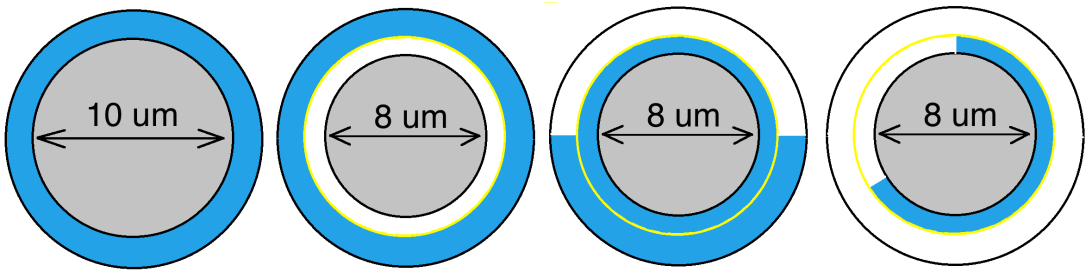

Figure 4.18 – First image: equatorial section of a 10 µm spherical alite grain at w/c = 0.32. At w/c= 0.32 the volume of water equals the volume of alite. On the second image, a 1 µm gap opens. On the third half of the initial water has flowed in: a 1 µm gap on a 10 µm grains means that the grain has lost about half its volume, this equal half of the initial volume of water at this w/c. Fourth image: when the water consumption is additionally taken into account, at DoH= 50% for a 10 µm grain at w/c = 0.32, the water left is not even sufficient to fill the inner space; the outer space filling is then maximal: hydrates can no more grow there. On this last image the white area is a mix of hydrates and air.

4.2.2 Examples on monodisperse powders

In table 4.1 are computed the volume fraction loss for 5, 10 and 20 μm grains where a gap of 1 μm and 2 μm respectively opens. The importance of this loss of space available for precipitation is highlighted in table 4.2 for a monodisperse powders at w/c = 0.32 and 0.5.

If the previous calculations are corrected for the water consumption, table 4.3 is obtained. Table 4.3 highlights the dramatic loss of space available for precipitation for all powder sizes at w/c = 0.32. For the coarsest powder, the capillary water left is only 27% of its initial volume so that impingement already plays a role. For the 10 μm powder, the whole external capillary water has vanished: impingement is maximal in outer space and no further hydrates can grow there. For the finest powder, both external and internal capillary reservoirs have been consumed: the only remaining one is the gel water. In this latter case the reaction carries on by densification and the reaction rate must then be slower.

Table 4.1 – Volume fraction loss of different grain size when a gap of 1 µm or 2 µm opens; this corresponds to the DoH. The maximum gap size for alite paste is about 1 µm whereas it is about 2 µm in PC pastes. In both case the volume fraction loss is significant even for 20 µm grains.

Initial grain size [μm] (spherical grains)	Volume fraction loss for a 1 μm gap	Volume fraction loss for a 2 μm gap
5 μm	78%	99 %
10 μm	49%	78%
20 μm	27 %	49%

N.B. The computations have been made here for spherical grains, but are not strictly correct for other shapes. In general when an ellipsoidal grain loses 1 µm in thickness, its form factor changes. Although real cement and alite grains are not spherical, they are close, as can be observed on the SEM pictures of this chapter, this approximation does not hinder the essential

Table 4.2 – Volume fraction of external capillary water that flows in the gap for a 1 µm gap opens for w/c = 0.32 and w/c = 0.5. Notice that for 10 µm grains at w/c=0.32, half of the external space available for precipitation has vanished, at 0.5 it is about one third.

Monodisperse powder size [μm]	External capillary water that flows in the gap if w/c = 0.32	External capillary water that flows in the gap if w/c = 0.5
5 μm	78%	50 %
10 μm	49%	31%
20 μm	27 %	17%

Table 4.3 – Volume of water left in the external (internal) capillary pores for different monodisperse powder at w/c = 0.32 and w/c = 0.5 when a 1 µm gap opens up and both the flow in and consumption are considered. Notice that at 0.32 the two finest powders have entirely lost their external available space for precipitation.

Monodisperse powder size [μm]	External capillary water that flows in the gap if w/c = 0.32	External capillary water that flows in the gap if w/c = 0.5
5 μm	0%(0%)	0 %(70%)
10 μm	0%(69%)	28%(28%)
20 μm	37%(100%)	60%(60%)

qualitative idea of this section that the volume opened by the gap is significant.

4.2.3 The polydisperse case, the "space-filling rule of thumb"

The computation made so far only concerns a monodispersed powder, but is there a general rule of thumb that yields the DoH at which the external capillary water is exhausted? Is there a formula valid for any PSD that yields the characteristic DoH at which the external space is completely filled with hydrates and/or air?

Yes, there is. By definition, the external capillary water is the initial amount of water minus the water that flows into the gap and minus the water consumed:

$$V_{H_{cap_{ext}}} = V_{H_{initial}} - V_{H_{gap}} - V_{H_{consumed}} \tag{4.3}$$

The external capillary water is exhausted when:

$$V_{H_{initial}} = V_{H_{gap}} + V_{H_{consumed}} \tag{4.4}$$

These terms can be re-expressed: $V_{H_{initial}} = w/c * d_{alite} * V_{alite_{initial}}$, $V_{H_{gap}} = V_{alite_{consumed}} = DoH * V_{alite_{initial}}$, $V_{H_{consumed}} = \eta_2/\eta_1 V_{alite_{consumed}}$, and reordering the equation yields:

$$DoH_{external-space-filled} = \frac{d_{alite}}{1+\eta_2/\eta_1} * w/c \tag{4.5}$$

Assuming a density of 3.15 for alite and $\eta_2/\eta_1 = 1.32$, we get the following rule of thumb: $DoH_{external-space-filled} \simeq 1.36 * w/c$. However, this equation assumes that the scaffold detachment to happen immediately from the beginning. In reality, this rather happens at a gel-space of about 20% as is shown later so that the correct rule of thumb is:

$$\boxed{DoH_{external-space-filled} \simeq 1.6 * w/c} \tag{4.6}$$

Alternatively, the fraction of external space filled can be quantified by: $f^{v}_{ext_{space}} = \frac{DoH}{1.6w/c}$.

For a w/c = 0.32, the external space is filled at a DoH of about 51.2%, whereas for a w/c = 0.5, the external space is filled at a DoH of 80%. The threshold w/c beyond which the external capillary water is never exhausted is 0.625. These values predict the DoH at which the calorimetry curves have an inflection point because of space-filling. This is exemplified on figure 4.19.

N.B. I- This rule of thumb is a priori only valid for alite pastes without fillers and as long as no inner C-S-H is forming. Because filler grains do not open a gap, this ruins the derivation of the formula. Because inner C-S-H is forming inside, it also ruins the derivation. In the filler case the formula underestimates the critical DoH for external space filling, in the second case it overestimates it. It thus does not hold for PC pastes because the belite, C3A, C4AF (and usually about 5% of limestone is found in PC) slightly behave as fillers at least during the first day.

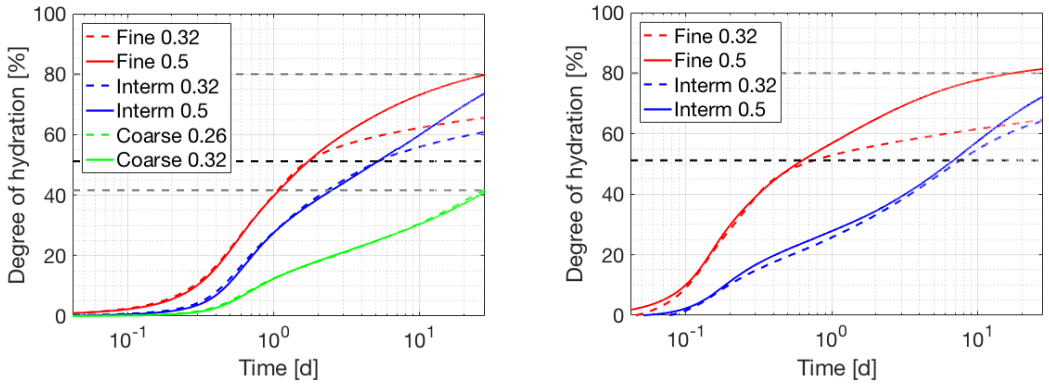

Figure 4.19 – Measured DoH of alite pastes computed from isothermal calorimetry experiments. Experiments made at different fineness (fine, intermediate and coarse), w/c ratios (0.26, 0.32 and 0.5) and temperatures (left: 20°C, right: 40°C). The continuous and dashed lines are superimposed up to a given DoH beyond which they abruptly separate because of the space filling. The horizontal dashed lines indicate the rule of thumb prediction of external space filling: the 80% line corresponds to the w/c = 0.5, the 51.2% to the w/c = 0.32 and the 41.6% to the w/c = 0.26. The black one in particular deals with the 0.32 w/c ratio case exactly crosses the point where the 0.32 curves diverge from the 0.5 ones. The grey lines intersect their correspond curves beyond the frame of these experiments. N.B. These experiments are a subset of the dataset to benchmark hydration models presented later in this chapter.

4.3 General idea of the upgraded needle model algorithm

This part assumes the reader is familiar with the later ages microstructural development, the main hydration peak model and the concepts defined in the former sections.

The structure is made so that the reader can skim through the section by reading only the headings of each subsection which summarize them.

In short, the model:

- computes the volume of each phase,
- distribute them in space
- considers the gap opening

The model emphases volume computations rather than moles or masses because the underlying motivation of the model is to test the space-filling hypothesis. It is important to understand that the phase distribution in space is not decoupled from the volume computation: at each time step, the distribution of phases define the impingement of the next time step which then influence the hydrates growth rate of the next one.

- In particular, the model focuses on computing carefully the C-S-H volume. It computes the volume of outer and inner C-S-H with time from measurements of the nucleation and growth rates of the C-S-H needles, the inner C-S-H thickness with time, the PSD and BET specific surface of the powder. The alite, water and Portlandite amounts are then obtained from the volumetric stoichiometric equation. From the enthalpy of dissolution of alite, the enthalpy of C-S-H and CH precipitation the overall heat and heat flow are computed.
- The distribution of phases in space stems from the observation that phases are not randomly distributed in space. SEM observations of the later ages microstructural evolution and thermodynamic arguments enable us to set some distribution rules, the C-S-H always precipitates heterogeneously on the scaffolds and air voids preferentially open in the biggest pores for instance. The distribution of phase in space is quantitatively described with DMDs.
- Other events that affect the distribution of phases are considered. Grains may detach from their scaffold, shells may get engulfed within Portlandite clusters, or lose their anhydrous core.

N.B. The present version of the code unfortunately does not consider the Portlandite phagocytose and the influence domains. The analytical derivation for them is still introduced.

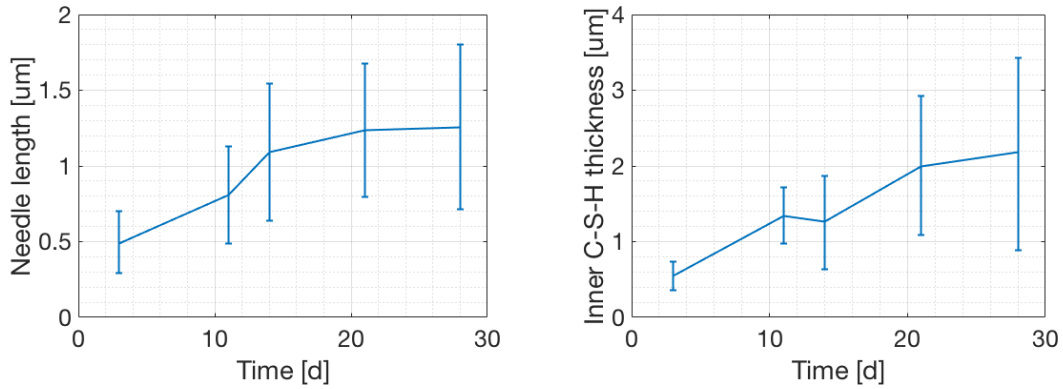

(a) *(b)*

Figure 4.20 – Measured C-S-H needles length with time (left) and inner C-S-H thickness (right) as of an alite paste hydrated at w/c = 0.7 (note the sectioning effect is not corrected). Both profiles initially grow fast and then slow down (note the inner C-S-H would not start at time zero but at half a day approximatively). The 28 days measurements were taken from the same sample as on figures 4.1 and 4.6.

4.3.1 It computes the volume of C-S-H with time from measurements

The total volume of C-S-H is the sum of the outer and inner C-S-H. The volume of outer C-S-H is computed in a similar manner to the main hydration peak: by summing the volume of needles over all generations (for one single grain) and then over the PSD (for the whole powder). The volume of inner C-S-H is simply the volume of a shell which nucleates and grow from the scaffold inward until it touches the anhydrous cores[6].

The needle length and inner C-S-H thickness with time on an alite paste hydrated at w/c = 0.7 are shown on figure 4.20.

The volume of outer C-S-H

The outer C-S-H volume is computed in the same manner as in the main hydration peak model. The volume of outer C-S-H is the number of needles times the size of each generation of needles. The number of needles with time requires the specific surface (measured by BET for instance) and PSD (measured by laser diffraction or BSE-SEM) of the powder to be measured together with the nucleation rate with time (measured by SE-SEM). The needles size with time needs to be measured by SEM or STEM.

[6] then the reaction is assumed to stop in the present version of the model. In reality, it should a priori carry on as long as the inner C-S-H contains gel pores.

The volume of one single needle Needles are assumed to be cylinders: the radius and length with time need to be measured to determine their volume. The function proposed to compute the length of a needle at time t which has nucleated at time τ is:

$$l_{needle_{normal}}(t,\tau) = l_{24h} * \left(1 - e^{\frac{-(t-\tau)}{t_{c_{24h}}}}\right) + \left(l_{28d} - l_{24h}\right) * \left(1 - e^{\frac{-(t-\tau)}{t_{c_{28d}}}}\right) \tag{4.7}$$

Where l_{24h} and l_{28d} are the characteristic lengths at 24 h and 28 d, $t_{c_{24h}}$ and $t_{c_{28d}}$ the characteristic growth times at 24 h and 28 d. This function simply illustrates the observations that the needles initially grow fast and then slow down as shown on figure 4.20.

Because of the possible perpendicular impingement against the other phases, if there is no more external capillary water but still water between the needles[7], this length needs to be corrected by the probability of impingement:

$$l_{needle}(t,\tau) = l_{needle_{normal}}(t,\tau) * \left(1 - P_{impingement}(t)\right) \tag{4.8}$$

This probability is discussed in subsection 4.3.7.

In addition, when the anhydrous core of the grain has completely dissolved, a further correction needs to be added because the needles may still grow if the shell is sufficiently close to a living cell:

$$l_{needle}(t,\tau) = l_{needle_{normal}}(t,\tau) * \left(1 - P_{impingement}(t)\right) * P_{living}(R,t) \tag{4.9}$$

This probability is discussed in the appendix of this chapter.

The radius of the needles is assumed proportional to their length according to their aspect ratio which typically is about 10. Users can also directly input any alternative closer to their experiments for the length and radius with time.

Finally, the volume of one single needle is the product of the base times the length of the needle:

$$v_{needle}(t,\tau) = \pi r(t,\tau)^2 * l_{needle}(t,\tau) \tag{4.10}$$

[7] In case of perpendicular impingement, if there is still water left between the needles, they are still allowed to grow radially.

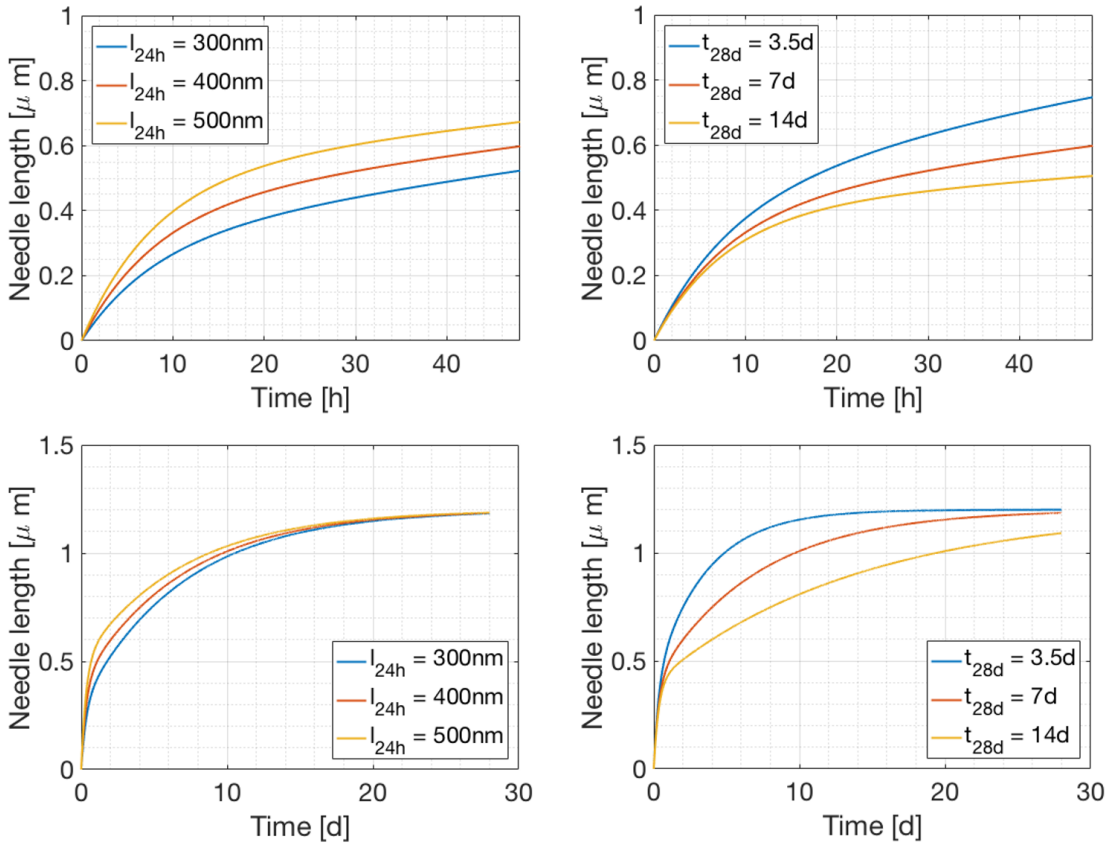

Figure 4.21 – Typical profiles of the needle length with varying characteristic lengths at 24h (left) or characteristic 28d growth times (right). On the left: $t_{c_{24h}} = 8h$, $t_{c_{28d}} = 7d$, $l_{28d} = 1.2\mu m$, *on the right:* $t_{c_{24h}} = 8h$, $l_{24h} = 400nm$, $l_{28d} = 1.2\mu m$.

The single grain model A grain and its scaffold are defined by three number: its radius, form and roughness factors as in the main hydration peak model. As hydration occurs, they are assumed to shrink concentrically: they keep their form and roughness factor but their radii decrease. The scaffold and grain radii are identical up the time of detachment when the gap opens. The criterion for detachment is based on the gel-space ratio threshold and is described in the corresponding paragraph within subsection 4.5.2.

For a given grain size, the number of needles at time step k is equal to the number of the needles at the last time step plus the newly generated needles:

$$N_{needles}(R,k) = N_{needles}(R,k-1) + k_n(k).S_{free}(R,k-1) \tag{4.11}$$

Where k_n is the nucleation rate per unit of free surface with time (the same for all grains) and $S_{free}(R,k)$ is the available surface for nucleation on a scaffold of size R at time k; it reduces at each time step due to the progressive covering of the needles and due to the receding effect.

The nucleation rate profile k_n is assumed to be Gaussian[8]:

$$k_n(t) = A_n e^{-\frac{t-t_n}{2\sigma_n^2}} \tag{4.12}$$

Where A_n, t_n and σ_n are the characteristic nucleation rate amplitudes, delay time and width. This function illustrates the observations that the needles nucleates. Users may alternatively use another nucleation rate profile that better suits their measurements.

Finally, the total volume of the needles on one grain can be computed by summing over all the needles generations:

$$V_{outer_{CSH}}(R,t) = \int_0^t N_{needles}(R,\tau) * \upsilon_{needle}(t,\tau) d\tau \tag{4.13}$$

The inner C-S-H model The volume of the shell with time is given by:

$$V_{inner_{CSH}}(t) = F.4/3\pi(R^3_{scaffold} - R^3_{inner}) \tag{4.14}$$

Where $R_{scaffold}$ and R_{inner} are the radii indicated on figure 4.22 and F is the form factor. The grain is assumed to shrink concentrically so that F is assumed constant throughout the reaction.

As hydration progresses, the inner C-S-H thickness increases and may come in contact with the anhydrous core. This contact depends on the gap size at the time of the inner C-S-H nucleation, the bigger it is the less likely it is to come into contact, the further growth of outer C-S-H (it consumes the anhydrous core), the densities of the outer and inner C-S-H.

As for the outer C-S-H, the inner C-S-H nucleation rate and thickness evolution with time are modeled by the same profile function: a Gaussian for the nucleation rate, and a set or two exponential functions for the thickness. Again, users may as well define their own functions.

Finally, the polydisperse case is treated by integration over the PSD as for the outer C-S-H.

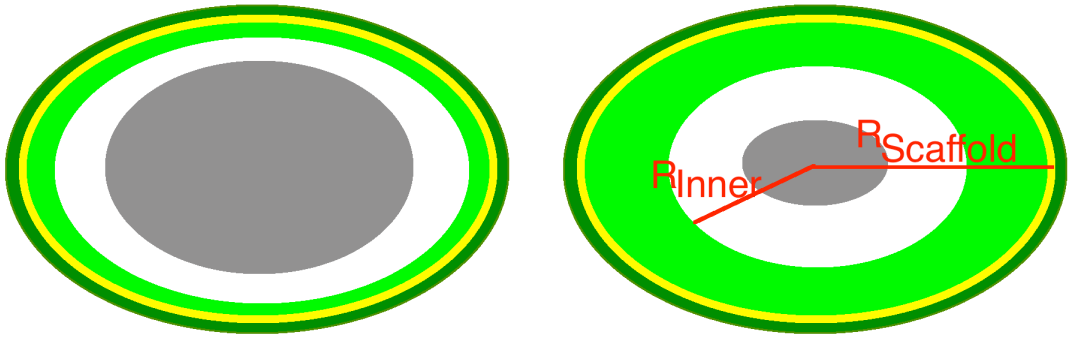

(a) *(b)*

Figure 4.22 – Representations of the inner C-S-H (in light green) growth within its cell. The yellow layer represents the scaffold, the dark green shell the outer C-S-H shell and the gray ellipse the anhydrous grain. The inner C-S-H thickness is the difference between the scaffold and inner radii. As the inner C-S-H grows the anhydrous core shrink so that it may or not eventually come in contact with the core.

4.3.2 The phase assemblage is derived from the C-S-H volume and the stoichiometric equation

The alite hydration equation is:

$$C_3S + yH \rightarrow C_xSH_{y+x-3} + (3-x)CH \tag{4.15}$$

Which rewritten in volumes gives:

$$\eta_1 V_{C_3S} + \eta_2 V_H \rightarrow \eta_3 V_{C-S-H} + \eta_4 V_{CH} \tag{4.16}$$

Once the Ca/Si and H/Si ratios and the C-S-H volume are determined, the whole phase assemblage is obtained thanks to the stoichiometric coefficients η_1 η_2, η_3 and η_4:

$$\frac{V_{C_3S}}{\eta_1} = \frac{V_H}{\eta_2} = \frac{V_{C-S-H}}{\eta_3} = \frac{V_{CH}}{\eta_4} \tag{4.17}$$

These coefficients may vary significantly with time, w/c ratios and temperature because the Ca/Si and H/Si ratio do. The Ca/Si variation was studied by Bazzoni and Marchon on alite on figure 4.23, and the H/Si variation by Muller on white Portland cement on figure 4.24.

[8] By contrast with the published main hydration peak model, this profile is closer to our latest observations (Yu Yan et al. 2019, to be submitted): the number of nuclei with time follow an S-shape curve so that its derivative, the nucleation rate, has a bell-shape profile. In addition, synthetic C-S-H nucleation rates also exhibit bell shape curves (Andalibi et al., 2017, fig. 5 a)). More fundamentally the nucleation rate is dependent on the pore solution concentration; but the relationship between both is unknown to this date.

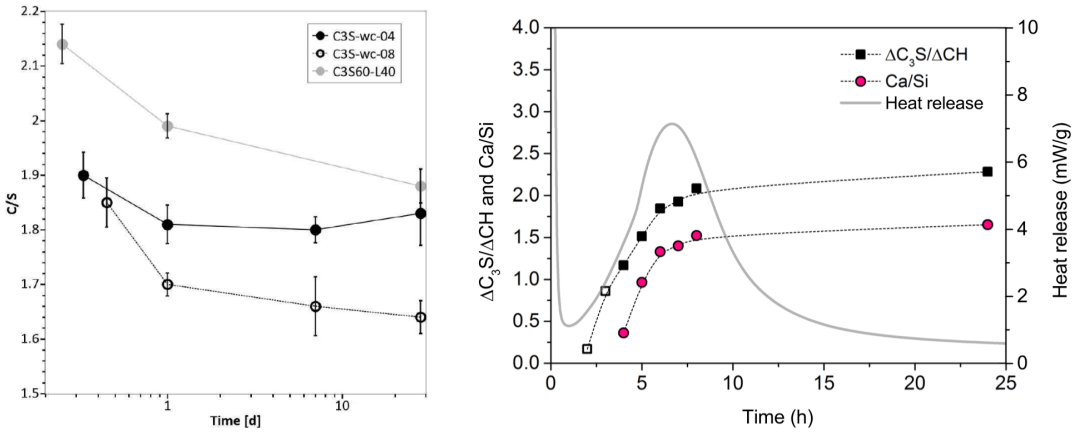

(a) *(b)*

Figure 4.23 – Variation of the Ca/Si ratios with time on C_3S pastes. The left plot show that the Ca/Si ratio evolve with time and w/c ratio over 28 days. The right plot shows a very strong variation of the Ca/Si ratio during even the first day which shows that Portlandite and C-S-H are not congruently precipitating during this period of time. Left: Evolution of the ratio with varying w/c ratios (bottom curves) and for C_3S with 40% of limestone filler (top curve); from (Bazzoni's thesis, fig. 5.8, p.117), the quantification was made by SEM-EDX. Right: evolution of the Ca/Si ratio together with the rate of C_3S/CH ratio and calorimetry curves; the Ca/Si ratio was determined by the mass balance; from (Marchon's thesis, fig. 4.2 p. 87).

The evolution of the volumetric coefficients for common Ca/Si and H/Si ranges are plotted on figure 4.25. On these figures the arrows represent the evolution of these coefficients over the course of a white Portland cement paste hydrated for 28 days at w/c = 0.4 (see the chapter of 4 of Muller's thesis for more details). They vary by 10 % to 20 %. These variations have an effect on the predicted phase assemblage, space filling and heat flow: they are a priori not negligible.

The derivation of the volumetric coefficients from which figure 4.25 plots are computed is detailed in the next subsection.

Derivation of the stoichiometric volumetric coefficients

By contrast with the main hydration model which assumed the Ca/Si and H/Si ratios constant and equal to 1.7 and 4 respectively, the later ages model considers possibly varying Ca/Si and H/Si.

By definition of the volumetric stoichiometric coefficients:

$$\frac{V_{C_3S}}{\eta_1} = \frac{V_H}{\eta_2} = \frac{V_{C-S-H}}{\eta_3} = \frac{V_{CH}}{\eta_4} \tag{4.18}$$

The coefficient η_1 is fixed at one by convention.

water volumetric stoichiometric coefficient

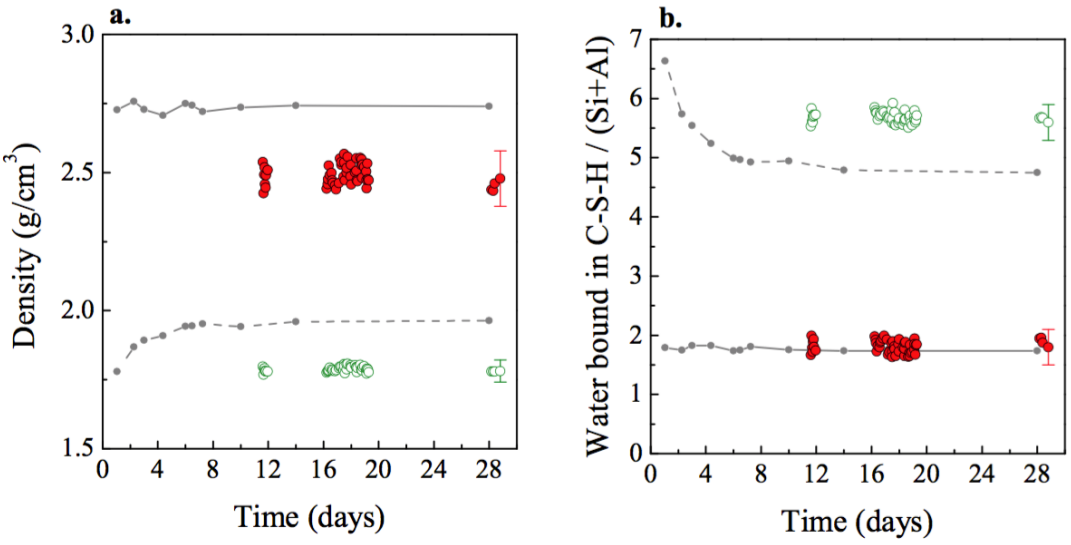

Figure 4.24 – Evolution with time of the C-S-H density (left) and water bound in atomic ratios (right) in a white Portland cement. Colored points correspond to a 10°C experiment, solid points are the C-S-H solid density while the empty ones include the gel water. The grey dashed lines correspond to the 20°C experiment. From [11, fig. 4. 28 p. 86].

From the previous equation, we get:

$$\eta_2 = \frac{V_H}{V_{C_3S}} = \frac{m_H * d_{C_3S}}{m_{C_3S} * d_H} = \frac{n_H M_H d_{C_3S}}{n_{C_3S} M_{C_3S} d_H} = y \frac{M_H d_{C_3S}}{M_{C_3S} d_H} \tag{4.19}$$

Where m_H and m_{C_3S} are the masses of water and alite,n_H and n_{C_3S} their moles, d_H and d_{C_3S} their densities (equal to 1 and 3.15 respectively), M_H and M_{C_3S} their molar masses (equal to 18.0 g/mol and 228[9] g/mol). For these numerical values, the calculation yields the formula:

$$\eta_2 = 0.249\, y \tag{4.20}$$

C-S-H volumetric stoichiometric coefficient

In a similar way:

$$\eta_3 = \frac{V_{CSH}}{V_{C_3S}} = \frac{n_{CSH} M_{CSH} d_H}{n_{C_3S} M_{c3S} d_{C_3S}} = \frac{M_{CSH} d_{C_3S}}{M_{C_3S} d_{CSH}} = \frac{x M_{CaO} + M_{SiO_2} + (y + x - 3) M_H)}{M_{C_3S}} * \frac{d_{C_3S}}{d_{CSH}} \tag{4.21}$$

Where n_{CSH} and n_{C_3S} are the moles of $C-S-H$ and C_3S, M_{C-S-H} and M_{C_3S} their molar masses, d_{C-S-H} and d_{C_3S} their densities. The term d_{C-S-H} is the average density of $C-S-H$

[9] As for the density, the molar mass could slightly vary for alite as other ions my incorporate within its structure, but the incorporation of other ions never exceeds a few percent, so that the density and molar mass of alite should also vary within a maximum of a few percent.

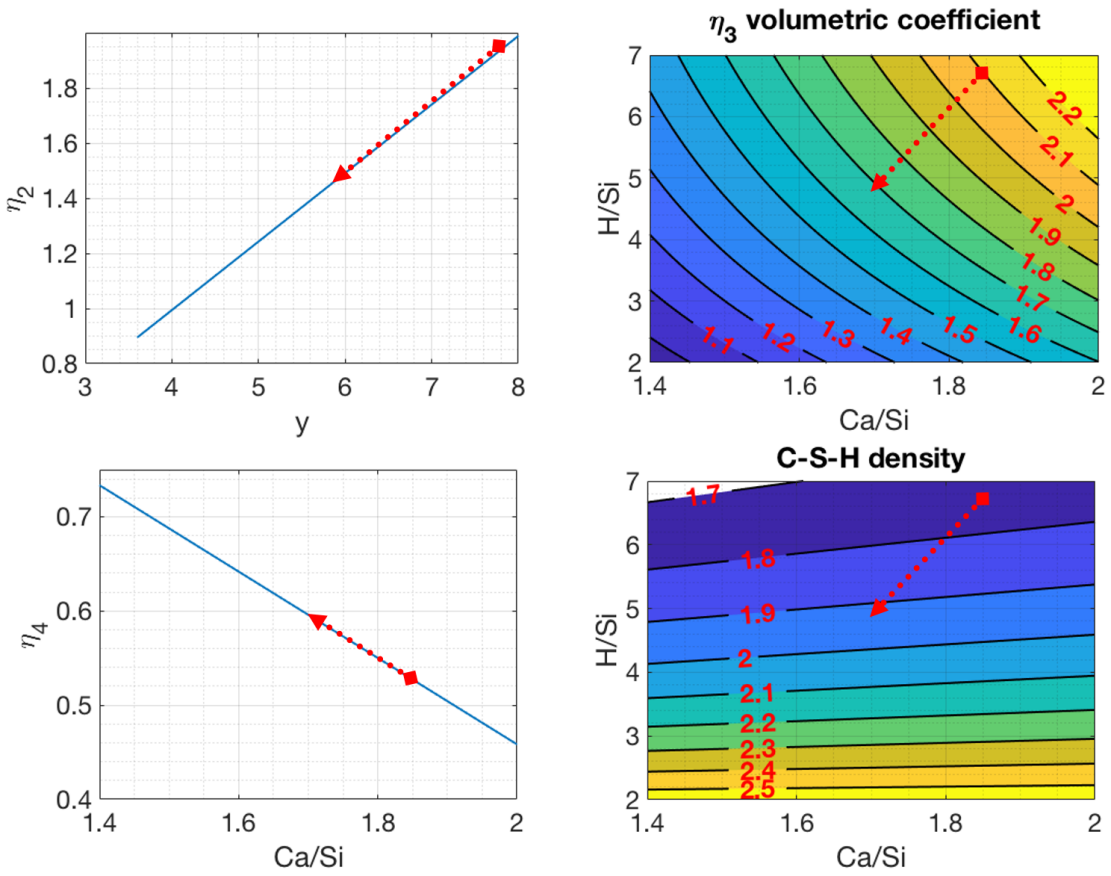

Figure 4.25 – Evolution of the volumetric coefficients with Ca/Si and H/Si. To appreciate how much these coefficients may vary over the course of hydration red arrows are plotted. They represent the volumetric coefficients evolution (the squares are the initial values and the arrows tips the 28 days ones) of Muller WPC experiment. The data used for plotting the arrows is taken from from [11, fig. 4.18 and 4.28 pp. 73 and 86].

which includes its gel water:

$$d_{C-S-H} = \frac{m_{C-S-H_{solid}} + m_{gel_{water}}}{V_{C-S-H_{solid}} + V_{gel_{water}}} = \frac{n_{C-S-H_{solid}} M_{C-S-H_{solid}} + n_{gel_{water}} M_{gel_{water}}}{\frac{m_{C-S-H_{solid}}}{d_{C-S-H_{solid}}} + \frac{m_{gel_{water}}}{d_{gel_{water}}}} \tag{4.22}$$

$$= \frac{n_{C-S-H_{solid}} M_{C-S-H_{solid}} + n_{gel_{water}} M_{gel_{water}}}{\frac{n_{C-S-H_{solid}} M_{C-S-H_{solid}}}{d_{C-S-H_{solid}}} + \frac{n_{gel_{water}} M_{gel_{water}}}{d_{gel_{water}}}} \tag{4.23}$$

Where $C-S-H_{solid}$ denotes the C-S-H without any gel pores or surface water, and has a 1.8 moles of water molecules per mole of C-S-H. Gel_{water} denotes the gel pores water as NMR defines them, which corresponds to the water contained within the needles and possibly within the inner C-S-H. The solid C-S-H density considered here is 2.65 g/cm^3 as it is the

average of the NMR value [11, p. 71 fig. 4.15] and small angle neutron scattering (SANS) [1]. Assuming that the gel water has the same density as the bulk water, the formula becomes:

$$d_{C-S-H} = \frac{xM_{CaO} + M_{SiO_2} + 1.8M_H + (y+x-3-1.8)M_H}{\frac{xM_{CaO}+M_{SiO_2}+1.8M_H}{d_{C-S-H_{solid}}} + \frac{(y+x-3-1.8)M_H}{d_H}} \tag{4.24}$$

With $M_{CaO} = 56.1g/mol$, $M_{SiO_2} = 60.1g/mol$ and $M_{CaO} = 18.0g/mol$, $d_{C-S-H_{solid}} = 2.65$ and $d_H = 1$, this yields:

$$d_{C-S-H} = \frac{56.1x + 60.1 + 32.4 + (y+x-4.8)*18}{\frac{56.1x+60.1+32.4}{2.65} + \frac{(y+x-4.8)*18}{1}} \tag{4.25}$$

Injecting this back to the volumetric coefficient gives:

$$\eta_3 = \frac{M_{C-S-H}d_{C_3S}}{M_{C_3S}d_{C-S-H}} = \frac{M_{C-S-H}d_{C_3S}}{M_{C_3S}} * \frac{1}{\frac{n_{C-S-H_{solid}}M_{C-S-H_{solid}}+n_{gel_{water}}M_{gel_{water}}}{\frac{n_{C-S-H_{solid}}M_{C-S-H_{solid}}}{d_{C-S-H_{solid}}} + \frac{n_{gel_{water}}M_{gel_{water}}}{d_{gel_{water}}}}} \tag{4.26}$$

$$= \frac{M_{C-S-H}d_{C_3S}}{M_{C_3S}} * \frac{\frac{n_{C-S-H_{solid}}M_{C-S-H_{solid}}}{d_{C-S-H_{solid}}} + \frac{n_{gel_{water}}M_{gel_{water}}}{d_{gel_{water}}}}{n_{C-S-H_{solid}}M_{C-S-H_{solid}} + n_{gel_{water}}M_{gel_{water}}} \tag{4.27}$$

$$= \frac{(56.1x + 60.1 + 18(y+x-3)) * 3.15}{228} * \frac{\frac{56.1x+60.1+32.4}{2.65} + \frac{(y+x-4.8)*18}{1}}{1*(65.1x+60.1+32.4)+(y+x-4.8)*18} \tag{4.28}$$

The Portlandite stoichiometric coefficient In a similar way:

$$\eta_4 = \frac{V_{CH}}{V_{C_3S}} = \frac{m_{CH} * d_{C_3S}}{m_{C_3S} * d_{CH}} = \frac{n_{CH} * M_{CH} * d_{C_3S}}{n_{C_3S} * M_{C_3S} * d_{CH}} = (3-x)\frac{M_{CH} * d_{C_3S}}{M_{C_3S} * d_{CH}} \tag{4.29}$$

Where m_{CH} and m_{C_3S} are the masses of Portlandite and alite, n_{CH} and n_{C_3S} their moles, d_{CH} and d_{C_3S} their densities (equal to 2.23 and 3.15 respectively), M_{CH} and M_{C_3S} their molar masses (equal to 74.1 g/mol and 228[10] g/mol). For these numerical values, the calculation yields the formula:

$$\eta_4 = (3-x) * 0.459 \tag{4.30}$$

[10] As for the density, the molar mass could slightly vary for alite as other ions may incorporate within its structure, but the incorporation of other ions never exceeds a few percents, so that the density and molar mass of alite should also vary within a maximum of a few percents.

4.3.3 The overall heat of reaction is computed from the volumetric coefficients and individual enthalpies

Once the evolution of the volumetric coefficients with time are known from Ca/Si and H/Si measurements, the heat and heat flow can be computed and compared with calorimetry.

$$\Delta_r H_{overall}(t) = n_{C_3S}^{consumed}(t).\Delta_r H_{C_3S}(t) + n_{C-S-H}^{produced}(t).\Delta_r H_{C-S-H} + n_{CH}^{produced}(t).\Delta_r H_{CH} \tag{4.31}$$

Where the n_i are the moles of each reactant or product and the $D_r H_i$ the individual enthalpy of reaction per moles:

- $D_r H_{C_3S}^{dissolution} = -145 kJ/mol$, value from [17, p. 148]
- $D_r H_{C-S-H}^{precipitation} = 25 kJ/mol$, value from [6] as cited in [3, p. 33]
- $D_r H_{CH}^{precipitation} = 16 kJ/mol$, value from [6] as cited in [3, p. 35]

The moles of each reactant and products are computed from the volume of C-S-H and volumetric coefficients:

$$n_{C_3S}^{consumed}(t) = \int_0^t \frac{d}{d\tau}\Big(\frac{d_{C_3S}(\tau)}{M_{C_3S}(\tau)} V_{C_3S}^{consumed}(\tau)\Big) d\tau = \frac{d_{C_3S}}{M_{C_3S}} \int_0^t \frac{d}{d\tau}\Big(\frac{\eta_1}{\eta_3(\tau)} V_{C-S-H}^{produced}(\tau)\Big) d\tau \tag{4.32}$$

4.3.4 DMDs are used to distribute the water between the external and internal capillary water

Air voids always start forming in the outer space because there is no other possibilities. Later on, as the gap progressively open there may be a competition between filling the inner or outer space. As explained in section 1-9, the capillary water is balanced between the inner and outer space by filling the DMDs from the right.

4.3.5 The water reservoirs are assumed to empty from the coarser ones to the finer ones

Once the external and internal capillary water are exhausted, the water between the needles is used. At this point, needles are no more allowed to grow longitudinally but only laterally.

When the water between the needles is exhausted, the present version of the code stops. This does not prevent thinking about a solution: the next step is naturally the densification of the C-S-H which uses its own gel water. One may assume that the rate of densification is proportional to the amount of gel water left, that is proportional to the density itself. The solution of this PDE is the decreasing exponential function.

4.3.6 The probability of Portlandite phagocytose

A first guess of the probability of Portlandite phagocytose may be the ratio of the Portlandite volume over the outer space volume. Closer examination challenges it: the whole volume of the Portlandite clusters is not effectively engulfing grains but only the cluster cores are as explained in subsection 4.1.10. The volume of Portlandite in the transition zone does not contribute to engulfing the grains but only to impingement.

The thickness of the transition zone then needs to be defined. This thickness depends on the grain size: bigger grains are less likely to get engulfed than smaller ones; bigger grains are more likely to be affected by Portlandite impingement rather than Portlandite engulfment.

The transition zone for a grain of size d_{grain} is the size of its cell which includes the shell plus the space closer to its shell than any other grain. As a consequence, the probability P for such a grain to be engulfed at time t or before is:

$$P(r_{cell}, \tau < t) = \frac{\sum V_{Cluster_{core}}}{V_{outer-space}} = \frac{\int_0^\infty p_{CH}(R_{cluster}, t) * F_{cluster}(R_{cluster}).4/3\pi(R_{cluster}^3 - r_{cell}^3)}{V_{outer-space}} \tag{4.33}$$

Where $R_{cluster}$ is the radius of a cluster, p_{CH} the PSD of the clusters at a given time, $F_{cluster}$ the form factor of the clusters (assumed constant throughout the reaction but may vary with size) and r_{cell} is the cell radius which equals $r_{cell} = r_{grain} * \sqrt[3]{1 + \frac{w}{c} * \frac{d_{alite}}{d_H}}$.

The volume of Portlandite used for engulfing grains is therefore the sum of the volume of Portlandite used to engulf each grain size:

$$V_{CH_{for-engulfment}}(t) = \int_0^\infty p_{alite}(r_{cell}) P(r_{cell}, \tau < t) * V_{CH_{for-engulfment}}(r_{cell}, t) dr \tag{4.34}$$

Where $p_{alite}(r_{cell})$ is the PSD of the cell, which equals the initial powder PSD, and $V_{CH_{for-engulfment}}(r_{cell}, t) = F(r_{cell}) * 4/3\pi * (r_{cell}^3 - r_{outer-shell}^3)$ where $F(r_{cell})$ is the cell form factor which is assumed to be equal to the initial grain form factor.

The volume of Portlandite used for impingement is then the complementary volume:

$$V_{CH_{for-impingement}}(t) = V_{CH}(t) - V_{CH_{for-engulfment}}(t) \tag{4.35}$$

N.B. The distinction between the two phenomena, engulfing and impinging, should be kept in mind as they do not have the same effect on the reaction. In cement pastes, clusters are much smaller and therefore mostly impinge against the cells rather than engulfing them. The reaction of these cells is then slowed down but they still have the chance to eventually completely hydrate. On the opposite, in alite pastes, clusters are much bigger and therefore mostly engulf the cells rather than impinging against them. The reaction of these cells is then

completely stopped and the paste never reach 100% of DoH.

4.3.7 The probabilities of internal and external impingement

A first guess of the probability of impingement may be the ratio of the (outer/inner) available space for precipitation over the total (outer/inner) space. The available space for precipitation is the (external/internal) capillary water. For the internal space:

$$P_{int_{impintement}}(t) = \frac{V_{cap_{int_{water}}}}{V_{inner-space}} = \frac{V_{cap_{int-water}}}{V_{cap_{int_{water}}} + V_{cap_{int_{air}}} + V_{CH_{int}}} \tag{4.36}$$

While this is valid for the inner space, the outer space needs a correction because the Portlandite phagocytose happens there. The part of space where impingement only occur, not Portlandite engulfment, is simply $V_{outer-space} - V_{CH_{for-engulfment}}$, so that the formula is:

$$P_{ext_{impingement}}(t) = \frac{V_{cap_{ext_{water}}}}{V_{outer-space} - V_{CH_{for-engulfment}}} \tag{4.37}$$

However, because the outer C-S-H does not precipitate randomly in space, but heterogeneously on the scaffolds, the probability of impingement of the C-S-H of neighboring grains is initially extremely low so that this formula will exaggerate the initial probability of impingement. Ruling the outer C-S-H out yields a formula symmetrical to the inner C-S-H:

$$P_{ext_{impintement}}(t) = \frac{V_{cap_{ext-water}}}{V_{cap_{ext_{water}}} + V_{cap_{ext_{air}}} + V_{CH_{ext}}} \tag{4.38}$$

4.3.8 Other upgrades of the later ages model over the published version of the previous chapter

The key novelties of the later age model are the introduction of the inner C-S-H nucleation and growth and the distribution of the water in different reservoirs according to DMDs. But the code also considers other upgrades.

- The Ca/Si and H/Si ratios can now be varied with time. This affects the C-S-H density and volumetric stoichiometric coefficients.
- The shape and roughness factors can now be varied with the grain size.
- Shells detach from the scaffold beyond a critical gel-space ratio.

4.4 Parametric study

The parametric study is made one factor at a time: all factors are assumed to be set according to table 4 except for the one under study. The PSD chosen is Costoya's 13 μm one (shown in red on figure 4.34) and the w/c is 0.5 (except in the w/c study).

4.4.1 Outer C-S-H nucleation and growth parameters

The influence of the outer C-S-H parameters on the hydration kinetics is only studied for the later ages as their influence on the main hydration peak was already made in section 2.7 (section 3.7 of the Chapter 3) and on figure 10 of [13].

The influence of the early needles length, parameter l_{24h}, and late needles length, parameter l_{28d}, were studied on figure 4.26a. Interestingly the influence of the early needles length is not monotonous: the curves cross at about 20 days. This may be caused by the coupling between the outer C-S-H and the inner C-S-H via the capillary water: if smaller needles grow then the gap opening is lower so that the inner C-S-H has less space to precipitate and therefore consume less water; this saved water can then be used later on by needles to carry on growing.

4.4.2 Inner C-S-H nucleation and growth parameters

In a similar fashion the influence of the early and later inner C-S-H thickness on the DoH are shown on figure 4.27.

4.4.3 Water to cement ratio

The influence of the water to cement ratio on the heat flow, DoH, probability of impingement and ratio of external capillary water over total capillary water are presented on figure 4.28.

The influence of the w/c ratio on the first day is negligible for the four graphs except for w/c lower or equal to 0.3. In the later ages, at least up to 28 days, w/c higher than 0.5 are barely distinguishable on the DoH plot though they have an influence on the probability of impingement and fraction of external capillary water.

4.4.4 Conclusion of the parametric study

The early needle length has the biggest influence on the DoH up to a week, and it takes one week to resorb. The later inner C-S-H has the biggest influence on the 28days DoH. The late needle length and early inner C-S-H thickness have lower influences.

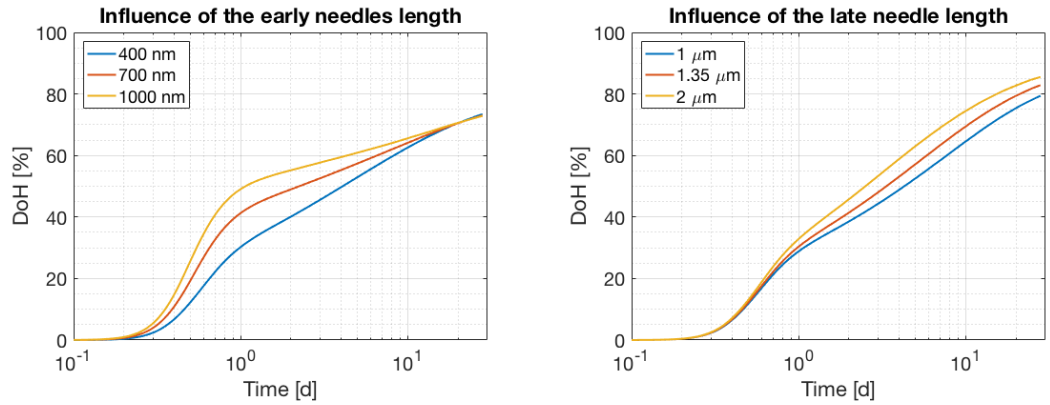

(a) *(b)*

Figure 4.26 – Parametric study of the early (left figure) and late (right figure) needle age parameter. The early needle length has a strong influence on the DoH up to one week. Surprisingly the low early needle length curve (400 nm curve on the left plot) crosses the high early needle length one (1000 nm) at about 28 days highlighting the non linearity of this factor: it is coupled other factors invisible here. The late needle length has a smaller effect.

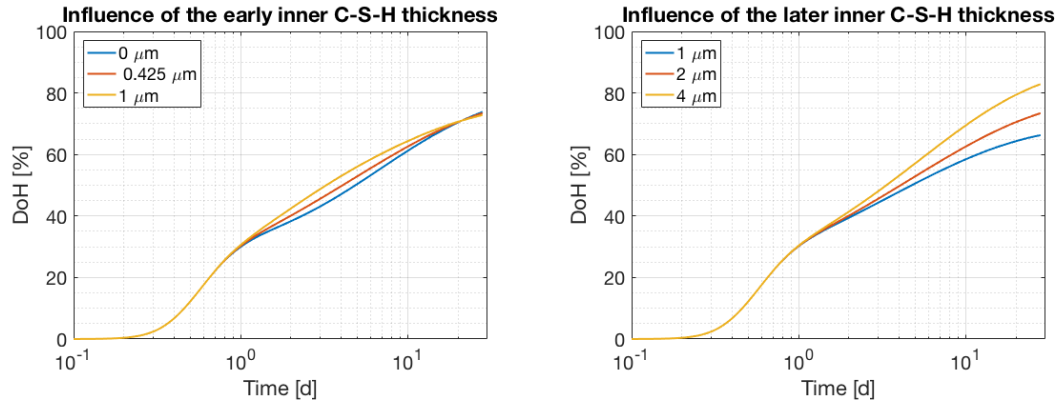

(a) *(b)*

Figure 4.27 – Parametric study of the early (left figure) and late (right figure) inner C-S-H parameter. The late inner C-S-H thickness has a strong influence on the DoH up to one week.

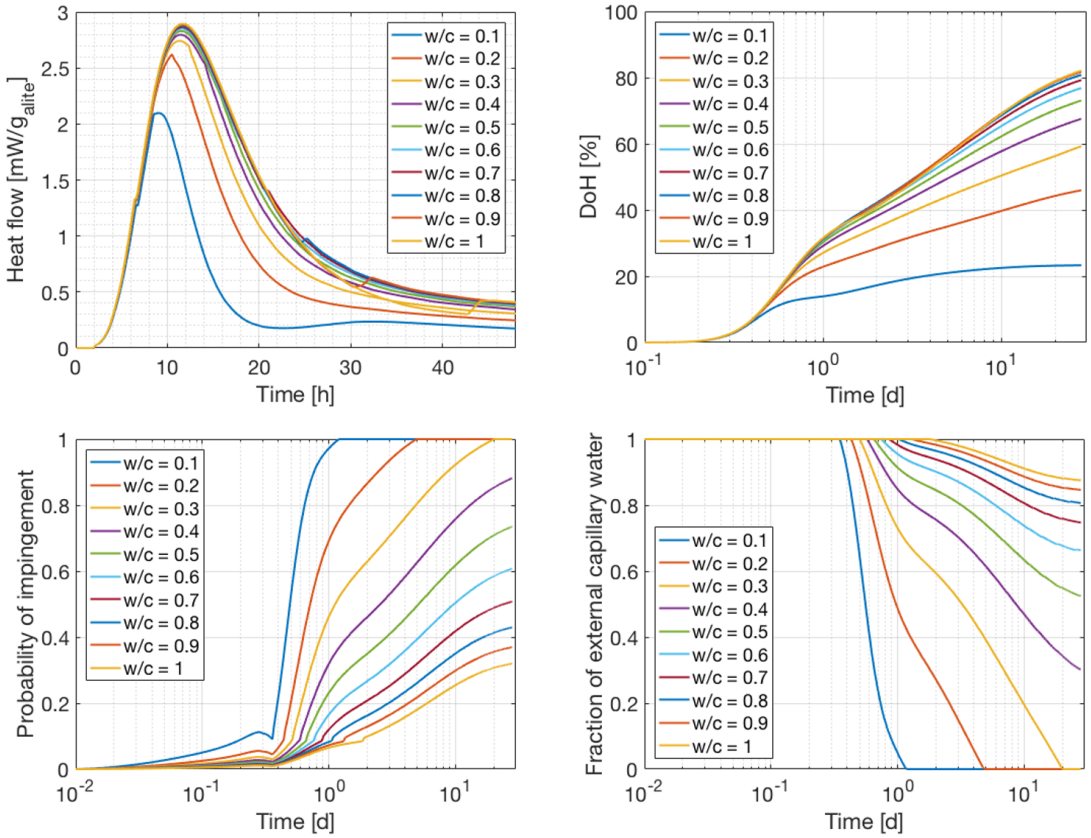

Figure 4.28 – Parametric study on the influence of the w/c on the heat flow, DoH, probability of impingement and ratio of external capillary water over total capillary water. Except for the w/c, the parameters of the simulation are those of table 4.4. The discontinuities mark the time at which the systems cross the critical gel-space threshold for scaffold detachment. Once this happens the inner C-S-H is allowed to grow if the time is more than 18 h.

4.5 Test of the model

4.5.1 Experiments to test the model

There does not exist yet in the literature a dataset specifically designed for benchmarking alite hydration models in the later ages. Following Popper in [15] and [14], datasets should push models to their limit so as to refute them, for example by varying the most impacting factors to extremal values. The dataset presented here vary: the PSD (coarse, intermediate, fine), w/c (0.26, 0.32, 0.5), and temperature (20°C and 40°C).

The input parameters for the model are all listed in table 4 and are kept identical for all experiments (except obviously for the PSD and w/c) so as to make the test more stringent.

The alite synthesis method closely follows the C_3S one detailed in [9]. Only the differences with this article are described here.

N.B. Only the experiment at 20°C are used for testing the model as only at this temperature could the outer and inner C-S-H parameters be retrieved.

Raw materials, mix design and calcination process

Calcium carbonate (VWR, 99.9% pure), SiO2 (7nm, Sigma-Aldrich, 99.9% pure), Al2O3 (Merck, 99.9% pure), MgO (Merck, 99.9% pure) and Fe2O3 (Acros Organics, 99.999%) were used for the synthesis of the yoghurt.

The mix design was initially based on the value given in [17, table 4.3 p. 105], but because of flash set, the amount of alumina was slightly reduced. Each jar contained:

- $CaCO_3$: 1271.6g
- SiO_2: 266.5g
- Al_2O_3: 10.2g
- MgO: 12.8g
- Fe_2O_3: 10.2g.

The alite was calcined at 1600°C for three hours after a four hours long heat ramp of 7°$C/minutes$.

Grinding process and storage

Because the disc mill is stored in a 60°C oven, and because the grinding process heats up the mill, the following cooling process was used. The disc mill was cooled in tap water, dried, wet

in isopropanol to remove any trace of water, and dried. Each grinding batch was 100g +/- 5g, 0.1wt. % of isopropanol was added. The control of the mass was observed to be critical to remain reproducible. The coarse powder was ground for 30 seconds, the intermediate one for 1 minute, the fine one for 5 minutes.

Once the alite was ground, it was stored in a 1L sealed plastic and used no more than two weeks before the calorimetry measurement.

Justification of the choice of the PSD, w/c and temperature levels

The PSD levels were chosen as a function of the disc mill: below 30s of grinding the PSD is not reproducible, beyond 5 minutes, the disc mill is too hot to be manipulated.

The upper bound w/c was limited by the bleeding effect. Bleeding was observed one hour after mixing. Beyond w/c = 0.5 bleeding was visible by eye on 2cm thick samples for the intermediate and fine powder; for the coarse powder bleeding started as low as w/c = 0.32. The lower bound was fixed by the homogeneity of the mixing process as observed by eye. Below the selected threshold the pastes were visibly not homogeneously mixed.

The $20°C$ and $40°C$ temperature levels were chosen because they are representative of the range where cement pastes operate and because these two temperatures are commonly used in the literature to assess the activation energy.

Calorimetry curves

The experimental calorimetry curves are presented in bright colors: red (fine powder), blue (intermediate powder) and green (coarse powder) on figure 4.37. In darker shades are plotted the model fit. The continuous and dashed lines respectively correspond to the high and low w/c. During the first day there is barely any difference with varying w/c as could be expected from the previous experiments presented in the literature review.

The corresponding DoH curves are shown next on figure 4.38. Continuous and dashed lines align up to a threshold DoH. This graph complements the study by Berodier in her thesis and replotted here on figure 4.29. Here it is clearly shown that the separation in stages is rather horizontal than vertical: continuous and dashed line only separate beyond a critical DoH rather than after a critical time (one day for example) even if in practice they often occur simultaneously.

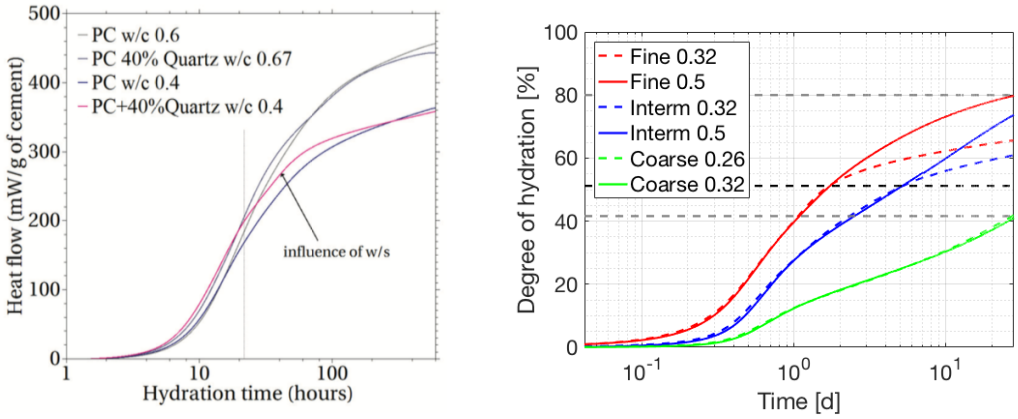

(a) *(b)*

Figure 4.29 – Left: Berodier's experiment on the effect of the w/c and w/s on PC. From (Berodier's thesis, fig. 5.13, p. 100). This figure suggests a change of mechanism occurring at one day (vertical line at 24 hours). Right: dataset at 20°C that show the change of mechanism is rather "horizontal": the green curves in particular did not split even by 28 days. The horizontal dash lies are defined by the rule of thumb explained in section 2.3.

4.5.2 Input parameters

Time step profile

In order to optimize the computation time the time step profile presented on figure 4.30 was chosen. The time step frequency is high during the main hydration peak so as to correctly capture the nucleation and growth of needles. Then it decreases as the reaction rates also diminishes.

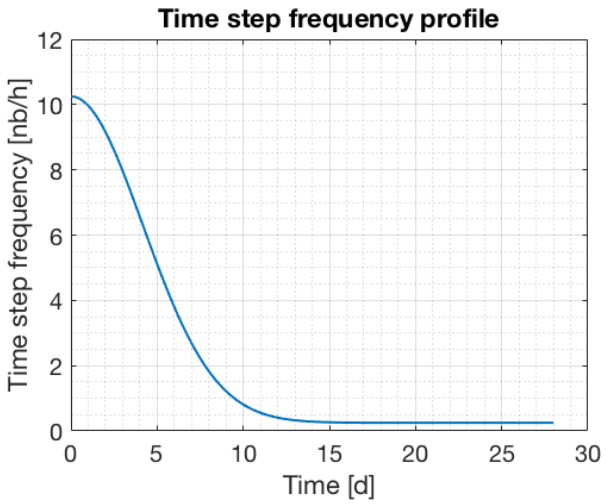

Figure 4.30 – Time step profile used for the simulations. During the first day, the time step is 10 per hours which makes one time step every 6 minutes, then it progressively decreases over a week down to 0.25 time steps per hour which makes one time step every 4 hours. The motivation behind this profile is to optimize the computation cost.

Outer C-S-H input parameters

The needle length with time is fitted on the measurement on figure 4.31. This corresponds to characteristic lengths of 400nm and 1350nm at respectively 24 hours and 28 days, characteristic growth time of 6 hours and 9 days at respectively 24 hours and 28 days.

Inner C-S-H input parameters

The inner C-S-H thickness were measured for the intermediate powder at w/c = 0.7 (figure 4.20b). These measurements suffer from the sectioning effect as illustrated on figure 4.32 on average grains are not sectioned at their equator but slightly higher. For monodisperse powders, the average sectioned diameter is 80% of the equatorial one [7, fig. 12.5 p. 208].

One figure 4.32 right is represented a grain of radius R with a shell of thickness r. The section cut slightly higher than the equator: the measured grain radius is R_s and the inner C-S-H

Table 4.4 – Input parameters used for the parametric and fitting the model. The parameters are kept identical for all simulations except obviously the w/c and PSD.

Numerical parameters		**Units (if any)**	**Remarks**
Number of time steps	336	No unit	See the time step profile on figure 4.30
Nb of alite grains	100	No unit	
DMD resolution	1	[nm]	
Powder parameters			
Roughness total	6	no unit	Identical to the value taken for the 14 experiments in (Ouzia and Scrivener, 2018)
Ellipse perimeter over equivalent disk perimeter	3.33	No unit	
Outer C-S-H parameters			
L_{24h}	400	[nm]	
L_{28d}	1350	[nm]	
$t_{c_{24h}}$	6	[hours]	
$t_{c_{28d}}$	9	[days]	
aspect ratio	0.1		
$\mu_{outer} C-S-H$ Gaussian nucleation	4	[hours]	
$\sigma_{outer} C-S-H$ Gaussian nucleation	2	[hours]	
final fraction covered	70	[%]	
Ca/Si	1.7		Average of Bazzoni's and Marchon's values
H/Si	5		Average value measured by Müller on WPC at 20°C
Density	1.89	$[g/cm^3]$	
Inner C-S-H parameters			
Thickness at 3 d	425	[nm]	
Thickness at 28 d	2000	[nm]	
$T_{c_{3d}}$	1.5	[days]	
$T_{c_{28d}}$	28	[days]	
$\mu_{inner} C-S-H$ Gaussian	24	[hours]	
$\sigma_{inner} C-S-H$ nucleation	6	[hours]	
Ca/Si	1.7		
H/Si	2.3		
Density	2.46	$[g/cm^3]$	Identical to Muller and Jennings
Thermodynamic parameters			
$\Delta_r H$ alite dissolution	-145	[kJ/mol]	
$\Delta_r H$ Portlandite precipitation	16	[kJ/mol]	
$\Delta_r H$ C-S-H precipitation	25	[kJ/mol]	
Density alite	3.15	$[g/cm^3]$	
Density CH	2.23	$[g/cm^3]$	
Density water	1	$[g/cm^3]$	
Others			
Gel space ratio scaffold detachment threshold	0.2		See section 5.2.4.

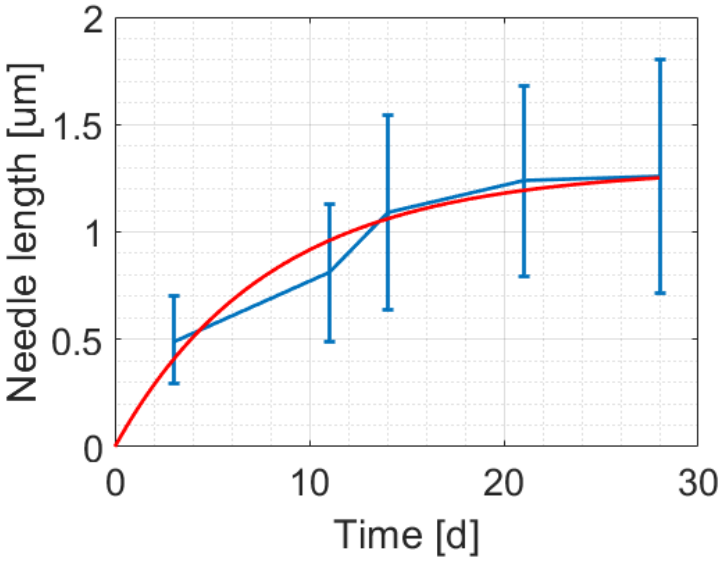

Figure 4.31 – Needle length measure (blue curve) with the fit function (red curves).

thickness is D. Applying twice Pythagoras theorem and solving the resulting trinomial yields:

$$r = \sqrt{R^2 + D^2 + 2R_s D} - R \tag{4.39}$$

In the case of a 13 μm grain, which is the dv_{50} of the intermediate powder, and a measured thickness of 2.2 μm, which is the average inner C-S-H thickness at 28 days, this yields r = 1.86 μm. The actual inner C-S-H is about 15% lower than the measured one.

As a consequence, the measured inner C-S-H thickness are reduced by 15%. The corrected C-S-H thickness together with the fit function used for all simulations are presented on figure 4.33.

PSD recovery

Unfortunately, the PSDs were not recorded so that they have to be estimated from similar experiments[11]. To constrain the fitting process, the following methodology was set.

The intermediate PSD powder is assumed to equal Costoya's 13 μm PSD powder The intermediate PSD powder has a very similar heat flow during the first day as the 13 μm experiment from Costoya. Both heat flows can be compared from figure 4.37 and figure 3 of chapter 2. Costoya's PSD is thus assumed to match this intermediate PSD.

[11] The actual PSD and specific surface measurement are planned to be measured and presented in a later publication most likely in 2020

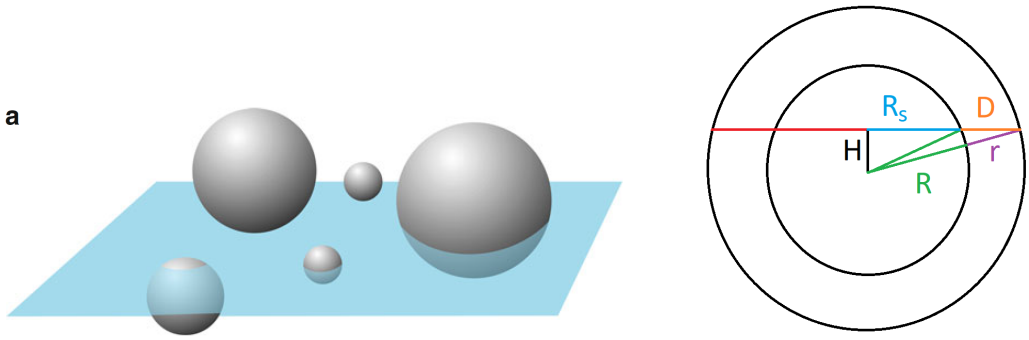

(a) *(b)*

Figure 4.32 – Left: Berodier's experiment on the effect of the w/c and w/s on PC. From (Berodier's thesis, fig. 5.13, p. 100). This figure suggests a change of mechanism occurring at one day (vertical line at 24 hours). Right: dataset at 20°C that show the change of mechanism is rather "horizontal": the green curves in particular did not split even by 28 days. The horizontal dash lies are defined by the rule of thumb explained in section 2.3.

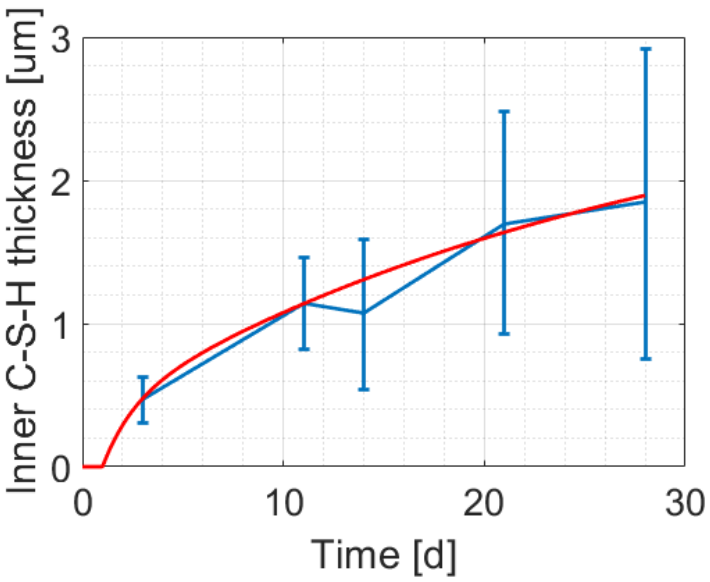

Figure 4.33 – Needle length measure (blue curve) with the fit function (red curves).

From the assumed average roughness of the grains, the BET specific surface is estimated
In (Ouzia and Scrivener, 2018), the average equivalent specific surface was assumed to be 6 for all 14 experiments tested. The equivalent specific surface of a grain, denoted Rou/F in the article, represents the ratio of the actual surface of a grain over the surface of the sphere of equal volume. A perfectly smooth sphere has an equivalent specific surface of 1, a smooth rugby ball is 4 and an elongated bottle of wine is 15. An equivalent specific surface of 6 means that grains can be represented on average as slightly rough rugby ball.

Table 4.5 – Translation coefficient used for the PSD recovery

	Intermediate powder	Fine powder	Coarse powder
Estimated BET specific surface $[m^2/g]$	1.00	1.28	0.44
Peak height $[mW/g]$	2.77	3.55	1.22

Knowing the equivalent specific surface and the PSD of a powder allow the calculation of its specific surface. The relation between the two was derived in appendix 1.2 of [13][12]

$$S_{spe} = \frac{3}{d_{alite}} * \frac{Rou}{F} * \frac{\int_0^\infty \frac{p_v(r)}{r} dr}{\int_0^\infty p_v(r) dr} \tag{4.40}$$

On Costoya's 13 μm PSD powder, this yields a specific surface of 1.00 m^2/g.

The other PSDs are obtained by a logarithmic translation. The other two PSDs, the fine and coarse ones, a translation of Costoya's PSD was made. The translation coefficient was determined thanks to the equation 16 derived in (Ouzia and Scrivener, 2018):

$$H(t) = \Delta_r H \frac{\eta_1}{\eta_3} S_{spe} l_{24h} d_{alite} * g(k_n, s_0, t_c, t) \tag{4.41}$$

Where H(t) is the heat flow, $\Delta_r H$ is the overall heat of reaction, S_{spe} is the specific surface, l_{24h} is the needle length at 24h, d_{alite} is alite density, g is a function of the nucleation rate k_n, the needles base surface s_0, t_c the needle characteristic growth rate.

This equation shows that the heat flow during the first day is proportional to the specific surface, in particular, the peak height is proportional to the specific surface area. This relation holds only as long as the dissolution of small grains is negligible, that is for DoH lower than 50%. By chance, this is the case for all three powders.

Assuming the PSD is the only parameter that changes, i.e. assuming all the other model parameters are constant (needles sizes, nucleation rates, etc.), from the estimated specific surface of the intermediate powder and the ratio of the peak heights, the fine and coarse powders specific surfaces can be computed with the rule of three. The results are presented in table 4.5.

Now that the specific surface of the other two powders are known, their PSD can be derived under the assumption that they are logarithmic translations of the intermediate PSD. A logarithmic translation means the PSDs appear translated when plotted in a semi-logarithmic scale.

[12] This equation holds when the parameter Rou and F are assumed independent of r, otherwise these should appear within the integral. As these are assumed to indeed constant (their ratio being 6 for all the experiments of this chapter), this equation can be applied here.

This actually amounts to a multiplication in linear scale. Therefore we are looking for the multiplication factors K_{fine} and K_{coarse} so that $p_v^{fine}(r) = p_v^{intermediate}(K_{fine} * r) and p_v^{coarse}(r) = p_v^{intermediate}(K_coarse * r)$.

These multiplication factors can be obtained by inversing equation 16 of [**Needle_article**]:

$$S_{spe} = \frac{3}{d_{alite}} * \frac{Rou}{F} * \frac{\int_0^\infty \frac{p_v(K_{fine} r)}{r} dr}{\int_0^\infty p_v(K_{fine} r) dr} \tag{4.42}$$

By the change of variables: $r' = K_{fine} * r$, this yields:

$$S_{spe}^{fine} = \frac{3}{d_{alite}} * \frac{Rou}{F} * \frac{\int_0^\infty \frac{p_v(r')}{K_{fine} * r'} dr'}{\int_0^\infty p_v(r') dr'} = \frac{1}{K_{fine}} * \frac{3}{d_{alite}} * \frac{Rou}{F} * \frac{\int_0^\infty \frac{p_v(r')}{r'} dr'}{\int_0^\infty p_v(r') dr'} \tag{4.43}$$

$$= \frac{1}{K_{fine}} * S_{spe}^{intermediate} \tag{4.44}$$

And finally: $K_{fine} = \frac{S_{spe}^{intermediate}}{S_{spe}^{fine}} = \frac{H_{peak}^{intermediate}}{H_{peak}^{fine}} = 2.77/3.55 = 0.78.$

In a similar way, $K_{coarse} = \frac{S_{spe}^{intermediate}}{S_{spe}^{coarse}} = \frac{H_{peak}^{intermediate}}{H_{peak}^{coarse}} = 2.77/1.22 = 2.27.$

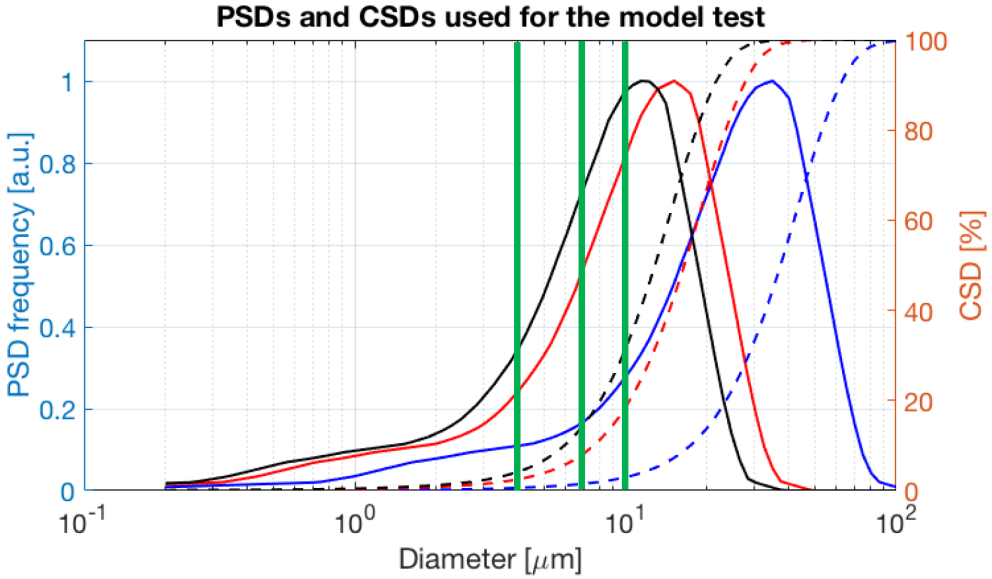

Figure 4.34 – Particle size distributions used to test the model and their associated cumulative size distribution in dashed lines. The middle red PSD is Costoya's 13 µm PSD. The vertical lines indicate the approximate threshold diameters below which grains have completely dissolved by 1, 7 and 28 days. These lines are the average on all simulations: there are variations of +/1 µm at 1 day, +/- 2 µm at 7 days and +/- 3 µm at 28 days.

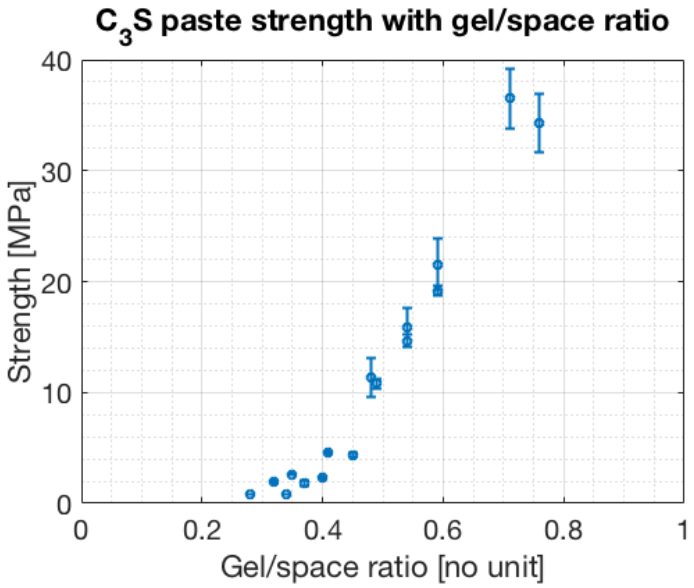

Figure 4.35 – Strength of C_3S pastes with gel-space ratio. The strength collapses around 0.2. The error bars are the standard deviation computed on 4 replicates. Note the error bars for the lower gel/space ratio points are so low they are contained within the circle symbols.

Threshold gel-space ratio for detachment

The threshold gel-space ratio for scaffold detachment was estimated from experiments made on C_3S following the protocol described in [13]. The plot is shown on figure 4.35. Note how small are the error bars on the low w/c points. The strength collapses below a gel-space ratio of 0.2.

C-S-H Ca/Si and H/Si ratios and density

The Ca/Si ratio was chosen at 1.7 because this is the average of two similar experiments made by Bazzoni and Marchon and replotted on figure 4.36. The H/Si was chosen at 5 following Muller NMR experiment on WPC replotted on figure 4.24.

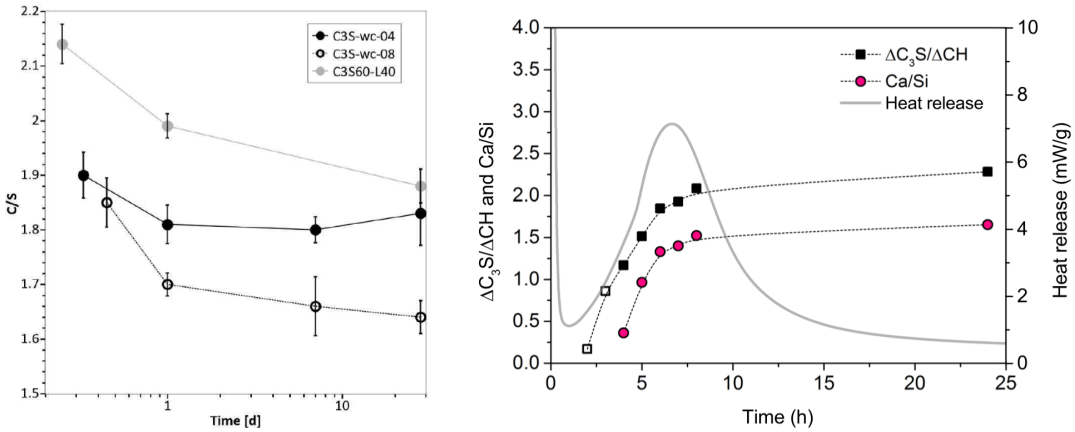

(a) *(b)*

Figure 4.36 – Left evolution of the Ca/Si ratio for alite experiments made by Bazzoni (Bazzoni's thesis, fig. 5.9 p. 118). Right: calorimetry curve and Ca/Si ratio for C_3S experiments made by Marchon (Marchon's thesis, fig. 4.2 p. 87)

4.5.3 Results and discussion

i) Calorimetry and DoH curves

The main hydration peak heights and positions during the first day are well captured by the model. Also, the 28 days DoH are very close to the experimental ones. The DoH throughout the reaction is well captured for the coarse powder, correctly captured for the intermediate powder, and poorly captured for the finer ones. These results rather comfort the hypotheses on which the model is built.

The probability of outer C-S-H growth is not linear with the space available

One striking difference however is the way the curves split: the model does predict a separation of the low w/c curves with the high w/c curves, and the separation quantitatively match the measured ones at 28 days, but **the separation is progressive by contrast with the experiments**. In the experiments, the continuous and dashed lines are very well aligned below the critical DoH of separation; then they **abruptly** split.

Where is the model wrong then? One may point at the list of approximations made, DMD do not exactly represent the reality, the error bars on the measurements are rather high and forcing them to be equal for all 6 systems may seem too stringent. Yet, any model that assumes the probability of impingement to be **proportional** to the available space will actually show this progressive trend.

Therefore, the probability of growth is not proportional to the space available, but must be non-linearly dependent on it. What are the sources of this non-linearity?

A first guess could be that impingement simply is not influencing the kinetics in the later ages, that some other unthought mechanisms have been missed. Nevertheless, the model still correctly captures four out of six curves, and correctly predict the 28 days DoH for all systems.

A second guess could be the combination of the densification and ions transport. As long as there is external capillary water left, the ions can travel easily through the structure and feed the growing or densifying needles (if they are blocked by impingement). But this remains to be quantitatively assessed as this boils down to the cell influence domain (see appendix), which at least during the first day was shown to be negligible in [13].

A third guess is the non-randomness of the space filling. Perhaps more work on the DMDs is needed to adequately represent the space filling. The way air voids open was simplified in the DMD treatment. In principle, air voids minimize the surface curvature and do not exactly fill the space from the right as it was assumed. Still this correction would not account for the impingement of C-S-H from neighboring grains or against CH clusters.

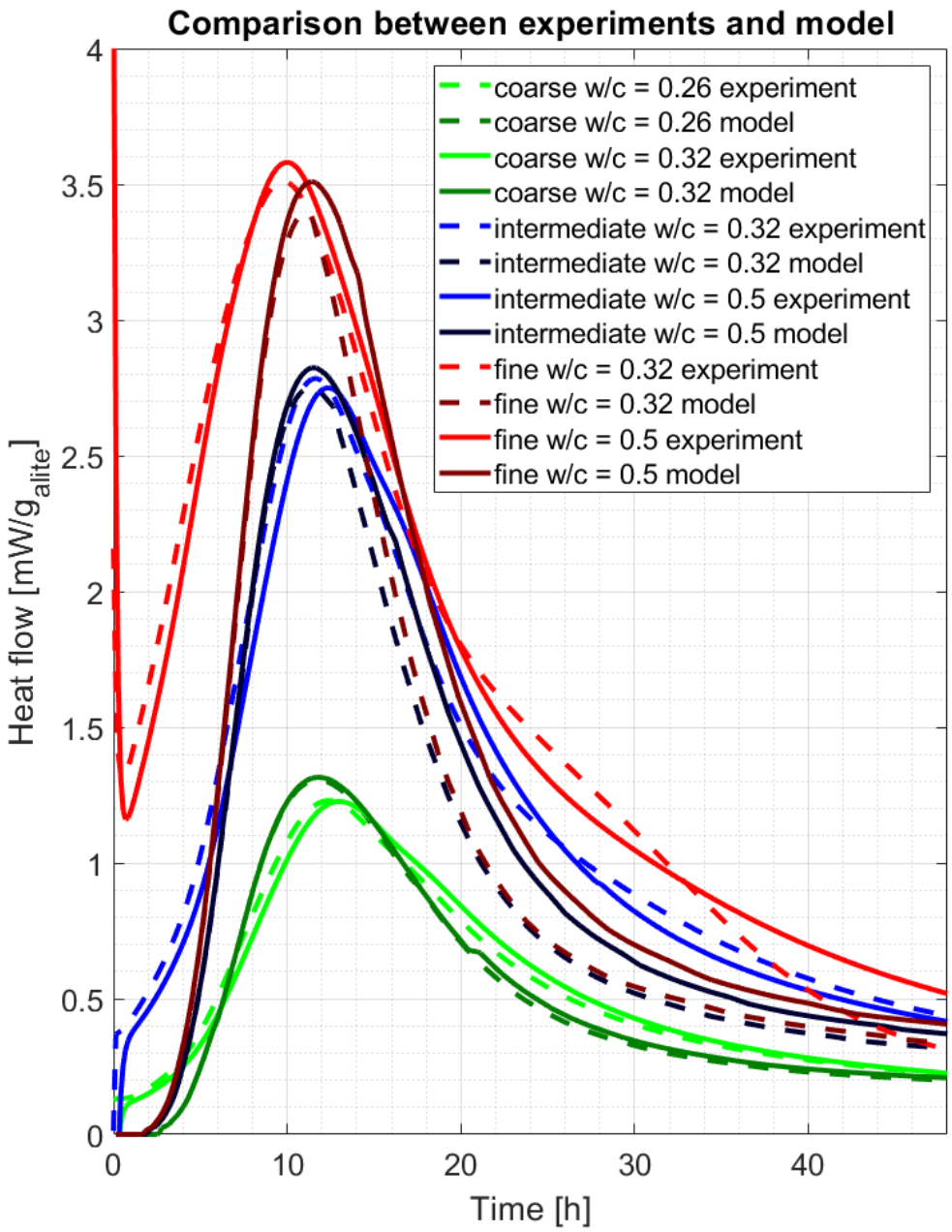

Figure 4.37 – Heat flow rates during the first day to test the model together with the model fits. Bright curves are the experimental ones, dark ones are the model fits. Dashed and continuous lines are respectively the lower and higher water to cement ratios.

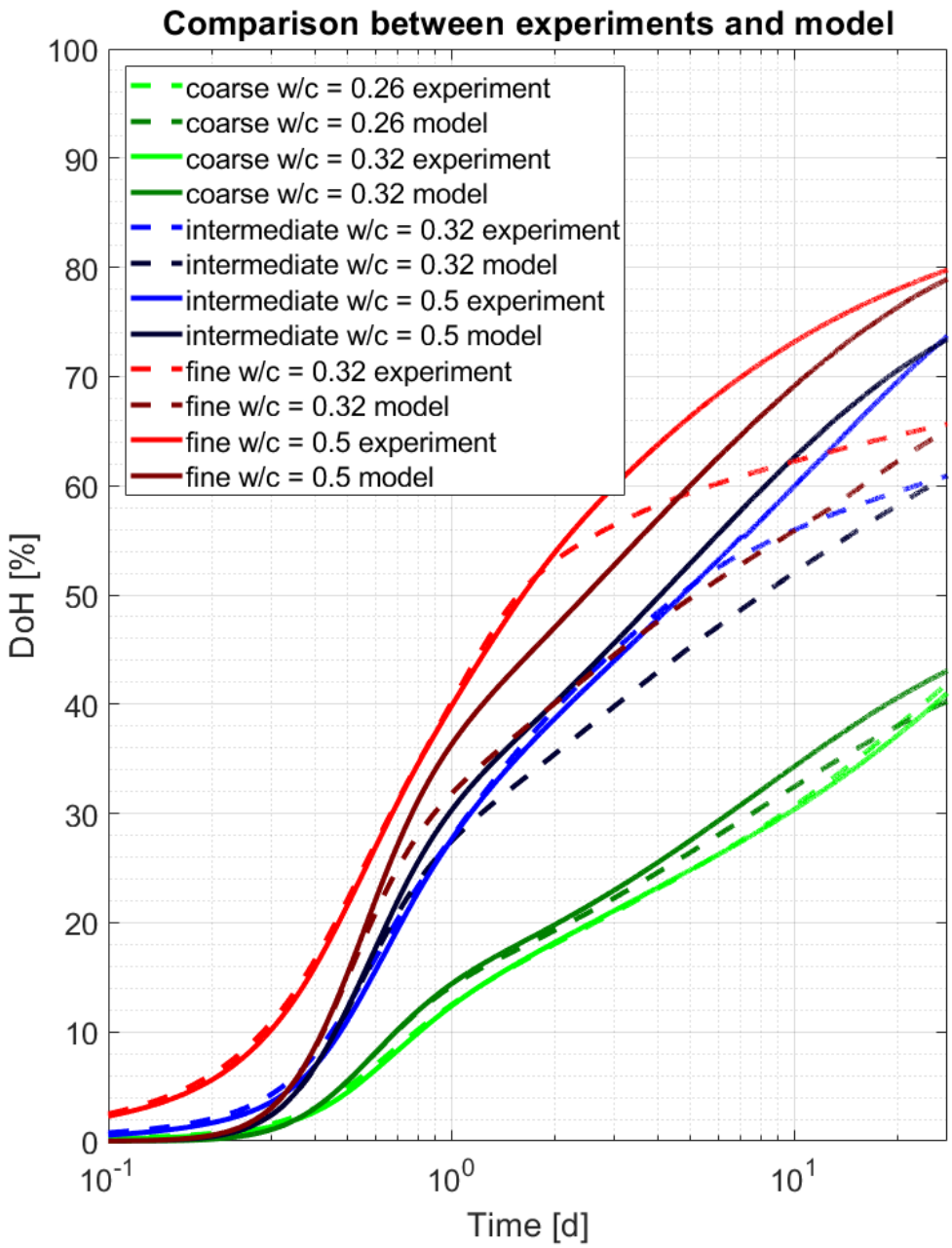

Figure 4.38 – Evolution of the DoH in the later ages. Comparison between the experiments (bright colors) and model (corresponding darker colors). Continuous and dashed lines are respectively high and low water to cement ratios.
By contrast with the previous figure, the fits are not that good, especially for the fine powder. Although the 28 days DoH are systematically well predicted there are large deviations before. This may come from the approximation used in the PSD recovery and the fact the needles N&G parameters may not be exactly identical with the powder fineness. Still one striking difference would remain: the split between the low and high w/c curves is abrupt *whereas it is* progressive *for the model curves. This may come from the fact that the phases are not randomly distributed in the external space so that the probability of impingement is not proportional to the external space available.*

ii) Powers diagrams

On figure 4.40 are presented the Powers diagram from the simulations of figure 4.37 and 4.38. All these plots exhibit a macroscopic shrinkage of about 1.5 to 2 %. This is directly determined from the critical gel-space ratio for detachment. Once the scaffolds have detached, the internal capillary water region develops (light blue). One of this Powers diagram is enlarged and described in figure 4.39.

The predominant role of the outer C-S-H over the inner C-S-H on the kinetics persists Although the inner C-S-H precipitation often coincides with the start of the later ages and is a prominent feature of the later age microstructure, its role on the later ages kinetics is not as important as SEM polished sections suggest.

- The Powers diagrams show that the volumetric fraction of outer C-S-H is always higher than the inner C-S-H fraction. Quantitatively, the inner C-S-H volumetric contribution to the total C-S-H is only about 30% ± 10% at 28 days. This fact could actually already be guessed even without any simulation: by 1 day only outer C-S-H has grown, yet the DoH in common PC systems or fine enough alite powders is already 50% by that time. From one day to 28 days, alite or cement never reach 100% so that the inner C-S-H amount must necessarily be lower than the outer C-S-H one.
- At sufficiently high w/c ratios and/or for coarse powders, the external capillary water is not exhausted so that the outer C-S-H still grows. In that case, it still contributes to about one third of the total heat flow all through the later ages.
- At sufficiently low w/c and/or for fine powders, the external capillary water is exhausted so that the outer C-S-H growth stops and the heat flow displays a characteristic inflection point. Because of the indirect influence of the outer C-S-H on the gap opening, the maximal thickness the inner C-S-H can reach is also reduced.
- The exhaustion of the external capillary water can in a sense cause the inner C-S-H precipitation. If there is no external capillary water left, but only internal capillary left, the system has no choice but to precipitate inside the gap.

The importance of the gap opening phenomenon. Water always flow from the external to the internal capillaries. The amount of volume freed by the gap opening is considerable. By 24 h the internal water fraction varies from 5 to 30%; by 7 days, it varies from 20 to 80%; by 28% it varies from 50 to 100%.

Moreover, the air pores always start forming in the external space as can be seen on the Powers diagram. This implies that the water always flows from the external capillary to the internal one. This can also be seen on the bottom right plot of figure 4.28: the fraction of external capillary water always decreases. This could be expected: once an air void has opened in the external space, it is hard to imagine it to shrink at the advantage of a void opening in the internal space; it may at best keep its size.

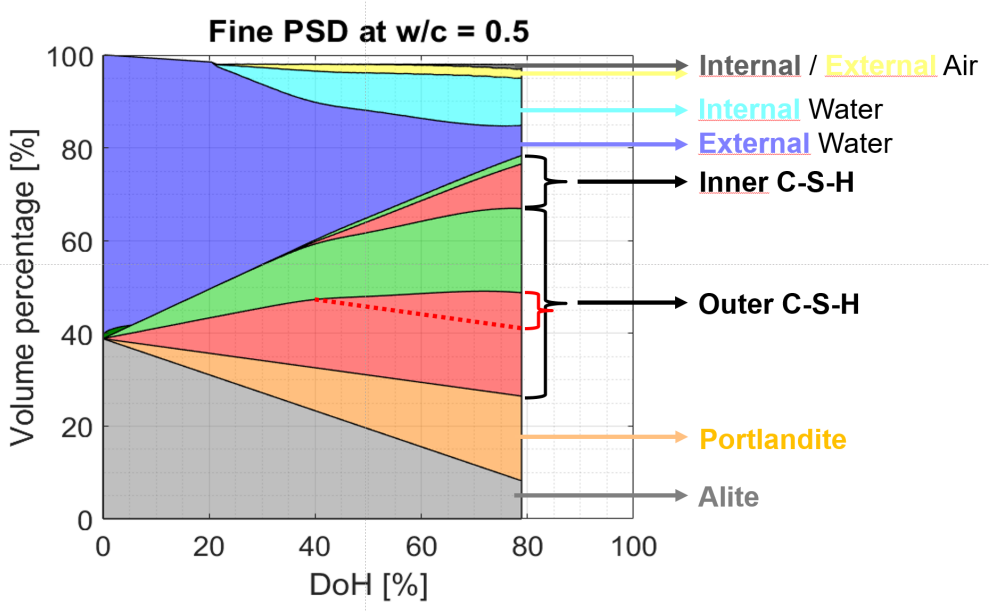

Figure 4.39 – Powers Diagram corresponding to the fine powder at w/c = 0.5. The outer and inner C-S-H are subdivided in two parts: the red parts represent the solid C-S-H and the green parts the gel-water as measured by NMR (see [11] for more details. - Note that because of chemical shrinkage the whole phase assemblage macroscopically shrinks by about 2% at the beginning up to the threshold gel-space ratio beyond which the scaffolds detaches from the shells. At this point, the gap opens and internal water and air can develop. The inner C-S-H appears at about 1 day which corresponds to a DoH of 40%. - Surprisingly, the amount of outer solid C-S-H produced from one to 28 days is about the same as the inner C-S-H produced during the same period (see the red dotted line and accolade). - Note that in this experiment, because the powder is very fine, there is a balance between external and internal air. This balance is computed with the help of DMDs. - Note that the volume of external water is always decreasing whereas the volume of internal water is always increasing which underlie that water always flow from the external water to the internal one.

Because of this unidirectional water flow, the gap opening removes available external space for the outer C-S-H precipitation, it accentuates the external impingement and therefore decrease the outer C-S-H growth and thus slows down the kinetics.

The curvature of the internal capillary water comes from mostly from the inner C-S-H growth, not from the balance between the external and internal capillaries A distinctive feature of the Powers diagram is the inflection point at the time of the inner C-S-H nucleation. Before it, the curve separating the external and internal capillaries is a straight line.

This inflection point could a priori come from two source: a flow of internal water in the external capillary, or the inner C-S-H growth. As explained in the previous subsection, the water always flow from the outside in, which leaves only the second option. This could also be seen directly from the volume fraction of internal air compared to the inner C-S-H volume fraction which is much bigger.

The inner C-S-H decreases the internal capillary water for two reasons: first it grows in the internal space and therefore at the expense of the internal water; second, when the external capillary is exhausted, it additionally consumes the inner water. This marks a second inflection point in the internal capillary water volume fraction observed on the top left Powers diagram.

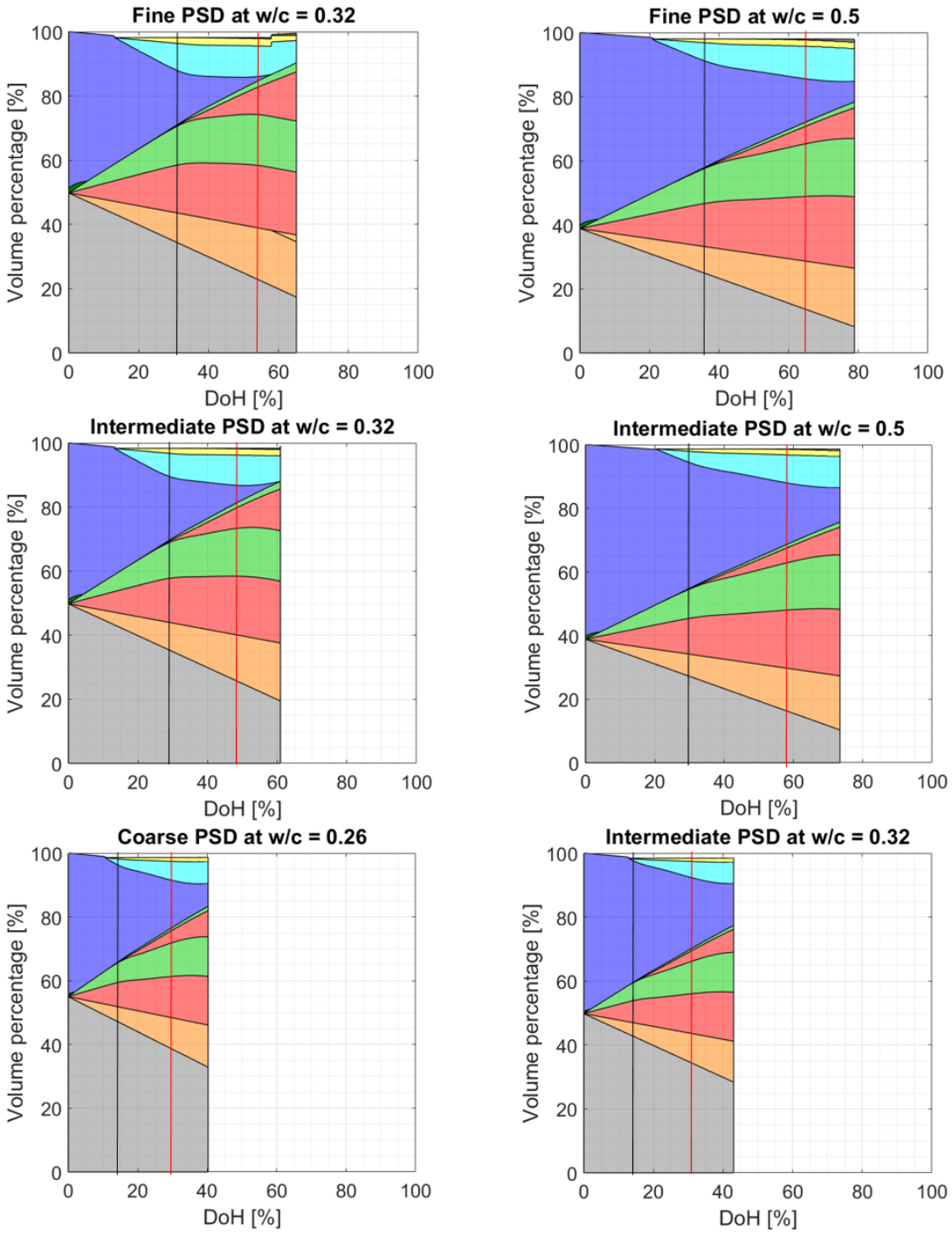

Figure 4.40 – Powers Diagram corresponding to the model fits presented on figures 4.37 and 4.38. Grey: alite, Orange: Portlandite, Red: compact C-S-H (the first to appear is the outer, the inner appears at about 20 – 40 % of DoH), green: water contained within the outer and inner C-S-H, dark blue: external capillary water, light blue: internal capillary water, yellow: external capillary air, black: internal capillary air. The vertical black lines are the DoH at 1 day, the red ones are the DoH at 7 days, and the diagrams stop at 28days.

iii) Evolution of the grains diameters during the later ages

Small grains carry on dissolving in the later ages and have a bigger importance than during the first day as the proportion of grains lying between 4 and 10 μm is higher than the proportion below 4 μm for common alite and cement PSDs (and as shown on figure 4.34).

The evolution of the grain sizes with time are presented on figure 4.41. The grain diameters pass by three distinctive steps: a first sharp decrease during the first day, then a long linearly decreasing section, and third a collapse to zero for sufficiently small grains.

At any time, small grains dissolve faster than bigger ones: the slopes of smaller grains are always steeper than those of bigger ones. As a consequence, they open larger gaps.

The higher the DoH and the coarser the PSD, the bigger the threshold grain size for dissolution.

- Grains below $7 \pm 2 \mu m$ completely dissolve within 7 days.
- Grains below $10 \pm 3 \mu m$ completely dissolve within 28 days.
- The maximum grain size that dissolves at 28 days is directly influenced by the initial amount of space available, that is the initial w/c. But the PSD indirectly influences it: finer powders quickly exhaust the external capillary water, which as a result diminishes the outer C-S-H growth, which leads to a lesser gap opening and therefore less inner C-S-H growth as well.

One issue: for big enough grains, the inner C-S-H does not touch the anhydrous surfaces
The 14 μm diameter grains shrinks by at least 4 μm (top left plot) and at most by 8 μm (bottom right plot). This is significantly more than the final inner C-S-H assumed in table 4 which means SEM polished sections should leave visible gaps between their anhydrous core and the inner C-S-H shell.

This is in contradiction with SEM observations: inner C-S-H are almost always in contact with the anhydrous cores at 28 days as seen on figure 4.6 and or on SEM polished sections of [5, chapters 4 and 5] and [10, chapter 4]. At least one assumption must therefore be wrong or missing.

Perhaps is the inner C-S-H not as dense as assumed ($2.46 g/cm^3$). In that case it would grow thicker faster and set contact with the anhydrous cores. However, to match the missing μm observed, the inner C-S-H density would need to be significantly lower than 2.46 and this would go against Muller's NMR experiment. Indeed, he observed a constant gel water during the later age [11, fig. 4.17] and suggested that the inner C-S-H must then be dense. But another interpretation is possible: the outer C-S-H may significantly densify and compensate the inner C-S-H gel pore production, and the inner C-S-H may as well later on densify.

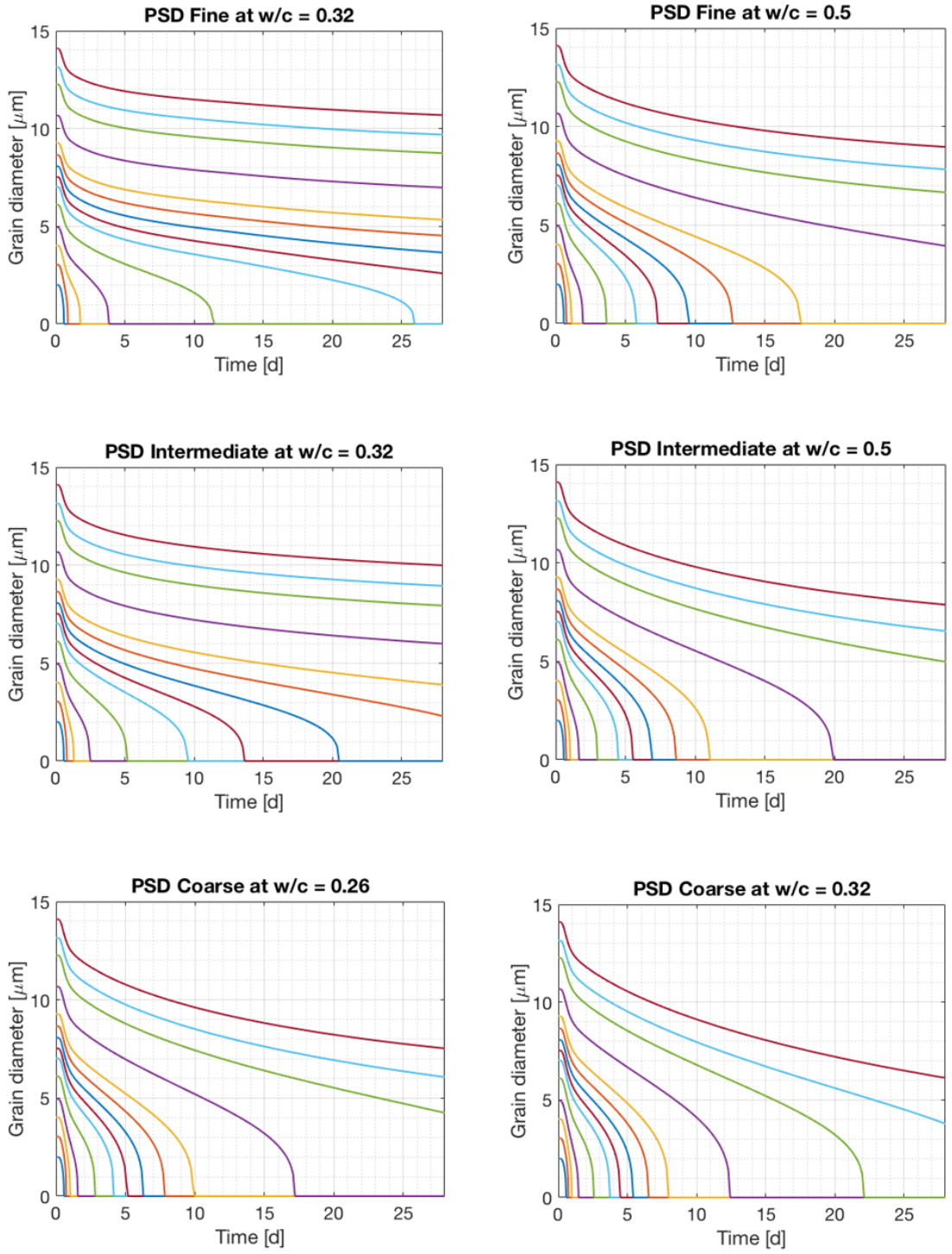

Figure 4.41 – Evolution of the grains diameters for the systems considered in the test of the model. Compare the left and right columns: increasing the w/c makes vanish bigger grains. Compare each line/PSD to the one below it: coarsening the PSD makes vanish bigger grains. Tracking the purple line (11 µm grain curve) helps to understand the influence of these two factors. The two extreme cases are the top left and bottom right plots. On the top left plot, grains below 7 µm dissolve by 28 days whereas on the bottom right plot, grains below 13 µm dissolve by 28 days (the volume of a 13 µm grain is 3.5 times larger than a 7 µm one).

4.5.4 DMDs

The external and internal DMDs at 28 days are presented on figure 4.42 and 4.43. The areas of each phase match those of the Powers diagrams, but the additional information of the distance to the scaffold provide additional insights.

First, most of the outer C-S-H actually grows within less than 1 μm far from the scaffolds although the maximum needle length inputted in the model is 1.35 μm. This comes mostly from the impingement of the C-S-H with the other phases. Other sources come from the way in which DMDs are built.

Second, the internal air pores develop only significantly in the finer powder and comes from the complete dissolution of some grain. Indeed, on the top right figure dealing with the fine PSD at w/c =0.5, there is some internal air pore 2.5 μm far from any scaffolds; but looking at the corresponding evolution of the grain diameter with time reveals that by 28 days all grains below 10 μm have vanished. As a consequence, this 2.5 μm air pore either comes from a 5 μm grain that dissolved early and did not have the opportunity to grow the inner C-S-H or a slightly bigger one, between 5 and 10 μm, which completely dissolved but had time to develop a thin inner C-S-H layer.

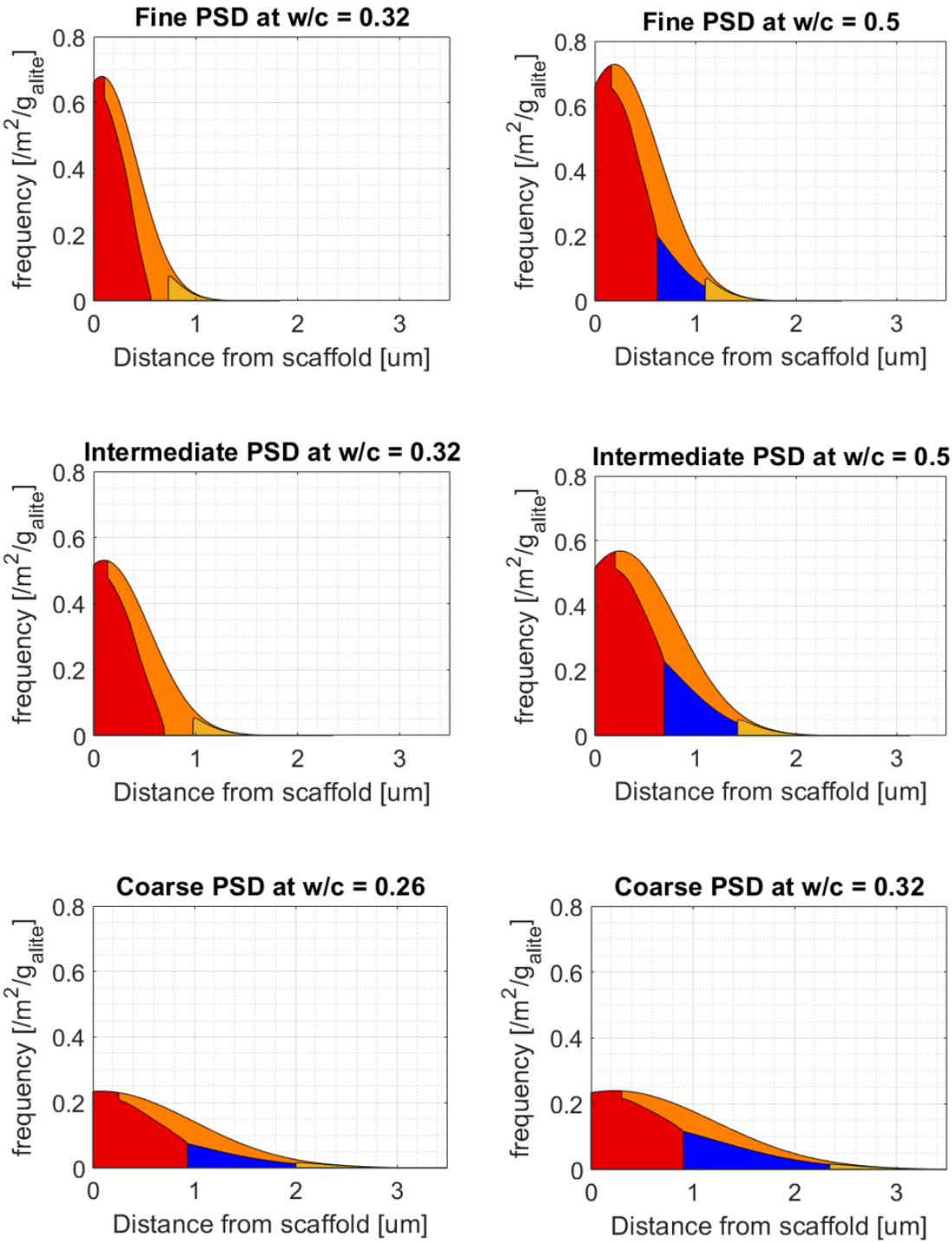

Figure 4.42 – External DMDs at 28days corresponding to the simulations made to test the model (cf figures 4.37 and 4.38). The coarser the PSD the coarser the maximum pore size (about 1 µm for the fine powder versus nearly 3 µm for the coarse powder). By 28 days the external water is depleted for the fine and intermediate powders at low w/c (compare with the corresponding Powers diagrams).

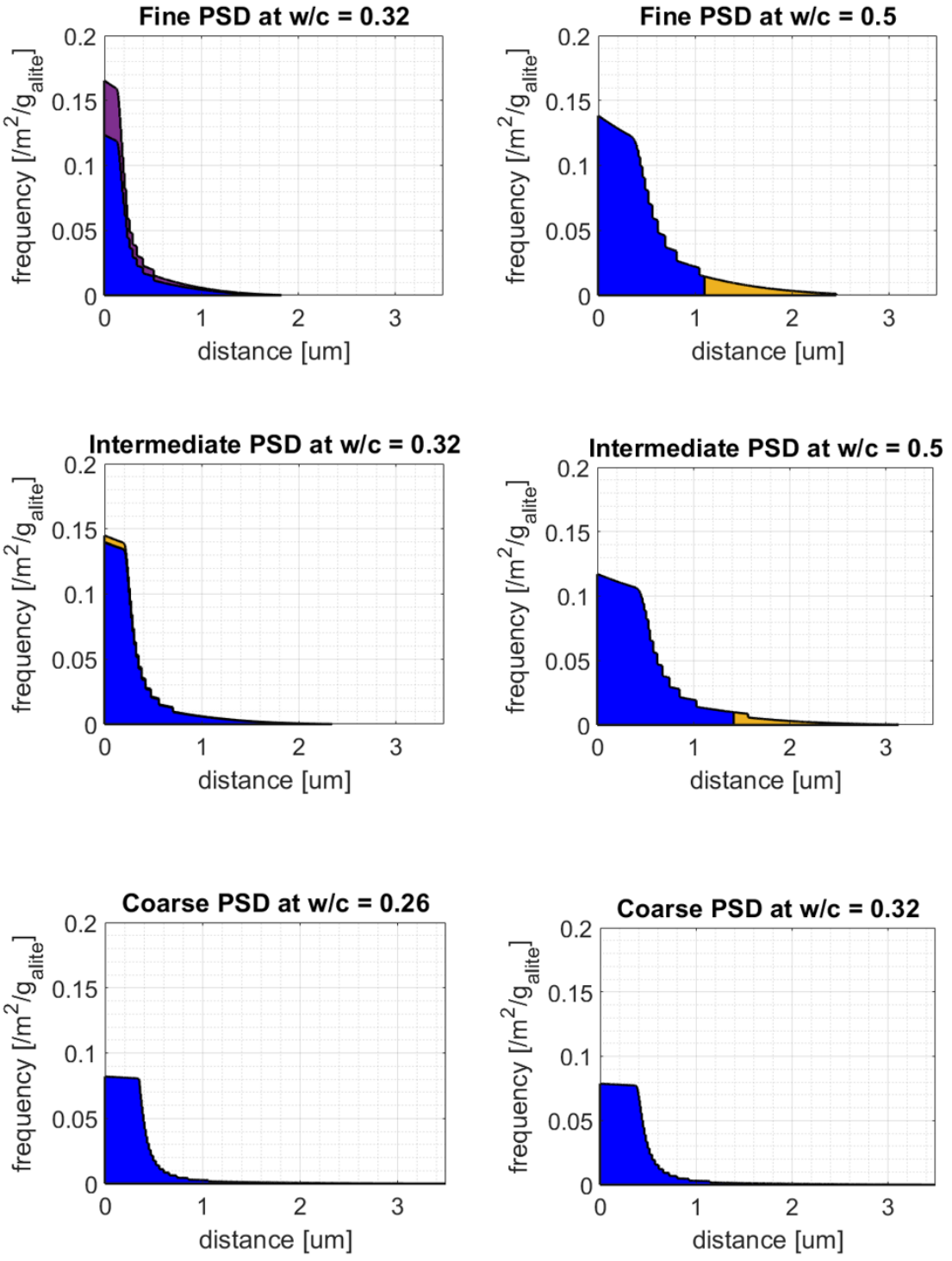

Figure 4.43 – Internal DMDs at 28 days corresponding to the simulation made to test the model (cf figures 4.37 and 4.38). The fine and intermediate powders at low w/c systems have exhausted their external water so that the representation of the air fraction is different to the other plots where there is a balance of air between the two reservoirs. The purple area in the top left plot highlights that not only air but also Portlandite is now precipitating inside (see the slight subdivision of the Portlandite area in the corresponding Powers diagram).

4.6 The complete dataset to benchmark alite hydration models

The need for a broad dataset was already mentioned by Taylor in 1986 [18, section 10]:

> The hydration of cement is a complex process, and the factors governing its kinetics are very imperfectly understood. For these reasons, the most practical attempts to model it have been those with a high proportion of empirical content. To exploit to the maximum the hight degree of predictive capacity that such approaches can provide, a broad base of experimental data is needed.
>
> This does not appear to exist at present, and its acquisition is probably the most important prerequisite for advances in the modelling of hydration kinetics.

Such a dataset still does not exist 34 years later and the first aim of this section is to fill this gap.

The dataset used in the last section is a subset of a complete one that aims at benchmarking alite hydration models. As there does not yet exist a dedicated dataset in the literature, models have often been tested only on Costoya's PSD experiment [13, section 5.3]. This is problematic for several reasons:

- The number of input parameters in existing models is always equal or higher than the number of experimental curves. Mathematically speaking the fits are underconstrained.
- Costoya's experiment only varies the PSD. Other factors which are known to influence the reaction like the temperature and filler effect for the first day, and additionally w/c for the later ages are not considered.
- Costoya's experiment only deals with the first hydration day. No dataset is yet available for the later ages.

For these reasons, models are often not stringently tested, to fit the data is too easy. In the absence of a dedicated dataset, the underlying mechanisms of these models cannot be rigorously tested and validated or refuted, their power of conviction is weak. As mentioned in [13, section 5.3] (section 6.3 of the previous chapter):

> It is remarkable that among the 5 models that attempted to fit Costoya's calorimetry curves [14,16,19,21] and the needle model) all of them succeeded though they defend quite different mechanisms as the cause of the transition from acceleration to deceleration. Even when they defend the nucleation and growth hypothesis their interpretations are significantly different: the model of Scherer [14] back-fitted parameters on Costoya's data indicates a decrease of nuclei density while an increase in perpendicular growth rate with increasing PSD size, the Bishnoi variable C-S-H density μic model indicates that the growth rate fluctuates over a one order of magnitude - a large interval without clear trend, and finally the needle model that these parameters remain constant.

Because the C-S-H parameters could not be measured at $40°C$ and because the model does not consider the filler effect, the model was tested only on a subset of the complete dataset. Nevertheless, the complete dataset still provides interesting insights into the later age mechanisms; that is the second aim of that section.

4.6.1 Presentation of the dataset

The dataset plays on four factors:

- PSD: coarse, intermediate or fine
- w/s in volume: 1.008 and 1.575 for the intermediate and fine powder, 0.26 and 0.32 in mass for the coarse powder
- Temperature: $20°C$ and $40°C$
- Filler: with or without Limestone addition (Limestone/alite = 0.25 in mass).

N.B. The coarse systems with limestone addition were ruled out because of segregation. The limestone used was much finer than the coarse PSD so that segregation happened within two hours after mixing; it was visible by eye.

4.6.2 Raw materials and mix design

The only new material used was limestone (BetoCarb, Omya) with a dv_{50} of 1.77 μm and a BET SSA of $8.96 m^2/g$. The limestone to alite mass ratio is 0.25.

The choice of the limestone fineness and mass replacement were guided by the motivation to reach a trade-off between:

- The need to see a significant effect on the kinetics. To maximize the heat flow increase, the powder should be as fine as possible and the replacement as high as possible.

- To stay close enough to the industrial reality: limestone finer than 1 μm are rarely used and blended cement typically are in the range 10 to 30% of replacement.

The water to solid ratio were chosen in volume instead of mass. This is necessary to enable a direct comparison regarding the goal of testing the space filling hypothesis. Otherwise the systems would start with different initial spaces which would hinder a direct analysis. For the systems without fillers, these w/c corresponds to 0.32 and 0.5 in mass. The systems with fillers are indicated with reference to their no filler counterpart as 0.32 and 0.5 on the legends of the plots.

N.B.: The choice of working in volume has the inevitable consequence of changing the shearing rate during the mixing and thus possibly changing the etch pits opening. Difference in the etch pits opening may then influence strongly the induction stages and slightly the main hydration peak and later stages.

4.6.3 Results and discussion

i) Influence of the w/s

During the first day, the w/s has no systematic effect on the peak height for the system without limestone. The systems with limestone addition are systematically slightly higher by $5\% \pm 2\%$.

The peak time is systematically shifted left for lower w/s by $40 \pm 20 min$.

The w/s has a dramatic impact on the later age kinetics. At $20°C$, for the intermediate and fine powders the higher w/s systems have $13\% \pm 1\%$ higher DoH at 28 days. At $40°C$, the higher w/s systems have $10.5\% \pm 3\%$ higher DoH at 28 days.

An observation made by Berodier [4, section 3 of chapter 5] is now confirmed on 18 experiments: the low and high w/s systems initially align before to suddenly separate. However, the separation does not occur beyond a given time, but beyond a given DoH: even at 28 days, the coarse powder curves align. This justifies the "horizontal rule of thumb" proposed in subsection 4.2.3.

As mentioned in the test of the model, the separation between the low and high w/s systems is abrupt which indicates that the space filling has a non-linear impact on the kinetics.

ii) Influence of temperature

As expected the higher the temperature the faster the kinetics. The activation energies were computed according to three methods and are given in table 6. At $20°C$, the average of the intermediate and fine powders at 1 day is 38.8% of DoH, and 73.6% at 28 days. At $40°C$ the averages are 47% and 73.4%. Because the $20°C$ experiments on average catch up on the $40°C$, the kinetics is actually faster in the higher temperature only during the first days: the slopes are steeper at $40°C$ than at $20°C$ only during that period.

iii) Influence of the PSD

The finer the PSD the more reactive the powder: peak height and DoH are systematically higher for finer powders.

$20°C$ **experiments** The peak height of the coarse powder is 55% lower than the intermediate one. The fine powders average is 30% higher than the intermediate one. At 28 days, the DoH of the coarse powder average is 39% lower than the intermediate powder. The fine powders average is 10% higher than the intermediate one.

$40°C$ **experiments** The peak height of the fine powders average is 210% higher than the intermediate one. At 28 days, the DoH of the fine powders average is 10% higher than the intermediate one.

Space filling only partly explains the later age kinetics The reduction of the difference between the PSD during the later age can partially be explained by space filling: because coarser powders consume less water by 24h, they still can grow outer C-S-H and catch on the finer powder. Nevertheless, there remains a significant and clear difference at 28 days which suggests that space filling might not be sufficient. Even in the $40°C$ experiment, which behaves like an accelerated $20°C$ system, the difference is 10% of DoH. As the Powers diagram of figure 4.40 suggests, the difference comes from the loss of outer C-S-H growth.

One possible explanation is the combination of the decrease of the supersaturation field with time and the thickening inner C-S-H shells. On the one hand, needles can only grow fast during the first 24 hours or perhaps until 48 hours, on the other hand the inner C-S-H layer at 28 days may eventually act as a diffusion barrier and considerably slow down the reaction. One may nevertheless argue that the blue and red curves seem to converge to the same point later in time. Longer experiments are required to definitely conclude.

An interesting difference between the $20°C$ and $40°C$ experiments regarding the influence of PSD is the presence of a second inflection point in the $40°C$ experiments that do not show up in the $20°C$ ones. At $40°C$, the yellow and red curves present and inflection point when they reach 80% of hydration.

iv) Filler effect: influence of the limestone addition

$20°C$ **experiments** The absolute peak height increases are + 1mW/g for both the intermediate and fine powders. The relative peak height increase is + 29% and + 37% for the fine and intermediate powders respectively. The absolute DoH increase at 28 days are +6 % for the fine powder and + 8% for the intermediate powder. The relative DoH increase are + 8% and + 11% respectively.

$40°C$ **experiments** The absolute peak height increase are + 2.5 mW/g and + 2.75 mW/g for the fine and intermediate powders respectively. The relative peak height increases are + 18% and + 46% respectively. The absolute DoH increase at 28days are + 6% and +0%. The relative increases are + 9% and 0%.

The filler effect may be detrimental to the DoH by 28 days or later Interestingly, the fine powder behavior differs from the intermediate one with regard to the filler effect. This is especially clear at $40°C$: whereas the red and yellow curves separate during the first day and then maintain their difference, which suggests the filler effect only acts during the first day, the

blue curves catch on the purple one and the continuous blue curve even crosses the purple one at 30 days.

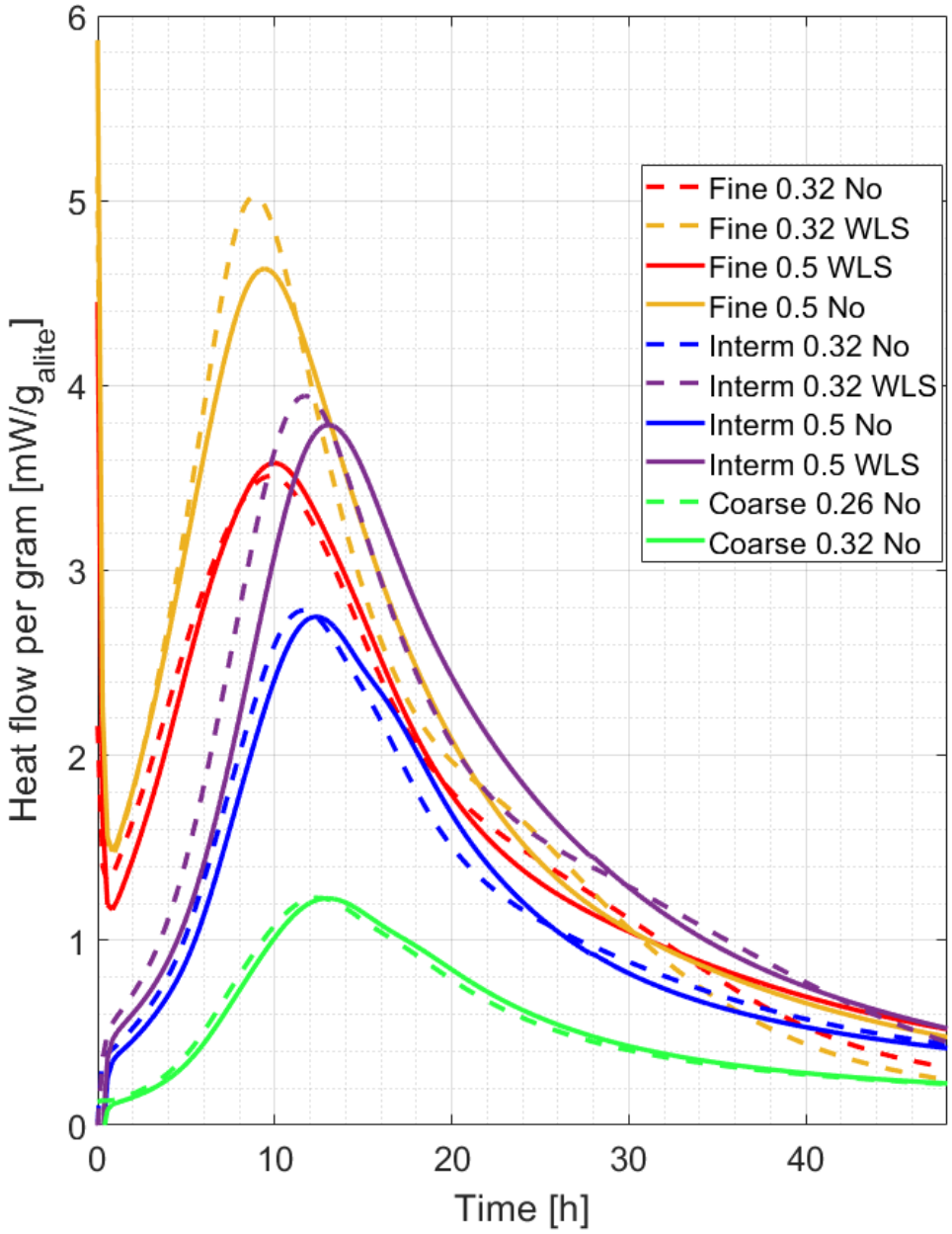

Figure 4.44 – 20°C dataset to benchmark alite hydration model. Dashed lines are the low water to cement ratio systems, continuous lines are the high water to cement ratio. During the first day, the w/c has nearly no influence. As already known, the the finer PSD the more reactive the system, and limestone additions increase the reactivity.

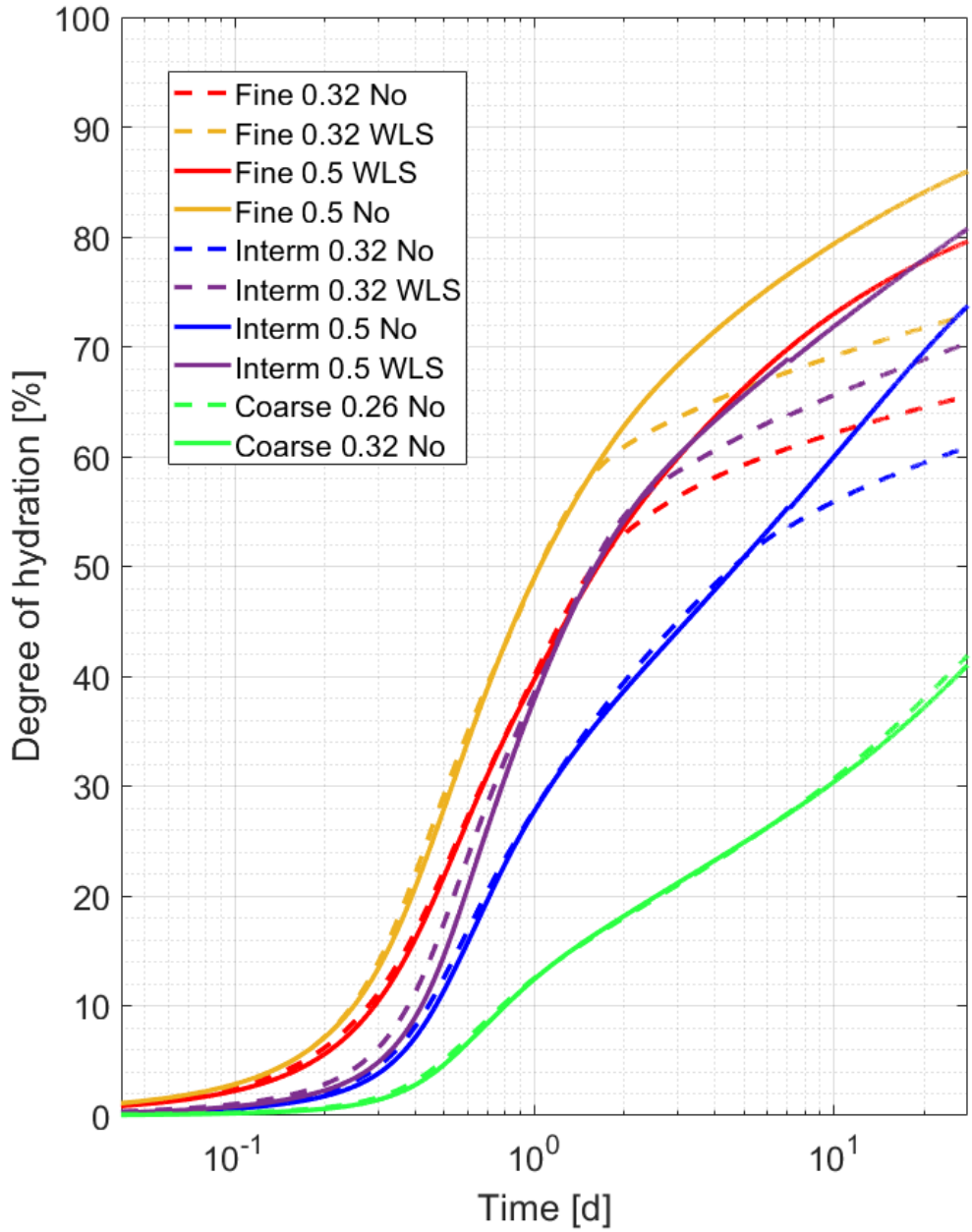

Figure 4.45 – Evolution of the DoH for the 20°C experiments. Note the significant influence of the w/c on the later ages kinetics: how the low w/c curves (dashed lines) and high w/c curves (continuous lines) initially align up to a given DoH beyond which they abruptly *split.*

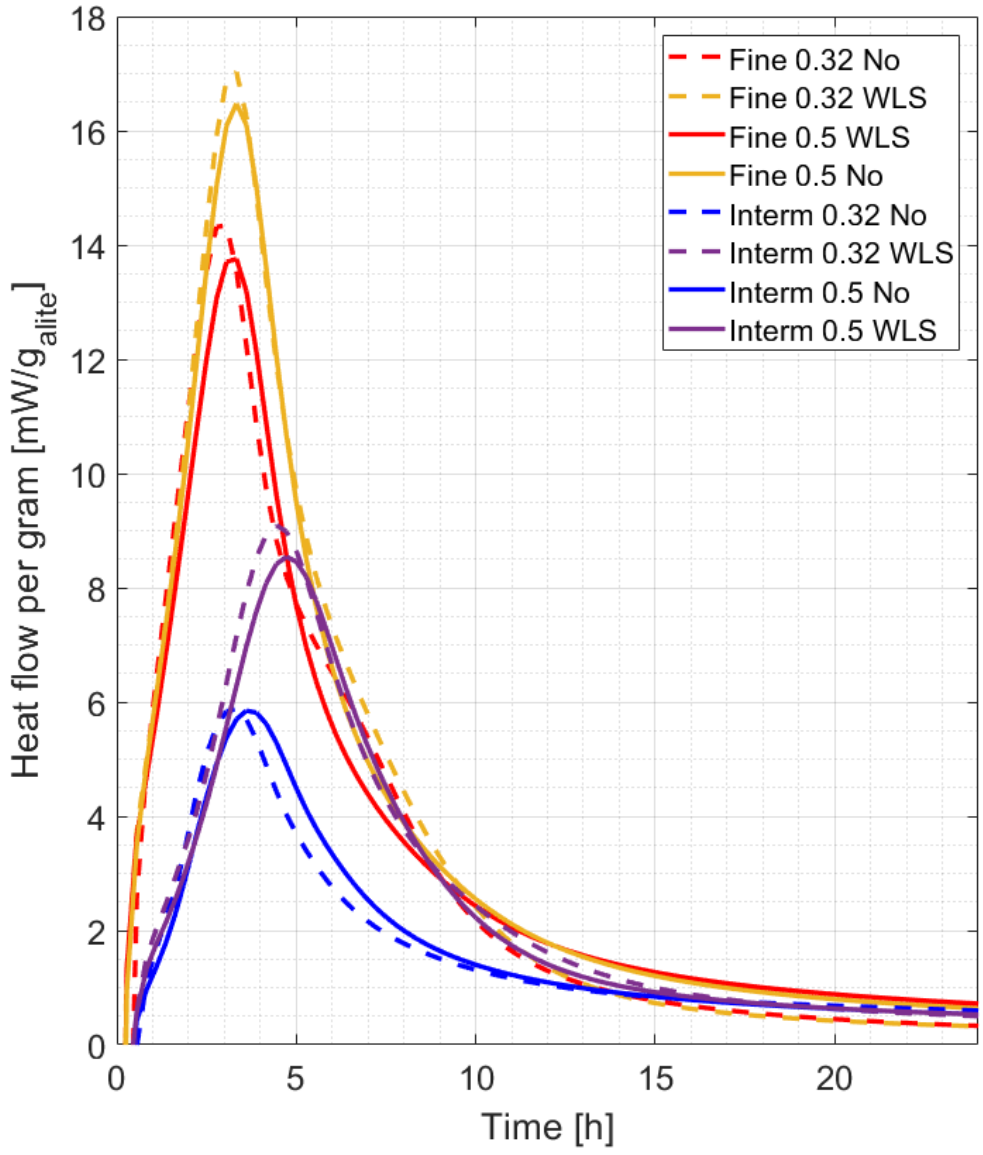

Figure 4.46 – Calorimetry curves of the 40°C experiments. Same remarks as for the 20°C experiment.

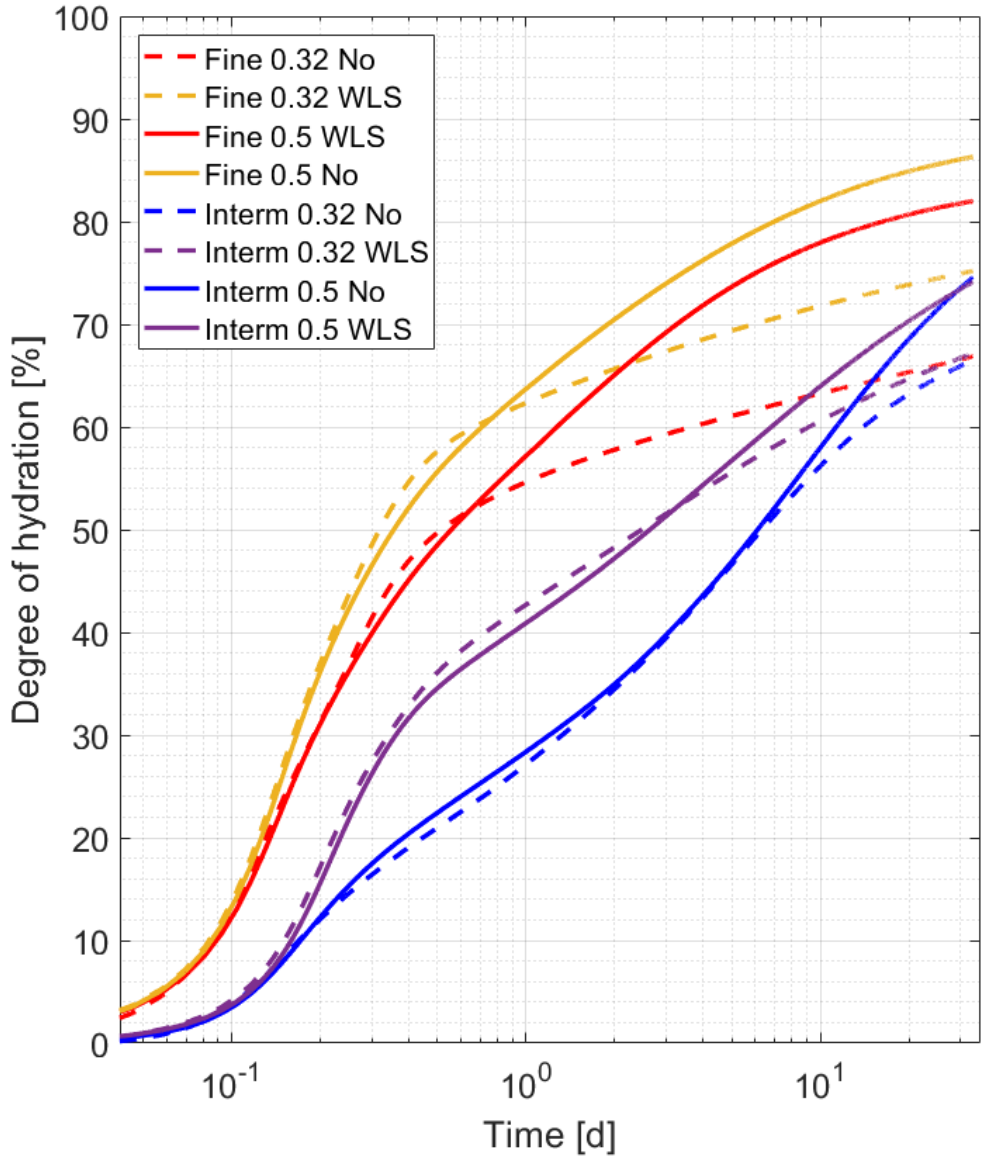

Figure 4.47 – DoH of the 40°C experiments. Same remarks as for the 20°C experiments. Note in addition that the low and high w/c curves split at the same DoH as at 20°C (though not at the same time): the yellow curves separate at about 60% DoH, the red, purple and blue ones at 53% DoH for both temperatures. In other words, the space filling rule of thumb holds at both temperatures.

4.7 Is space-filling the leading mechanism during the later ages?

Space filling certainly influences the later ages kinetics, but it entails different sub-mechanisms and other known mechanisms (the dissolution of the small grains, the decrease in supersaturation, diffusion limitation), hypothetic (like the C-S-H densification) or yet unknown (why is the probability of growth not linear with the available space for precipitation?) also account for the slowdown in the kinetics. In short, the later age kinetics is not controlled by a overwhelming single mechanism but by the cumulative effect of several non linear and coupled mechanisms. To quantitatively account for the later age kinetics all these effects and their coupling should be considered.

4.7.1 Space filling certainly influences the later ages kinetics

The points in favor of space filling influencing the later ages kinetics stem from theoretical and experimental arguments. Alternative hypotheses about the later age kinetics are not alone sufficient to explain it.

Arguments in favor of space-filling influencing the later ages kinetics

The space available for precipitation must first be the capillary water for thermodynamic reasons: it is always more favorable to precipitate in big pores than in small pores because of the crystallization pressure. The exhaustion of capillary water must therefore necessarily influence the kinetics: the system is then left with the only choice of precipitating within the only available remaining space: the gel pore. Although this rationale seems irrefutable, it is only qualitative and does not tell the pore size threshold below which the energetical cost is sufficiently high to prevent precipitation: the gel pore could be much larger than this threshold and C-S-H could a priori precipitate simultaneously in the capillaries and the gel pores.

NMR experiments made by Muller however set bounds to this scenario. His experiments on white Portland cement [11, fig. 4.26] and blended system [11, fig. 5.1] show a sharp increase of the gel water and the expense of the capillary water during the first day. In addition, the gel pore signal increase is linear with the solid water signal during the first day which indicates that C-S-H is not densifying during that period.

Even if further experiments were to reveal that C-S-H densification happens within the first day, the exhaustion of the capillary water would still shut off one mode of C-S-H growth and necessarily slowdown the kinetics.

Alternative hypotheses fail to account for the sharp and systematic split of the heat curve of the dataset of the previous section

Moreover, alternative hypotheses concerning the later age kinetics, drop in supersaturation, diffusion limitation or dissolution limitation cannot easily explain the systematic split between the low and high water to cement ratio of the 16 experiments of the dataset presented in the previous section.

A drop of supersaturation cannot alone explain why the kinetics slowdown above a given horizontal DoH threshold rather than a vertical time threshold. Measurements of supersaturation fields summarized in (Nicoleau and Nonat, 2016, a new view on the kinetics of C_3S hydration) show a dependence with time, not with DoH. In addition, the average supersaturation of the system should a priori not vary significantly, let alone increase, from 0.32 to 0.5 w/c.

The diffusion barrier hypothesis also fails to explain the w/c influence. For any PSD, the inner plus outer C-S-H shells are on average thicker on high w/c ratio systems: yet the higher w/c systems have a systematic higher DoH at any time. If the diffusion barrier was right, the w/c should not play a role at all once it is formed.

For a similar reason, a dissolution limitation as proposed in [12] cannot alone explain the w/c influence. Indeed, at higher w/c the DoH is higher which implies that grains react more and therefore shrink more and faster. The actual specific surface at any given time is therefore lower in higher w/c systems. Yet on the 16 experiments shown on figure 4.45 and 4.47, both the DoH and the slope are steeper during the later ages in the 0.5 w/c systems than in the 0.32 systems. Even at 28 days, when the grains have developed a 2 μm thick inner C-S-H plus 1 μm thick outer C-S-H layer, and when the grains have significantly more shrinked in the 0.5 systems than in the 0.32 systems (compare the left and right columns of figure 4.41), the slopes of all 0.5 systems are steeper than the 0.32 systems.

As a conclusion, these other alternative hypotheses are not alone sufficient to explain the w/c influence, though they may partially contribute to the later ages slowdown.

4.7.2 Space filling entails sub-mechanisms

The gap opening phenomenon

As already explained in subsection 4.5.3 within the Powers diagram discussion, the gap opening drag external water in and therefore increases the impingement in the external space.

Interaction between the outer and inner C-S-H

The outer C-S-H production directly influences the inner C-S-H potential of growth. The outer C-S-H is responsible for opening the gap during the first day: the inner C-S-H cannot by definition grow in the absence of a gap. Moreover, the higher the outer C-S-H production, the bigger the gap and the thicker the final possible inner C-S-H shell.

The inner C-S-H growth also influences the outer C-S-H growth though indirectly via the intermediary of the space available for precipitation. As explained in subsection 4.5.3, the water only flow from the external capillary water to the internal capillary water. As a consequence, the inner C-S-H production consumes the external capillary water rather than the internal one. This reduction of the external capillary water then increases the probability of external impingement which then slows down the outer C-S-H growth.

Non-Linearity of the kinetics with the amount of space available for precipitation

The fact that the low w/c curves abruptly split beyond a critical DoH instead of progressively entails this conclusion. The source of this non-linearity remains an open question: how much does the non-randomness of the phase distribution in space account for this abrupt split?

4.7.3 Grains still completely dissolve and slow down the kinetics

As for the first day, the progressive loss of the grains during the reaction slowdown the kinetics. As mentioned in 7.1.2, it is not the only mechanism playing a role though it certainly does.

4.7.4 Progressive contact between the inner C-S-H and the anhydrous grains

For grains that do not completely dissolve, the inner C-S-H shells eventually reach the receding anhydrous grain. Once this is done, the reaction must naturally slow down though this may happen only by the end of the first month.

4.7.5 Portlandite clusters

Although not considered in the model yet, the Portlandite clusters must necessarily decrease the reaction rate as they engulf alite grains. Estimations on Bazzoni's systems on figure 4.16a gives an estimate: $6\% \pm 2\%$ decrease of DoH by one month.

4.8 Appendix: The living and dead subdomains

N.B. Unfortunately, by lack of time, this was not included in the code and therefore does not appear in the main section of the thesis. Yet this provides a first analytical derivation of the problem and provide I believe some valuable insights on how the problem should be formulated.

4.8.1 The probability for an empty scaffold to lie in a living subdomain

Let us mathematically set the problem described qualitatively in part 1.5 on the cell influence domain. The goal is to define the probability for an empty shell to carry on growing. The probability for an empty shell to grow is assumed as a first order approximation to be proportional to the local supersaturation field. Therefore, the supersaturation field must be solved.

Derivation of the supersaturation field

Let us assume the domain to be spherical with the ion source, the anhydrous core, at its center as shown in grey on figure 4.48. The red part represents the mixture of hydrates (empty shells and Portlandite) air and capillary water, the black layer the limits of the domain. On the right picture is in addition represented the living subdomain, where empty shells are close enough to the ion source to be fed and grow.

The supersaturation field S, like a concentration field, obeys the diffusion equation:

$$\frac{dS}{dt} = D\Delta S + q_{v_{sink}} + q_{s_{source}} \tag{4.45}$$

Where D is the diffusion coefficient, $q_{v_{sink}}$ is the volume sink term which corresponds to the hydrates absorbing ions through precipitation, and $q_{s_{source}}$is the source term which corresponds to the surface of the anhydrous core which release ions through dissolution.

Because the diffusion of species is fast compared with the reaction rate at any time (the saturation field of the solution is stable with time in the alite later ages as ICP measurements suggest), the time dependent term can be neglected so that the equation becomes:

$$0 = D\Delta S + q_{v_{sink}} + q_{s_{source}} \tag{4.46}$$

N.B.: The supersaturation field necessarily has a gradient (it is the driving force for transport) as is highlighted in [12, fig. 3]. The question is quantitative: how strongly bended is the supersaturation field? This depends on the space filling: in high w/c systems the external capillary pores remain filled with water so that the supersaturation is only slightly bended,

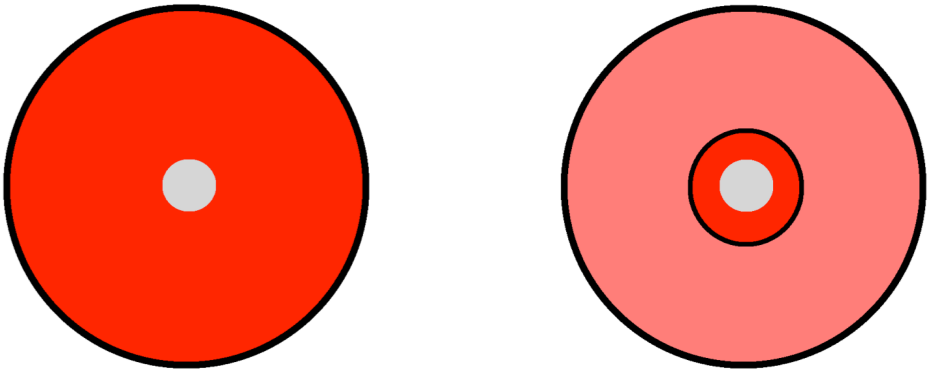

(a) (b)

Figure 4.48 – Geometrical simplified representation of the cell influence domain problem. The anhydrous core is represented in grey, red represents a mixture of empty C-S-H shells, portlandite and water, and black the boundary of the domain. On the right, the subdomain circumscribes the living domain: empty shells that are close enough to the ions source to maintain growth.

in low w/c systems the opposite is true. Without a quantitative calculation with a realistic microstructure it is not possible to know whether the curvature of the supersaturation can be assumed to be nil. However the following intuitive argument can be raised: in the later age, after 1 week of hydration for instance, the sum of the outer plus inner C-S-H shell is about $3\mu m$ to that the concentration of the species are likely different between the internal and external spaces. The time at which this effect start to be significant is an open question and an so is the time at which the simplification of the PDE is justified. The following derivation only aims at giving a hint of how the problem could be formulated.

The diffusion coefficient is assumed proportional to the fraction of external capillary water, the more water the easier the diffusion,

$$D = K_{diff} * f_{cap_{ext}} \tag{4.47}$$

The sink term is assumed proportional to the amount of hydrates at a distance r $4\pi r^2 * f_{hydrates}$ where $f_{hydrates}$ is the hydrates volume fraction, and local deviation from the C-S-H equilibrium $S(r) - S_{eq_{CSH}}$:

$$q_{v_{sink}} = -k_{sink} * 4\pi r^2 f_{hydrates} * (S(r) - S_{eq_{C-S-H}}) \tag{4.48}$$

It is negative because the sink absorbs the ions. The source term is positive because it produces ions. The source term is assumed proportional to the anhydrous surface and local deviation from alite solubility:

$$q_{v_{source}} = k_{source} * 4\pi R^2_{anhydrous} f_{hydrates} * (S_{eq_{alite}}(r) - S(R_{anhydrous}) \tag{4.49}$$

Because the source term is null everywhere except at the interface, the PDE in the bulk shortens to:

$$D\Delta C - k_{sink} * 4\pi r^2 f_{hydrates} * (S(r) - S_{eq_{C-S-H}}) = 0 \tag{4.50}$$

Replacing the Laplacian for its spherical expression yields:

$$\frac{d^2S}{dr^2} + \frac{2}{r} - \frac{dS}{dr} - \frac{k'_{sink}}{D} r^2 S = -\frac{k'_{sink}}{D} r^2 S_{eq_{C-S-H}} \tag{4.51}$$

Where $k'_{sink} = k_{sink} * 4\pi f_{hydrates}$. A particular solution to the inhomogeneous equation is $S(r) = S_{eq_{C-S-H}}$. Let us know solve the homogeneous equation:

$$\frac{d^2S}{dr^2} + \frac{2}{r} - \frac{dS}{dr} - \frac{k'_{sink}}{D} r^2 S = 0 \tag{4.52}$$

Using Wolfram mathematica online (Wolfram Research, Inc. (www.wolfram.com), Mathematica Online, Champaign, IL (2018)), the homogeneous solution is:

$$S_{homogeneous}(r) = \frac{1}{r} * \Big(C_1 \exp\big(-\frac{1}{2}\sqrt{\frac{k'_{sink}}{D} r^2}\big) * H_{-\frac{1}{2}}\sqrt[4]{\frac{k'_{sink}}{D}} r + \frac{C_2 \Gamma(\frac{3}{4})}{\sqrt{2}} * \sqrt[4]{\sqrt{\frac{k'_{sink}}{D}} r^2} \quad B_{\frac{-1}{4}} \frac{\sqrt{\frac{k'_{sink}}{D}} r^2}{2} \Big) \tag{4.53}$$

Where C_1 and C_2 are integration constants, H is the fractional Hermite polynomial, B is the fractional Bessel function of the first kind, and Γ the Euler gamma function.

Because $B_{\frac{-1}{4}}(r^2)/\sqrt{r}$ diverges at infinity, the constant C_2 equals zero. The formula boils down to:

$$S_{homogeneous}(r) = \frac{1}{r} * \Big(C_1 \exp\big(-\frac{1}{2}\sqrt{\frac{k'_{sink}}{D} r^2}\big) * H_{-\frac{1}{2}}\sqrt[4]{\frac{k'_{sink}}{D}} r \Big) \tag{4.54}$$

Setting $a = \sqrt{\frac{k'_{sink}}{D}}$ and solving the equation at the anhydrous grain interface r_i yields C_1:

$$C_1 = \frac{4\pi r^2_{interface}(k_{sink} S_{eq_{C-S-H}} + k_{source} S_{eq_{alite}}}{\exp(-\frac{1}{2} a r_i^2)\Big(H_{-\frac{1}{2}}\sqrt{a r_i}\Big(4\pi r_i (k_{sink} + k_{source}) - Da(a r_i - \frac{1}{r_i})\Big) - Da^{\frac{3}{2}} H_{\frac{3}{2}}\sqrt{a r_i} - \frac{3Da}{r_i} H_{\frac{5}{2}}\sqrt{a r_i}} \tag{4.55}$$

Where the H functions are Hermite fractional functions. After calculations, the field at the interface $r = r_i$ is equal to:

$$S(r_i) = \frac{(k_{sink} S_{eq_{C-S-H}} + k_{source} S_{eq_{alite}}}{k_{sink} + k_{source}} \tag{4.56}$$

To conclude, the supersaturation field general solution is the sum of the particular and homogeneous solutions:

$$S(r) = S_{eq_{C-S-H}} + \frac{C_1}{r} * \exp\left(-\frac{1}{2}\sqrt{\frac{k'_{sink}}{D}}r^2\right) * H_{-1/2}\left(\sqrt[4]{\frac{k'_{sink}}{D}}r\right) \qquad (\forall r > r_{interface}) \tag{4.57}$$

The inverse function here is a very slowly decreasing function of r compared to the Gaussian one, and the Hermite function is even slower than the inverse function so that the Gaussian gives the overall profile of the supersaturation field. The supersaturation field is thus a steeper version of the right arm of a Gaussian.

The characteristic distance and living subdomain

The quantity $1/\sqrt[4]{k'_{sink}}D$ is homogeneous to a distance and is the standard deviation of the Gaussian: beyond this distance, the function has lost about half of its initial height. This distance therefore is he characteristic size the living subdomain indicated on figure 4.48.

Injecting the definitions of k'_{sink} and D in this quantity, yields the characteristic living subdomain thickness $T_{living-domain}(t)$:

$$T_{living-domain}(t) = K_{living-domain}\sqrt[4]{\frac{f_{cap_{ext}}(t)}{f_{hydrates}(t)}} \tag{4.58}$$

Where $K_{living-domain}$ is a constant that aggregates k_{sink} and k_{source}.

When the diffusivity is very high compared to the hydrates sink, i.e. when $f_{cap_{ext}}(t) >> f_{hydrates}(t)$, that is typically early on or at large w/c ratios, this distance is very high: empty shells far from the source are still fed, the living domain practically equals the whole domain. Figure 4.6, with a w/c = 0.7, illustrates this case.

On the opposite, when the external capillary water is low and the hydrates fraction high, this distance is short and only the closest empty grains may carry on growing; the living domain lies close to the anhydrous core. Figure 4.7b right illustrates this case.

Back to the probability of lying within the living subdomain

The probability for an empty shell to lie within the subdomain is assumed to be the ratio of the volume of the living subdomain over the whole domain:

$$P_{living-subdomain} = \frac{V_{living-subdomain}(t)}{V_{whole-domain}(t)} \tag{4.59}$$

Let us consider the average living cell radius at time t $r_{eq_{living-cell}}(t)$, then the volume of the living subdomain is on average the volume of the shell of thickness $T_{living-domain}(t)$:

$$V_{living-subdomain}(t) = F_{average}\frac{4}{3}\left((r_{eq_{living-cell}}(t) + T_{living-domain}(t))^3 - r^3_{eq_{living-cell}}(t)\right) \quad (4.60)$$

The volume of the whole domain is the average space volume per remaining living cell:

$$V_{whole-domain}(t) = \frac{\int_0^\infty p(r) * Heaviside(r - r_{min-living}(t))dr}{V_{tot}} \quad (4.61)$$

Where $p(r)$ is the powder PSD in number, Heaviside is the Heaviside step function, $r_{min-living}(t)$ is the threshold radius below which anhydrous core have completely dissolved and V_{tot} is the total volume of the system.

4.9 References

[1] Andrew J. Allen, Jeffrey J. Thomas, and Hamlin M. Jennings. "Composition and density of nanoscale calcium-silicate-hydrate in cement". *Nature materials* 6 (2007), pp. 311–316.

[2] Amélie Bazzoni. *Study of early hydration mechanisms of cement by means of electron microscopy*. Doctoral Dissertation Ecole Polytechnique Fédérale de Lausanne (EPFL), 2014.

[3] Farid Begarin. *Etude de paramètres endogènes et exogènes au ciment Portland ordinaire influençant l'hydratation de sa phase principale: le silicate tricalcium*. Doctoral Dissertation Université de Dijon, 2012.

[4] Elise Berodier. *Impact of the Supplementary Cementitious Materials on the kinetics and microstructural development of cement hydration*. Doctoral Dissertation Ecole Polytechnique Fédérale de Lausanne (EPFL), 2015.

[5] Mercedes Costoya. *Effect of Particle Size on the Hydration Kinetics and Microstructural Development of Tricalcium Silicate*. Doctoral Dissertation Ecole Polytechnique Fédérale de Lausanne (EPFL), 2008.

[6] Sandrine Garrault. *Etude expérimentale et par simulation numérique de la cinétique de croissance et de la structure des hydrosilicates de calcium, produits d'hydratation des silicates tricalcique et dicalcique*. Doctoral Dissertation Université de Dijon, 1998.

[7] Renée Heilbronner and Steve Barrett. *Image analysis in the earth sciences: microstructures and textures of earth materials*. Springer Science & Business Media, 2013.

[8] S.F. Jones, G.M. Evans, and K.P. Galvin. "Bubbles nucleation from gas cavities - a review". *Advances in Colloid and Interface Science* 80 (1999), pp. 25–50.

[9] Xuerun Li, Alexandre Ouzia, and Karen L. Scrivener. "Laboratory synthesis of C3S on the kilogram scale". *Cement and Concrete Research* 108 (2018), pp. 201–207.

[10] Berta Mota-Gasso. *Impact of alkali salts on the kinetics and microstructural development of cementitious systems*. Doctoral Dissertation Ecole Polytechnique Fédérale de Lausanne (EPFL), 2015.

[11] Arnaud Charles Albert Muller. *Characterization of porosity and C-S-H in cement pastes by H1-NMR*. Doctoral Dissertation Ecole Polytechnique Fédérale de Lausanne (EPFL), 2014.

[12] Luc Nicoleau and André Nonat. "A new view on the kinetics of tricalcium silicate hydration". *Cement and Concrete Research* 86 (2016), pp. 1–11.

[13] Alexandre Ouzia and Karen L. Scrivener. "The needle model: A new model for the main hydration peak of alite". *Cement and Concrete Research* 115 (2019), pp. 339–360.

[14] Karl R. Popper. *Conjectures and refutations*. Routledge & Kegan Paul, 1963.

[15] Karl R. Popper. *The logic of scientific discovery*. Hutchinson & Co, 1959.

[16] George W. Scherer et al. “Hydration and percolation at the setting point”. *Cement and Concrete Research* 42 (2012), pp. 665–672.

[17] H.F.W. Taylor. *Cement chemistry, Second edition*. Thomas Telford, 1997.

[18] H.F.W. Taylor. “Chemistry of Cement Hydration”. *8th International Congress on the Chemistry of Cement, Rio de Janeiro* (1986).

[19] Jian-jun Zheng, Jie Zhang, and George W. Scherer. “Prediction of the degree of hydration at initial setting time of cement paste with particle agglomeration”. *Cement and Concrete Research* 42 (2012), pp. 1280–1285.

5 Conclusions

This chapter sums up the contribution of the thesis and opens perspectives for future experimental and modelling programs of research.

Contents

5.1 Contributions of this thesis

The conclusions brought forward in this section draw on the test of the model on 14 experiments, which is a wider set of experiments than any other alite hydration model yet published. All the model parameters were constrained within experimental confidence intervals, in particular they are quantitatively true to SEM observations. Across the 14 experiments, the average error on the heat flow and DoH were respectively of 16.2%±9.1% and 10.1%±9.9%.

The main hydration should be seen as a single event, the separation into acceleration and deceleration period is arbitrary and a heritage of Kondo and Ueda in 1968 who were the first to qualitatively describe the calorimetry curve of alite hydration. There is no qualitative change of mechanisms, only a quantitative and progressive one. Their division of the peak into two stages biased the debate for the following five decades.

5.1.1 Contributions to the main hydration peak debate

Rebuttal of the diffusion barrier and nucleation and growth by impingement

One of the main output of the literature review in chapter 2 is the rebuttal of the two main hypotheses present in the textbooks of Taylor, Lea, Bye and Matsuyuma: the diffusion barrier hypothesis and nucleation and growth by impingement. The evidence raised against both hypotheses over the past decade of research is overwhelming. The theses adds a few arguments on top of the already published ones.

Evidence against the diffusion barrier hypothesis

- There is no uniform /dense layer forming around alite / cement grains; C-S-H nucleates as needles or foils leaving the anhydrous grain in direct contact with the pore solution
- The presence of a gap between the receding anhydrous grain and the outer CSH scaffold
- The activation energy is constant throughout the whole peak
- The CSH diffusion coefficient of models based on this hypothesis vary by an order of magnitude with the PSD: it does not make sense
- The ability to fit a bell shape curve with four freely varying parameters or more is not convincing
- There is no publication in favor of it in one decade or having answered any of the former arguments

Evidence against the nucleation and growth by impingement

- Impingement is barely visible on SEM polished sections
- The value of the nucleation and growth rates of existing nucleation and growth models lie beyond experimental incertitude intervals
- The main hydration peak still occurs at w/c = 50 where there is clearly no perpendicular impingement
- Parallel impingement is not valid as well because it would lead a transition to a lesser, still positive, slope or a plateau, not a decrease.
- The ability to fit a bell shape curve with four freely varying parameters or more is not convincing

A quantitative deepening of Bazzoni's thesis

The qualitative microstructural evolution proposed by Bazzoni in her thesis has been quantitatively demonstrated, though with some shades.

- The transition from the acceleration to the deceleration period coincides with the covering of the alite grain surface in combination with the progressive slowdown of the needles growth. Neither the full coverage of the surface nor the progressive slowdown of the needles is alone sufficient to account for the transition.
- The contribution of the inner C-S-H to the output heat flow is quantitatively negligible up to the end of the deceleration period. Even if the inner C-S-H starts to form as early as at the peak time as Bazzoni observed, the computation of the heat released demonstrate it is quantitatively negligible: at least 80% of the heat released during the deceleration is accounted by the outer C-S-H only.
- To model C-S-H as needles enabled to show that the increase of needle size due to the Zinc doping quantitatively explains the heat flow increase
- 90% of the needles nucleate within a window of 4 hours ± 1 hour.

The role of small grains

The impact of the small grain dissolution on the hydration has been quantified for the first time.

- Grains below $4\mu m \pm 1\mu m$ completely dissolve within 24 hours for w/c between 0.32 and 0.5.
- The heat flow release of PSDs that incorporate a large fraction of small grains are sharpened and shifted left, but the overall shape remains the same. The dissolution of the small grain is not per se the mechanism causing the transition except perhaps for PSDs entirely below 1 μm.

- For log-normal PSDs commonly encountered for alite and cement powders, the impact of the small grains dissolution on the heat flow is negligible below 50% DoH.

5.1.2 Two linear equations with needles length and powder specific surface

Two equations of linearity for the heat and heat flow for needle length and specific surface were derived:

$$DoH = \frac{\eta_1}{\eta_3} * S_{spe} * M_{alite} * l_{24h} * f(k_n, s_0, t_c, t) \tag{5.1}$$

$$HF = \Delta_r H \frac{\eta_1}{\eta_3} * S_{spe} * M_{alite} * l_{24h} * \frac{df(k_n, s_0, t_c, t)}{dt} \tag{5.2}$$

These equations show that the DoH and heat flow are *proportional*, not simply monotonously increasing, to the 24 hours needle length and specific surface of the powder. These equations hold for the first day as long as the DoH is lower than 50%.

The slop of the acceleration period when plotted per unit of surface is a characteristic function of the surface chemical reactivity

Within the range [1 100]μm where the model has been tested, the slope of the acceleration period when plotted per unit of surface is independent of the PSD and w/c (within the range 0.32 to 0.5 at least). In this sense, it allows for the comparison of the reactivity of different alites.

In particular, the fact the model could fit 20 experiments with very similar parameters entails that the reactivity of grains is independent of their size within the range [1 100] μm and w/c: 1μm grains react in exactly the same manner as 100μm, and at whatever w/c within [0.32 0.8]. The difference in specific surface is sufficient to account for the increased reactivity of smaller grains, there is a priori no need to invoke a higher density of defects for all experiments quoted or made in this thesis.

Whenever it comes to comparing the chemical reactivity of alites, the representation per unit surface is thus more relevant than the widespread representation per unit of mass.

5.1.3 Contributions on the later ages mechanisms

The conclusions of this section rely on a test on only 6 experiments. Although the model was shown to fit all these 6 experiments with the same set of input parameters, the conclusions are less solid than for the main hydration peak.

The role of small grains

- Grains below $7 \pm 2 \mu m$ completely dissolve within 7 days.
- Grains below $10 \pm 3 \mu m$ completely dissolve within 28 days.
- The maximum grain size that dissolve at 28 days is directly caused by the initial amount of space available, that is the initial w/c. But the PSD indirectly influences it: finer powders quickly exhaust the external capillary water, which as a result diminishes the outer C-S-H growth, which leads to a lesser gap opening and therefore less inner C-S-H growth as well.

The predominant role of outer C-S-H over the inner C-S-H on the kinetics persists

Although the inner C-S-H precipitation often coincides with the start of the later ages and is a prominent feature of the later age microstructure, its role on the later ages kinetics is not as important as SEM polished sections suggest.

- The volume fraction of outer C-S-H is always higher than the inner C-S-H fraction. Quantitatively, the inner C-S-H volumetric contribution to the total C-S-H is only about $30\% \pm 10\%$ at 28 days for the systems studied in the thesis.
- At sufficiently high w/c ratios and/or coarse powders, the external capillary water is not exhausted so that the outer C-S-H still grows. In that case, it contributes to about one third of the total heat flow all through the later ages.
- At sufficiently low w/c and/or fine powders, the external capillary water is exhausted so that the outer C-S-H growth stops and the heat flow displays a characteristic inflection point. Because of the indirect influence of the outer C-S-H on the gap opening, the maximal thickness the inner C-S-H can reach is also reduced.
- The exhaustion of the external capillary water in a sense provokes the inner C-S-H precipitation. If there is no external capillary water left, but only internal capillary left, the system has no choice but to precipitate inside the gap.

The probability of outer C-S-H growth is not linear with the space available

One striking difference between the model and the experiment is the manner in which the low w/c curve diverge from the high w/c. In the experiments, the curves exactly align up

to a given point beyond which they abruptly diverge. In the model, because the probability of impingement is assumed proportional to the amount of space, the curves progressively separate.

The importance of the gap opening phenomenon, the water alwasy flows from the external to the internal capillary for the system considered in this thesis

The amount of volume freed by the gap opening is considerable. For the experiment considered in this thesis, by 24h the internal water fraction varies from 5 to 30%; by 7 days, it varies from 20 to 80%; by 28% it varies from 50 to 100%.

In addition, it was shown that the capillary water always flowed from the external space to the internal one. As a consequence, the gap opening suck the space available for the outer C-S-H precipitation. This accentuates the external impingement and slows down the kinetics.

Alternative explanations of the later ages kinetics are not alone sufficient to explain the later ages kinetics. The later age kinetics cannot be simplified by one overwhelming mechanism: it is caused by the cumulative effect of several coupled mechanisms.

As it was shown in section 7.1 of chapter 4, the later age kinetics is not controlled by a single mechanism, be it a drop in supersaturation, diffusion limitation or dissolution limitation but by the cumulative effect of several non-linear and coupled mechanisms. To quantitatively account for the later age kinetics all these effects and their coupling should be considered.

Conclusions: space filling is a leading mechanism in the later ages, but it entails several sub-mechanisms and other different mechanisms should be considered to quantitatively account for the kinetics.

Space-filling is certainly an important mechanism in the later ages but entails the sub-mechanisms describe in the previous subsections. Furthermore, it was not shown to be sufficient per se to quantitatively account for the experiments.

Space filling does explain part of the divergence between the low and high water to cement ratio. However, the probability of outer C-S-H impingement is strongly non-linear with the volume of space. Interestingly, the space filling "horizontal rule of thumb" is better at predicting the inflection point than the model. This rule of thumb state that the inflection point happens at:

$$DoH_{ext-space_{filled}} = 1.6 * w/c \tag{5.3}$$

$w/c = 0.45 \pm 0.01$ marks the threshold below which there is no external capillary left at 28 days for PSD considered in this thesis. At 0.5 there is still external capillary water at 28 days. At 0.4 there is none. The kinetics slowdown is thus significant only for system below 0.45.

5.1.4 Experimental contributions

New SEM observations showed that needles still grow significantly in the later ages. Measurements showed they grow as much in the first 24 hours than in the following 27 days. Also, the thickness of the inner C-S-H was quantified for the first time.

A new dataset to benchmark alite hydration models was built. Three new factors are added to Costoya's PSD experiments: water to solid ratio, filler effect and temperature. This dataset brought forward new information in its own right: first it shows the abrupt split between the low and high w/c is valid for 16 experiments, and second it showed the filler effect may actually be detrimental to the 28 days DoH.

5.2 Perspectives

5.2.1 Questions left

Why do needles slow down?

If the transition corresponds to the time when most of the surface is filled and most of the needles are in their fast growth mode, what then control the nucleation and growth rates profile? Why is there a burst of nucleation within only very few hours? Why do needles exhibit a transition from a fast growth mode to a slow growth mode? The mechanisms behind them remain unspecified despite their importance in causing the transition; the model takes the nucleation and growth rates as input parameters says nothing regarding their causes.

Could these be explained only because of the drop of the supersaturation? Perhaps needles incorporate defects during their growth, thus modifying their interfacial energies, to the point where their structure is too defective to carry on growing? This is difficult to experimentally assess, and C-S-H is known to have an intrinsic defective structure. Or is it a combination of the two effects?

Why is there a transition to the inner C-S-H? Why are the outer and inner C-S-H growing simultaneously in the later ages? What is the structural difference with the outer C-S-H

Why is there a transition from one phase, the outer C-S-H needles, to another one, the inner C-S-H? Thermodynamically, the local nucleation and growth of a phase are determined by the local temperature, pressure and chemical potentials fields. Given that the temperature and pressure fields remain uniform and constant in an isothermal calorimetry experiment, the composition of the pore solution and the interfacial energies of the anhydrous grains and the hydrates are the only possible causes for this transition.

Perhaps there is a change in the calcium to silicon ratio that would favour the inner over the outer C-S-H. This seems unlikely as Bazzoni did not measure any significant difference between the end of the first day, when there are mostly outer C-S-H needles, and one month, when there is a mixture of outer and inner C-S-H.

A change of supersaturation is almost certain: it is well known it decreases and then plateaus with time, but is it more than that? The pore solution concentrations are likely not uniform - the outer and inner C-S-H growth overlaps: perhaps there is a gradient from each anhydrous grain surface to the outward extremity of its outer C-S-H shell that combined with a global decrease of the supersaturation would account for the transition? perhaps the local concentrations of species between the inner gap solution and the outer shell solution slightly changes?

Portlandite cluster impact

SEM polished sections surely set bounds to their impact. Image analysis of Bazzoni's observations set a range of 6% ± 2% DoH loss.

5.2.2 The necessity of mathematical models to understand the later ages mechanisms

Space-filling, grain consumption, Portlandite phagocytose, outer and inner C-S-H nucleation and growth, and possibly C-S-H densification and influence domains all have a cumulative and effect on the hydration kinetics while interacting between them. It is hard to imagine how the later ages mechanisms could be understood without integrating quantitatively the full list of these coupled mechanisms.

In other words, qualitative one-factor-at-a-time experimental approaches that show a given factor X influence the kinetics are doomed to only a vague conclusion as X may well interact with all other factors.

5.2.3 Recommendations for future hydration models

Modelling approach: coupling between dissolution and growth through the pore solution supersaturation

So far hydration models have endeavored to test whether one single mechanism was rate-controlling. Yet the experiments made on dissolution alone and C-S-H precipitation alone indicate that the pore solution composition has a dramatic impact on both phenomena. Marchon (Marchon's PhD Thesis, ETH, 2016) , Bullard et al. (Bullard et al., "Time dependent driving forces and the kinetics of tricalcium silicate hydration", Cement and Concrete Research, 2015) and Ouzia & Scrivener (chapter 3 of this thesis) researchers have underlined that there is likely a "mixed-control" between dissolution and precipitation. Therefore, there is a need to develop models that consider both effects simultaneously together with the other factors like space-filling for instance.

To achieve that, models that can capture dissolution or precipitation independently should first be built, in a similar fashion to Andalibi et al. (Andalibi et al., "On the mesoscale mechanism of synthetic calcium-silicate-hydrate precipitation: a population balance modeling approach", 2017). Simultaneously, experiments are required to allow for testing these models in a variety of situation, if possible as close to realistic systems as possible.

Modelling approximations that should not be made to avoid misinterpretations

Given the simple shape of the calorimetry and DoH curves, models can easily fit them and tack onto them a biased interpretation. Some approximations have been shown to bias the interpretation and should not be made:

- Grains should not be approximated by smooth spheres
- Because the probability of impingement is not linear with the available space, models that do not rely on an explicit 3D microstructure should consider the non-random distribution of phases in space.
- The nucleation rate cannot be assumed constant. A fixed initial number of nuclei is also in contradiction with experiments. Needles nucleates within a window of $4h \pm 1h$.
- The outer and inner C-S-H growth rates should not be assumed linear: measurements show they initially grow fast and then slow down.

Methodological recommendations

Whether dealing with the main hydration peak or later ages, modelers should note the critical importance of having at hand a well-made dataset before spending time on developing their models. Otherwise no strong and decisive conclusions can be reached and no hypothesis firmly validated/refuted.

As the past decades have demonstrated in the case of the main hydration peak, the ability for a model to fit on dots a few experimental curves proves nothing. The underlying mechanisms may completely be wrong, like the Avrami, diffusion-based or BNG models for instance, and still the model fits the calorimetry curves *on dots*. Therefore, the ability for a model to fit curves is *necessary but never sufficient*.

Therefore, other criteria are required to properly assess models. For instance:

1. **The ability to fit a large enough dataset.** As a rule of thumb models should at least be able to fit twice the number experiments than input parameters. Note only the size of the dataset but also its quality matters: the dataset parameters should vary over the widest relevant span so that to push the models to their limits. The dataset provided in this thesis is a start.
2. **The dataset should consider all the key experimental parameters** that are known to strongly influence the reaction and commonly vary in real life applications. At least the amount and PSD of each phase. Models dealing with the later ages should at least take the w/c into account and the small grain dissolution as they have a strong effect on the reaction. Ideally, the Portlandite phagocytose, the filler effect, and possibly the diffusion should be added.
3. **Whenever possible, the input parameters should ideally be retrieved directly from experiments and constrained as much as possible within narrow confidence intervals** instead of calibrating them on some data. When this is not possible, two datasets should be used: one for calibration and one for prediction.
4. **Parameters should at least be measurable and have a clear physical meaning.** Parameters like the fractional n-exponent of the Avrami law are meaningless and cannot be used to assess the nature of the C-S-H growth. Parameters that do not have a clear physical meaning, because of geometrical approximations made for instance, should be avoided: whenever the model does not fit perfectly the experiments, the approximation is raised as an explanation and no further investigation is done. On the contrary, if the model only relies on measured quantities and does not fit the experiments within the experimental confidence intervals, this pushes the investigation forward: either some assumption is wrong or missing. Only then is progress possible.

5. **The ability to fit simultaneously several techniques**, in particular SEM, XRD and NMR, instead of only calorimetry. For example, nucleation and growth rates found by fitting the calorimetry curve that are within the confidence intervals measured by SEM and that lead to Powers diagrams validated by NMR experiments reinforce the model and/or the underlying hypothesis credibility.

6. **An objective fitting process**. Fitting requires an error function to be defined followed by a standard fitting method such as the gradient method, the simplex method, genetic algorithms to be applied. In all cases, the uniqueness of the solution should be addressed.

7. **Cross-comparison by testing the model on a common dataset**. So far Costoya PSD experiment has served such a purpose for alite hydration but only deals with five curves. Now this expanded dataset can replace it.

These recommendations are not exhaustive but mere interpretations of Karl Popper's falsfiability as the criterion of demarcation: theories that avoid a direct and stringent test, theories that do not take the risk of being refuted (by remaining qualitative, by introducing non-measurable quantities, by making geometrical approximations, etc.) should be looked at suspiciously:

> The amount of positive information about the world which is conveyed by a scientific statement is the greater the more likely it is to clash, [...] The more it prohibits, the more it says.
>
> This makes our methodological rule that those theories should be given preference which can be most severely tested.
>
> Karl Popper, *The Logic of Scientific Discovery* (1959), Hutchinson & Co Editors, pp. 41 and 121.

Alexandre Ouzia

Ph.D

École Polytechnique Fédérale de Lausanne (EPFL)
Switzerland
☎ *+41 21 69 37786*
✉ *alexandre.ouzia@epfl.ch*
Citizenship : french

Education

2007 **Scientific Baccalaureate**, *Prytanée National Militaire*, La Fleche, *Highest Honours*.

2007–2009 **Classes préparatoires aux grandes écoles**, *Lycée Lakanal*, Sceaux, .
Preparation in Mathematics, Physics and Chemistry in order to enter the "Grande écoles".

2009–2012 **Polytechnical Institute of Grenoble**, Grenoble, *Grande école d'ingénieur*.

2011–2012 **Technical University of Darmstadt**, Darmstadt, 2^{nd} *year of M.Sc*.

Nov 2012 **Reception of the master and engineering diploma**, *Master of Materials science and Engineering diploma from Grenoble and Darmstadt, highest honours*.

2013–2014 **Université Pierre et Marie Curie**, Paris, *Bachelor in fundamental mathematics. (From home)*.

Bachelor thesis

2011 **Center for Heavy-Ion Research (G.S.I.)**, Darmstadt, Germany.

title *Ion beam induced damages in graphite*

Master thesis

2012 **European Organisation for Nuclear Research (C.E.R.N.)**, *EN-STI-TCD team*, Geneva, Switzerland.

title *Feasibility study of a slit for the LBS line of the Linac 4*

Ph.D thesis

2015 - 2019 **École Polytechnique Fédérale de Lausanne**, *EPFL*, Laboratory of Construction Materials, Lausanne, Switzerland.

title *Modelling the main hydration peak and later age kinetics of alite hydration*

supervisor Karen L. Scrivener

description A new model and interpretation for the main hydration peak has been developed and validated against a wide range of experiments. For the first time the space-filling hypothesis has been quantified and tested for the later age kinetics.

Teaching assistantship
- Probability and Statistics. In particular, I built all the exercises for a one semester long course. 112 hours over 4 years.
- labwork: fresh concrete, mortar elaboration, wood hygroscopic and mechanical properties (responsible for this labwork) and thermal properties of construction materials (responsible for this labwork). 144 hours over 4 years.

Projects supersivion
- SEM study of C-S-H precipitation during the first week of cement hydration (B.Sc project. 6 hours / week over one semester.)
- C_3S synthesis, analysis by SEM of its hydration and relationship between gel-space and strength (B.Sc project. 6 hours / week over one semester.)
- Quantitative microstructural analysis of alite pastes beyond one day (M.Sc project. 10 hours / week over one semester.)
- Quantitative limitations of chemical shrinkage by dilatometry. (Entry level engineer. 1 year.)

Professional Experience

European Organization for Nuclear Research (C.E.R.N.)

2013–2014 **Technical student**, *TCD team*.

- Realization of the future P.S.B. (Proton Synchrotron Booster) injection dump
- Test campaign on silicon carbide - molybedum brazed joint

Languages

French	**Mother tongue**	
English	**Advanced**	*TOEFL iBT : 111; studied, passed exams and worked in english.*
German	**Intermediate**	*can read and watch news.*

Computer skills

O.S. Windows, Linux and Mac at work and home.

Programming basics of C++, regular use of the numerical simulation software ANSYS and the Monte-Carlo code SRIM/TRIM when at CERN, regular use of matlab during my PhD.

Articles

published Ouzia, A. and Antonakakis, T. (2016). *Uncoupled thermoelasticity solutions applied on beam dumps.* Physical Review Accelerators and Beams, 19(6), 063501.

published Li X, Ouzia, A. and Scrivener, K. (2017) *Laboratory synthesis of C_3S on the kilogram scale*. Cement and Concrete Research.

published Ouzia, A. and Scrivener, K. (2019) *The needle model: a new model for the main hydration peak of alite*. Cement and Concrete Research.

reviews Reviewed 15 articles for Cement and Concrete Research.

Conferences and workshops

Attended COST Action TU1404 in Vienna on cement and concrete modelling, October 2015.

Presented CEMNET meeting in Bern. February 2016.

Poster 36th Cement and Concrete Science conference in Cardiff, best poster, September 2016.

Workshop Rilem committee on hydration models in Delft, November 2016.

Workshop Joint Workshop EPFL-PSI-Konstanz University on nucleation and growth, May 2017.

Workshop Nanocem Workshop on C-S-H modelling by MD and DFT, May 2017.

Poster The Future of Cement, 200 years after Louis Vicat, June 2017.

Presented 37th Cement and Concrete Science conference in London, September 2017.

Invited speaker Materials Science department weekly seminar, Strathclyde University Glasgow, September 2017.

Attended 2nd International conference on calcined clay cement (LC3), La Havana , december 2017.

Presented Workshop of the Joint International Laboratory for Advanced Construction Materials (LACM), Southeast university, Nanjing, May 2018.

Presented 4th international Symposium on Design, Performance and Use of Self-Consolidating Concrete, Hunan university of technology, Changsha, May 2018.

Invited speaker Prof. Tung-Chai Ling lab seminar, Hunan university of technology, Changsha, May 2018.

Invited speaker Prof. Suping Cui (Beijing University of Technology) and Wensheng Zhang (China Building Academy) lab seminar, May 2018.

Interests

Trail running. Violin at Lausanne "Amati" orchestra. Philosophy of science.

Theater: Wrote and played part of the "Origine(s)" piece in Lyon and Paris in 2017 and 2018.

Co-Founder of the "Break and Brain" talks on Science and Society at EPFL.

**Ce document a été imprimé au Centre d'impression EPFL,
imprimerie climatiquement neutre, certifiée myClimate.**